# Structure and dynamics of the aggregation mechanism of the Parkinson´s disease-associated protein α-synuclein

Dissertation

zur Erlangung des Doktorgrades

der Mathematisch-Naturwissenschaftlichen Fakultäten

der Georg-August-Universität zu Göttingen

vorgelegt von

Carlos Walter Bertoncini

aus Santa Fe, Argentinien

Göttingen, 2006

D7

Referent: Prof. Ralf Ficner

Korreferent: Prof. Reinhard Jahn

Tag der mündlichen Prüfung: 05.07.06

# Abstract

In Parkinson's disease (PD), intracellular neuronal inclusions containing amyloid-like aggregates of the protein α-synuclein (αS) are deposited in the pigmented nuclei of the brainstem. The mechanisms underlying the structural transition of innocuous, presumably natively unfolded αS to oligomeric neurotoxic forms of the protein are largely unknown.

The major aim of this thesis has been the characterization of the ensemble of conformers that αS populates in its monomeric native state and the early transitions that lead to protein oligomerization, by the use of nuclear magnetic resonance (NMR) spectroscopy. The conformational flexibility inherent to this kind of proteins places them beyond the reach of classical structural biology, and a special set of NMR-based experiments had to be implemented in order to study the native soluble state of αS, namely paramagnetic relaxation enhancement (PRE) from nitroxide spin labels and residual dipolar couplings (RDCs).

Our results show evidence that monomeric αS assumes conformations that are stabilized by long-range interactions and act to inhibit aggregation. As probed by RDCs, these auto-inhibitory conformations are formed on a ns to μs timescale that is precisely that in which secondary structure elements form during folding. In addition, PRE-derived distance restraints have been employed to derive a low resolution model for the ensemble of structures of αS compatible with the experimental findings.

The conformations populated by αS under disease-state circumstances were further investigated. Missense mutations linked to early onset PD, and environmental conditions that promote αS aggregation were found to release the inherent tertiary structure of the protein. Thus mutant or ligand bound αS overcomes more easily the energetic barrier for self-association, leading to an increased tendency to oligomerize.

The homologous protein βS, which is proposed to inhibit the toxicity of αS, has been also characterized by means of high resolution NMR. It was found that the conformations populated by this protein do not account for long range interactions as αS does, but a higher degree of residual structure is attained, likely polyproline II extended conformations.

Finally, the binding of divalent transition metal cations to αS was studied by a set of spectroscopic techniques. It was found that among several transition metals, Cu(II) is strongly bound by the N-terminus of the protein with an affinity of ~ 100 nM, and the complex is more prone to aggregate that the free protein. Other metals as Fe(II), Mn (II), Ni(II) and Co(II) do not influence protein aggregation since they bind to the C-terminus of the protein

with $10^4$ lower affinities. Our results suggest that impairment of Cu(II) homeostasis links the three major amyloid neurodegenerative disorders Alzheimer's, Prion and Parkinson's disease.

From the therapeutic point of view, it is foreseen that the reinforcement of these native, auto-inhibitory, long-range interactions in αS may be a (the) key target of new pharmacological agents designed to impede or even reverse aggregate formation in Parkinson's disease. Conformationally altered αS may also constitute a general molecular mechanism underlying the induction of PD by both environmental and genetic conditions. Thus, agents specifically designed to stabilize the native state of αS may also prove useful in impeding or reversing its pathologic aggregation in familial forms of PD.

# Table of contents

# Abbreviations

| | |
|---|---|
| $A\beta$ | Amyloid-$\beta$ peptide |
| AD | Alzheimer's disease |
| APP | Amyloid precursor protein |
| $\alpha S$ | $\alpha$-synuclein |
| ATP | Adenosine -5'-Triphosphate |
| $B_0$ | External magnetic field |
| $\beta S$ | $\beta$-synuclein |
| CD | Circular dichroism |
| DEPC | Diethylpyrocarbonate |
| DLB | Dementia with Lewy bodies |
| CMA | Chaperone-mediated autophagy |
| DNA | Desoxyribonucleic acid |
| $^1D_{NH}$ | N-H residual dipolar coupling |
| DSSE | Doublet Separated Sensitivity Enhanced |
| DTNB | 5,5'-Dithiobis(2-nitrobenzoic acid) |
| DTT | Dithiothreitol |
| EDTA | Ethylenediamine tetraacetic acid |
| EPR | Electron paramagnetic resonance |
| ER | Endoplasmic reticulum |
| FRET | Förster resonance energy transfer |
| FTIR | Fourier-transform infrared spectroscopy |
| $\gamma S$ | $\gamma$-synuclein |
| HMQC | Heteronuclear double quantum coherence |
| HSQC | Heteronuclear single quantum coherence |
| HSPs | Heat shock proteins |
| INEPT | Insensitive nuclei enhanced by polarization transfer |
| IPAP | In-Phase-Anti-Phase |
| IPTG | Isopropyl-$\beta$-D-thiogalactopyranoside |
| $^1J_{NH}$ | N-H scalar coupling |
| $^3J_{HNH\alpha}$ | HN-H$\alpha$ scalar coupling |
| LBs | Lewy bodies |
| MES | 2-Morpholinoethanesulfonic acid |

| | |
|---|---|
| MPP+ | 1-Methyl-4-phenylpyridinium |
| ms | Milliseconds |
| μs | Microseconds |
| MTSL | (1-oxy-2,2,5,5-tetramethyl-D-pyrroline-3-methyl)-methanethiosulfonate |
| NAC | Non-Aβ Component of Alzheimer's disease amyloid plaques |
| NMR | Nuclear magnetic resonance |
| NOE | Nuclear overhausser effect |
| ns | Nanoseconds |
| PAR | 4-(2-pyridylazo)resorcinol |
| PCR | Polymerase chain reaction |
| PD | Parkinson's disease |
| PFG-NMR | Pulse field gradient-NMR |
| PG-SLED | Pulse gradient stimulated echo longitudinal encode-decode |
| PMSF | Phenylmethylsulfonyl fluoride |
| PII | Polyproline II |
| PRE | Paramagnetic relaxation enhancement |
| PrP | Prion protein |
| ps | Picoseconds |
| RDCs | Residual dipolar coupling |
| $R_g$ | Radius of gyration |
| $R_h$ | Hydrodynamic radius |
| RT-PCR | Reverse transcription-polymerase chain reaction |
| SAXS | X-ray scattering |
| SDS | Sodium Dodecyl Sulphate |
| SDS-PAGE | SDS-polyacrylamide gel electrophoresis |
| TF | Trigger factor |
| Thio-T | Thioflavin-T |
| Ub | Ubiquitin |
| UCH-L1 | Ubiquitin Carboxy-Terminal Hydrolase-L1 |
| UPS | Ubiquitin-proteasomal system |
| wt | Wild type |

# *Introduction*

# 1. Introduction

## 1.1. Protein folding

Organisms have evolved such as the native states of proteins are required to perform diverse biochemical functions, ranging from mere pillars of the overall cellular architecture, like actins and tubulin, up to exquisitely complex molecular machines, as the DNA and RNA polymerases. In all cases adopting a proper structure is essential if the proteins are to carry out their biological function. Failing to do so has often critical consequences for cellular homeostasis (Dobson, 2003).

The mechanism by which a polypeptide chain attains its unique native three dimensional structure is known as protein folding. Inside a cell proteins fold during, or immediately after, their synthesis in response to the crowding nature of the media and the concerted action of chaperones (Young et al., 2004). Nevertheless the fold of a protein appears to be solely encoded in the primary amino acid sequence, inasmuch as polypeptide chains fold *in vitro* in the absence of any auxiliary factors (Anfinsen, 1973; Dobson and Karplus, 1999). Indeed, the self assembly capability of proteins has allowed the occurrence of the early biologically-driven chemical processes, and the stability of such catalytically-competent polypeptide-based systems is believed to have been crucial for evolution to have taken place.

## 1.1.1. The energy landscape of protein folding

An unbiased search for the most stable structure of a protein would demand the population of all possible conformations that the polypeptide chain could adopt, until the state with the lowest energy is attained. As the average size of naturally occurring proteins is about 300 amino acids, it would take an astronomical amount of time for a polypeptide to fold via a random search of the conformations (Fersht, 1999). However, most proteins fold in the order of μs to ms, suggesting a preferential population of conformational states, as already proposed by Levinthal in the late ´60s (Dill and Chan, 1997).

Several models have emerged to explain the existence of folding pathways, from the framework model according to which secondary structure forms locally followed by collision of the folded segments, to the nucleation model in which folding is initiated locally and propagated through the chain. A third model, the hydrophobic collapse model, hypothesizes that the polypeptide would collapse rapidly around its hydrophobic side chains and then rearrange from the restricted conformational space that is then sampled (Fersht, 1999). All

three models are reasonable and fit experimental data, such that a single generic mechanism for protein folding may not exist in nature.

A conceptual mechanism for understanding how a protein folds while avoiding the Levinthal paradox is a folding funnel, described by the most probable pathways leading to the adoption of the unique native structure of a protein (Wolynes et al., 1995; Dill and Chan, 1997; Dinner et al., 2000). In a folding funnel, as schematized on figure 1.1, the unfolded state possesses the highest free energy and comprises an ensemble of multiple conformations constituting the starting point of the folding pathway. The fast dynamics and low conformational restriction that characterize this state allow the occurrence of interactions between different parts of the chain, and, among them, native-like contacts involving key residues are energetically favored. This causes a fast collapse of the polypeptide chain, often driven by the formation of hydrophobic clusters decreasing the free energy of the system. Thus proteins may fold from the random state by collapsing and reconfiguring (Fersht, 1999). A loosely collapsed state with fluctuating tertiary interactions and very weak secondary structure, known as the "molten globule", may be observed, and some times isolated.
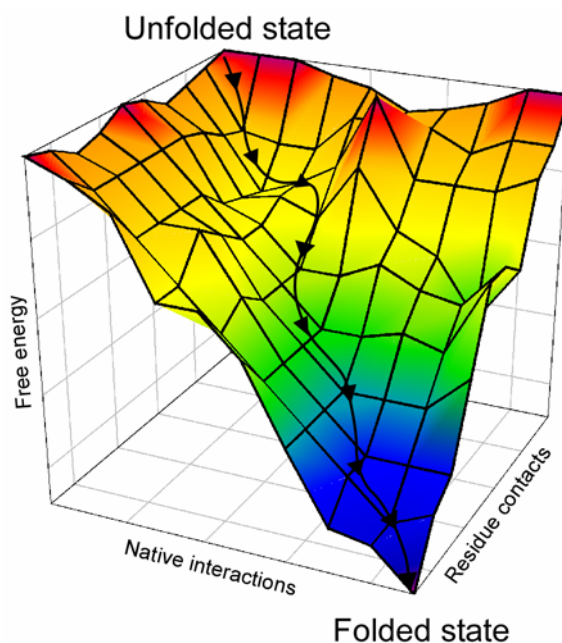


**Figure 1.1. Landscape for protein folding.** Theoretical folding surface for a polypeptide chain. One folding pathway is indicated by the continuous arrowed line, where the rapid collapse of the chain is represented by the population of the first valley, which makes that only few particular conformations overtake the higher free energy of the transition state. After the saddle point is reached folding readily occurs downhill. Adapted from Dinner et al. (Dinner et al., 2000).

Neighboring residues start then to populate conformations with increasing amount of stable secondary structure, with turns and helices forming more rapidly than beta sheets (Eaton et al., 1998; Plaxco et al., 1998; Mayor et al., 2003). The population of a defined secondary structure requires that many residues concomitantly adopt concerted backbone conformations capable of forming hydrogen bonds between amide and carbonyl groups of the main chain, which further reduce the degree of freedom of the system. In many cases, depending on the mechanism by which the protein folds, a relatively stable transition state is populated, which adopts an overall three-dimensional shape that closely resembles the one of the native state of the protein (Vendruscolo et al., 2003). After the transition state the protein folds downhill until it attains the single unique state with the lowest energy.

In summary, the native state of a protein is achieved through a precise interplay of both short- and long-range interactions, determining that only a small number of conformations need to be sampled, thereby speeding up the process.

### 1.1.2. Protein folding in the cell

In a cellular environment protein folding occurs co-translationally in the cytoplasm, mainly due to the slow synthesis rate by the ribosome, of ~ 8 amino acid residues per second. The concerted effect of chaperones prevents hydrophobic stretches from newly synthesized polypeptides to be exposed and to self-interact, avoiding protein aggregation (Hartl and Hayer-Hartl, 2002). Major cytosolic chaperones belong to the class of small heat shock proteins (HSPs), like the HSP60s (GroEL-GroES, CCT/TRiC), HSP70s, HSP90s and HSP100s, and another important class is represented by foldases, like the peptidyl-prolyl *cis-trans* isomerases, which isomerases peptidyl-prolyl bonds in proteins (Bukau and Horwich, 1998).

Insights into the mechanism of protein folding *in vivo* were recently provided by high resolution structural studies of bacterial chaperones, but mammalian systems are homologous and very likely to proceed similarly (Bukau and Horwich, 1998). In bacteria protein synthesis occurs at a speed of 20 residues per second, and the nascent polypeptide leaves the ribosome through a 10 nm exit tunnel placed in the large subunit. This hollow cage may accommodate up to 35 residues, but its narrow diameter (about 15 Å) impedes folding. To the end of this tunnel is recruited the ribosome-associated chaperone trigger factor (TF), a 48 kDa protein which provides a cage where hydrophobic residues of the nascent polypeptide are able to fold. TF possess high affinity for emerging exposed hydrophobic stretches but the interaction weakens as the protein folds and such residues are buried, leading to detachment from the

complex (Maier et al., 2005). Two other systems provide folding assistance either co- or post-translationally, the DnaK-DnaJ chaperone complex (HSP70 family) and the GroEL-GroES chaperonin (HSP60 family). In contrast to TF, these two mechanisms require ATP and co-chaperone systems. DnaK preferentially associates with elongating polypeptides larger than 20 to 30 kDa and thus acts on nascent chains subsequent to TF. It does not posses a cage, and rather facilitates the posttranslational folding of multidomain proteins through cycles of binding and release (Teter et al., 1999). The GroEL-GroES system forms a hydrophobic cage (also termed "Anfinsen cage") in which non-native proteins up to 60 kDa can be encapsulated and are free to fold. Folding is allowed to proceed for 10 s, as timed by the hydrolysis of ATP (Hartl and Hayer-Hartl, 2002).

The concerted action of the three chaperone-based system ensures proper folding in the cell; however it remains to be determined which fraction of proteins does entirely rely on chaperones to fold. For example a recent quantitative assessment of the GroES-GroEL chaperone function *in vivo* suggests that it may only be involved in the folding of ~ 100 proteins in *E. coli*. (Kerner et al., 2005).

Proteins that are directed to the secretory pathway or to mithocondria do not fold in the cytoplasm since they have to traverse the phospholypidic bilayers, remaining thus unfolded until they reach their final destination. Protein folding in the endoplasmic reticulum (ER) is also assisted by chaperones of the HSP70 and HSP90 class, GrpE-like and DnaJ-like, among others, and foldases, lectines and N-linked oligosaccharide-modifying enzymes are also present to ensure that polypeptides adopt their proper structure. Importantly, prior to vesicular release, folded proteins suffer a tight quality check based on glycosylations and de-glycosilations by the proteins UGGT and BiP (Schroder and Kaufman, 2005).

*In vitro*, re-folding after denaturation seems to be successful only for small to medium-size proteins, and very often large multidomains proteins fail to re-fold, mainly due to intra- and inter-molecular interactions (Kiefhaber et al., 1991). The picture *in vivo* is very similar, where off-pathway conformations are more likely to be populated if chaperones would not protect hydrophobic patches and force nascent polypeptide domains to fold independently and in a subsequent manner. Thus, in kinetic terms, chaperones do not themselves increase the rate of folding, rather they foster the overall efficiency of the process by reducing the probability of competing reactions, in particular aggregation (Schmid et al., 1994). In addition, confinement in the chaperone cage may smooth the energy landscape of folding for some larger proteins, either by preventing the formation of certain kinetically

trapped intermediates or by facilitating their progression toward the compact, native state (Hartl and Hayer-Hartl, 2002). As a conclusion, the evidence points that *in vivo* the folding of a protein is also exclusively dictated by the amino acid code of the polypeptide chain, and thus the generic applicability of the principles of protein folding (Dobson, 2003).

### 1.1.3. Quality control mechanisms of protein folding

Cells possess quality control mechanisms that ensure a proper folding of proteins and facilitate removal of misfolded species, mainly based on the concerted action of chaperones and the ubiquitin-proteasomal system (UPS). Although the buffering capacity of chaperones may be sufficient for counterbalancing small changes in the amount of non-native proteins, it is often required to clear species that do not properly re-fold and may aggregate (Buchner, 1996). To achieve such a task, cells couple the chaperone system to proteasome-based pathways of protein degradation, like the chaperone BiP (HSP70 class), which binds to a mutant Prion protein and mediates its degradation by the proteasome (Jin et al., 2000). The proteasome is a multisubunit complex that manages protein turnover, either by direct interaction with the protein substrate or by recognition of ubiquitinated substrates. Three different proteasomes are found in mammalian cells, two which are ubiquitin-independent, the 20S and 26S, and one ubiquitin-dependent, the 26S, the latter being the main degradation pathway of the cell (Ciechanover, 2005).

Chaperones are not only able to protect proteins as they fold, but they also rescue misfolded and aggregated proteins, providing them a new chance to get properly folded (Hartl and Hayer-Hartl, 2002). In particular, the chaperone HSP100 is thought to participate in ATP-dependant dissagregation of proteins, and polyglutamine-expanded ataxin 1 misfolding and aggregation is suppressed by chaperones of the HSP70 family (Cummings et al., 1998).

Extracellular protein-rich depositions are also in part derived from the misfolding of polypeptides, and in the light of few molecular chaperones present outside the cell, extracellular membrane or secreted proteins undergo a tight quality check in the ER. The concerted action of glycosilases and deglycosilases determines the fate of proteins that cannot fold correctly (Schroder and Kaufman, 2005). Indeed, it was observed that a large fraction of newly synthesized proteins fail to pass the stringent checks at the ER, and are thus degraded by the proteasome (Schubert et al., 2000).

## 1.2. Protein misfolding and disease

The quality control mechanisms of protein folding discussed above are often overpowered in a disease state of the cell, increasing the chances for a polypeptide chain to adopt conformations that are not conductive to the native structure of proteins. Furthermore, feedback to such impairment of cell homeostasis will come from proteins that do not fold correctly, or do not remain correctly folded, since they are often prone to aggregate and to form toxic oligomers, which sustain proteasomal impairment (Dobson, 2003) .

For example, a primary trigger for proteasomal failure is a massive overloading of unfolded substrates, but UPS malfunction may also arise from deficiencies in ubiquitinating enzymes responsible for determining the fate of misfolded proteins (Ciechanover and Brundin, 2003). Ubiquitin-independent degradation via the proteasome is also heavily challenged upon stress situations or when chaperones are incapable of refolding proteins, and accumulated misfolded proteins, which are not able to be cleared under these conditions, are progressively deposited in protein-rich aggregates called aggregosomes (Johnston et al., 1998). Moreover, recent studies suggest that such protein aggregates cause cytotoxicity by inhibiting proteasomal and/or UPS function, which may be causative of neurodegenerative disorders such as Alzheimer's, Parkinson´s, Huntington's and Prion diseases (Bence et al., 2001; Ciechanover and Brundin, 2003). Indeed, impairment of proteasomal function in the *substantia nigra* has been described for Alzheimer's and Parkinson´s patients (McNaught and Jenner, 2001; Keck et al., 2003). The mechanism by which this inhibitory effect takes place is largely unknown, but supports the idea of a generic toxic property of protein aggregates (Dobson, 2003).

In addition, the function of the ER is perturbed when the influx of unfolded polypeptides exceeds its folding capacity, which is often the case upon over-expression of proteins such as antithrombin III or blood coagulation factor VIII, which sequester chaperones and form protein aggregates. The ER normally responds by a complex signaling cascade known as the unfolded protein response, increasing the expression of chaperones and generally repressing transcription and translation (Schroder and Kaufman, 2005). Misfolded proteins in the ER are retro-translocated to the cytoplasm and degraded by the 26S proteasome (Mayer et al., 1998). Nevertheless, long-term abnormal accumulation of folding-incompetent proteins may produce oligomers resistant to proteasomal degradation, which completely disrupts the ER and activates apoptotic signaling pathways, leading to a disease-state of the cell (Davis et al., 1999; Nakagawa et al., 2000).

It is therefore not surprising that aberrations in the folding and abnormal deposition of certain proteins are now associated with a wide range of human diseases, collectively known as misfolding diseases (table 1.1). Such disorders may arise from the presence of mutations that impede a proper folding of the polypeptide chain or from stress factors that specifically trigger the misfolding of the protein, escaping control mechanisms and forming toxic species to cells (Dobson, 2004).

| Disease | Protein | Site of folding |
|---|---|---|
| Hypercholesterolaemia | Low-density lipoprotein receptor | ER |
| Cystic fibrosis | Cystic fibrosis transmemb. regulator | ER |
| Phenylketonuria | Phenylalanine hydroxilase | Cytosol |
| Amyot. lateral sclerosis | Cu, Zn, superoxide dismutase | Cytosol |
| Huntingston´s disease | Huntingtin | Cytosol |
| Sickle cell anemia | Haemoglobin | Cytosol |
| Alzheimer´s disease | **Amyloid $\beta$-peptide / Tau** | ER |
| Parkinson´s disease | **$\alpha$-synuclein** | Cytosol |
| Creutzfeld-Jakob disease | **Prion protein** | ER |
| Familial amyloidoses | **Transthyretin / Lysozyme** | ER |
| Cataracts | Crystallins | Cytosol |
| Cancer | P53 | Cytosol |

**Table 1.1. Representative protein folding diseases.** Selected disorders that are linked to the misfolding and aberrant deposition of proteins are listed. Proteins responsible of such deposits and the respective cellular compartment of folding are also depicted. Proteins displaying amyloid deposition in disease are highlighted in bold. Adapted from Dobson, 2004 (Dobson, 2004).

A common denominator of many if not all of these diseases is the modern-man intervention. For example, spanning our life-term permits accumulating damage to cells reducing the stringency of quality control mechanisms, in particular for protein folding, facilitating the occurrence of Alzheimer's (AD) and Parkinson´s disease (PD). Exposure to environmental toxins, like MTTP or Rotenone is another major cause of PD, and medical treatments as long-term dialysis unexpectedly cause deposition of proteins in liver or

osteoarticular tissue. The outburst of mad-cow disease during the last decade have also been a consequence of man's intervention in the feeding of animals, allowing misfolded proteins to cross natural barriers. The current idea behind these afflictions is that the actions of modern man have radically altered the evolutionary pressure on proteins. Thus the challenge to science strategists is to device the means for circumventing interventions with deleterious effects while promoting those offering ecologically responsible benefits to the human race.

### 1.2.1. Amyloid diseases

A sub-set of these pathologies, including AD, PD, Prion diseases and late-onset diabetes, among others, are associated with the deposition of structurally defined protein aggregates in the tissue known as amyloid fibrils (Koo et al., 1999; Serpell, 2000). Amyloid in disease is generally defined to be extracellular, although intracellular structures sharing the same core structures are described in PD (Serpell et al., 2000).

Amyloid is defined in terms of empirical observations from X-ray fiber diffraction, electron microscopy, FTIR and specific chemical staining with dyes such as Congo Red and Thioflavine T. Thus to be classified as an amyloid protein, its deposits should be straight, unbranched, of about 10 nm in diameter, reach a μm in length, present a cross-β diffraction with two sharp reflections at 4.7 Å and 10 Å, and display green birefringence after staining with Congo Red.

The pathological hallmark of these conformational diseases is not constrained to the formation of amyloid-like fibrils. In several disorders, protein deposits are composed of amorphous aggregates, without micro- or macroscopical order. Similarly, stable soluble oligomers derived from the self-association of soluble misfolded species, could be the final product of the aggregation process, and the culprit of many of these disorders (Caughey and Lansbury, 2003).

### 1.2.2. Molecular basis of amyloid formation

In order to deposit in the form of ordered filamentous protein-rich aggregates, a dramatic change in the structure of a protein has to occur. A conformational change triggered on the polypeptide chain cause a transition from its natural soluble conformation towards a more insoluble state. Although more than 20 proteins are known to be involved with such pathological depositions, they do not share any sequence homology, and may be either rich in β-sheets, α-helix, or lack significant secondary structure in their native states (Uversky and Fink, 2004). However, independently of the originating protein, they all form a common

cross-β structure in which continuous β-sheets are formed with β-strands running perpendicular to the fibril axis (Makin and Serpell, 2005).

To reconcile this observation, it has been proposed that fibrillation may occur when the rigid native structure of a protein is destabilized, favoring a partial unfolding. Such partially or completely unstructured conformations of the polypeptide chains are particularly high aggregation-prone, presumably via specific non-native intermolecular interactions conductive for oligomerization (Uversky and Fink, 2004). Indeed, many of the pathogenic mutations that are associated with familial deposition diseases increase the population of partially unfolded states by decreasing the stability of the native state or reducing its global cooperativity, as observed for lysozyme (Booth et al., 1997; Dumoulin et al., 2005). For Transthyretine it has also been postulated that pathogenic mutants destabilize the native tetramer of the protein, favoring a kinetic partition towards the monomeric state which easily destabilizes and aggregates (Hammarstrom et al., 2002).

Conformations that lead to misfolded states of a protein are not dictated by the polypeptide sequence, and thus are not generally part of the folding funnel, which is sequence-specific, giving rise to a second energetic landscape known as misfolding pathway (Figure 2.1). Although misfolded structures possess a low free energy, and could even be more stable than the native state of the protein, the energetic barrier dictates that the unfolded state has to be attained earlier than such conformations are populated (Uversky and Fink, 2004).

*In vitro* assembly of recombinantly expressed amyloid proteins has given sustained to such findings, demonstrating that fibrils readily form when the native state is destabilized by addition of denaturant or organic solvents, low pH, high temperature, pressure, or amino-acids substitutions. In most of these conditions, the population of a partially unfolded conformation has been documented (Uversky and Fink, 2004).

However, exceptions to this empirically-derived rule have been described. For example β2-microglobulin has been found to fibrillate through a native-like folding intermediate. This amyloidogenic conformation involves the formation of a non-native trans-prolyl isomer which is part of the folding pathway of the protein, but is just rarely populated in native conditions. This suggests that the folding and aggregation landscapes of this protein are, at least, partially overlapping (Jahn et al., 2006). Similarly, an acylphosphatase variant was found to aggregate via the population of a conformation that retains its enzymatic

activity and native-like structure. Afterwards, this intermediate species interconverts slowly into enzymatically inactive amyloid-like protofibrills (Plakoutsi et al., 2005).
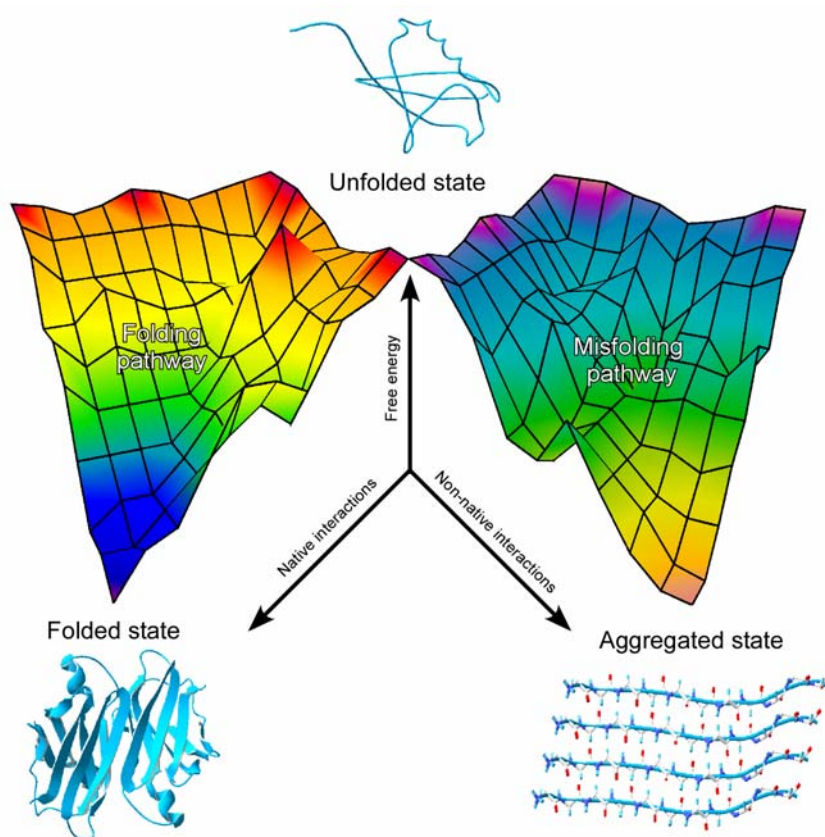


**Figure 1.2. Landscape for protein misfolding.** Analogous to the folding funnel determined for the folding of a protein, a similar landscape for the adoption of stable misfolded conformations of a protein is devised. The misfolding pathway is linked to the folding pathway through the unfolded state, and necessarily involves self-oligomerization of the polypeptide chain. In contrast to the folding situation where a single native structure is attained, several misfolded species may be populated in a stable manner, and are kinetically related. Depicted are the native and misfolded states of the amyloidogenic protein Transthyretine (native state based on 1bmz and fibril state based on 1rvs). Adapted from Jahn, 2005 (Jahn and Radford, 2005).

Limited proteolysis may also give rise to the exposure of highly aggregation prone regions, which readily self-associate, as in the process of the amyloid precursor protein APP, or in some cases with αS, giving raise to a C-terminal truncated species (Li et al., 2005). This may be explained in terms of cooperativity, another crucial factor in enabling proteins to remain soluble, ensuring that the equilibrium population of unfolded regions is minimal.

The tendency of proteins to form amyloidogenic conformations has been the subject of intense speculation by theoreticians. Electrostatic repulsion, hydrophobicity and secondary

structure propensity have all been shown to have a major influence on the tendency of fully or partially unfolded conformations to aggregate (Chiti et al., 2003). Interactions between solvent exposed, hydrophobic and flexible regions that lack stable hydrogen bonded elements of secondary structure are also suggested as factors initiating fibrillation (Uversky and Fink, 2004). Nevertheless, a specific conformational state seems not to be required for ordered aggregates to form, provided that the solution conditions permit relatively stable intermolecular interactions (Calamai et al., 2005).

### 1.2.3. Conformational plasticity in amyloid formation

Kinetic studies of *in vitro* protein aggregation have revealed a conserved fibrillation pathway for amyloid proteins, characterized by the intermediacy of ordered prefibrillar aggregates of distinct morphology  (Figure 1.3) (Caughey and Lansbury, 2003). After partially unfolded states are reached, conformations rich in β-sheet secondary structure content are populated, concomitantly with oligomerization (Uversky and Fink, 2004).

Soluble oligomers rapidly convert to fibrillation intermediates, designated protofibrils, which were first described for Aβ but now seem to be a general feature of amyloid formation (Harper et al., 1997; Walsh et al., 1997; El-Agnaf et al., 2001; Haass and Steiner, 2001; Bucciantini et al., 2002; Poirier et al., 2002). Early formed metastable protofibrils typically comprise 10 to 50 monomers, depending on the protein involved, and appear to be spherical in nature. These spheres may anneal to form chainlike protofibrils, which can further form annular pore-like species or proceed to amyloid fibrils (Harper et al., 1999; Ding et al., 2002; Lashuel et al., 2002a; Lashuel et al., 2002b; Nichols et al., 2002).

Cellular studies with several amyloidogenic proteins suggest that the pathogenic species on this kind of disorders is an ordered oligomeric intermediate and not the fibrilar end-product of the protein aggregation pathway (Caughey and Lansbury, 2003). In particular for Aβ and αS, a possible link between a subpopulation of circularized chain-like protofibrils, the so-called amyloid pores, and neuronal death, has been proposed (Lansbury, 1999; Goldberg and Lansbury, 2000; Haass and Steiner, 2001; Lashuel et al., 2002b). The toxicity of protofibrils is also supported by studies demonstrating that antibodies raised against soluble Aβ oligomers are capable of blocking the toxicity of these fractions to cultured neurons (Lambert et al., 2001).

It appears that the toxicity of protofibrils is related to their structure, not their sequence, as protofibrilar material comprising unrelated proteins showed similar toxicity in cell culture, while amyloid fibrils were non-toxic (Bucciantini et al., 2002; Fezoui and

Teplow, 2002). The generic nature of such aggregates and their effects on cells has recently been supported by the development of antibodies that can cross-react with protofibrills of different amyloidogenic peptides and proteins, and moreover inhibit their toxicity (Kayed et al., 2003).
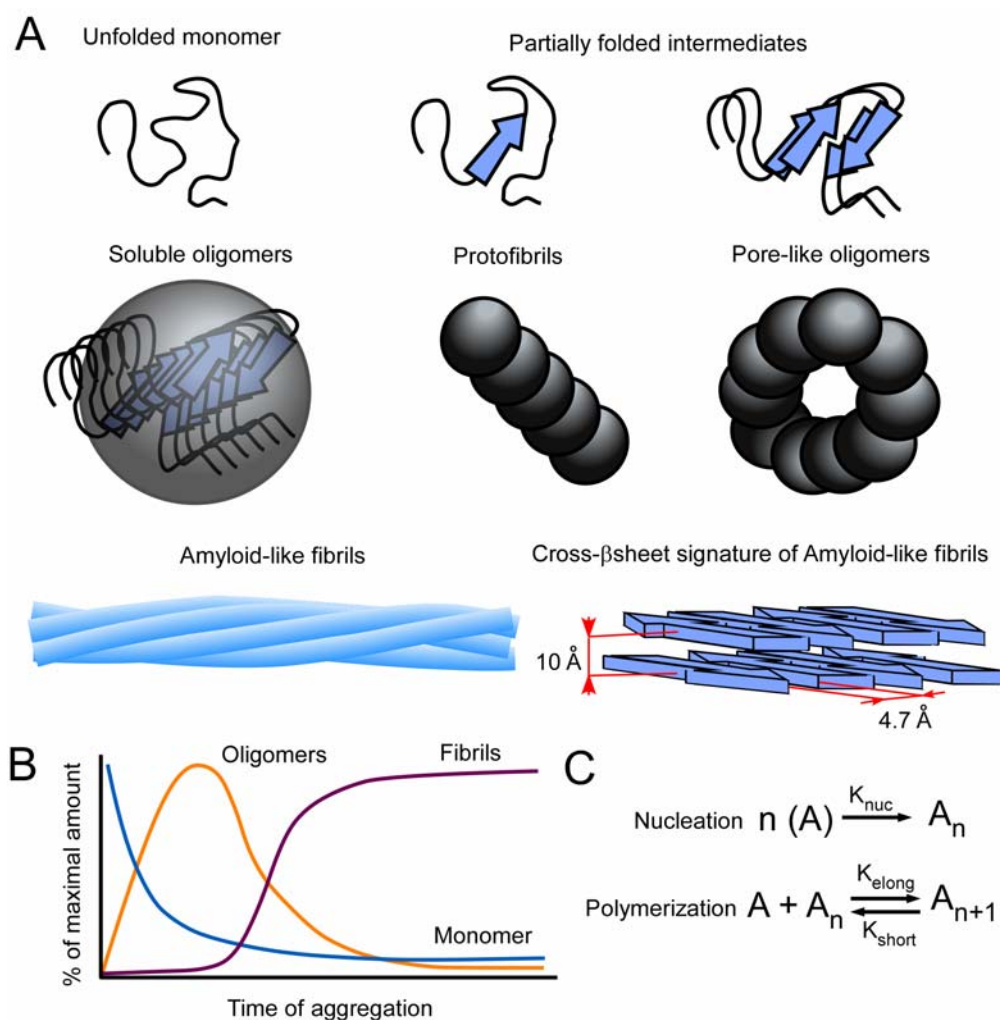


**Figure 1.3. Conformational plasticity in amyloid formation. A.** Different conformational assemblies that may be populated during the amyloid conversion of a protein. From a completely unfolded monomer to a partially folded, β-sheet rich, monomeric or dimeric intermediates, up to oligomers and protofibrills, a extensive variety of states are populated by a protein until it reaches the formation of an amyloid fibril. **B.** Ideal traces for the time-dependent occurrence of the above mentioned species during aggregation. Monomer consumption (blue) is rapid, as oligomeric conformations are populated (orange). Depending on the stability of such high molecular species, oligomers coalesce into protofibrils which mature into amyloid fibrils (violet). Simultaneously, monomeric species are able to directly aggregate into fibrils (direct monomer addition), but monomer consumption is not complete as a critical concentration is always in equilibrium with the fibrils. **C.** Simplified nucleation-polymerization kinetic model for amyloid formation, considering a nucleation event ($K_{nucleation}$) and a polymerization, or monomer addition, event ($K_{elongation}$ and $K_{shortening}$).

The search for the pathogenic conformation has practical implications because its formation and the proteins with which it interacts are potential targets for therapeutic intervention. Although the protofibril hypothesis has displaced the amyloid hypothesis, controversy still exists as to which is the pathogenic species. As recently suggested by Lansbury (Caughey and Lansbury, 2003), the "culprit" should have the following properties:

- "(*i*) its stability and/or the rate of its formation should be sensitive to disease-associated mutations;

- (*ii*) it should also be accessible to the wild-type protein because most of these diseases are predominantly sporadic;

- (*iii*) it should be linked to a potential pathogenic mechanism (for example, sequestration of a critical protein, disruption of a membrane, or initiation of apoptosis);

- (*iv*) its formation/stability should be sensitive to the effects that distinguish the various cell types in the brain, since all of these diseases are selective with respect to the anatomical distribution of neurodegeneration; and

- (*v*) its formation/stability should be sensitive to cellular defense mechanisms that may play a role in determining disease susceptibility, such as heat shock, chaperones, proteasomal degradation, or aggregosome formation".

At first glance it is very unlikely that a single toxic species could account for such diverse features. However, a concerted action of the different intermediates in the amyloid formation, each of them challenging a different cellular target, may reconcile the current disparate views of these sorts of afflictions.

## 1.3. Protein misfolding in Parkinson's disease

Parkinson's disease (PD) is a progressive, neurodegenerative, and age-related movement disorder affecting more than 1% of the population over 65 years of age (Goedert, 2001). It arises from the loss of dopaminergic neurons in the *substantia nigra* pars compacta of the brain and is accompanied by the presence of eosinophilic intracellular inclusions known as Lewy bodies (LBs) and Lewy neurites, which are confined largely to nerve cells (Galvin et al., 1999). LBs are also found in other major neurodegenerative disorders that occur increasingly with aging, including dementia with LBs and Alzheimer's disease (Dawson and Dawson, 2003). Ultrastructurally, LBs are protein rich depositions in the form of long amyloid-like fibrils, the major component of which is the pre-synaptic protein α-synuclein (αS) (Spillantini et al., 1997). The second most common component of LBs is ubiquitin (Ub) (Forno, 1996) and other proteins that are predominantly found are heat shock proteins, neurofilaments, Tau, synphilin-1 and tubulin, among others (Shults, 2006).

The etiology of PD is not yet fully understood, but genetic analysis, neuropathologic investigations, and experimental models of PD have provided fundamental insights into its pathogenesis (Figure 1.4). Impairment of mitochondrial complex I, leading to an increase of reactive oxygen species, plays a central role in the pathogenesis of sporadic PD (Jenner and Olanow, 1998; Schapira et al., 1998; Sherer et al., 2002). PD models based on MPP+ administration feature loss of dopaminergic neurons due to inhibition of complex I with the presence of intracellular inclusions strongly immunoreactive for αS and Ub (Vila et al., 2000), and other complex I inhibitors such as paraquat or rotenone also produce symptoms of Parkinson in various animal models (Thiruchelvam et al., 2000; Manning-Bog et al., 2002; Sherer et al., 2003).

In addition to oxidative stress, impairment in the ubiquitin-proteasomal system contributes to the disease condition in PD (McNaught et al., 2001), as has been linked to many neurodegenerative disorders (Ciechanover and Brundin, 2003). Failure of the UPS to adequately remove misfolded or abnormal proteins may underlie demise of nigral cells in sporadic PD (McNaught et al., 2001). Furthermore, deficits in the 26/20S proteasome pathways are accompanied by protein accumulation and aggregation, which may also cause neurodegeneration (Chung et al., 2001), and recently it has been demonstrated that soluble aggregated proteins can inhibit the UPS (Bence et al., 2001). These combined pieces of evidence have attracted much attention as they imply that LBs could originate from ubiquitin-

rich aggregosomes that the proteosomal components may not be able to process (McNaught et al., 2002).
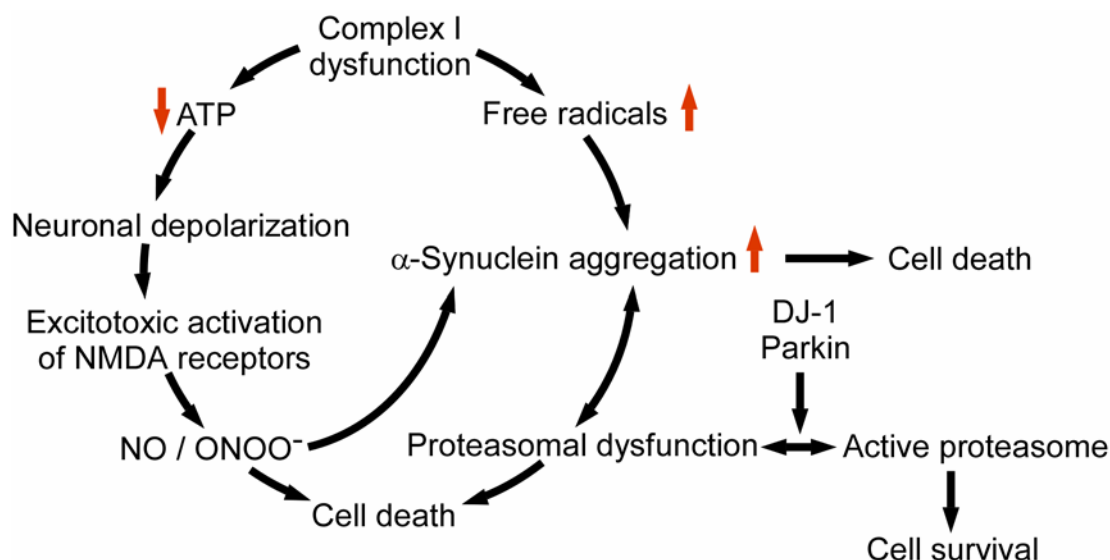


**Figure 1.4. Molecular pathways to Parkinson´s disease.** PD is a complex disorder that involves impairment of cellular homoestasis a various levels. Three main events may trigger PD, (i) damage to mitochondria accompanied by an increase in reactive oxygen species, (ii) impairment of the ubiquitin proteasomal system, and (iii) misfolding of αS. Evidence suggests that all of these disease-associated mechanisms are tightly interconnected in a single pathological pathway that cause the demise of dopaminergic neurons in the brain stem. Adapted from Dawson, 2003 (Dawson and Dawson, 2003).

### 1.3.1. α-Synuclein aggregation is linked to Parkinson's disease

Although PD is primarily a sporadic disorder, more than 10 different loci are responsible for rare Mendelian forms of PD, and the study of these gene products has provided new insights that assisted experimental models of neurodegeneration (Dawson and Dawson, 2003).

αS has been unequivocally linked to PD due to the discovery of genetic mutations. Three different missense mutations in the *αS* gene result in early onset PD (A30P, E46K and A53T), and additionally, a locus triplication causing an increased dosage of the *wild type* (*wt*) *αS* gene potentiates the disease (Polymeropoulos et al., 1997; Kruger et al., 1998; Singleton et al., 2003; Zarranz et al., 2004). The role of αS in the formation of Lewy bodies and the pathogenesis of PD has been compared to the role of Aβ peptide and amyloid plaques in Alzheimer's disease.

The appealing hypothesis for Lewy body formation is that αS monomers combine to form oligomers (or protofibrils), which coalesce into fibrils and then co-aggregate with other proteins into Lewy body inclusions (Conway et al., 1998; Wood et al., 1999). While the

monomers and oligomers of αS are soluble, the fibrils and Lewy bodies are insoluble in the neuronal cytoplasm. Some controversy arises from the roles of the various physical forms of αS in PD pathogenesis. LBs have been proposed to be both neurotoxic (El-Agnaf et al., 1998; Giasson and Lee, 2001), and protective (Rochet et al., 2000; Mouradian, 2002). Other hypotheses state that the protofibrilar intermediates, made of αS oligomers, are the main species toxic to dopaminergic neurons (Conway et al., 2000). Lansbury and co-workers have recently shown that αS protofibrils can form elliptical or circular amyloid pores in cell membranes (Lashuel et al., 2002b; Volles and Lansbury, 2002), and cell culture studies found that they reduce cell viability, disrupt lysosomes and induce Golgi fragmentation (Stefanis et al., 2001; Gosavi et al., 2002). In line with these findings, the A30P and A53T mutants of αS share an increased tendency to form soluble oligomeric intermediates, whereas the E46K and A53T mutants fibrillate faster than the *wt* protein (Conway et al., 2000; Choi et al., 2004).

Other important genetic mutations suggest the involvement of UPS in PD, and major interest arouse with the identification of mutations in the E3 ubiquitin ligase Parkin as a cause of autosomal recessive PD (Kitada et al., 1998). Both the loss of E3 activity and the possibility of incomplete or aberrant ubiquitination are proposed as causes of Parkin-related PD (Giasson and Lee, 2003). A second member of the UPS involved in PD is the Ubiquitin Carboxy-Terminal Hydrolase-L1 (UCH-L1), and mutations in the *uch-l1* gene cause dysfunction of this enzyme and lead to accumulation of toxic products (Leroy et al., 1998).

The shared symptoms of PD associated with the different genetic mutations raises the possibility of a molecular intersection in the pathogenic mechanisms driven by both protein degradation and aggregation. One plausible mechanism would involve αS mutations populating abnormal protein conformations and overwhelming the cellular protein degradation systems, whereas mutations in the UPS machinery would challenge the cell's ability to detect and degrade misfolded proteins that can result in the formation of toxic early aggregates (McNaught et al., 2002) . The common outcome of this failure at different levels is thus expected to be a cellular buildup of such unwanted toxic species that should have been cleared in healthy conditions. Minimal defects in the crucial protein turnover machinery may suffice to cause a slow demise of dopaminergic neurons, which may explain the relentless, progressive nature of the disease (Vila and Przedborski, 2003).

**1.3.2. The physiological role of α-Synuclein**

αS is member of a closely related group of brain-enriched proteins (αS, βS and γS) that have been implicated in neurodegenerative disorders and cancer, among others (Clayton and George, 1998). αS and βS are predominantly cytosolic proteins and co-localize in presynaptic nerve terminals, close to synaptic vesicles, while γS appears to be axonal and cytosolic (Buchman et al., 1998).

Despite the involvement of αS in neurodegenerative diseases, the normal biological function of this family of proteins is still unclear. Expression of both αS and βS is minimal in the embryonic rat brain, thus the function of synucleins is more relevant for the adult than for the developing nervous system (Clayton and George, 1999). They are related to presynaptic terminal function, although not being vesicle proteins, yet being able to influence vesicle fusion and membrane trafficking at the presynaptic terminal (Clayton and George, 1998). In particular, αS is proposed to regulate dopamine neurotransmission by modulation of vesicular dopamine storage (Lotharius and Brundin, 2002).

An overall role of αS on brain neurotransmitter function is still elusive, since the absence of αS in mice appears associated with only mild behavioral changes. Mice lacking αS show only subtle changes in dopamine-dependent behavior and are not impaired in spatial learning (Abeliovich et al., 2000; Chen et al., 2002). In addition, mice deficient in either αS or βS, or lacking both proteins are viable, fertile, and display no major phenotype (Chandra et al., 2004). Nevertheless, αS overexpression rescues lethality associated with the lack of CSPα, a co-chaperone (HSP40 kind) associated with synaptic vesicles and implicated in folding of SNARE proteins, suggesting that αS may act as an auxiliary chaperone preserving the function and integrity of the synapse (Chandra et al., 2005).

**1.3.3. The native unfolded state of α-synuclein**

αS is only 140 amino acid long and lacks a defined secondary structure in aqueous solution, populating random-coil conformations (Weinreb et al., 1996). Hence it belongs to the group of "natively unfolded" or "intrinsically disordered" proteins (Uversky et al., 2000). Three distinct regions are identified in the αS polypeptide sequence (Figure 1.5):

(i)     the N-terminal domain (residues 1–60), which is positively charged and contains five imperfect repeats of the highly conserved KTKEGV motif,

(ii)    the central NAC domain (residues 61–95), which is highly hydrophobic

(iii)     The C-terminal region (residues 96–140), which is very acidic, containing 10 Glu, 5 Asp and 5 Pro residues.
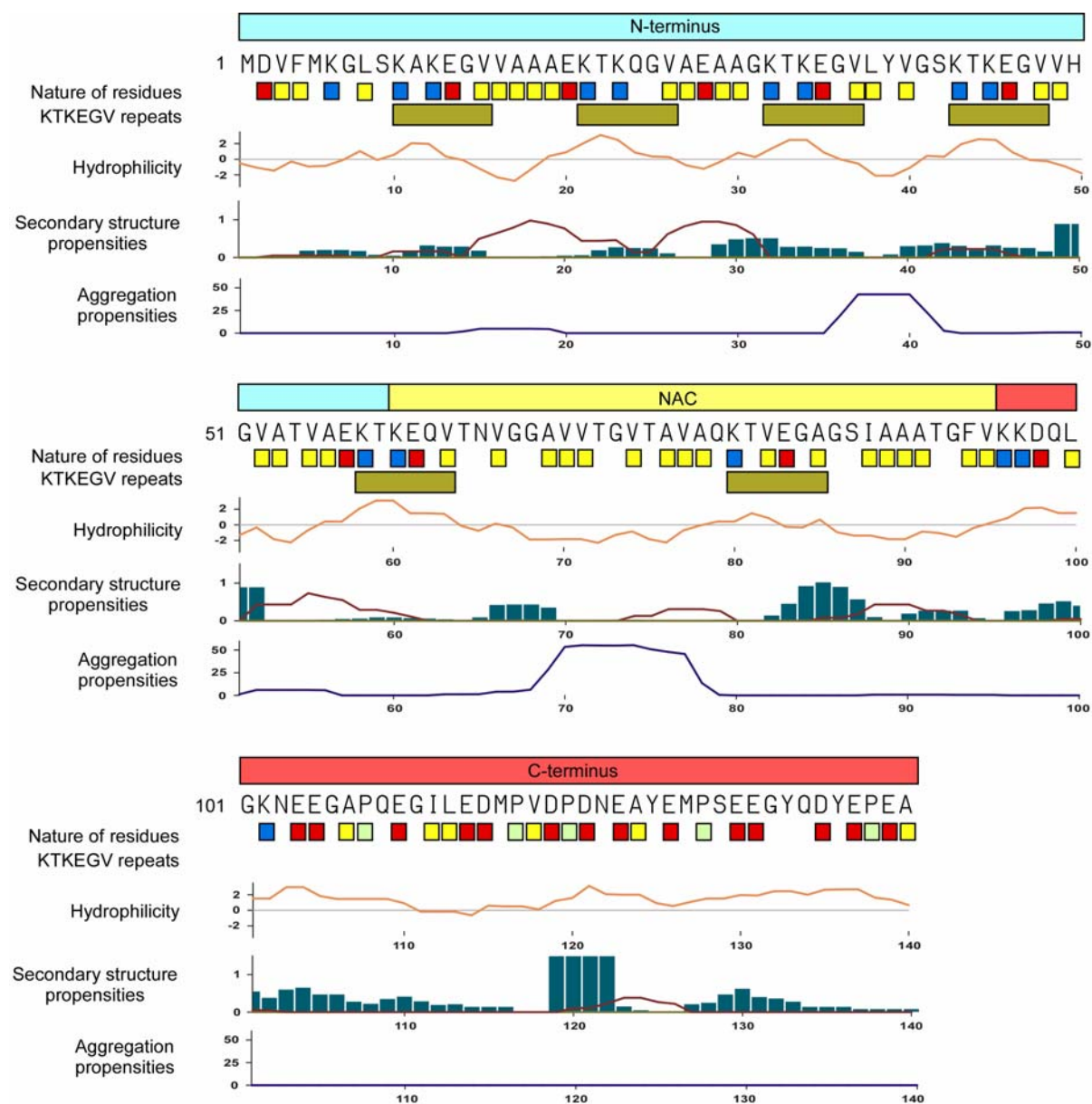


**Figure 1.5. Structural features associated with the primary sequence of αS.** From top to bottom: Domain organization (N-terminus, NAC and C-terminus) and amino acid sequence of αS. Nature of residues colored as follows: blue (+), red (-), yellow (hydrophobic), light blue (Pro). Hydrophilicity plot (Kyte-Doolitle) calculated with a 9 residue window. Secondary structure propensity calculated using TANGO (red line α-helix, green line β-sheet, blue bars β-turns). Aggregation propensity according to TANGO (Fernandez-Escamilla et al., 2004).

Due to the despair nature of its constitutive residues, each region on αS displays a different feature associated with the disease-state. The N-terminus and the NAC region, up to residue 87, increase in α-helical structure upon association with lipid vesicles, adopting a

broken amphypatic helix, important for the physiological state of the protein (Davidson et al., 1998; Jensen et al., 1998; Jo et al., 2000; Narayanan and Scarlata, 2001; Bussell and Eliezer, 2003; Chandra et al., 2003; Ulmer and Bax, 2005; Ulmer et al., 2005). The NAC region, due to its hydrophobic nature is proposed to initiate aggregation, and indeed includes a 12 residue stretch essential for fibril formation (Giasson et al., 2001). The C-terminus of the protein is responsible for the high thermostability of the protein and is essential for the chaperone function of αS by serving as a solubilizing domain (Kim et al., 2000; Souza et al., 2000; Kim et al., 2002; Park et al., 2002b; Park et al., 2002a). Upon αS binding to lipids the C-terminus remains disordered and does not interact with the micelles (Bussell et al., 2005; Ulmer et al., 2005). Moreover, it regulates aggregation of αS since C-terminally truncated fragments are found to aggregate faster than the full-length protein (Crowther et al., 1998; Serpell et al., 2000; Murray et al., 2003). This later finding correlates with recent evidence from PD patients, in whom a C-terminal truncated αS was isolated from brain-deposited fibrilar material (Li et al., 2005).

### 1.3.4. Ligand induced aggregation of α-synuclein

The idea that early steps in neuronal damage by PD are governed by the oligomerization of αS is leading a number of groups to identify factors that induce a conformational change in the αS molecule. Protein and other ligand-induced conformational changes on the native conformation of the polypeptide chain might have dramatic effects on its ability to interact with itself.

Indeed, various molecules and solution conditions of manifold chemical nature have been shown to accelerate αS aggregation such as low pH, increased temperature (Uversky et al., 2001b), certain metal cations (Uversky et al., 2001c), pesticides (Uversky et al., 2001a), oxidized catecholamines (Conway et al., 2001), phospholipid vesicles, detergents and organic solvents (Perrin et al., 2000; Perrin et al., 2001). The aggregation promoting effects are suggested to be caused by a preferential population of a partially folded αS conformation which constitutes a critical intermediate on the aggregation pathway (Uversky et al., 2001b).

### 1.3.5. Polycation-induced α-synuclein fibrillation

The transitions of monomeric αS toward oligomeric amyloid structures have been extensively investigated in the laboratory where this thesis work was carried out. The diversity of aggregate morphology upon variation in solution conditions was studied employing different spectroscopy and microscopy techniques. It was found that upon pH

decrease from 7.0 to 4.0 or upon addition of polycations, fibril networks and amorphous aggregates are observed. Those aggregates retain characteristics of amyloid and presumably share a common nucleation event with the ordered fibrilar structures (Hoyer et al., 2002). The impact of the C-terminal region on the aggregation kinetics was assessed by comparing the full length with C-terminally truncated αS under solution conditions affecting the C-terminal charge state. The solution dependence of aggregate morphology was attributed to charge shielding at the C-terminal region comprising the amino acids 109-140 (Hoyer et al., 2004). Moreover, the modulatory effect of solution conditions on A30P and A53T disease-related mutants of αS was investigated. The aggregation kinetics of wild-type αS, A30P, and A53T were modulated differently by changes of the solution conditions, suggesting long range interactions between the C-terminus with the central and N-terminal parts of the protein (Hoyer et al., 2004).

In addition to the above-mentioned conditions, work performed by our group recently demonstrated that natural polyamines promote the aggregation of αS (Antony et al., 2003). Polyamines are cellular stabilizers of nucleic acids and membranes, being essential for growth and differentiation. In the central nervous system, they mediate channel and receptor gating, immune responses to infection (Soulet and Rivest, 2003) and are involved in neurodegenerative disorders as AD (Morrison and Kish, 1995). At high intracellular levels spermidine and spermine are toxic (Auvinen et al., 1992); they are significantly elevated in the red blood cells of AD and PD patients (Gomes-Trolin et al., 2002) and can produce oxidative intermediates during polyamine retro-conversion. For these reasons, it was postulated that at physiological concentrations and in a cellular context these natural compounds may modulate the propensity of αS to form fibrils, thereby playing a significant role in the formation of cytotoxic aggregates (Antony et al., 2003).
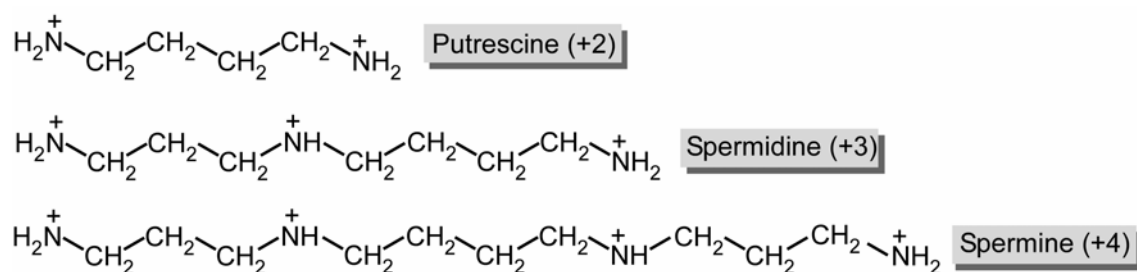


**Figure 1.6. Structure of natural polyamines accelerating αS aggregation.** The polyamines studied on this thesis work are depicted, whereas the net charge at neutral pH is consigned.

The binding site of polyamines to αS was determined by high resolution Nuclear Magnetic Resonance (NMR), and chemical shift perturbations were detected on a defined region at the C-terminal domain of the protein (Fernandez et al., 2004). This report constitutes the first evidence that residue-specific changes in this domain are linked to the acceleration of fibrillation, and is in line with previously mentioned housekeeping effect that the C-terminus has on the aggregation of αS. Binding constants were determined for the association of the different polycations to the protein, and ranged from 0.6 mM (Spermine) to 10 mM (Putrescine).

It was hypothesized that binding of polyamines might modulate structural and dynamic properties of the free protein and thereby influence intermolecular interactions required for the aggregation process. In the unliganded native conformation, the dynamic C-terminal domain could block the self-aggregating domain(s), assigned by many studies to the central core of the molecule, and C-terminal modifications such as charge neutralization by polyamine binding would release the self-aggregating domain and promote its transition to a β-sheet conformation. Further evidence supporting these findings is provided by intensity changes of the signals belonging to this domain upon polyamine binding (Fernandez et al., 2004), and by our own studies showing that C-terminally truncated αS aggregates much faster than the *wt* protein (Hoyer et al., 2004).
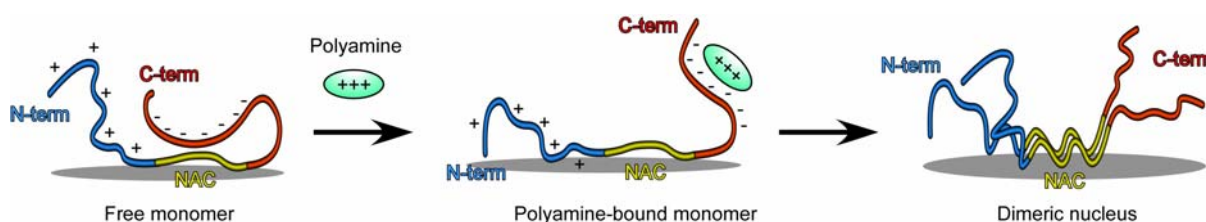


**Figure 1.7. Biochemical cartoon model for the polyamine-induced aggregation of αS.** The unliganded monomer is auto-inhibited for aggregation due to interactions between the NAC region and the C-terminus. Upon polyamine binding the C-terminus shielding effect is removed and the protein readily dimerizes, nucleating the aggregation process. Adapted from Hoyer et al. (Hoyer et al., 2004).

The αS-polyamine system is very suitable for study since (i) it is physiologically relevant to the pathogenesis of PD; (ii) it allows characterization of the early transitions that lead to αS fibrillation; (iii) the liganded protein is still soluble and do not readily associate at low temperature, permitting high resolution structural studies to be performed; and (iv) the charge-dependent effect on the binding affinity for the different polyamines allows a comparative assessment of the structural perturbations.

### 1.3.6. Metal induced α-synuclein fibrillation

Metal cations have been frequently recognized as risk factors in neurodegenerative disorders (Sayre et al., 1999; Bush, 2000). Brain lesions associated with Alzheimer's disease are rich in Fe(III), Zn(II) and Cu(II) (Lovell et al., 1998). Recent biophysical and structural studies of the amyloid precursor protein (APP) and the amyloid-β peptide (Aβ) have provided strong evidence linking Cu(II) with AD (Atwood et al., 1998; Huang et al., 1999; Bush et al., 2003; Brown and Kozlowski, 2004). Furthermore, a role for copper in prion disease has also been suggested and the interaction of Cu(II) with fragments of the prion protein (PrP) was structurally characterized (Viles et al., 1999; Aronoff-Spencer et al., 2000; Garnett and Viles, 2003; Brown and Kozlowski, 2004).

Although less well defined, the metallobiology of PD is attracting increasing attention. Iron deposits have been identified in Lewy bodies in the *substantia nigra* (Castellani et al., 2000) and elevated Cu(II) concentrations have been reported in the cerebrospinal fluid of PD patients (Pall et al., 1987). Based on this evidence, a role was suggested for copper and iron in the catalysis of oxidative oligomerization and subsequent aggregation of αS in the presence of hydrogen peroxide (Hashimoto et al., 1999; Paik et al., 2000).

A systematic analysis of the effect of various metal ions revealed that Al(III), Fe(III) and Cu(II) accelerate AS fibrillation *in vitro* (Uversky et al., 2001c) and another study showed that Cu(II) is the most effective ion in promoting αS oligomerization (Paik et al., 1999). The enhancement of fibrillation by metals has been attributed to Coulombic screening of charge-charge repulsion associated with the highly acidic C-terminal domain (Paik et al., 1999; Uversky et al., 2001c). Cu(II), Fe(II) and Mn(II) quench tyrosine fluorescence and are presumed to form stable metal-protein complexes with αS and cause a significant acceleration of αS fibril formation (Uversky et al., 2001c; Golts et al., 2002).

## 1.4. The unfolded state of proteins

As stated before, the unfolded state of a protein represents the starting conformation for the folding pathway, and partially or completely unfolded conformations are also key intermediates in amyloid formation. In addition, the proteins investigated in this thesis work are classified as natively unfolded proteins. It is thus instructive to comment at this point on the particular characteristics of this conformational state of the polypeptide chain.

### 1.4.1. Intrinsic conformational restrictions in the unfolded state

As originally defined by Tanford (Tanford, 1968), the conformations populated by an unfolded polypeptide chain are true random coils, retaining no element of their original native structure. Nevertheless, even in the most expanded unfolded protein sequence, local elements of the chain are held in proximity via the peptide bond, leading to the Flory isolated pair hypothesis (Flory, 1969), which states that in a random coil conformational restrictions do exist, but are limited to nearest neighbor interactions. However, it was recently suggested that systematic local steric effects can extend beyond nearest-chain neighbors and may restrict the size of accessible conformational space (Pappu et al., 2000). Shortle has recently restricted the definition of a random coil state of a polypeptide as the well defined reference (and perhaps ideal) state in which no sidechain-sidechain interactions occur (Shortle, 1996). Thus the characteristics of a random coil state of a protein will depend on the intrinsic molecular features of the amino acids that compose the particular polypeptide chain.

In a polypeptide chain the peptide bond is planar, and the main-chain trace of the backbone can be described in terms of peptide planes connecting the C$\alpha$ atoms. The relative orientation of two of these planes (i and i + 1) will be determined by the pair of torsion angles $\phi_i$ and $\psi_i$, defining the rotation about the bonds connecting the C$\alpha_i$ (Figure 1.8).
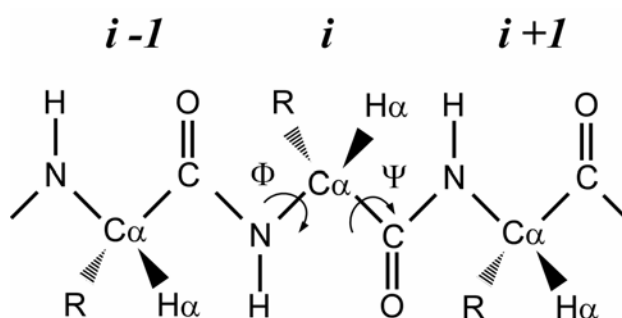


**Figure 1.8. A polypeptide chain.** Schematic diagram of a polypeptide chain showing the torsion angles f and y, which determine the backbone conformation.

The combination of φ and ψ angles for each of the amino acids composing the chain defines the specific conformation of the polypeptide backbone. Thus for proteins that retain a single structure, each residue populates a defined φ, ψ conformation, with small fluctuations, contrasting a random coil conformation, where there will be a distribution of φ, ψ angles for each residue, giving rise to an ensemble of conformers (Smith et al., 1996).

Ramachandran in the late 60´s observed that steric considerations in the backbone atoms are sufficient to restrict the permissible φ, ψ values for a given amino acid in a polypeptide chain, providing the basis for the description of conformational spaces for secondary structure formation in proteins (Ramachandran et al., 1963). The Ramachandran plot depicts the distribution of φ, ψ torsion angles that are evidenced in a polypeptide and relates those values with the adoption of helical or sheet backbone conformations (Figure 1.9). Thus the measurement of torsion angles for a given residue may, in general, report on the conformation in which a certain amino acid is embedded.



| Conformation | Φ | Ψ |
|---|---|---|
| α-helix | - 57 | - 47 |
| β-sheet parallel | - 119 | + 113 |
| β-sheet anti-parallel | - 139 | + 135 |
| Left α-helix | + 57 | + 47 |
| Poly-Pro II | -78 | + 149 |
| Beta turn | - 60 | + 120 |
| 3-10 helix | - 49 | -26 |
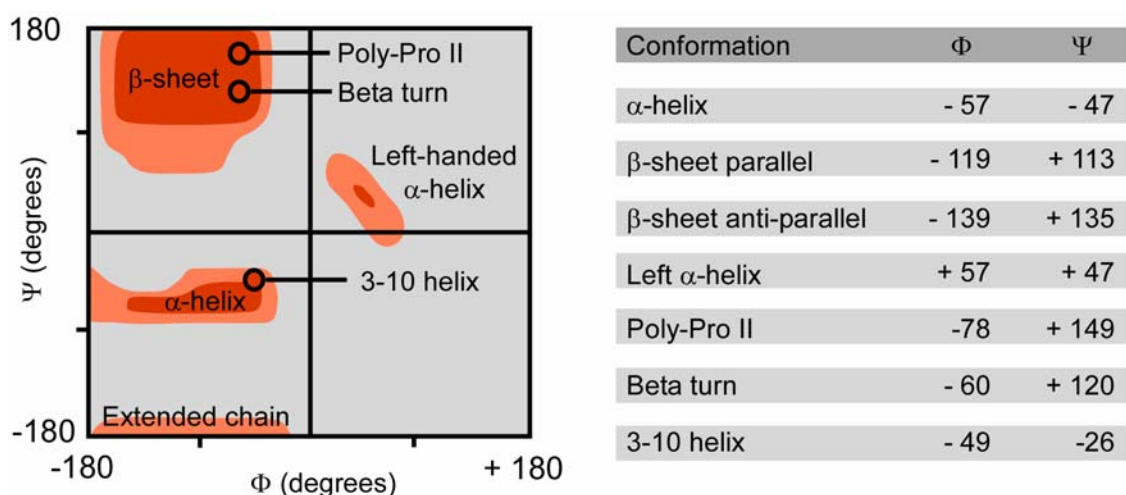
**Figure 1.9. Ramachandran plot and dihedral angles for secondary structure conformations in polypeptides.** Diagram of the φ, ψ torsion angles distribution for residues in a polypeptide chain. The average conformational parameters are consigned for each secondary structural element.

In the absence of secondary structure, the values of φ, ψ torsion angles for a given residue will not be correlated with the φ, ψ angles for all the other residues, and will exclusively report on the conformational space that the residue is sampling (Smith et al., 1996). A database analysis of residues in coil regions of known structures of proteins, i.e. residues not in α-helices and not in β-sheets, has determined the intrinsic residual preferences for amino acids, in the absence of interactions stabilizing secondary structural motifs. The striking conclusion from such studies is that the distribution of φ, ψ angles in coil regions of

proteins is far from random, with backbone angles heavily biased to those corresponding to α-helices and β-sheets. (Serrano, 1995; Swindells et al., 1995). Within this framework, specific residues have preferences for particular areas of conformational space, and these preferences are heavily influenced by neighboring residues (Griffiths-Jones et al., 1998). Nevertheless, the high population of α and β space predicted for residues in a random coil does not itself imply a persistent population of α-helices or β-sheets, since such population requires repeated values (at least five) of the appropriate $\phi$, $\psi$ dihedral angles along a given sequence (Smith et al., 1996). Questions remain, however, regarding the length scale over which the distribution of $\phi$, $\psi$ torsion angles becomes uncorrelated, giving rise to the concept of persistence length of the chain, which could define some sequence-local structure (McCarney et al., 2005).

### 1.4.2. Structural studies on the unfolded state of proteins

Investigation of non-native states of proteins is now possible through a wide variety of techniques, which provide information on global parameters, such as the radius of gyration or sedimentation coefficient, and on local properties of the chain, like the NMR-derived constraints (Table 1.2).

The concerted use of several of these techniques is necessary, due to the very flexible nature of the chain and to the absence of a defined conformation. Different properties of the polypeptide are probed by each of these methods which provide complementary information to characterize such dynamic state. However, in particular for the study of the denatured state of proteins, it has been difficult to reconcile the results arising from many of these methods. For example, the overall topology of the unfolded state fits the expected for a random coil polymer, deprived of conformational preferences, challenging fluorescence and NMR-derived parameters, which unequivocally show the presence of long-range and residual local structure (Smith et al., 1996; McCarney et al., 2005).

This scenario rise the important question as to what extent are the structures of unfolded proteins disordered. It also points towards how general are structural propensities in unfolded proteins, questioning whether they are sequence-specific or denaturant-induced (Baldwin, 2002). Recently, computer simulations on ensemble-averaged structural coil models have reconciled this view (Bernado et al., 2005b; Jha et al., 2005a). The presence of defined local backbone structure in unfolded proteins suggests that conformations populated under strong denaturing conditions are not as heterogeneous as previously supposed, with a

consequent reduction in the entropy of the unfolded state relative to predictions from the random coil model (Fitzkee and Rose, 2004).

| Technique | Information content |
|---|---|
| Ultracentrifugation | Sedimentation coefficient, shape. |
| Dynamic Light Scattering | Diffusion coefficient, hydrodynamic radio |
| X-ray, Neutron Scattering | Radius of gyration (small angle scattering) |
| Circular Dichroism | Secondary structure content |
| FTIR Spectroscopy | Secondary structure content |
| Raman Spectroscopy | Secondary structure content |
| EPR Spectroscopy | Local order, distances via couplings. |
| Fluorescence Spectroscopy | Denaturation by exposure of Trp residues or by binding of fluorescent dyes. Distribution of distances by FRET. Size changes by anisotropy. |
| NMR Spectroscopy | Hydrodynamic radio by pulse field gradient NMR. Secondary structure by backbone chemical shifts. Order parameters and fast backbone dynamics by $^{15}N$ and $^{13}C$ relaxation. Slow backbone dynamics and local structure by RDCs Long range distance information on the ensemble by paramagnetic spin labels. $\Phi$ / $\Psi$ angles via coupling constants and NOEs. Low populated states by relaxation dispersion. |

**Table 1.2. Methods to study conformational properties of the unfolded state of proteins.** Adapted from (Smith et al., 1996; Dyson and Wright, 2004).

A considerable body of data has been generated to date on the denatured state of proteins, providing structural details on the conformations that are particularly populated. The

most important characteristics of unfolded polypeptides can be summarized as follows: (i) the global dimensions of the denatured states of proteins exhibit the size dependence expected for self-avoiding random coil polymers, as measured by hydrodynamic methods and small angle X-ray scattering (SAXS); (ii) they possess very little residual secondary structure as probed by circular dichroism (CD), Fourier-transform infrared spectroscopy (FTIR), although Raman spectroscopy suggests the existence of some PII helical conformations, as is often supported by CD; (iii) the random coil behavior of the backbone is observed through NMR measurements of chemical shifts, though $\phi$ dihedral angles measured through $^3J_{HNH\alpha}$ couplings suggest preferential sampling of helical conformations, indicative of $\alpha$-helix or PII conformations; (iv) significant degrees of local residual structure are detected by NMR Residual Dipolar Couplings (RDCs), which probe the orientation of bond vectors relative to an alignment tensor fixed in the molecular frame; (v) the long range interactions and native-like topology are evidenced for some proteins, even at high denaturant concentration, detected by NMR Paramagnetic Relaxation enhancement (PREs) and single-molecule Förster resonance energy transfer (FRET); and (vi) the persistence of hydrophobic clusters could be probed by NMR relaxation or Trp fluorescence quenching.

### 1.4.3. Structural studies on α-synuclein

Intrinsically unstructured proteins have challenged the paradigm of the structure-function relationships in current biology since they are now recognized to play essential roles in transcription, translation and signal transduction pathways. A disorder-to-order transition induced in natively unfolded proteins during the binding of specific targets in vivo represents a simple mechanism for the regulation of numerous cellular processes (Dyson and Wright, 2005). The absence of defined structure allows disorder regions of proteins to attain functional plasticity in physiological states of cells but also represents an easy target for misfolding, leading often to disease conditions (Uversky, 2002).

High resolution structural studies of natively unfolded proteins are very difficult, since they can not be studied by means of crystallography or standard NMR spectroscopic techniques. It is only now, with the advent of higher field spectrometers and more powerful computer methods, that NMR spectroscopy is able to reveal the unfolded state of proteins at atomic resolution (Dyson and Wright, 2004).

A large variety of biophysical and biochemical methods has been applied for the structural description of these proteins, and αS is no exception. Briefly, αS has been studied using CD, intrinsic and extrinsic fluorescence, SAXS, light scattering, FTIR and

heteronuclear NMR (reviewed in (Uversky, 2003)). These data demonstrate that αS is essentially disordered but surprisingly adopts a more compact conformation that the one expected for a random coil configuration (Uversky et al., 2002). Nevertheless, previous NMR determinations were unable to provide evidence for structural constraints in αS, only suggesting a slight tendency of the N-terminal domain to adopt α-helical conformations (Eliezer et al., 2001). Changes in secondary structure are visible in the far-UV CD spectrum of αS, when the protein is exposed to conditions of high temperature or low pH, data that correlate with the increment of fibrillation. This conclusion led to the hypothesis that the process of αS fibrillation may be dramatically accelerated by the partial folding of the intrinsically unstructured protein, and suggests that this conformation is a key intermediate along the fibril-forming pathway (Uversky et al., 2001b). However, all these methods have failed to reveal information regarding the early structural transitions that take place on αS under fibrillation conditions.

Inasmuch as there is not structural model for the ensemble of conformers that αS populates, no information is available on the transitions that take place on the protein under conditions conductive to self-oligomerization. Such information is necessary to shed light into the mechanism of amyloid deposition and toxicity in PD, as it will be very valuable for the rational design of therapeutic agents.

# Aims of the Thesis

## 2. Aims of the thesis

The misfolding, oligomerization and amyloid formation of the small pre-synaptic protein αS are believed to be central to the development of neurodegenerative disorders as Parkinson´s disease (PD) and dementia with Lewy bodies. The mechanisms by which the innocuous, presumably natively unfolded, αS protein oligomerizes and forms neurotoxic species are yet elusive, mainly due to the conformational flexibility inherent to this kind of proteins.

Since PD is primarily a sporadic disease, and αS is an abundant protein in the neuronal cytoplasm of healthy individuals, it is believed that a conformational change has to occur in the protein in order to trigger its oligomerization. The hypothesis of this thesis work was that, although devoid of secondary structure, the ensemble of conformations that αS populates may account for long-range interactions which aid the protein to remain soluble and avoid aggregation. Thus we have sought to employ high resolution NMR to determine the presence of contacts between different domains of the polypeptide chain in the native state of the protein. In addition, the study of the protein under aggregation prone states, namely binding of polyamines or transition metals, high temperature, or presence of genetic mutations, would provide information on the early structural transitions that render αS oligomerization.

The results obtained in this study are divided in 4 chapters. The first chapter describes that αS is not a true random coil and rather populates compact conformations which account for long range interactions. We report the application of a set of NMR-based experiments optimized for the study of unfolded states of polypeptides, which provide residue-specific information on the structure and dynamics of the ensemble of conformations that αS adopts in solution. We further prove that these long range interactions are impaired upon chemical denaturation of the protein or upon binding of polycations or increase of temperature.

Chapter 2 describes the application of the above mentioned set of experiments to two mutants of αS linked to early-onset PD. We show that long range contacts are altered in the A30P and the A53T αS mutants and that these proteins populate destabilized conformations and easily overcome the energetic barrier for self association.

A comprehensive NMR-based characterization of the homologous protein βS is provided in chapter 3. This protein, a member of the synuclein family of proteins, does not aggregate and is proposed to inhibit αS neurotoxicity. We assigned the backbone resonances of βS and studied the conformations populated by this natively unfolded protein. We show

the absence of long range interactions in βS and identify regions with a particular tendency to adopt conformations rich in residual structure.

In chapter 4 the formation of complexes between αS and transitions metals, known from epidemiological studies to increase the risk of neurodegeneration, is systematically studied. We report that the only divalent metal ion which significantly interact with αS at physiological conditions is Cu(II), and show that it binds to the N-terminal domain of the protein. Based on different low and high resolution spectroscopic techniques we propose a common link between Cu(II) binding to αS and the formation of Cu(II) complexes in other amyloid proteins.

A final summarizing discussion provides evidence for the origin of the long-range interactions in the native state of αS and suggests that conformational restrictions in αS arise in the ns to μs timescale, only probed successfully by our experimental setup. The biological significance of our findings is discussed herein and the implications for the design of wide-ranging anti-αS oligomerization drugs are further commented.

In the Appendix, the set up of a variety of fluorescence-based techniques to study αS is shown. Lifetime and time-resolved anisotropy measurements were taken on fluorescently labeled αS and βS proteins, and information on the local motions of the polypeptide chain was obtained. The data, although preliminary, is complementary to the main results of this thesis, and represent the first steps towards the characterization of the aggregation mechanism of αS by means of intrinsic fluorescence probes.

# Materials and Methods

## 3. Materials and methods.

### 3.1 Materials.

#### 3.1.1. Equipment.

| | |
|---|---|
| - Bench top centrifuge | Eppendorf mini spin plus |
| - Centrifuge | Beckman Avanti J-25 |
| - Ultracentrifuge | Beckman TL-100 |
| - Thermocycler | Thermo Hybaid PCR Express |
| - Incubation shaker cabinet | B. Braun Biotech Centromat *IS* |
| - Perfussion chromatography workstation | Applied Biosystems Biocad 700 E |
| - UV-Vis spectrophotometer | Cary 100 Scan |
| - UV-Vis CD spectrophotometer | Jasco J-720 |
| - Fluorescence spectrophotometer | Varian Cary Eclipse |
| - Protein electrophoresis chamber | Invitrogen X-SureLockII |
| - EPR spectrometer | Varian Century-Line 9-GHz |
| - NMR spectrometers | Bruker DRX 600 MHz, triple axis gradient |
| | Bruker Avance 600 MHz, with cryoprobe, z-axis gradient |
| | Bruker Avance 700 MHz, triple axis gradient |
| | Bruker DRX 800 MHz, triple axis gradient |
| | Bruker Avance 900 MHz, with cryoprobe, z-axis gradient |
| - Electron microscope | Philips CM12 |

#### 3.1.2. Bacterial strains.

- *Escherichia coli DH5α.* F⁻, *end*A1, *hsd*R17 ($r_k^-$ $m_k^-$), *sup*E44, *thi*1, *rec*A1, *gyr*A(Nal$^r$), *rel*A1, Δ(*lac*ZYA-*arg*F)U169, φ80-d *lac*ZΔM15.

- *Escherichia coli BL21 (DE 3).* F-, *omp*T, *hsd*Sβ(rβ-mβ-), *dcm*, *gal*, (DE3) tonA.

### 3.1.3. Reagents.

During the development of the present thesis work the following reagents from the mentioned suppliers were employed:

Restriction enzymes and buffers used for digestion of DNA were from NEB, while the site directed mutagenesis kit was from Stratagene. Primers were synthesized by Metabion, Martinsried Germany. Agarose gels (1.5 %) were prepared with agarose (Gibco, Invitrogen) dissolved in 1 x TBE buffer (Roth, Karlsruhe, Germany) and supplemented with 1 μg/ml ethidium bromide (Merck, Darmstadt, Germany).

SDS-Polyacrylamide gel electrophoresis was performed with buffers (SDS-MES), pre-cast ready-to-use gels (10 % and 12%) and Coomasie stain (Simply Blue safe stain) from Invitrogen, following instructions from the supplier.

For NMR measurements, $^{15}NH_4Cl$, $^{13}C$-D-glucose and $D_2O$ were purchased from Cambridge isotope laboratories, Andover, MA. The paramagnetic nitroxide spin label MTSL (1-oxy-2,2,5,5-tetramethyl-D-pyrroline-3-methyl)-methanethiosulfonate was from Toronto Research Chemicals, Toronto, Canada. The phages solution employed for the alignment of proteins was Pf1 from Asla, Riga, Latvia, and the liquid crystal phase employed for alignment were prepared with *n*-octyl-penta(ethylene glycol) ($C_8E_5$) and octanol, or with *n*-dodecyl-penta(ethylene glycol) ($C_{12}E_5$) and hexanol, all from Sigma.

The natural polyamines spermine, spermidine and putrescine were from Sigma and Fluka, while urea and guanidinium hydrochloride were from Sigma.

The salts employed for the studies with metal ions were $CuSO_4$, $NiSO_4$, $MnCl_2$, $CoCl_2$, and $FeCl_2$, of the highest purity available, form Merck or Sigma. The reagents employed for quantization of the metals in solution were 4-(2-pyridylazo)resorcinol (PAR), Fura-2 pentapotassium salt and 1,10-Phenanthroline, and were purchased from Sigma, Molecular Probes (Invitrogen) and Fluka (Sigma), respectively.

### 3.2. Methods.

### 3.2.1. Molecular biology.

All molecular biology experiments described here were performed at the Department of Molecular Biology, MPI-BPC.

### 3.2.1.1. αS-containing plasmids.

The coding sequences for wild type (*wt*) human αS and the two genetic mutants A30P and

A53T were kindly provided by Dr. Peter Lansbury, Harvard Medical School, Cambridge, MA. All the three constructs were cloned *NdeI/EcoR*I in the plasmid PT7.7 (Tabor, 1990), under the strong promoter T7.

The construction of the C-terminal deletion of αS (αS1-108) was already reported elsewhere (Hoyer et al., 2004).

### 3.2.1.2. βS-containing plasmids.

The cDNA sequence of human βS was isolated from a cDNA sample obtained from RT-PCR of total mRNA from human brain (a kind gift from Dr. L. Pardo, MPI-EM, Göttingen), via PCR using the specific primers βS-*wt*-Fwd and βS-*wt*-Rev, containing *Nde*I and *Hind*III restriction sites for cloning (Figure 3.1). The amplified product was ligated in the plasmid pT7-7 employing *Nde*I/*Hind*III sites and transformed into *E. coli* DH5α. The nature of the DNA cloned product was validated by DNA sequencing.
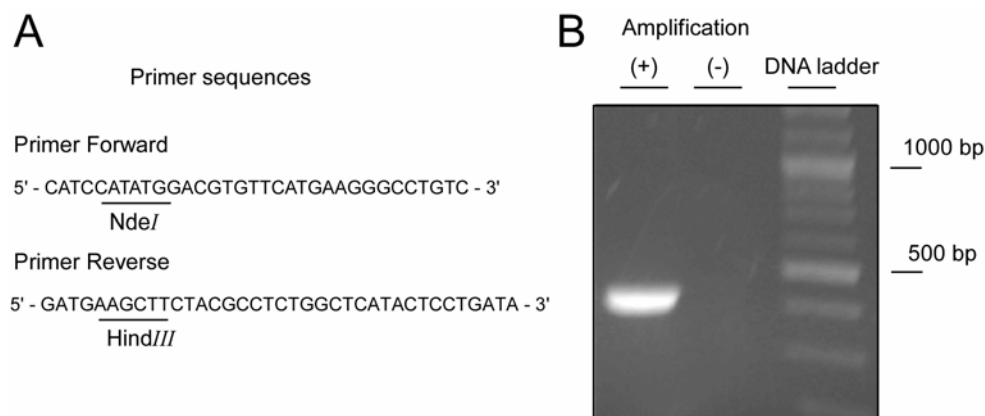


**Figure 3.1. Amplification of the cDNA coding for βS. A**. Primers used for amplification of βS cDNA. **B**. 1.5% agarose gel showing successful PCR-based amplification of βS DNA on the sample using as template cDNA derived from coding mRNA (+). Negative control shows no amplification on the sample using cDNA derived form non coding mRNA (-) as template.

### 3.2.1.3. Construction of αS and βS Cys-containing mutants.

In order to provide an attachment site for the nitroxide spin label employed in PRE studies, three different αS cysteine-containing mutants Ala[18]Cys (A18C), Ala[90]Cys (A90C), and Ala[140]Cys (A140C) were constructed on the *wt*, A30P and A53T protein using the Quick-Change site directed mutagenesis kit (Stratagene, La Jolla, CA) and following the manufacturer's protocol. Briefly, for each mutant two complementary 20-30 bp DNA primers are designed, containing the point mutation in the center of the primer plus long (~ 12 basis) flanking sequences on both 5′and 3′directions. These 5′and 3′ branches are complementary

to the sequence flanking the site of the mutation, allowing the annealing of the primers to the *wt* DNA (parental).

| | |
|---|---|
| αS-A18C F | 5′-gggagttgtggcttgtgctgagaaaaccaaacaggg-3′ |
| αS-A18C R | 5′-ccctgtttggttttctcagcacaagccacaactccc-3′ |
| αS-A90C F | 5′-gcagggagcattgcatgtgccactggctttgtc-3′ |
| αS-A90C R | 5′-gacaaagccagtggcacatgcaatgctccctgc-3′ |
| αS-A140C F | 5′-caagactacgaacctgaatgctaagaaatatctttgctcc-3′ |
| αS-A140C R | 5′-ggagcaaacatatttcttagcattcaggttcgtagtcttg-3′ |
| βS-A18C F | 5′-gagggcgttgtggcatgcgcggagaaaaccaag-3′ |
| βS-A18C R | 5′-cttggttttctccgcgcatgccacaacgccctc-3′ |
| βS-A79C F | 5′-gcagggaacatcgcatgcgccacaggactggtg-3′ |
| βS-A79C R | 5′-caccagtcctgtggcgcatgcgatgttccctgc-3′ |

**Table 3.1. DNA primers employed for the construction of Cys-containing mutants.** Sequence of DNA primers forward (F) and reverse (R) employed for the construction of the Cys-containing mutants in αS and βS. The combination of primers used in *wt* αS was further employed for the construction of the same substitution mutants in A30P and A53T αS.

The PCR is carried out with sense and antisense primers in the same reaction tube, each of them promoting the full-length amplification of the two strands of the DNA plasmid. After the amplification, two populations of DNA are found, the parental circular DNA, which does not contain the mutation, and the amplified linear DNA which harbors the substitution. The parental, *wt*, DNA is selectively degraded by addition of the enzyme *Dpn*I, an exonuclease recognizing methylated DNA (only the one synthesized in bacteria). The amplified mutant DNA is then transfected into chemically competent bacteria (DH5α), which recognize the DNA as a plasmid and catalyse both the circularization and synthesis of the complementary strand. Successful transformation is determined by the selection marker of the vector, ampicilline resistance. Ten transformants are selected for screening and plasmid DNA is obtained through a small scale preparative procedure (miniprep). Incorporation of the desired modifications are afterwards verified by DNA sequencing. The rate of success of the methodology was greater than 80 % in all the cases. Once sequenced, plasmids are transfected into *E. coli* BL21(DE3) in order to achieve a high level of protein expression.

The cysteine-replacements on βS mirror the ones employed for αS studies, and were selected to report long range interactions on the protein. The Ala$^{18}$Cys (A18C) and Ala$^{79}$Cys (A79C) βS cysteine-containing mutants were constructed using the same protocol as for αS

mutants. The primers employed are described on table 1. The introduced modifications were further verified by DNA sequencing.

### 3.2.2. Protein biochemistry

All experiments described in this section were performed at the Department of Molecular Biology, MPI-BPC.

### 3.2.2.1. Expression and purification of αS and βS.

The same protocol was applied for purification of all the αS variants, as well as for βS production. Following transformation, *E. coli* BL 21 cells were grown overnight in 10 ml of LB medium containing 100μg/ml ampicillin. The pre-culture was diluted (10 ml in 1 l LB containing 100 μg/ml ampicillin) and allowed to grow at 37°C until an O.D of 0.6-0.8. Expression of the desired gene construct was then induced with 1 mM IPTG (Roth, Karlsruhe, Germany). Cells were then harvested, after 3-4 hours of incubation at 37 ºC, by centrifugation at 3000 x g for 10 minutes.

The bacterial pellet was resuspended in 10 ml of 10 mM Tris-HCl, pH 8.0, 1 mM EDTA and 1 mM PMSF, and lysed by multiple freeze-thaw cycles and sonication. The cell lysate was boiled for 20 minutes and centrifuged at 20000 x g (30 minutes at 4 °C), in order to precipitate the heat-sensitive proteins (synucleins remain soluble). Streptomycin sulphate (Sigma) was added to the supernatant from the previous step (final concentration 10 mg/ml) for precipitation of DNA. The mixture was stirred at 4 °C for 15 minutes, followed by centrifugation at 20000 g (30 minutes at 4 °C). The synuclein protein (αS or βS) was then precipitated by addition of ammonium sulphate (Merck, Darmstadt, Germany) (361 mg/ml) to the supernatant from previous centrifugation. The solution was stirred at 4°C for 15 minutes and centrifuged once again at 20000 x g (30 minutes at 4 °C).

The protein pellet was resuspended in 20 ml of 25 mM Tris-HCl, pH 7.7, and loaded onto a POROS HQ/M anion exchange column (PerSeptive Biosystems, Cambridge, MA) in a Biocad 700E perfusion chromatography workstation (Applied Biosystems, Foster City, CA), equilibrated with 25 mM Tris-HCl, pH 7.7. Full length αS and βS proteins were eluted with a salt gradient at ~ 300 μM NaCl. The C-terminal truncated mutant of αS was eluted in the flow trough, since lacking the acidic C-terminus impaired ability of the protein to bind to the column. The fractions containing protein (determined spectrophotometrically) were pooled together and concentrated using Centriprep YM-10 filter devices (10000 Da molecular weight cut off) (Amicon, Bedford, MA) to a final concentration of ~ 300 mM. Concentrated

proteins were dialyzed overnight against the desired buffer (buffer A, 25 mM Tris-HCl, pH 7.4, 100 mM NaCl or buffer B, 20 mM MES, pH 6.5, 100mM). Purity of the protein was assessed by SDS-PAGE and the concentration was determined with absorbance at 275 nm using an extinction coefficient of 5600 $M^{-1}$ $cm^{-1}$, for the full length proteins, or 1460 $M^{-1}$ $cm^{-1}$ for the C-terminally truncated. Proteins were aliquoted, flash frozen in liquid $N_2$ and stored at -80 °C.

Purification of Cys-containing mutants was performed similarly to *wt* proteins but 1 mM dithiothreitol (DTT) (Roth, Karlsruhe, Germany) was included throughout the different purification steps in order to avoid Cys oxidation and disulfide-linked dimer formation.

Preparation of $^{15}$N- and $^{13}$C/$^{15}$N labelled proteins was carried out exactly as for the non-labelled proteins with the only difference that LB medium was replaced by M9 minimal medium supplemented with $^{15}$NH$_4$Cl or $^{15}$NH$_4$Cl and $^{13}$C-D-glucose (Cambridge Isotope Laboratories, Andover, MA). A 5x stock solution of M9 salts, with the absence of NH$_4$Cl, was prepared adding 64 g Na$_2$HPO$_4$-7H$_2$O (Sigma), 15 g KH$_2$PO$_4$ (Sigma), 2.5 g NaCl (Sigma), adding water to a final volume of 1 l and autoclaving. For 500 ml of final culture media 100 ml of M9 5x stock salt solution are mixed with 1 ml of 1M MgSO$_4$, 50 µL of 1 M CaCl$_2$, 0.5 g of $^{15}$NH$_4$Cl, 10 ml of 20 % D-glucose ($^{13}$C-D-glucose for double labelled proteins) and autoclaved H$_2$O to a final volume of 500 ml. The pH of the solution was adjusted to 7.3 and the media was filter-sterilized (0.2 µm filter). Previous to culture, 100 µg/ml of ampicillin were added.
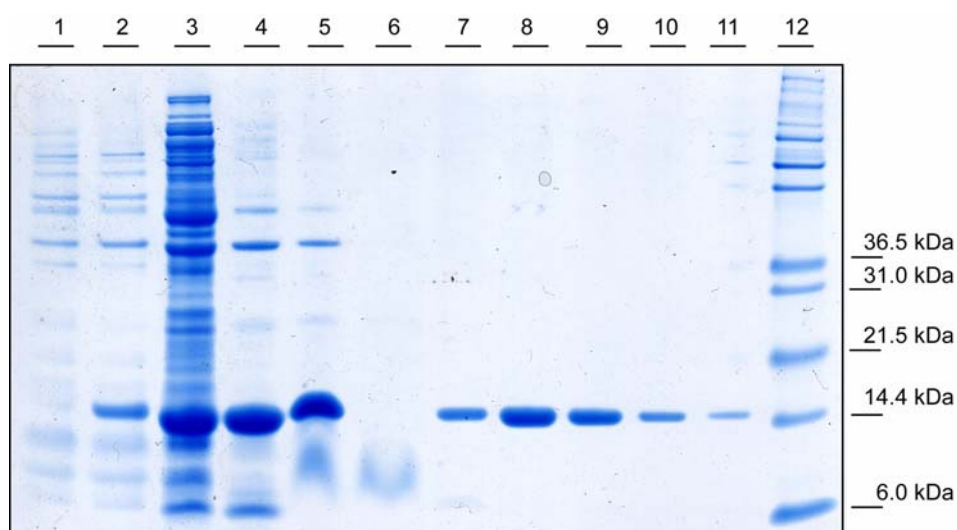


**Figure 3.2. Expression and purification of βS in *E.Coli*.** SDS-PAGE following the outcome of the set up protocol for purifying recombinant human βS from *E. coli*. Lane 1, total protein extract from un-induced cells. Lane 2, total protein extract from IPTG-induced cells. Lane 3, total protein extract following sonication. Lane 4,

soluble protein fraction after boiling and centrifugation. Lane 5, soluble protein after precipitation of DNA with streptomycin sulphate. Lane 6, protein remaining in the supernatant following ammonium sulphate precipitation. Lane 7 to 11, fractions eluted from the anion exchange column (eluates 4, 8, 11, 14 and 16. Lane 12, molecular weight marker.

### 3.2.2.2. Synthesis of C-terminal peptides of αS.

The C-terminal αS peptides were kindly synthesized by Kerstin Overkamp at the Department of NMR-based Structural Biology, MPI-BPC. Peptides comprising residues 105 to 136 and 95 to 136 of *wt* αS were synthesized employing standard solid-phase Fmoc chemistry. The peptides were purified by semipreparative reverse phase HPLC and the purity (>95%) were analyzed by mass spectrometry.

### 3.2.2.3. Spin-labelling of proteins.

Studies of paramagnetic relaxation enhancement by nitroxide spin labels involve the site-directed addition of a nitroxide radical in the evaluated position of the protein. An easy procedure to achieve such a task is to engineer a Cys replacement in the residue that is investigated, with the condition that this one is the only Cys amino acid present in the protein. Thus, a methanethiosulfonate-based nitroxide spin label can be efficiently coupled to the reduced sulfhydryl of the cysteine under physiological buffer conditions.
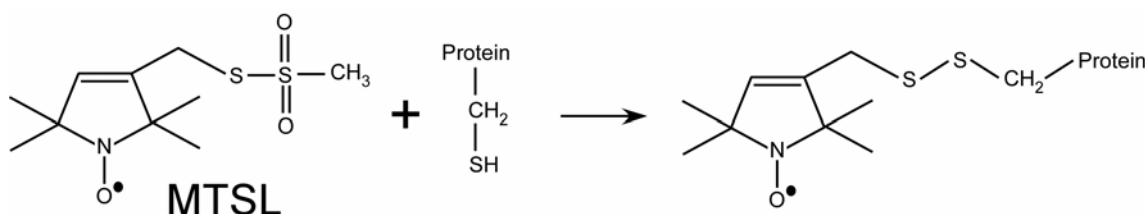


**Figure 3.3. Reaction of the nitroxide-maleimide MTSL with a Cys residue in the target protein.** Chemical structure of the spin label reagent MTSL and the disulfide bond adduct formed with the side-chain of the single Cys residue in the protein.

The reaction of αS and βS Cys-containing mutants with the nitroxide spin label MTSL (1-oxy-2,2,5,5-tetramethyl-D-pyrroline-3-methyl)-methanethiosulfonate was carried out essentially as described in Der-Sarkissian et al. (Der-Sarkissian et al., 2003) with some modifications. Briefly, DTT was removed prior to labelling from the buffer using Sephadex-G25 fast desalting columns (PD-10 columns, Amersham Biosciences) and the proteins were equilibrated in 20 mM Tris-HCl, pH 7.4, 100 mM NaCl (or 20 mM MES, pH 6.5, 100 mM NaCl). Free sulfhydryl groups were reacted with a 5-fold molar excess of the MTSL-

maleimide regent solubilized in acetone, at 4 °C for 16 h, in the dark. Unreacted spin label was removed using PD-10 columns and spin-labeled proteins were concentrated using Microcon YM-3 filter devices (3000 Da molecular weight cut off) (Amicon, Bedford, MA). Complete labelling with the nitroxide radical was verified by mass spectrometry or reaction with DTNB to measure unreacted sulfhydrils. Proteins were aliquoted, fast frozen in liquid $N_2$ and stored at -80 °C

Importantly, all the buffers employed through the labelling procedure were de-gased under $N_2$ in order to avoid the presence of oxygen which readily oxidizes the free sulfhydryl of the Cys residue.

### 3.2.2.4. Alignment of αS in anisotropic media.

Residual dipolar couplings are orientational restraints that report on the degree of orientation of a $^{15}N$-$^1H$ or $^{13}C$-$^1H$ bond respect a molecular alignment tensor. In order to observe non vanishing RDCs the solution in which the protein is dissolved has to be slightly anisotropic, causing all orientations of the protein not to be equally probable (Bax, 2003). Thus RDCs are measurable in solution conditions in which a relatively small population of molecules adopts a net orientation with respect to the externally applied magnetic field. In solution this is possible when the protein experience an asymmetric environment, such as in the presence of liquid crystals. Under such circumstances, a protein will tumble anisotropically, preventing the one-bond internuclear dipoles average to zero. The RDC signal will depend on the degree of asymmetry of the anisotropic environment, and on the defined orientation(s) adopted by the bond vector (Prestegard et al., 2004).

Alignment media for the measurement of RDCs include charged or uncharged lipid bicelles, ether/alcohol lamellar phases, Pf1 filamentous phage, purple membranes, and mechanically stressed polyacrylamide gels. We selected for our studies the ether/alcohol liquid crystalline phases, which are uncharged and relatively insensitive to pH and ionic strength (Rückert and Otting, 2000). As a second independent alignment medium we employed Pf1 filamentous phage, which are rods 2 μm in length and 6.5 nm in diameter that align under the magnetic field (Hansen et al., 1998). While ether/alcohol phases cause alignment by steric obstruction, Pf1 has a negative surface charge and provokes the alignment by charge repulsion (Bax, 2003).

Thus, RDCs were measured in αS or βS aligned in 10 mg/ml bacteriophage Pf1 or in 5 % w/v *n*-octyl-penta(ethylene glycol)/octanol ($C_8E_5$). Pf1 phages are commercially available and were used with no further treatment. The $C_8E_5$/octanol phase was prepared as

described by in Alexandrescu and Kammerer (Alexandrescu and Kammerer, 2003). Briefly, $C_8E_5$ was added to the protein sample (5% vol/vol) and the pH was checked and further adjusted if necessary. Octanol was added in 1 µl increments to the protein incubated at 10 °C. Formation of the opalescent anisotropic phase was observed after 2-3 µl of added octanol and was stable after a total of 4-5 µl of octanol (final $C_8E_5$/octanol molar ratio $0.75 < r < 0.90$).

Alignment in the presence of urea was performed by addition of octanol to the sample-urea- penta-ethylene glycol solution. Changing the alignment medium to 5 % w/v *n*-dodecyl-penta(ethylene glycol)/hexanol ($C_{12}E_5$) (r = 0.7) (Sigma) (Rückert and Otting, 2000) allowed RDCs measurements at higher temperatures.

In all cases, the homogeneity and stability of the anisotropic phase was assessed by determining the quadrupolar splitting of the deuterium signal in the NMR sample (Rückert and Otting, 2000).

### 3.2.2.5. Protein aggregation assays.

Aggregation measurements of αS were performed with 100 µM protein samples in buffer A (20 mM Tris-HCl, pH 7.4, 100 mM NaCl) plus 0.01% Na-azide (Sigma), or buffer B (20 mM MES, pH 6.5, 100 mM NaCl) in the case of the studies with metal cations. In all experiments 300 µl of protein sample were incubated in glass vials (Zinsser Analytik, Frankfurt, Germany) at 37 ºC under constant stirring (300 rpm) with magnetic microbars.

Determination of the amount of fibril formation at different time points was carried out by the Thioflavin-T assay (Thio-T) (Sigma) (Conway et al., 2000; Hoyer et al., 2002). Briefly, 5 µl aliquots were withdrawn from the assay and diluted in 2 ml of 50 µM Thio-T in 50 mM Glycine buffer, pH 8.0 (or 50 mM MES, pH 6.5 for assays with metal cations). ThioT fluorescence was measured in a Varian Cary Eclipse spectroflourimeter, with an excitation wavelength of 446 nm. Emission wavelengths from 460 to 600 nm were collected. Fluorescence at 480 nm was employed for determination of the relative content of αS fibrils in the sample.

Analysis of the aggregation traces were performed as previously described, assuming a nucleation polymerization model (Fernandez et al., 2004). Thio-T fluorescence values were normalized to the values at the end of the aggregation assay and the averaged data points were fitted to equation 1:

$$\alpha_{(t)} = \frac{1 - e^{-kapp\, t}}{1 + e^{-kapp\,(t - t_{1/2})}} \tag{1}$$

The quantities $k_{app}$ and $t_{1/2}$ are related to the aggregation reaction as follows:

$$K_{app} = k \times \varepsilon \times [\alpha S], \text{ and} \qquad (2)$$

$$t_{1/2} = \frac{\ln(\varepsilon \times [\alpha S]/[nc])}{k_{app}}, \qquad (3)$$

where $k$ is the rate constant for incorporation of monomers into growth points located in aggregates, $[\alpha S]$ = total concentration of $\alpha S$ monomer units, $[nc]$ is the concentration of nucleation centers and $\varepsilon$ denotes the fraction of addition-competent monomer sites in already formed aggregates. This approximation assumes that $[nc] << \varepsilon \times [\alpha S]$. In all cases, the reported $t_{1/2}$ values correspond to the average of three to five independent aggregation assays carried out simultaneously.

### 3.2.2.6. Metal content determination in $\alpha S$-metal(II) complexes.

Cu(II) concentrations were measured using 4-(2-pyridylazo)resorcinol (PAR) (McCall and Fierke, 2000). The calibration curve yielded the relationship $[Cu(II)](\mu M) = (27.1 \pm 0.3) \times \Delta A_{504nm} + (0.1 \pm 0.1)$. To estimate $[Cu(II)]$ in $\alpha S$ aggregates, 150 $\mu l$ of the sample at the end of the aggregation assay were withdrawn and centrifuged at 90,000 x $g$. The pellets were separated from supernatants and re-dissolved in 150 $\mu l$ of 5.75 M GdnHCl. Cu(II) concentrations were then measured in both fractions (supernatants and re-dissolved pellets).

Co(II) and Ni(II) concentrations were also measured using PAR, whereas the fluorescence probe Fura-2 was used for Mn(II) and 1,10-Phenanthroline for Fe(II) (Margerum and Banks, 1954; McCall and Fierke, 2000). The calibration curves yielded the relationships $[Co(II)](\mu M) = (17.3 \pm 0.2) \times \Delta A_{514nm}$, $[Ni(II)](\mu M) = (24.4 \pm 0.2) \times \Delta A_{514\,nm}$, $[Fe(II)](\mu M) = (84.0 \pm 0.2) \times \Delta A_{500nm}$ and $[Mn(II)](\mu M) = (1.0 - F/F_0)/0.05$, where $F$ and $F_0$ are the fluorescence of the Fura-2 probe in the presence and absence of the metal ion, respectively.

### 3.2.2.7. Equilibrium dialysis assays.

Equilibrium dialysis was used to determine the binding of transition metals to monomeric $\alpha S$ at different metal(II) concentrations. 150 $\mu l$ of a 300 $\mu M$ metal-free $\alpha S$ solution in Buffer A were dialyzed for 24 h against 500 ml of the same buffer containing 0, 0.1, 1 or 10 $\mu M$ solution of metals. The buffer solution was changed every 12 h. Anaerobic conditions were used in the experiments performed with Fe(II). Metal content was determined inside and outside the dialysis container with the above mentioned reagents.

**3.2.2.8. Chemical modification of His residues in αS.**

The sole histidine residue of αS was modified using diethylpyrocarbonate (DEPC). Pure DEPC (6.8 M) (Sigma) was diluted in ethanol to a final concentration of 68 mM and added to the protein solution to reach a molar ratio of 5:1 (DEPC:protein). Modification of the residue was monitored by studying the change in absorption at 240 nm. Excess of DEPC was removed from the protein solutions by gel filtration chromatography using spin columns (Biorad).

**3.2.3. Spectroscopic determinations.**

**3.2.3.1. Absorption and CD spectroscopy.**

Visible electronic absorption spectra for the αS-Cu(II) complexes were acquired from 800 nm to 240 nm on a Varian Cary 100 Scan spectrophotometer (Palo Alto, CA), while CD spectra, also from 800 nm to 240 nm, were acquired with a Jasco 720 spectrapolarimeter (Groß-Umstadt, Germany), at the department of Molecular Biology, MPI-BPC.

Cu (II) titration experiments were performed on samples containing 300 μM protein in buffer 20 mM MES, pH 6.5, 100mM. Aggregation did not occur under these conditions of low temperature and absence of stirring.

Data were expressed as difference absorbance (ε) or circular dichroism (Δε) per molar concentration of protein. Spectrophotometric data were fit using the program DynaFit (Kuzmic, 1996).

**3.2.3.2. EPR spectroscopy.**

EPR spectra were recorded on a Varian Century-Line 9-GHz spectrometer at the department of Spectroscopy, MPI-BPC. Samples containing 300 μM protein in buffer 20 mM MES, pH 6.5, 100 mM NaCl were placed in a standard quartz EPR tube, and immersed in a liquid-nitrogen dewar. The static magnetic field was measured with a Bruker ER 035M NMR magnetometer (Karlsruhe, Germany) and the microwave frequency with a Hewlett-Packard 5345A/5355A frequency counter (Palo Alto, CA).

**3.2.3.3. NMR spectroscopy.**

NMR spectroscopy was performed at the department of NMR-based structural biology, MPI-BPC. The following spectrometers, all from Bruker AG (Karslruhe, Germany), listed in increasing field, were employed alternatively during the thesis work:

- Bruker DRX 600 MHz, triple axis gradient.
- Bruker Avance 600 MHz, with cryoprobe, z-axis gradient.
- Bruker Avance 700 MHz, triple axis gradient.
- Bruker 800 MHz, triple axis gradient.
- Bruker Avance 900 MHz, with cryoprobe, z-axis gradient.

NMR spectra were generally acquired at 15º C on a 100 µM sample of $^{15}$N labeled αS or βS in Buffer A (25 mM Tris-Cl, pH 7.4, 0.1 M NaCl) or B (20 mM MES, pH 6.5, 100mM). Triple resonance experiments were acquired on $^{15}$N-$^{13}$C labeled αS or βS protein, and concentration was raised to 300 µM in order to improve signal to noise ratio and reduce the acquisition time. Aggregation did not occur under these conditions of low temperature and absence of stirring. All spectra were processed and analyzed using nmrPipe (Delaglio et al., 1995), nmrView (Johnson and Blevins, 1994) and SPARKY (Goddard and Kneller).

Several standard NMR-based experiments were acquired on αS and βS proteins, and a comprehensive description of them may be found in the book "150 and More Basic NMR Experiments" written by S. Braun, H.-O. Kalinowski & S. Berger (Braun et al., 1999). However, most of this thesis work was conceived as the application of non-standard NMR techniques, optimized for the study of unfolded states of polypeptides. Thus, a brief theoretical background and description of methods is included for residual dipolar couplings, paramagnetic relaxation enhancement and pulse-field gradient NMR. In addition, a short insight into the $^1$H-$^{15}$N HSQC, the most often standard-NMR experiment employed on this work is provided.

*- $^1$H-$^{15}$N-HSQC.*

Heteronuclear NMR involves the transfer of magnetization between nuclei of different nature ($^1$H, $^{15}$N, $^{13}$C, etc.), however, from a sensitivity point of view, it is highly advantageous to excite the proton ($^1$H), followed by polarization transfer to the heteronucleus ($^{15}$N, for example), and subsequently reverse polarization transfer to the proton for detection. Two pulse sequences are based on this proton-detected heteronuclear correlation technique, the heteronuclear double quantum coherence (HMQC) (Bax et al., 1983) and the heteronuclear single quantum coherence (HSQC) (Bodenhausen and Ruben, 1980). The distinction between these two is that spin coherence is stored as multi-quantum (HMQC) or single-quantum (HSQC) during the evolution period (Bax et al., 1990).

The pulse sequence for a basic HSQC experiment is shown in figure 3.4. The experiment employs two INEPT magnetization transfers. The first one creates anti-phase heteronuclear coherence ($I_Y \rightarrow 2\, I_Z\, S_Y$) and the second is used to convert this coherence back to observable magnetization ($2\, I_Z\, S_Y \rightarrow I_Y$). It can be summarized as follows (Mandal and Majumdar, 2004):

- The first INEPT step creates a proton anti-phase magnetization ($2\, I_X\, S_Z$) during $\tau$. To refocus chemical shift modulation during this period, a 180° pulse on both spins is introduced in the middle of $\tau$ period.

- Coherence is subsequently transferred to the directly attached heteronucleus ($^{15}N$ for example) by simultaneous 90° pulses on both spins ($2\, I_Z\, S_Y$).

- The S-spin coherence is frequency-labeled during the $t_1$ period. The 180° pulse on the $I$-spin in the middle of $t_1$ refocuses the evolution of heteronuclear $J_{IS}$ coupling.

- A 90° pulse on both spins transfer the magnetization back to proton as anti-phase $I$-spin magnetization ($2\, I_Y\, S_Z$).

- The final spin-echo period converts this anti-phase term into in-phase proton magnetization ($2\, I_Y\, S_Z \rightarrow I_X$).
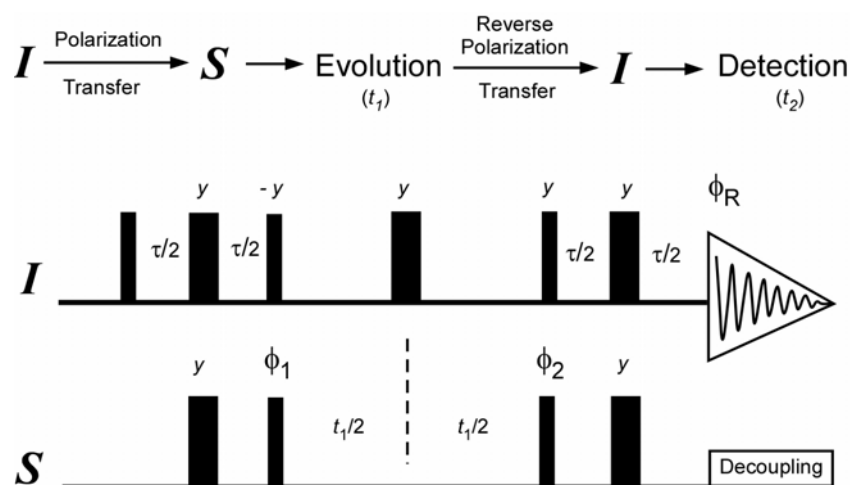


**Figure 3.4. Fundamental pulse sequence for a HSQC experiment**. Narrow and wide pulses correspond to 90° and 180° flip angles, respectively, with the indicated phase. The delay $\tau$ is set to $1/(2\, J_{IS})$. Decoupling of the S-spins during acquisition is accomplished using the Waltz-16 sequence. The basic phase cycling is $\phi_1$ ( x, -x, x, -x), $\phi_2$ ( x, x, -x, -x), and receiver $\phi_R$ (x, -x, -x, x) is applied in the sequence.

In the conventional HSQC sequence, heteronuclear single quantum evolves under the influence of the S-spin chemical shift during $t_1$ to yield two-orthogonal terms proportional to $2\, I_Z\, S_Y$ and $2\, I_Z\, S_X$. One of the two anti-phase magnetization terms is not refocused by the reverse INEPT sequence and consequently does not contribute to the final observed

magnetization. Therefore, on average one-half of the initial *I*-spin polarization does not contribute to the detected signal. A sensitivity-enhanced version of this experiment enhances the signal to noise ratio by $\sqrt{2}$ relative to the phase-cycled version (Palmer et al., 1991). In addition, pulsed-field gradients are used to suppress undesirable coherence pathways and to suppress solvent in a single transient (Zhu et al., 1998).

The outcome of such a pulse sequence is a signal, detected in the proton dimension (F2), which contains information on the chemical shifts of both $^{1}$H and $^{15}$N nuclei, for a given nitrogen frequency observed. The desired frequency space is sampled by repeating the pulse sequence for variable frequencies on the nitrogen dimension (F1), and the set of one-dimensional spectra is merged in a single bi-dimensional representation, the 2D $^{1}$H-$^{15}$N HSQC spectrum. NH bonds will thus be seen as cross-peaks situated at the intersection between the $^{1}$H and $^{15}$N resonant frequencies or chemical shifts.

$^{1}$H-$^{15}$N HSQC experiments in αS and βS were recorded using 256 x 1024 complex incremental data points in F1 ($^{15}$N) and F2 ($^{1}$H) dimensions, with 8 to 32 scans per increment and a relaxation delay of 1.2 s. The sampled frequency space (sweep width) was in general 26 ppm for the nitrogen dimension (from 106 to 132 ppm, centered in 119 ppm) and 8.6 ppm for the proton dimension (from 0.4 to 9.0 ppm, centered in 4.7 ppm).

*- Measurement of paramagnetic relaxation enhancement.*

Distance restraints between residues in the denatured state of proteins can be obtained by covalently attaching a probe containing a free radical to a unique cysteine residue introduced by mutagenesis. The magnetic interaction between the unpaired electron in the spin label and a proton in the same molecule is similar to the Nuclear Overhausser Effect (NOE) between pairs of protons. Unlike an NOE, whose measurable effect is limited to distances less than ~ 5 Å, the electron-proton interaction extends over approximately 20 to 25 Å, making it a workable probe for distances in the range from 10 to 20 Å (Gillespie and Shortle, 1997a). The parameterization of the magnetic interaction of a free electron with a proton is described by the Solomon-Bloembergen equations (Kosen, 1989), which parameterize the enhancement of the proton's transverse relaxation rate due to the paramagnetic effect (1):

$$R_{2P} = \frac{K}{r^6} \times \left( 4\,\tau_C + \frac{3\,\tau_C}{1 + \omega^2\,\tau_C^2} \right), \qquad\qquad (1)$$

where *K* is 1.23 x $10^{-32}$ cm$^6$s$^{-2}$ for the interaction between a single electron radical and a proton, r is the vector distance between the spin label electron and the HN proton, τc is the correlation time for the electron-proton vector (4 ns, as determined for the unfolded state of

sthaphilococal nuclease, which has a similar size as αS) (Gillespie and Shortle, 1997a), and ω is the Larmor frequency of the proton (dependent on the field at which the NMR experiment is acquired). The equation is based on the assumptions that the vector between the electron and the proton is free to undergo isotropic rotational diffusion and that its length r is fixed.

The paramagnetic effect is consequently related to the intensity of an amide cross-peak as follows (2) (Battiste and Wagner, 2000):

$$\frac{I_{para}}{I_{diam}} = \frac{R_{2D} \times e^{(-R_{2P}\,t)}}{R_{2D} + R_{2P}} \tag{2}$$

, where $I_{para}/I_{diam}$ is the ratio of peak intensities for an amide resonance between the paramagnetic and diamagnetic state of the spin label, $R_{2D}$ is the transverse relaxation rate of the amide proton measured in the absence of the spin label, $R_{2P}$ is the paramagnetic enhanced transverse-relaxation rate, and t is the duration of the INEPT delays (~ 10 ms) in the HSQC pulse sequence (the proton magnetization is in the transversal plane).
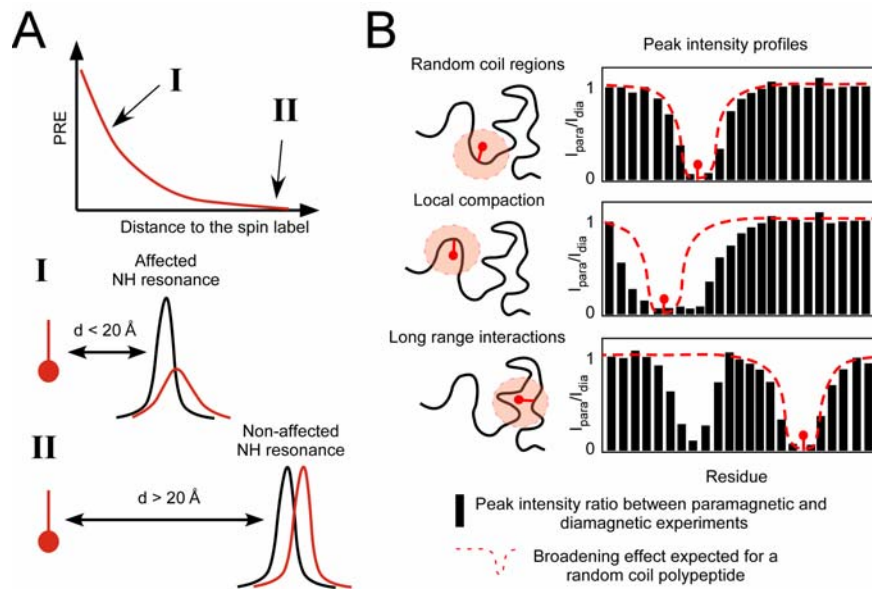


**Figure 3.5. Paramagnetic relaxation enhancement in protein studies. A.** The unpaired electron from a nitroxide spin label causes perturbation of amide resonances up to ~ 20 Å from the attachment site. The paramagnetic effect is measured as an enhancement of proton $R_2$ transverse relaxation rates ($R_{2P}$), and this effect is related to the distance between the affected amide proton and the spin label ($r$) by the relationship $R_{2P} \propto r^{-6}$. **B.** The targeted placement of the spin label provides information on local compaction and long range interactions, useful for the structural characterization of the unfolded states of polypeptides

Paramagnetic relaxation enhancement effects in αS and βS Cys-containing mutants were measured from the peak intensity ratios between two-dimensional ^{15}N-^{1}H HSQC

experiments acquired in the presence ($I_{para}$) and absence ($I_{diam}$) of the nitroxide radical attached to the Cys residue. HSQC experiments were recorded using 256 x 1024 complex data points in F1 and F2 dimensions with 8 scans per increment and a relaxation delay of 1.2 s. The removal of the spin label for measurement of the diamagnetic state was accomplished by addition of 0.5 mM DTT to the protein solution and 30 min incubation at room temperature. The reported intensity ratios are averages over repeated measurements for up to three different protein preparations.

*- Measurement of residual dipolar couplings.*

Dipolar couplings are large interactions caused by the magnetic flux lines of the spins of one nucleus affecting the magnetic field at the spin of another nucleus. The parallel component of the dipolar field of one nucleus ($^1$H, for example) to the external magnetic field ($B_0$) will change the resonance frequency of the bonded nucleus ($^{15}$N for the amide bond), by an amount that depends on the internuclear distance ($r_{NH}$), and on the orientation of the internuclear vector relative to $B_0$.
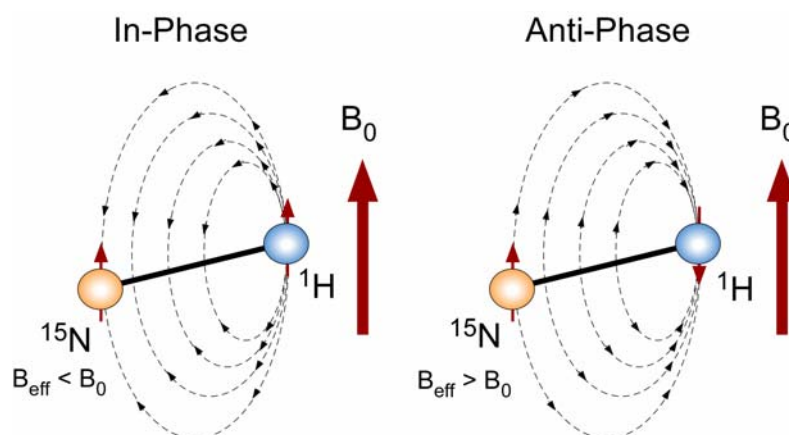


**Figure 3.6. Occurrence of dipolar couplings.** Magnetic dipole-dipole coupling for a $^{15}$N-$^1$H spin pair is illustrated. $^{15}$N and $^1$H magnetic moments are aligned parallel or antiparallel to the static magnetic field $B_0$. The effective magnetic field in the $B_0$ direction at the $^{15}$N position can increase or decrease relative to $B_0$ depending on the orientation of the $^{15}$N-$^1$H vector and the spin state of the proton (parallel or antiparallel to $B_0$) (Bax, 2003).

Thus, for the amide bond, the $^1$H nuclear spin can increase or decrease the total magnetic field at the $^{15}$N nucleus, depending whether is parallel (In-Phase) or antiparallel (Anti-Phase). In an ensemble of molecules, half of the nuclei will be parallel to Bo, and the other half will be antiparallel, thus the $^{15}$N nucleus will show two resonances (doublet),

separated in frequency by the N-H dipolar coupling ($D_{NH}$) (Bax, 2003). The magnitude of the $D_{NH}$ is given by (1):

$$D_{NH} = D_{NH}^{max} \times \left\langle \left(3\cos^2\theta - 1\right)/2 \right\rangle, \qquad (1)$$

where $\theta$ is the angle between the internuclear bond vector and $B_0$, and the brackets denote time and ensemble average. The maximum dipolar coupling for the amide bond is given by (2):

$$D_{NH}^{max} = -\mu_0\left(h/2\pi\right)\gamma_N\gamma_H / \left(4\pi^2 r_{NH}^3\right), \qquad (2)$$

where $\mu_0$ is the magnetic permittivity of vacuum, h is Planck´s constant, and $\gamma_N$ and $\gamma_H$ are the magnetogyric ratios of the $^{15}N$ and $^1H$ nuclei respectively. The value of the maximum $D_{NH}$ is 21 KHz, observable only in solids, but it averages to zero in isotropic solution due to the rapid molecular tumbling, giving sharp single resonance cross-peaks for amides. The slight anisotropy provoked by the alignment media causes that not all orientations are equally to occur such that the order parameter $\left\langle \left(3\cos^2\theta - 1\right)/2 \right\rangle \neq 0$, allowing measurement of RDCs in the range of few Hz.

RDCs are generally measured for N-H-groups in non-decoupled, spinstate separated, HSQC-based experiments like the In-Phase-Anti-Phase (IPAP) (Ottiger et al., 1998) or the Doublet Separated Sensitivity Enhanced (DSSE) (Cordier et al., 1999). Theses experiments are not proton-decoupled during nitrogen evolution and therefore yield the NH-splitting.

Since in the partial alignment condition used, the value of one-bond N-H RDCs ($D_{NH}$) is rather small (< 15 Hz), an accurate determination of these values is obtained by measuring them simultaneously with the larger one-bond N-H scalar coupling ($^1J_{NH}$) of ~ 94 Hz. $D_{NH}$ are thus determined as the difference between the NH splitting measured in an anisotropic phase ($D_{NH}$ + $^1J_{NH}$) and in isotropic solution ($^1J_{NH}$). In addition, to a decreased spectral overlap in the determination of the NH splitting, the two components of the doublets are separated into two different spectra, and thus are recorded in an interleaved manner (A+B spectrum for the Anti-Phase condition and A-B spectrum for the In-Phase condition). Briefly, the IPAP strategy can be described as follows. First, a regular $^1H$-coupled $^1H$-$^{15}N$ HSQC generates in-phase doublets in the nitrogen dimension. A second HSQC experiment, with a $^{15}N$ refocusing period $\Delta=2J_{NH}^{-1}$ inserted at the beginning of the evolution period plus a 90° phase decrement on the first 90° *S* pulse, relative to the regular HSQC experiment, allows detection of anti-phase doublets (Figure 3.7). Evolution during this period is terminated by a $^1H$ purge pulse.
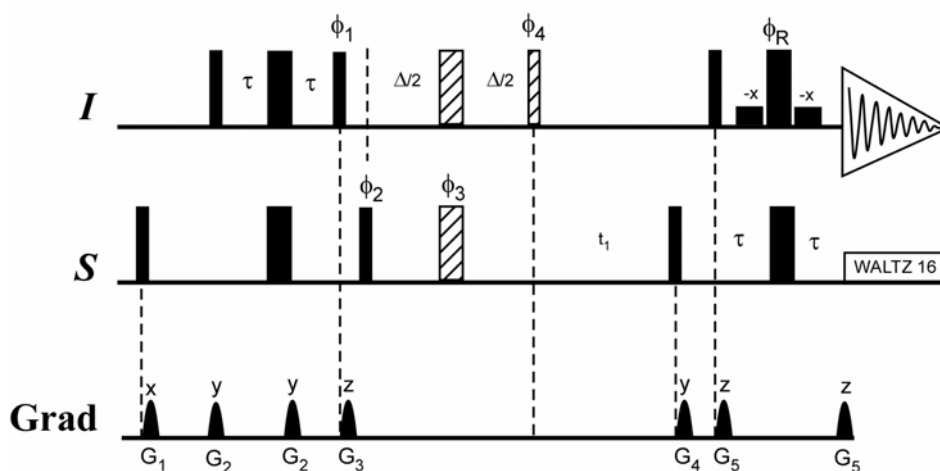
**Figure 3.7. Pulse sequence for the IPAP 1H-15N HSQC experiment.** Narrow and wide pulses correspond to 90° and 180° flip angles, respectively, with phase *x*, unless indicated. The $\Delta/2-180°(^1H/^{15}N) -\Delta/2-90°_{\phi4}$ sequence (open pulses) is only used in the experiment for generating the anti-phase (AP) spectrum and is omitted for generating the in-phase (IP) spectrum. IP and AP spectra are recorded in an interleaved manner. The low power $90°_{-X}$ pulses surrounding the final $^1H$ 180° pulse are part of the WATERGATE solvent suppression scheme. Delay durations: $\tau$ = 2.5 ms; $\Delta$ = 5.3 ms. All gradients are sine-bell shaped with 25 G/cm at their center. Gradient durations: $G_{1,2,3,4,5}$ = 2, 0.4, 2, 1, 0.4 ms. Phase cycling: $\phi_1$ = -*y*, *y*; $\phi_2$ = 2(*x*), 2(-*x*) for IP; $\phi_2$ = 2(-*y*), 2(*y*) for AP; $\phi_3$ = 4(*x*), 4(*y*), 4(-*x*), 4(-*y*); $\phi_4$ = 8(*x*), 8(-*x*) ; $\phi_R$ = *x*, 2(-*x*), *x* for IP; $\phi_R$ = *x*, 2(-*x*), *x*, -*x*, 2(*x*), -*x* for AP. Quadrature detection in the *t*1 dimension is obtained by altering $\phi_2$ (IP) or $\phi_2$ and $\phi_3$ simultaneously (AP) in the States–TPPI manner.

We measured $D_{NH}$ in αS and βS proteins using the IPAP $^1H$-$^{15}N$-HSQC sequence. Spectra were recorded with 512 x 1024 complex data points in F1 and F2 dimensions with 32 scans per increment and a relaxation delay of 1.2 s. Each experiment consisted of the acquisition of a first IPAP determination (A+B-iso and A-B-iso spectra) for the protein in buffer solution, to determine the isotropic contribution to the NH splitting ($^1J_{NH}$), and a second IPAP determination (A+B-aniso and A-B-aniso spectra) with the protein diluted in the alignment media, which provided the anisotropic + isotropic contributions ($D_{NH}$ + $^1J_{NH}$). $D_{NH}$ values were afterwards calculated as the difference between NH splittings measured in the aligned sample and those measured in an isotropic sample (i.e. the RDCs were not corrected for the negative gyromagnetic ratio of $^{15}N$). RDCs observed under different conditions were normalized according to the size of the quadrupolar splitting of the deuterium signal (relative to RDCs for free αS).
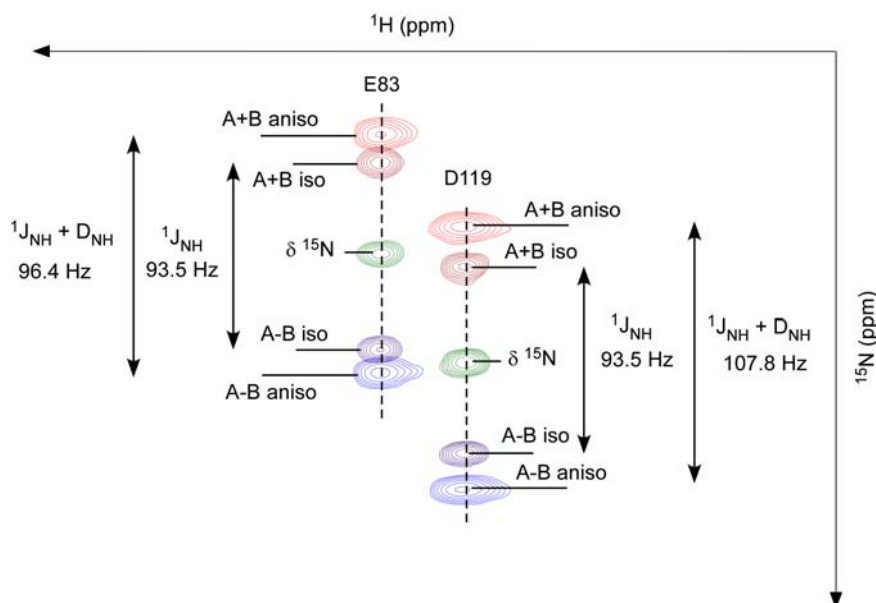
**Figure 3.7. Measurement of residual dipolar couplings**. Scheme showing the different experiments carried out for the determination of NH RDCs ($D_{NH}$) in proteins. A proton-decoupled standard HSQC provides single amide-cross peaks (green), positioned at the resonant frequency ($\delta$ $^{15}$N). The absence of proton decoupling in the nitrogen dimension allows determination of positive and negative $^{1}$H spin-state contributions to the externally applied magnetic field sensed by $^{15}$N nuclei (the peaks are split in two). The one-bond $^{1}$J$_{HN}$ couplings are measured in isotropic solution (buffer) in an interleaved manner, employing the IPAP sequence, resulting in the spectra A+B iso (dark red) and A-B iso (dark blue). The same IPAP experiment is afterwards measured under slight anisotropic conditions (Pf1 or $C_8E_5$ alignment media) to determine $^{1}$J$_{HN}$ + $D_{NH}$, and the spectra A+B aniso (light red) and A-B (light blue) are obtained, allowing calculation of $D_{NH}$ by subtraction of the previously determined $^{1}$J$_{HN}$ value. The broadening in the proton dimension observed in anisotropic conditions is caused by $^{1}$H-$^{1}$H dipolar couplings.

*- Pulse field gradient NMR.*

Pulse field gradient NMR (PFG) techniques are used extensively to measure translational diffusion in solution (Bernado et al., 2004). In the presence of a spatially inhomogeneous field (a field gradient), transverse magnetization from nuclei located in different points of the sample acquire different phases. This spatially-encoded phase induced by a field gradient can be reversed by the application of a second field gradient with exactly the same spatial distribution and intensity but opposite sign. Due to diffusion, molecules will change their spatial localization between the application of the first and second gradient, and thus they will experience an inhomogeneous total field, causing an attenuation of the measured signal. For unrestricted diffusion of a molecule in an isotropic liquid, the PFG NMR signal amplitude, A, normalized to the signal obtained in the absence of gradient pulses, is related to the diffusion coefficient D by (1):

$$A = e^{-\left(\gamma^2 \delta^2 D(\Delta - \delta/3)\right) \times g^2} ,  \tag{1}$$

where $\gamma$ is the gyromagnetic ratio of the observed nucleus, g and $\delta$ are the magnitude and duration of the magnetic field pulses, and $\Delta$ is the time between the gradient pulses (Stejskal and Tanner, 1965). The term $\gamma^2 \delta^2 D(\Delta - \delta/3)$ is called the decay rate ($d_D$) and is proportional to the diffusion coefficient. The determination of D is achieved by acquiring a series of 20 one-dimensional PFG spectra at different gradient strengths, and fitting the decay of the signal intensity to a Gaussian function with the form (2):

$$I_{(g)} = a \times e^{-d_D \times g^2} ,  \tag{2}$$

where $I_{(g)}$ is the ratio between the intensity of the signal measured at gradient strength g and in the absence of gradient, and *a* is the pre-exponential factor ($\sim 1$).

The Stokes-Einstein equation relates D to the hydrodynamic radius, $R_H$, as follows (3):

$$D = k_B T / 6 \pi \eta R_H ,  \tag{3}$$

where $k_B$ is the Boltzman constant, $T$ is the temperature of the sample and $\eta$ is the viscosity of the solution. Thus determination of the $R_H$ of a polypeptide chain requires the determination of the viscosity of the solution. In order to overcome this, a viscosity probe of known size is included in the determination, usually dioxane (Jones et al., 1997), providing the relationship (4):

$$R_H^{prot} = \frac{D^{ref}}{D^{prot}} \times R_H^{ref}  \tag{4}$$

If the standard is placed in the measurement solution together with the protein, the determination of $R_H$ is thus made relative to the measured decay rates of the individuals components, as follows (5):

$$R_H^{prot} = \frac{d_D^{ref}}{d_D^{prot}} \times R_H^{ref}  \tag{5}$$

Pulse field gradient NMR experiments for $\alpha$S and $\beta$S were acquired at 15 ºC on a 200 $\mu$M unlabeled protein sample dissolved in 99.9 % $D_2O$, 20 mM phosphate buffer pH 7.0 (uncorrected), and containing dioxane ($\sim 20$ mM) as an internal radius standard and viscosity probe (Wilkins et al., 1999). Deuterium oxide was employed instead of water in order to minimize the power level necessary for water pre-saturation. Twenty one-dimensional ${}^1$H spectra were collected as a function of gradient amplitude employing the PG-SLED sequence (Jones et al., 1997). The gradient strength was shifted from 1.69 to 33.72 Gauss cm${}^{-1}$, in a

linear manner. Each $^1$H spectrum comprised 32 scans plus 16 steady-state scans. Sixteen K complex points were acquired with a spectral width of 6,000 Hz. The signals corresponding to the aliphatic region of the $^1$H spectra (3.3-0.5 ppm) were integrated and the decay of the signal as a function of the gradient strength was fitted to a Gaussian function to determine $d^{prot}$. The same procedure was applied for the dioxane peak (~ 3.6 ppm) and the $d^{ref}$ was measured. The $R_H$ for the protein was calculated from the known $R_H$ (2.12 Å) for the dioxane and the ratio between the measured $d^{ref}/d^{prot}$.

*- Determination of dissociation constants for polyamine-synuclein complexes.*

For the association of a ligand L to a receptor protein P to give the complex PL, the following equilibrium exists (1):

$$P + L \underset{K_{off}}{\overset{K_{on}}{\rightleftharpoons}} PL \qquad (1)$$

with $K_{on}$ and $K_{off}$ being the association (on) and dissociation (off) rate constants.

The dissociation constant $K_D$ is given by (2):

$$K_D = \frac{[P] \times [L]}{[PL]} = \frac{K_{off}}{K_{on}} \qquad (2)$$

where [P], [L] and [PL] are concentrations at equilibrium.

With $[P]_0$ and $[L]_0$ being the initial concentration of protein and ligand, the equation (2) can be written as follows (3):

$$K_D = \frac{([P]_0 - [PL]) \times ([L]_0 - [PL])}{[PL]} \qquad (3)$$

Equation (3) can be transformed into a quadratic equation with the solution given in (4):

$$[PL] = 1/2 \left(K_D + [P]_0 + [L]_0\right) - \sqrt{1/4 \left(K_D + [P]_0 + [L]_0\right)^2 - [P]_0 + [L]_0} \qquad (4)$$

For a ligand binding to a protein in slow exchange on the NMR chemical-shift time scale, the difference in chemical shift for a given nuclei between the bound and free state relates to the fraction of bound ligand by (5):

$$\frac{[PL]}{[P]_0} = \frac{\Delta^{15N}\delta}{Max\, \Delta^{15N}\delta} \qquad (5)$$

where $\Delta^{15N}\delta$ is the chemical shift difference of the observed amide nitrogen between the bound and free state and $Max\, \Delta^{15N}\delta$ is the value at saturation. Equation (5) and can be written as follows to determine the concentration of complex (6):

$$[PL] = \frac{\Delta^{15N}\delta \times [P]_0}{\text{Max } \Delta^{15N}\delta} \qquad\qquad (6)$$

Combining equations (4) and (6), the concentration of complex can be expressed in terms of the initial concentration of protein and ligand, and the change in chemical shift measured for the observed amide nitrogen (7):

$$\Delta^{15N}\delta = \frac{\text{Max } \Delta^{15N}\delta}{[P]_0} \times 1/2\left(K_D + [P]_0 + [L]_0\right) - \sqrt{1/4\left(K_D + [P]_0 + [L]_0\right)^2 - [P]_0 + [L]_0}$$

A non-linear global fit for $[L]_0$ to the $\Delta^{15N}\delta$ for amide nitrogens of each residue involved in the binding site provides a single $K_D$ and the corresponding chemical shifts at saturation ( $\text{Max } \Delta^{15N}\delta$ ).

*- Triple resonance experiments.*

To obtain sequence-specific assignments for the backbone of βS, the following three-dimensional triple-resonance experiments were collected at 900 MHz, employing standard pulse sequences (Ikura et al., 1990):

| | Spectrometer field (MHz) | Real points | | | Spectral width (ppm) | | |
|---|---|---|---|---|---|---|---|
| | | $^{15}$N | $^{13}$C | $^{1}$H | $^{15}$N | $^{13}$C | $^{1}$H |
| HNCACB | 600 | 40 | 70 | 1024 | 23 | 60 | 9 |
| CBCACONH | 900 | 35 | 60 | 1024 | 23 | 60 | 9 |
| HNCO | 900 | 45 | 25 | 1024 | 22 | 8.8 | 9 |
| HNCACO | 900 | 64 | 40 | 1024 | 22 | 8.8 | 9 |
| | | $^{15}$N | $^{15}$N | $^{1}$H | $^{15}$N | $^{15}$N | $^{1}$H |
| HNN | 900 | 35 | 62 | 1024 | 23 | 23 | 9 |
| | | $^{15}$N | $^{1}$H | $^{1}$H | $^{15}$N | $^{1}$H | $^{1}$H |
| HNHA | 900 | 60 | 128 | 1024 | 26 | 9 | 9 |

**Table 3.2. Triple resonance experiments acquired to facilitate the backbone assignment of βS.** Briefly, the information provided by each experiment is as follows: HNCACB, sequential connectivity via Cα and Cβ (i-1, i) and $^{13}$Cα and $^{13}$Cβ chemical shifts; CBCACONH, complement to HNCACB, shows connectivity via Cα and Cβ (i-1), HNCO, sequential connectivity via CO (i-1, i); HN(CA)CO, sequential connectivity via CO (i) and C′ chemical shifts; HNN, sequential connectivity via amide $^{15}$N (i-1, i)

solves overlap in unfolded proteins; HNHA ($^3J_{HNH\alpha}$ coupling constants and H$\alpha$ chemical shift constraints). All these experiments were acquired at 15 ºC on a 400 μM βS protein sample in buffer B.

Secondary shift values were calculated as the differences between the measured Co/C$\alpha$/C$\beta$ chemical shifts and the empirical random coil values reported by Wishart *et al.* (Wishart and Sykes, 1994).

$^{15}$N relaxation data were acquired with modern versions of pulse sequences based on those described by Farrow et al. (Farrow et al., 1995). Spectra used for longitudinal relaxation $R_1$ analysis were collected using the following relaxation delay times (in ms): 20, 100, 200, 500, 100, and 20. $R_2$ data were measured using a pulse sequence employing a CPMG pulse train with the following relaxation delays (in ms): 3.8, 19, 38, 57, 114, 228, 2.8, and 228. Duplicate spectra were collected at several time points to estimate uncertainty. The delay between 180 °C pulses in the CPMG pulse train was ~ 1 ms. Resonance heights were extracted and fit as a function of the relaxation delay time using Sparky routines in order to determine $R_1$ and $R_2$ relaxation rates. Steady state NOE values are reported as the ratio of peak heights in paired spectra collected with and without an initial period (4 s) of proton saturation during the 5-s recycle delay.

In the case of $\alpha$S, a three-dimensional HNCACB experiment was used to facilitate backbone assignments under denaturing conditions (Bax and Grzesiek, 1993).

*- Metal-induced paramagnetic broadening.*
In a similar manner as occurs with the effect of a nitroxide spin label, the interaction of the free electron from a paramagnetic metal ion with the side chains of residues in a protein causes a perturbation of the magnetic field that is sensed by the nuclei. Thus, through bond or through space electronic interactions account for the broadening of amide resonances up to ~ 11 Å from the binding site of the metal.

For studies of the formation of $\alpha$S-metal complexes $^1$H-$^{15}$N HSQC spectra were recorded using 256 x 1024 complex data points in F1 and F2 dimensions with 16 scans per increment and a relaxation delay of 1.0 s. In general, spectra were acquired on 100 μM protein samples in buffer B at 15 °C to avoid protein aggregation. Similarly to PRE studies, for the determination of the paramagnetic broadening caused by binding of the paramagnetic ion, intensities of amide cross-peaks were compared in the presence ($I_{para}$) and absence ($I_{dia}$) of the metal in the protein solution. The $I_{para}/I_{dia}$ ratios of 95-105 non-overlapping cross peaks were plotted as a function of the protein sequence to obtain the intensity profiles.

*- Measurement of metal-induced relaxation enhancement.*

Proton longitudinal relaxation rates ($R_1$=1/$T_1$) were measured with the standard inversion recovery pulse sequence, and the paramagnetic relaxation rate enhancement ($R_{1p}$) determined on samples containing 5 μM Mn(II) and increasing concentrations of αS (100-800 μM). The Mn(II) binding affinity was estimated according to the following equation (1):

$$C_L = C_M (R_{1M}/R_{1p}) - K \qquad [1]$$

where $C_L$ is the protein concentration, $C_M$ is the metal ion concentration, $R_{1M}$ is the longitudinal relaxation rate in the paramagnetic site, $R_{1p}$ is the longitudinal relaxation rate enhancement and $K$ is the dissociation constant (Bertini and Luchinat, 1996). Equation 1 is valid under fast exchange conditions and if the concentration of the αS-Mn(II) complex is always much smaller than $C_L$. In these cases, from constant $C_M$, a plot of 1/$R_{1p}$ against $C_L$ gives a straight line; $R_{1M}$ can be obtained from the slope, and $K$ can be found form the intercept on the $C_L$ axis.

## 3.3. Miscellaneous

### 3.3.1. Calculation of distance restraints from PRE.

Distance restraints were calculated as previously described from the intensity ratio between two $^{15}$N-$^1$H HSQC NMR spectra, in the diamagnetic and paramagnetic state of the protein (Gillespie and Shortle, 1997b). The paramagnetic enhanced transverse relaxation rate ($R_{2P}$) was calculated using equation (2) described in PREs measurement section. Experimental values for the diamagnetic transverse relaxation rates ($R_{2D}$) (Bussell and Eliezer, 2001) and the measured intensity ratios for each resonance were used to linearly fit for $R_{2P}$ (Battiste and Wagner, 2000). This value was inserted into equation (1) (section 3.2.3.3, Measurement of PREs) to calculate the distance $r$ between each proton and the unpaired electron on the nitroxide radical. The correlation time for the electron-nuclear interaction $\tau_c$ was set to 4 ns, in agreement with previous studies (Gillespie and Shortle, 1997a). For amides that were broadened beyond detection in the oxidized spectra, an upper limit for the intensity ratio was estimated from the spectral noise in the oxidized spectrum.

### 3.3.2. Structure determination and analysis.

Structure calculations were performed using Xplor-NIH version 2.0.6 (Schwieters et al., 2003). Torsion angle dynamics were started at 3000 K from a random coil conformation with the temperature reduced to 20 K during simulated annealing, followed by a short energy

minimization. An all atom representation of αS was used. Structural energy terms from steric repulsion, bond length, bond angles, dihedral angles and favored regions of the Ramachandran map were used.

Intensity ratios for almost the whole N-terminus of αS A140C were below 0.8. In order to avoid an overly restrained structure, only intensity ratios < 0.75 were regarded as significant for this mutant, whereas a cutoff of 0.8 was allowed for the A18C and A90C mutants. However, changing these cutoff values in a reasonable range did not change the main structural features. Peaks with intensity ratios below these cutoffs were restrained to the calculated distance ± 5 Å using a harmonic square well potential. For intensity ratios above these cutoffs, a target distance was calculated from an intensity ratio of 0.9 and the lower distance bound was restrained to – 5 Å of the calculated value. All distances were imposed as restraints between the backbone amide proton of the residue with the cysteine-MTSL group and residue-specific amide protons.

Structure calculations were also performed with a modified version of the *ab initio* structure prediction program ROSETTA that allows inclusion of experimental distance restraints (Simons et al., 1997; Bowers et al., 2000). In using ROSETTA we assumed that despite the high conformational flexibility present in αS all residues favor a distribution of dihedral angles corresponding to those seen in structures of native proteins in agreement with previous studies (Bolin et al., 1996). Distance restraints were imposed as described above with the modification that no lower bounds were enforced.

Clustering was performed using the molecular dynamics program GROMACS version 3.2.1 with a cutoff of 0.9 nm and 1.0 nm for Xplor-NIH and Rosetta structures, respectively (Lindahl et al., 2001). Atom density maps were calculated using VMD-XPLOR (Schwieters and Clore, 2002) and represent a 5 % amplitude isosurface of the density of atoms in the peptide main chain of the structures comprising each cluster. Average contact maps were generated using MOLMOL (Koradi et al., 1996) and are for structures calculated using Xplor-NIH and ROSETTA.

### 3.3.3. Electron microscopy

An aliquot was removed from the aggregation incubation mixture and adsorbed onto a carbon film as described (Hoyer et al., 2002). The samples were analyzed with a Philips CM12 electron microscope in an angular dark-field mode.

*Results*

## 4. Results. Chapter I: "NMR identifies long-range auto-inhibitory interactions in the native state of αS".

NMR spectroscopy is a very powerful tool for studying the conformation and dynamics of proteins at atomic resolution. In the case of natively unfolded proteins like αS, heteronuclear NMR is the most suitable methodology to investigate the ensemble of conformations populated by the disordered polypeptide chain (Dyson and Wright, 2004).

With the fundamental aim of elucidating the ensemble of conformations populated by αS in solution we employed NMR methods developed for the study of denatured and transition states of folded protein, namely paramagnetic relaxation enhancement by nitroxide spin labels and residual dipolar couplings. Thus PREs would report on long range contacts in the protein, and RDCs would detect residual structure in the polypeptide chain. The hierarchy of such structural elements will be assessed by comparison of native and amyloidogenic conditions of the protein.

### 4.1 Heteronuclear 2D NMR spectroscopy probes conformational transitions on αS.

αS has been previously studied by NMR both in is native unfolded state and in the state associated to vesicles (SDS-micelles), therefore the assignments of backbone resonances corresponding to both states was available at the beginning of this thesis work (Bussell and Eliezer, 2001; Chandra et al., 2003). In addition, work performed in our laboratory had independently corroborated the assignment of αS in physiological aqueous solution (Fernandez et al., 2004).

In figure 4.1 a $^1$H-$^{15}$N Heteronuclear Single Quantum Coherence (HSQC) spectra of $^{15}$N-labelled αS is shown. This spectra is acquired with a particular sequence of magnetic pulses and time delays which allows the transfer of magnetization between amide protons and the amide nitrogens of amino acids, and detects the resonances corresponding to the H-N amide bond of each residue in the polypeptide chain (including amino acids side chains and excepting Pro which does not contain any amide proton). Changes in the chemical environment surrounding a particular amino acid can thus be efficiently evaluated by means of intensities or chemical shifts perturbations on resonances of amide protons. Thus, the HSQC sequence will be the method of choice in most of the experiments throughout this work, providing also a combination of adequate spreading of signals and low time required for acquisition of the spectra (45 minutes for a solution of 100 μM αS). However, this type of

experiment does not provide quantitative information about secondary structure propensities, therefore requiring in most cases recourse to triple resonance experiments (Chapter 3).
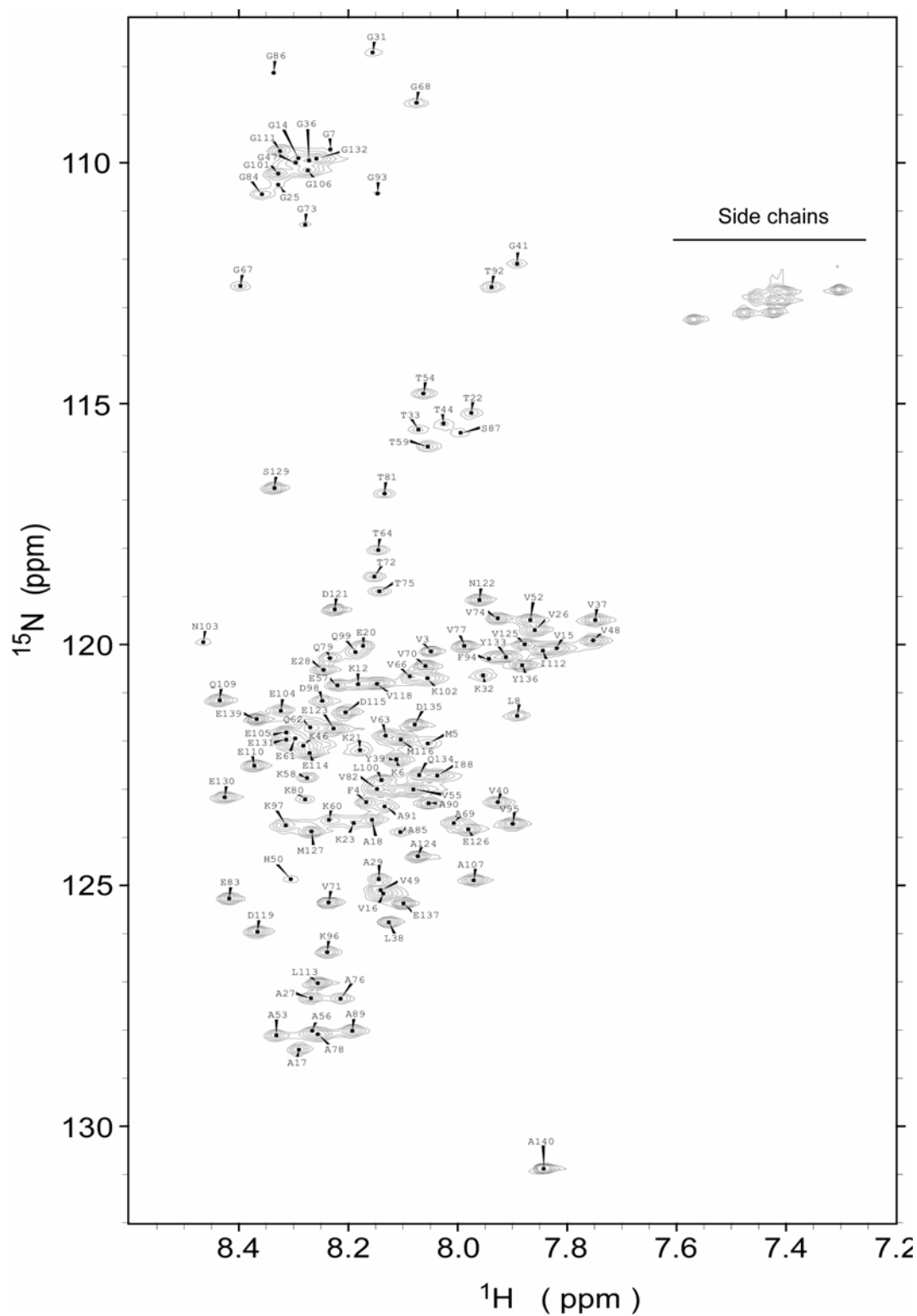


**Figure 4.1. ¹H-¹⁵N HSQC spectra of αS.** An HSQC spectrum of a 100 μM solution of αS protein was acquired at 600 MHz. Solution conditions were Tris-HCl 20 mM, pH 7.4, 100 mM NaCl (buffer A), and the temperature was 15 °C.

Several features of the polypeptide chain may be evaluated by the mere observation of the characteristics of this spectrum. For example, the lack of defined secondary structure in αS is evident from the narrow distributions of the resonance on the proton dimension (~ 0.8 ppm). Another signature of the state of the polypeptide chain is the cluster of resonances as a function of the residue nature, as Gly, Ser and Thr amide crosspeaks, for example, are detected into regions typical of the residue random coil positions (Figure 4.1). These signatures are identical to those of strongly denatured ubiquitin (Peti et al., 2001).

For a completely unfolded polypeptide, most resonances would be expected to be very sharp and detectable (except the ones from the first and second residues). For αS, under the conditions of pH and temperature evaluated, several peaks diminished in intensity, or were not detected at all. This suggests that the some regions of the protein could be involved in conformational exchange, as observed with molten globules states of proteins or for the natively unfolded HIV-TAT (Schulman et al., 1997; Shojania and O'Neil, 2006b). Indeed, it has been suggested for αS a reversible intermediate conformational exchange involving the first 100 amino acid residues of the protein (McNulty et al., 2006b).

The affected resonances correspond to residues $Met^5$, $Lys^6$, $Gly^7$, $Ser^9$, $Lys^{10}$, $Ala^{11}$, $Lys^{21}$, $Thr^{22}$, $Ala^{30}$, $Gly^{31}$, $Lys^{32}$, $Thr^{33}$, $Lys^{35}$, $Ser^{42}$, $Lys^{43}$, $Thr^{44}$, $His^{50}$, $Asn^{65}$, $Gly^{73}$, $Gly^{84}$, $Gly^{86}$, $Ser^{87}$, $Gly^{93}$, $Asn^{103}$ (Figure 4.2, green bars). The weak and medium intensity peaks fall all at the N-terminus and NAC region of the protein, whereas Val residues and the whole C-terminus feature resonances 2 to 4 times higher than the average for the protein.

Interestingly, the intensity of the signals increased at lower pH, but diminished upon increasing the temperature. As shown on figure 4.2 (blue line), a relative increase (~ 2 folds) was observed for the N-terminal and NAC resonances when the pH in αS was decreased from 7.4 to 6.5. Conversely, the increase of the temperature to 47 degrees caused a selective and strong reduction of those resonances (Figure 4.2, red line).
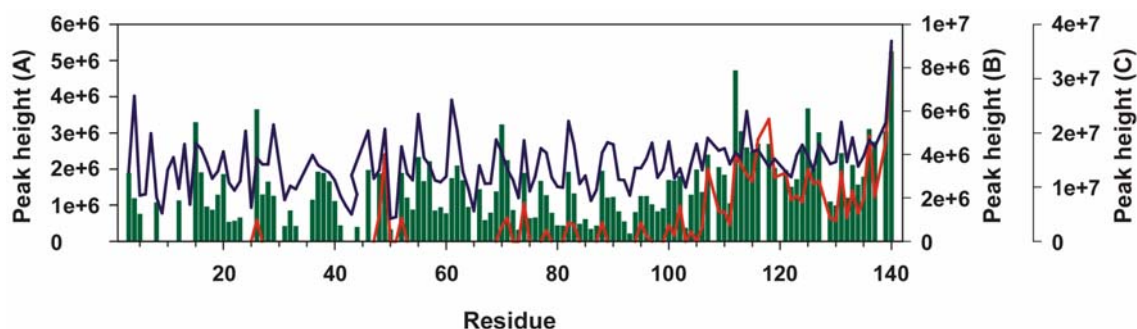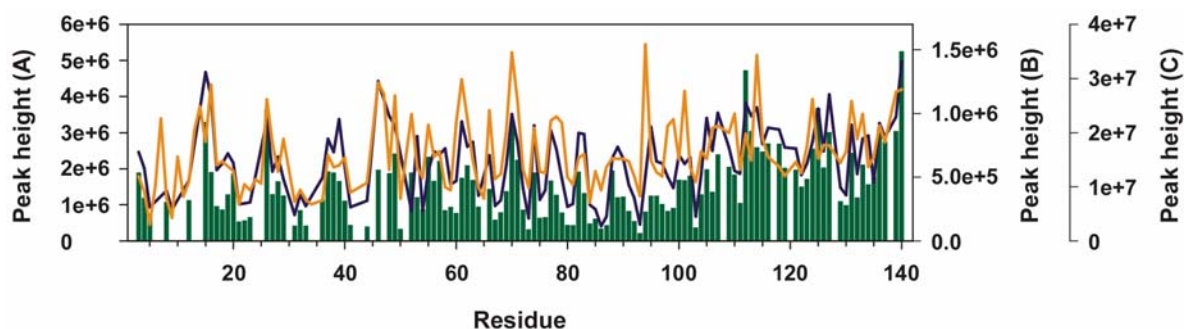
**Figure 4.2. Peak height profile for αS (I).** Peak intensity plot of amide backbone resonances from the spectra of αS acquired at different solution conditions. **A**: pH 7.4, 288 K (green bars). **B**: pH 6.5, 288 K (blue line). **C**: pH 7.4, 320 K (red line). Several resonances feature reduced intensities, which are not residue-specific (see text). However highest resonances at the N-terminus correspond to Val residues (Val[3], Val[15], Val[26], Val[37], Val[40], Val[52], Val[55], Val[66], Val[70]). Number of scans for acquisition were not similar in all the three experiments, thus peak height scales are set at equivalent maximum (resonance corresponding to Ala[140] in all cases).

There are two possibilities to explain the temperature-induced changes, one in terms of the size of the ensemble of conformations populated by αS, and the other assuming a modulation of the dynamics of partition between conformers of the ensemble. The first line of reasoning would suggest that the backbone of αS samples a restricted number of conformations at physiological pH and low temperature, since most of the peaks are observed (~ 80% at pH 7.4 and 310K), while a wider ensemble of conformations is accessible at high temperature as the total energy of the system significantly increases, und thus resonances become broadener (~ 20% at pH 7.4 and 320 K). The second hypothesis would state that the ensemble of conformations remains identical, but at higher temperatures a greater extent of partitioning between different conformers is achieved, leading to lower signal intensities. Either mechanism would displace the equilibrium towards conformations of the protein that are not significantly populated at native conditions. For αS it was found that increasing the temperature of incubation to 47 °C caused a radical acceleration of the self-assembly process of the protein, and fibrils form more rapidly ($t_{1/2}$ of 60 h at 37 °C vs. $t_{1/2}$ of 12 h at 47 °C). Thus partition towards amyloidogenic conformers is predicted at these conditions.

A different picture was observed at lower pH. Upon reduction of pH there is a significant change in the exchange rates of amide protons which may account for more residues becoming detectable (~ 95% at pH 6.5). However, chemical shifts perturbations were evidenced surrounding the sole residues which could be titrated at such neutral pH, the N-terminus or the His 50 (Pujato et al., 2005). Therefore, intensity changes may also be

caused by structural re-arrangement involving these residues. Indeed, this event has been found to strongly influence the amyloidogenic properties of αS, since fibrillation rates increased almost 4 fold as the pH of the protein decreased from 7.0 to 6.0 ($t_{1/2}$ of 80 h at pH 7.0 vs. $t_{1/2}$ of 6.5 hs at pH 6.0) (Hoyer et al., 2002). It is likely that in αS a slight change in the pH may facilitate population of particular backbone conformations of the protein.

In line with these findings, the intensity of particular resonances at the N-terminus and NAC region of the protein are enhanced similarly upon polyamine binding to the C-terminus of αS (Fernandez et al., 2004). As observed in figure 4.3 (dark blue line), upon spermine binding, many resonances, mostly corresponding to Thr and Ser residues at the central hydrophobic domain of the protein, increased ~ 2 fold in intensity. The addition of spermine did not perturb the pH of the solution and thus modulation of exchange rates was not the cause of these intensity changes. It is interesting to note that spermine increases nucleation of the aggregation process up to $10^5$ folds, resulting in a fast fibrillation of the protein, and that the hydrophobic region selectively affected is the one responsible to initiate fibrillation (Giasson et al., 2001). Thus conformers with amyloidogenic characteristics are present in the ensemble populated by the protein under physiological conditions, and particular modifications on the protein could unbalance the equilibrium towards conformers with higher tendency to self-associate.



**Figure 4.3. Peak height profile for αS (II).** Plot of peak intensities corresponding to amide backbone resonances from the spectra of αS acquired at different solution conditions. **A**: pH 7.4, 288 K (green bars). **B**: pH 7.4, 288 K, 3 mM spermine (dark blue line). **C**: pH 7.4, 288 K, 8 M urea (orange line). Under these conditions several resonances feature reduced intensities, in particular at the N-terminus and NAC region. Peak height scales are set at equivalent maximum (resonance corresponding to Ala[140] in all cases) due to different number of scans during acquisition.

One hint on the nature of the ensemble of conformers may also be evaluated from the $^1$H-$^{15}$N-HSQC spectrum of αS under the presence of strong denaturing conditions (Urea 8M).

As observed on figure 4.4, the amide crosspeaks do not significantly deviate from those corresponding to the physiological buffer conditions, confirming the absence of secondary structure in αS. What can be noticed is that almost all resonances become very sharp as the denaturant is added (Figure 4.3, orange-line), in a similar manner as evidenced with chemically unfolded structured proteins or molten globules (Wijesinha-Bettoni et al., 2001).

This would suggest that addition of denaturant to a native unfolded protein still causes slight structural perturbations able to re-distribute the ensemble of conformations. In addition, a possible scenario is that the mechanisms by which αS aggregation is triggered could involve population of completely unfolded conformers, as evidenced for many folded proteins (Uversky and Fink, 2004). The mechanisms of urea denaturation are still largely unknown, and it could involve direct binding of urea to the protein surface or indirect perturbation of solvent-mediated hydrophobic interactions, or a combination of these mechanisms.

Altogether, these preliminary data indicate that a conformational change has to occur at the level of the backbone of the protein in order to trigger the transition of the ensemble towards a more aggregation-prone conformational state. It thus can thus be hypothesized that αS, despite lacking a defined secondary structure, is not a random coil polypeptide, a perception leading to the quest for restricted auto-inhibitory conformations in the native unfolded state of the protein. At this juncture we foresee that the application of other NMR techniques for studying the native state of αS would serve to uncover such structural re-arrangements.
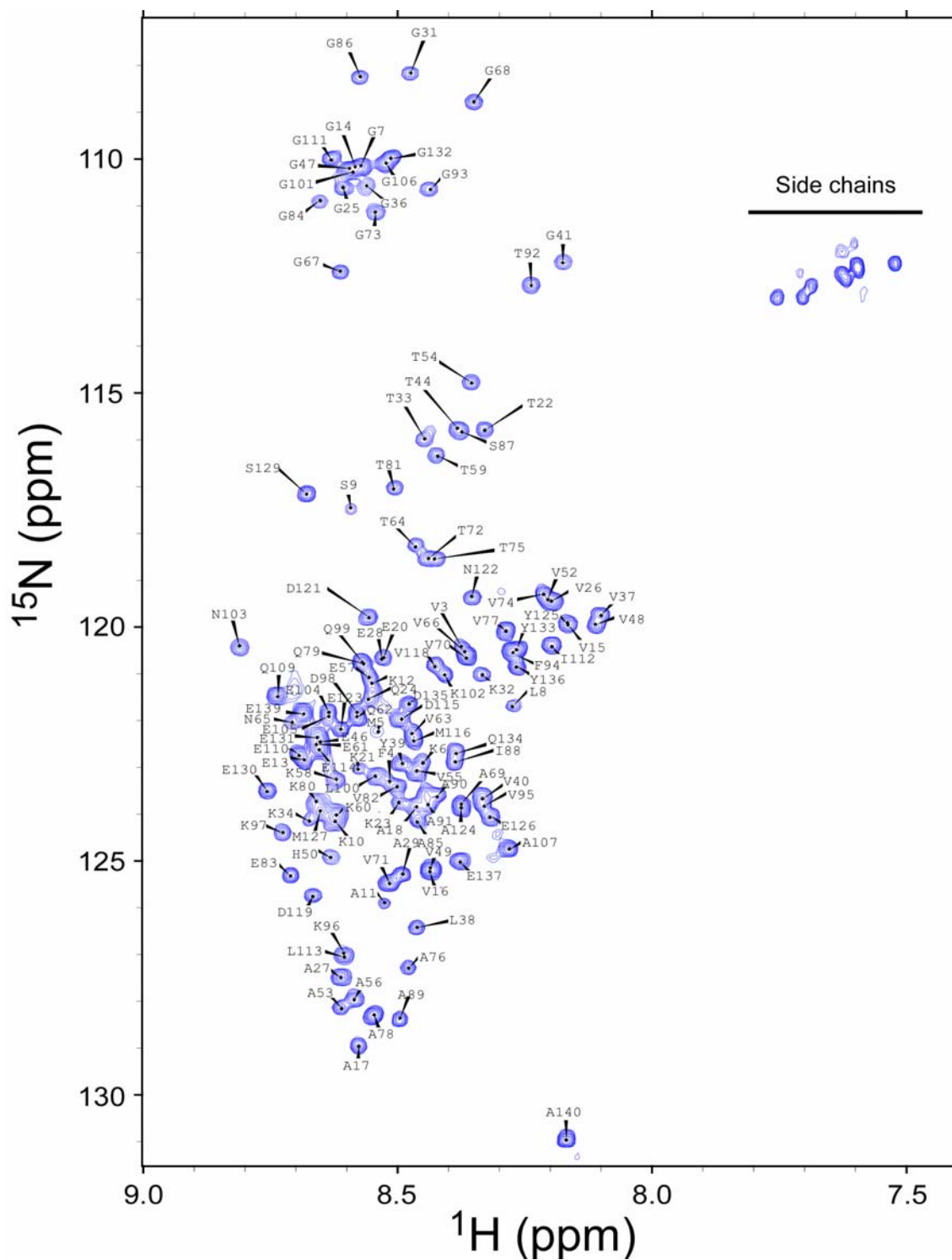
**Figure 4.4. $^1$H-$^{15}$N HSQC spectra of αS in 8 M urea.** An HSQC spectrum of a 100 μM solution of αS protein was acquired at 600 MHz. Solution conditions were buffer A + 8 M urea, and the temperature was 15 °C.

**4.2. Residual dipolar couplings evidence residual structure in native αS.**

The measurement of residual dipolar couplings in a weakly aligned protein, for which the large one-bond internuclear dipolar interactions no longer average to zero, provides long-range orientational information (Tjandra and Bax, 1997). On a folded protein, RDCs report on the orientation of each bond vector relative to the alignment tensor of the entire molecule, while for unfolded proteins, due to the absence of a global alignment tensor, RDCs are attributed to alignment of statistical or valence chain segments, or to transient elements of secondary structure (Louhivuori et al., 2003; Mohana-Borges et al., 2004). In addition, a recent report on a mutant variant of the protein acyl-coenzyme A binding protein (ACBP), showed how RDCs are also reporter on long range interactions in the denatured state (Fieber et al., 2004). Thus RDCs are excellent reporters of residual structure and conformational restrictions in the unfolded states of proteins (Shortle and Ackerman, 2001; Ackerman and Shortle, 2002; Alexandrescu and Kammerer, 2003; Ohnishi et al., 2004).

We decided to apply this technique in the search for structural constraints in the native state of αS, first evaluating whether structural elements could be identified on the protein, and then whether those elements modulate the re-distribution of the ensemble of conformations upon the amyloidogenic conditions reported above. In addition, the use of urea denatured αS will provide a reference frame for the observations.

The measurement of RDCs requires the introduction of a slight anisotropic media into the protein solution, in order to allow the net alignment of a fraction of the molecules respect the externally applied magnetic field. A modification of the HSQC pulse sequence has been implemented in order to measure $^1D_{NH}$ (Ottiger et al., 1998). The so called In-Phase Anti-Phase sequence (IPAP-HSQC), allows measurement of $^1D_{NH}$ as the parallel (positive) and anti-parallel (negative) contributions to the $^1J_{NH}$ scalar coupling, providing better accuracy. Thus $^1J_{NH}$ (~ 93 Hz) are measured in isotropic conditions (absence of alignment media) and $^1D_{NH} + {^1J_{NH}}$ are measured in anisotropic conditions. $^1D_{NH}$ are determined as the difference between the couplings measured in the anisotropic conditions and those determined in the isotropic solution (Figure 4.5).

$^1D_{NH}$ were measured for αS aligned in bacteriophage Pf1 suspensions (Hansen et al., 1998) and in *n*-octyl-penta(ethylene glycol)/octanol ($C_8E_5$) (Rückert and Otting, 2000) (Figure 4.6A). The highly reproducible RDC pattern in the two media and the absence of induced chemical shifts changes indicated that the alignment media did not appreciably perturb the ensemble of conformations (Figure 4.6B).
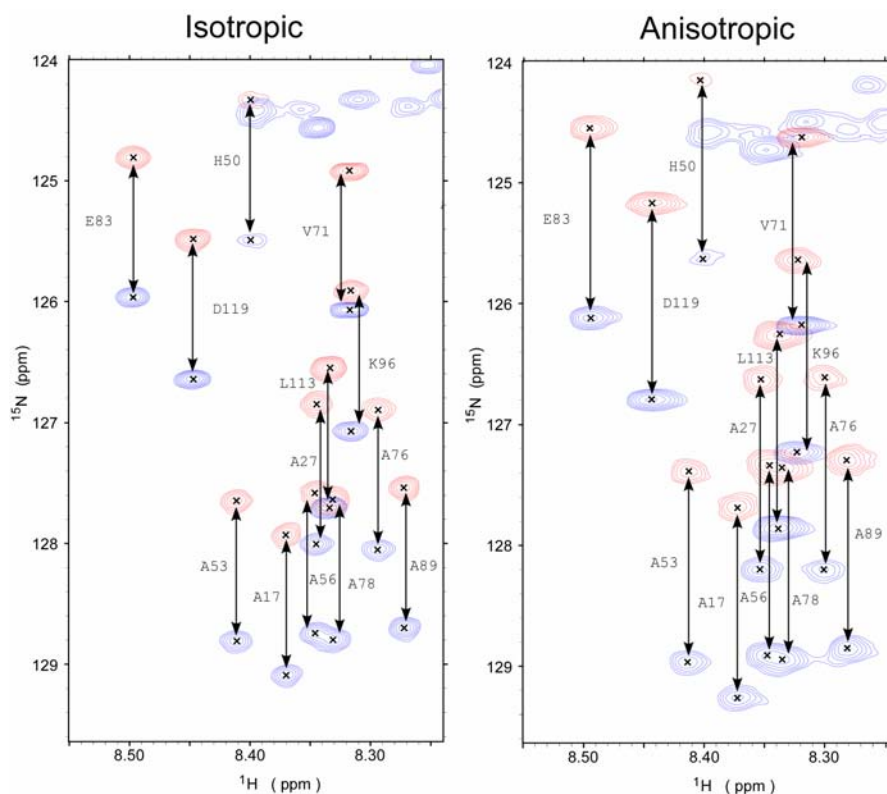
**Figure 4.5. Measurement of RDCs on αS.** IPAP-HSQC spectra of αS in buffer A (isotropic) and aligned in 5mg/ml of Pf1 phages (anisotropic). The In-Phase (blue) and Anti-Phase (red) spectra are overlapped to evidence the increment of the $^1J_{NH}$ coupling due to the residual dipolar coupling $^1D_{NH}$.

In contrast to the bell-like smooth distribution of dipolar couplings expected for a random coil polypeptide chain (Louhivuori et al., 2003), a very specific distribution of positive couplings was observed for αS (Figure 4.6). Five different domains could be identified. The N-terminus is subdivided into two regions with similar RDCs (domain I: residues 1-28; domain II: residues 33-65) with a linker sequence showing couplings close to zero (residues 28-32). The NAC domain (residues 61-95) exhibits large couplings about its central core, is flanked by two regions with reduced RDCs (residues 66-70 and 88-92) and is followed by a fourth domain (IV) comprising residues 95-101. The C-terminus (domain V) displays exceptionally large couplings with two major peaks for residues 115 to 119 and 125 to 129.
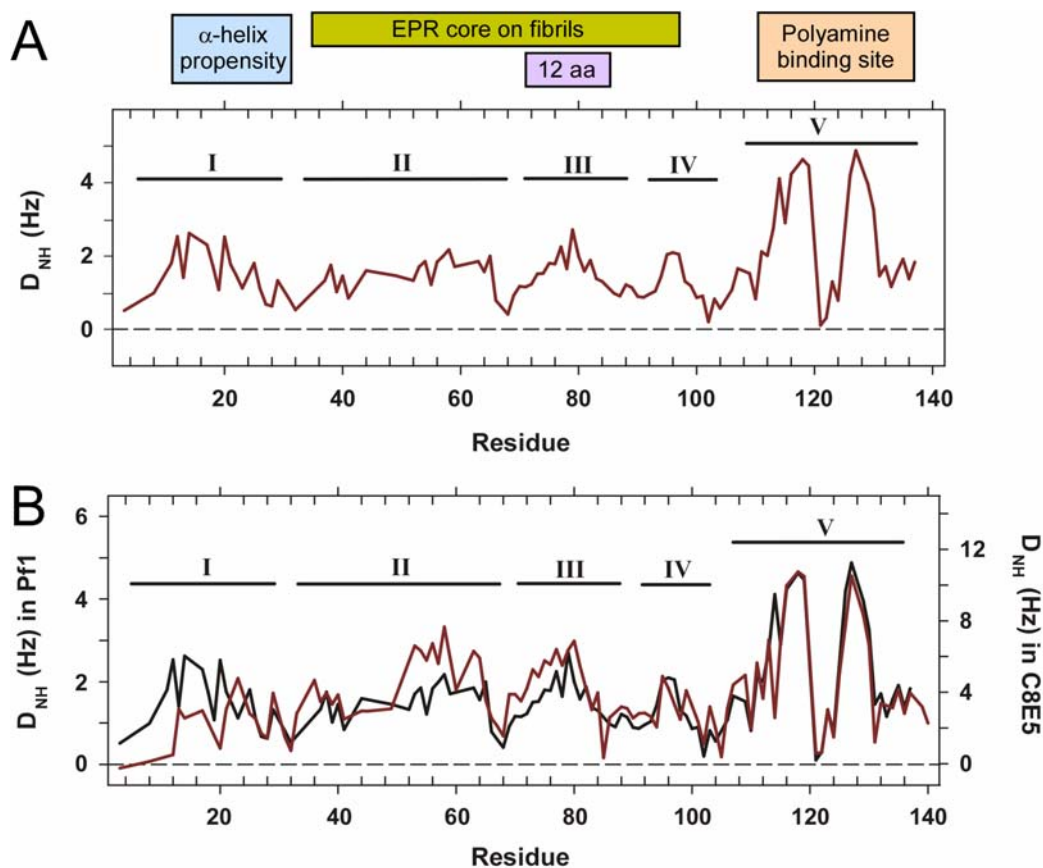
**Figure. 4.6. Residual dipolar couplings in native αS**. $^1D_{NH}$ dipolar couplings measured on αS at 15 °C. **A**. RDCs profile of αS aligned with 5 mg/ml Pf1 (dark red). Five domains with concerted motions are identified by RDCs (I to V). Functional domains of αS are display for comparison with the RDCs derived-domains (Bussell and Eliezer, 2001; Giasson et al., 2001; Der-Sarkissian et al., 2003; Fernandez et al., 2004). **B**. RDCs profile of αS aligned with 5 % $C_8E_5$/octanol mixture (dark red) compared with the couplings profile measured in Pf1 (black line).

The five domains identified by RDCs are consistent with the interpretations of previous biophysical studies (Figure 4.6A, top). A weak α-helical propensity has been determined for the first domain (Bussell and Eliezer, 2001), while RDC domain III overlays with the center of the NAC region. Domains II, III and IV represent the part of αS that is highly ordered in fibrils (Der-Sarkissian et al., 2003) and domain V comprises the polyamine binding site (Fernandez et al., 2004).

The 100 N-terminal residues of αS assume a α-helical conformation upon binding to phospholipid membranes with helix fraying for residues 30 to 42, residues 60 to 65 and 82 to 100 (Chandra et al., 2003). These regions of helix fraying roughly correlate with the hinge regions between RDC domains I and II, II and III and the small RDC domain IV, indicating

that the manner in which αS interacts with membranes is already encoded in its solution state.

Linker regions with couplings close to zero can be rationalized by the presence of residues with predominantly small side chains (Ala[29]-Ala[30]-Gly[31], Gly[67]-Gly[68]-Ala[69] and Ala[89]-Ala[90]-Ala[91]). Local interactions between side chains and the backbone are minimized enabling higher flexibility of the polypeptide backbone and effectively decoupling the five domains exhibiting concerted motion.

Computer simulated RDCs on random coils reported earlier that a flexible polypeptide chain would give a flatten pattern of couplings, but recent refinement of the model including steric hindrance between residues, which limit the main chain $\phi$ and $\psi$ angles, demonstrated that RDCs are indeed sensitive to residue-based conformational restrictions (Louhivuori et al., 2004). Thus local regions with residual structure would adopt a defined alignment and display high RDCs, while stretches of residues with enhanced flexibility would decrease the magnitude of alignment and report lower coupling values. Our observations are in agreement with this theoretical framework, as well as with other experimental evidences (Mohana-Borges et al., 2004).

The highly acidic C-terminus of αS exhibited very large dipolar couplings, which were modulated by the residual structure of this domain. Addition of 4 and 8 M urea progressively decreased the RDC values in this region down to a magnitude similar to the rest of the protein, while other features remained stable (Figure 4.7).
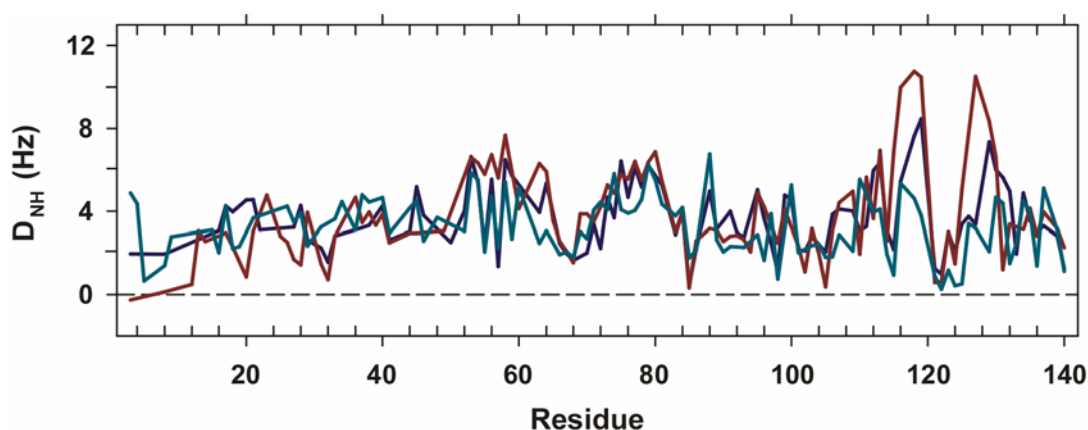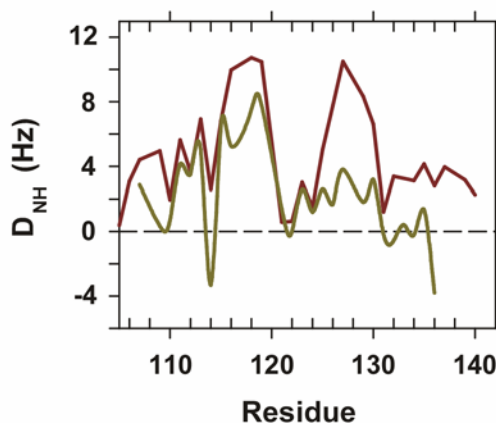


**Figure 4.7. Residual dipolar couplings in urea denatured αS**. $^1D_{NH}$ dipolar couplings measured on αS aligned with 5 % $C_8E_5$/octanol mixture (dark red) and in the presence of 4 M Urea (cyan) and 8 M urea (dark blue).

Since urea mainly abolishes hydrophobic interactions, the RDCs are suggestive of a hydrophobic cluster in the C-terminus involving residues 115 to 119 (Met[116], Val[118]) and 125

to 129 (Tyr[125], Met[127]). The 30 % smaller RDC values for residues 75 to 81 in 8 M urea (Figure 4.7) and the strong paramagnetic broadening of the C-terminus for the A90C mutant (see below), identify the hydrophobic NAC region as major contributor.

Additional information about the long-range nature of the hydrophobic cluster was derived from RDCs measured for a C-terminal peptide of αS (residues 105-136). Although the overall RDC patterns for the peptide and the full-length protein were similar (Figure 4.8), the two regions showing very large RDCs in case of the full-length protein were reduced, particularly for residues 125-129, suggesting that long-range interactions with other domains of the protein serve to stabilize this intrinsic structure.

[105] EGAPQEGILEDMPVDPDNEAYEMPSEEGYQDY [136]



**Figure. 4.8. Residual dipolar couplings of an αS C-terminal peptide.** A peptide comprising residues 105 to 136 from αS was synthesized and $^1D_{NH}$ dipolar couplings were measured for the peptide aligned in 5 % $C_8E_5$/octanol mixture (dark yellow). Couplings are compared with RDCs from the C-terminal region obtained under the same alignment condition of the full length αS protein (dark red).

**4.3 Paramagnetic resonance enhancement on αS detects long range interactions.**

The identification of long range interactions in αS by RDCs prompt us to investigate further the occurrence of such contacts between different domains of the protein employing NMR paramagnetic resonance enhancement (PRE) by nitroxide spin labels. Site-directed spin labeling by nitroxide tags provides a valuable tool for determining long-range structure in denatured states of proteins, and has been widely used to study characteristics of the ensemble of conformations in folding intermediates (Gillespie and Shortle, 1997a; Lietzow et al., 2002; Teilum et al., 2002; Lindorff-Larsen et al., 2004). The interaction between a specifically attached paramagnetic nitroxide radical and nearby (< ~25 Å) protons causes broadening of their NMR signals due to an increase in transverse relaxation rate (Gillespie

and Shortle, 1997a). This effect has an $r^{-6}$ dependence on the electron–proton distance and thus allows the detection of long-range interactions in proteins.

To provide a specific attachment of the nitroxide probe, Cys-reacting derivatives, as maleimides or iodoacetamides are employed. Since the primary sequence of αS lacks cysteine, three different cysteine-containing mutants (A18C, A90C and A140C) were constructed in order to provide attachment points for the nitroxide radical MTSL (maleimide). The design of the mutants was biased towards proving the interactions evidenced by RDCs, but taking care in not disrupting those (A90C and A140C mutants), while the selection of the A18C was intend to report on structural changes on the N-terminus of the protein. Neither the mere introduction of these mutations nor the addition of the MTSL radical modified the hydrodynamic radii or altered the time course of aggregation for αS (Figure 4.9). In addition, the RDCs pattern for A18C was not significantly perturbed besides the site of mutation (Chapter 2).
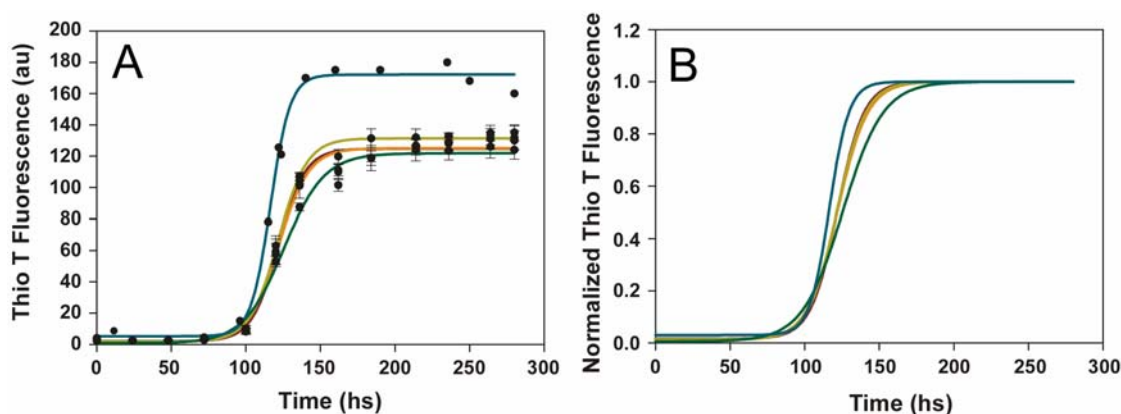


**Figure 4.9. Aggregation kinetics for αS Cys-containing mutants. A**. ThioT traces for the time-dependent aggregation of αS wt (dark red), A18C (orange), A90C (dark yellow), A140C (dark green) and A140C-MTSL labeled (cyan). Solution conditions were buffer A plus 100 μM DTT, except for the MTSL labeled mutant. A higher ThioT fluorescence for the sample containing MTSL was evidence from the starting of the assay, and could be attributed to an interaction between the dye and the paramagnetic tag. **B**. Normalized kinetic traces for the samples shown in A. The average half time of aggregation was 120 hs ± 5 hs, suggesting that the mutations do not perturb the fibrillation pathway of the wt protein.

In order to quantitatively assess the paramagnetic effect cause by the nitroxide tag, peak intensity ratios between two $^{15}$N-$^1$H HSQC NMR spectra, i.e. in the presence and absence of the nitroxide radical ($I_{param}/I_{diam}$), are determined, which permits the estimation of distances between the spin-label and the affected amide protons in the protein (Lietzow et al., 2002; Teilum et al., 2002). As observed in figure 4.10 for the A90C mutant, the paramagnetic

effect caused a distance-dependent broadening of amide resonances, which is reflected as a reduction of the peak heights.
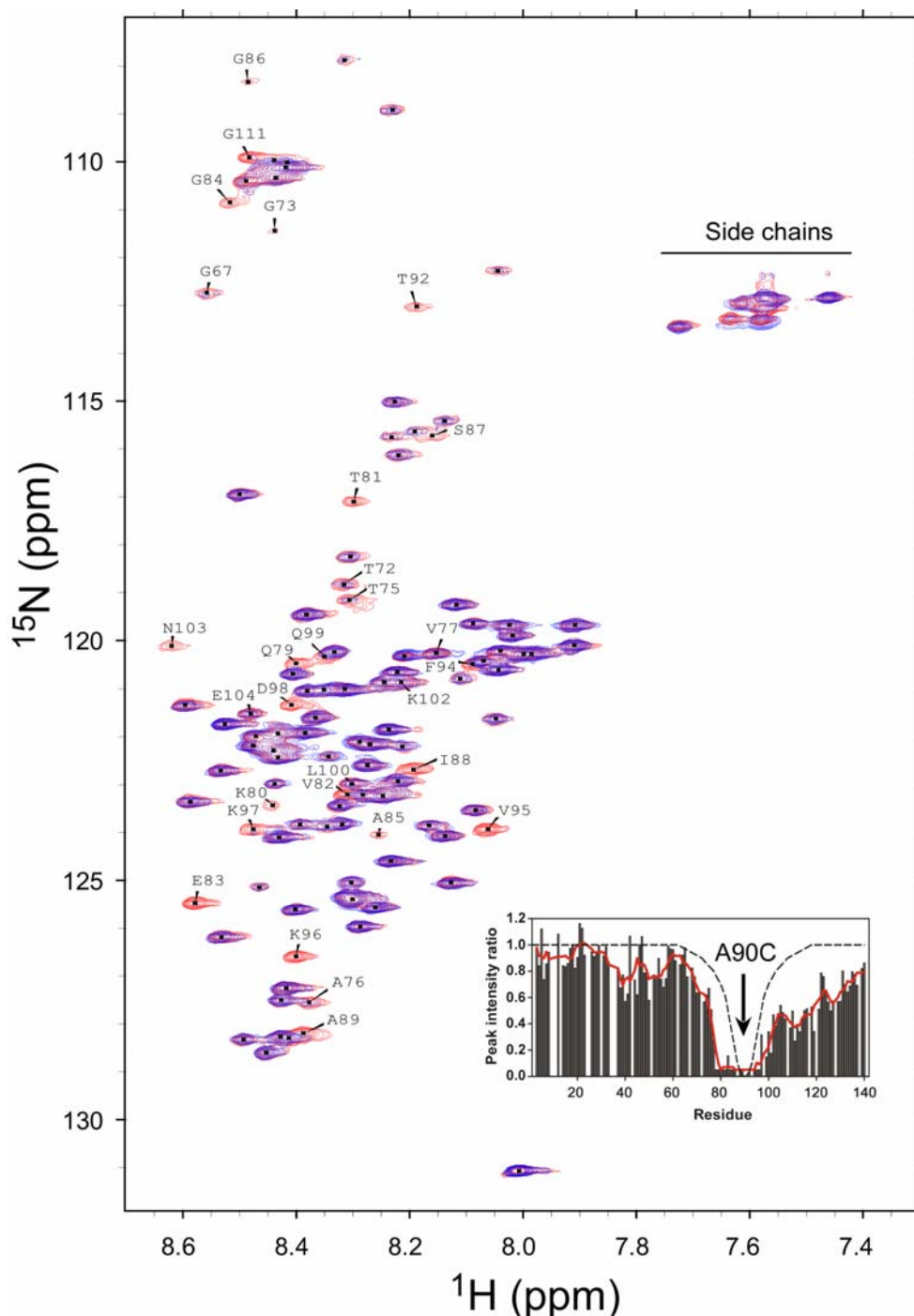


**Figure 4.10. PRE effect on αS-A90C.** The Cys containing mutant of αS (A90C) was labeled with the nitroxide spin label MTSL and $^1$H-$^{15}$N-HSQC spectra were acquired in the presence (blue) and absence (red) of the paramagnetic tag, resulting in the selective disappearance of peaks in the close vicinity of the probe. Ratios of peak intensities between both conditions ($I_{param}/I_{diam}$) are plotted (black bars) and compared with the profile expected for a random coil polypeptide (black dashed line). Deviations from the coil state reflect chain compaction or long range contacts. In

red a mobile 5 residue average of the peak intensity ratio is plotted to account for small fluctuations in the measured values.

For a random coil polypeptide the PRE effects would be expected to be restrained to the close vicinity of the attachment site (up to ~ 15 residues), and only upon chain compaction or long range interactions the effect would reach other resonances. Such features are reflected in the broadening effect caused by the nitroxide radical on the NMR spectra for the three studied Cys positions, as follows:

(i)     The profile of intensity ratios for the A18C mutant showed a broad paramagnetic effect extending to residue 60 and long-range interactions with the C-terminal residues 115 to 140 (Figure 4.11A).

(ii)    The paramagnetic tag at residue 90 strongly reduced the intensity ratios for all C-terminal residues (Figure 4.11B).

(iii)   The A140C mutant showed an unbroadened core in the C-terminus (residues 110-125), but a considerable PRE effect was present in the central region of the protein (residues 80-100) (Figure 4.11C).

Addition of 8 M urea led to a restriction of paramagnetic broadening to 15 residues from the position of the nitroxide radical (Figure 4.11D and 4.11E), indicating that the protein was fully unfolded. Interestingly, in the case of the A18C a considerable paramagnetic effect on the C-terminus remained even under strong denaturant conditions. The extended relaxation enhancement observed in urea for the A140C (Figure 4.11F) was likely due to the very high flexibility of the C-terminal residue (Teilum et al., 2002).
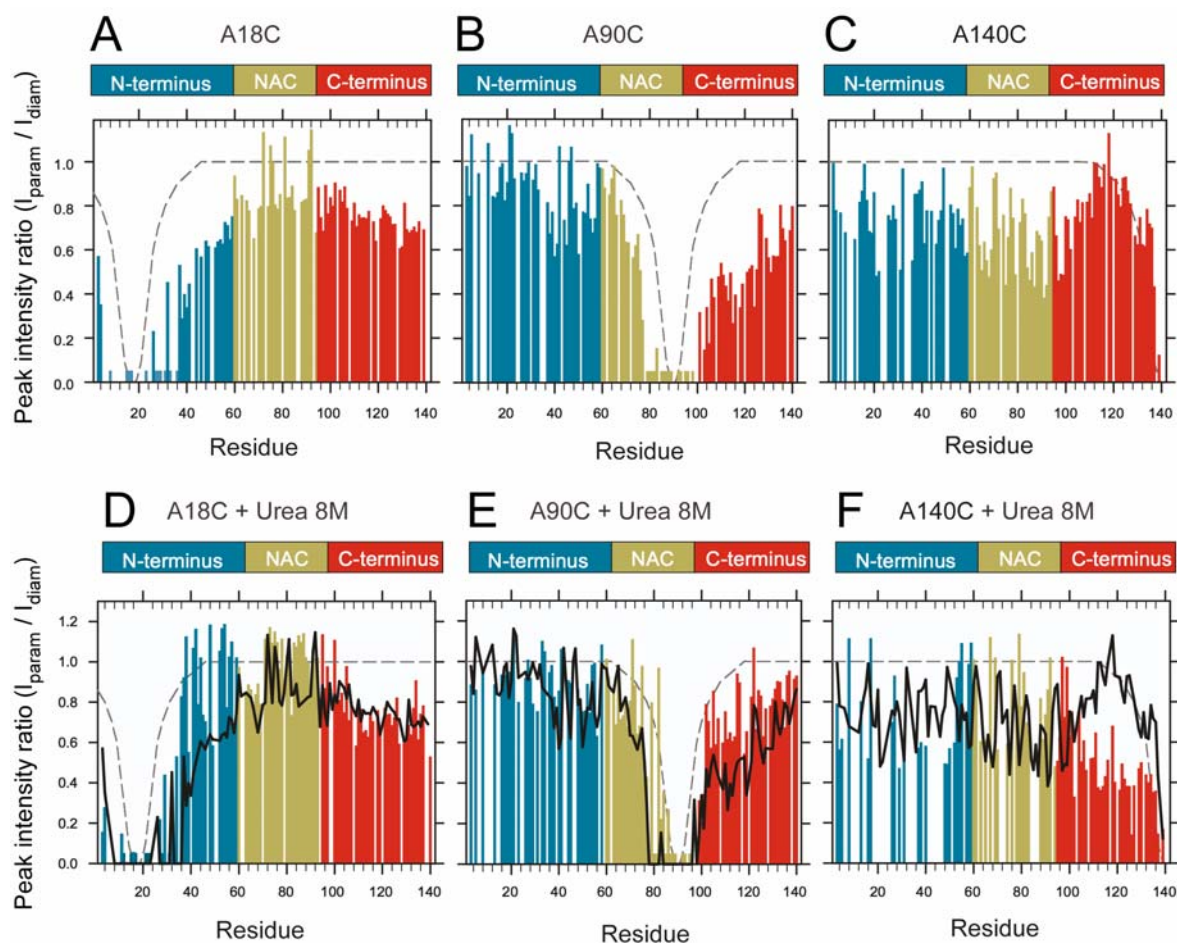
**Figure 4.11. Paramagnetic relaxation enhancement of amide protons in spin-labeled αS.** Three cysteine mutants of αS (A18C, A90C and A140C) were labeled with MTSL. HSQC spectra in the presence (paramagnetic) and absence (diamagnetic) of spin label were recorded at 15 °C and the intensity ratio ($I_{param}/I_{diam}$) of the resonance peaks was determined. **A, B and C.** MTSL-labeled cysteine mutants of αS in buffer A (colored bars). **D, E and F.** MTSL-labeled cysteine mutants of αS in buffer A + 8 M urea (colored bars), and the corresponding mutants of αS in buffer A (bold black line). Dashed grey lines indicate paramagnetic effects expected for a random coil polypeptide with the paramagnetic tag in the same position as the αS mutant (Teilum et al., 2002).

## 4.4. A conformational ensemble representative of the native state of αS.

In order to determine an ensemble of conformations consistent with the PRE measurements, intensity ratios were converted into distance restraints. Inasmuch as large errors are associated with distances calculated from PRE data and intensity ratios are averages over a broad ensemble of structures, the calculated distances were employed as semi-quantitative restraints in structure calculations using Xplor-NIH (Gillespie and Shortle, 1997a; Schwieters et al., 2003). The seven most representative conformations of the native state of αS are shown in figure 4.12A.
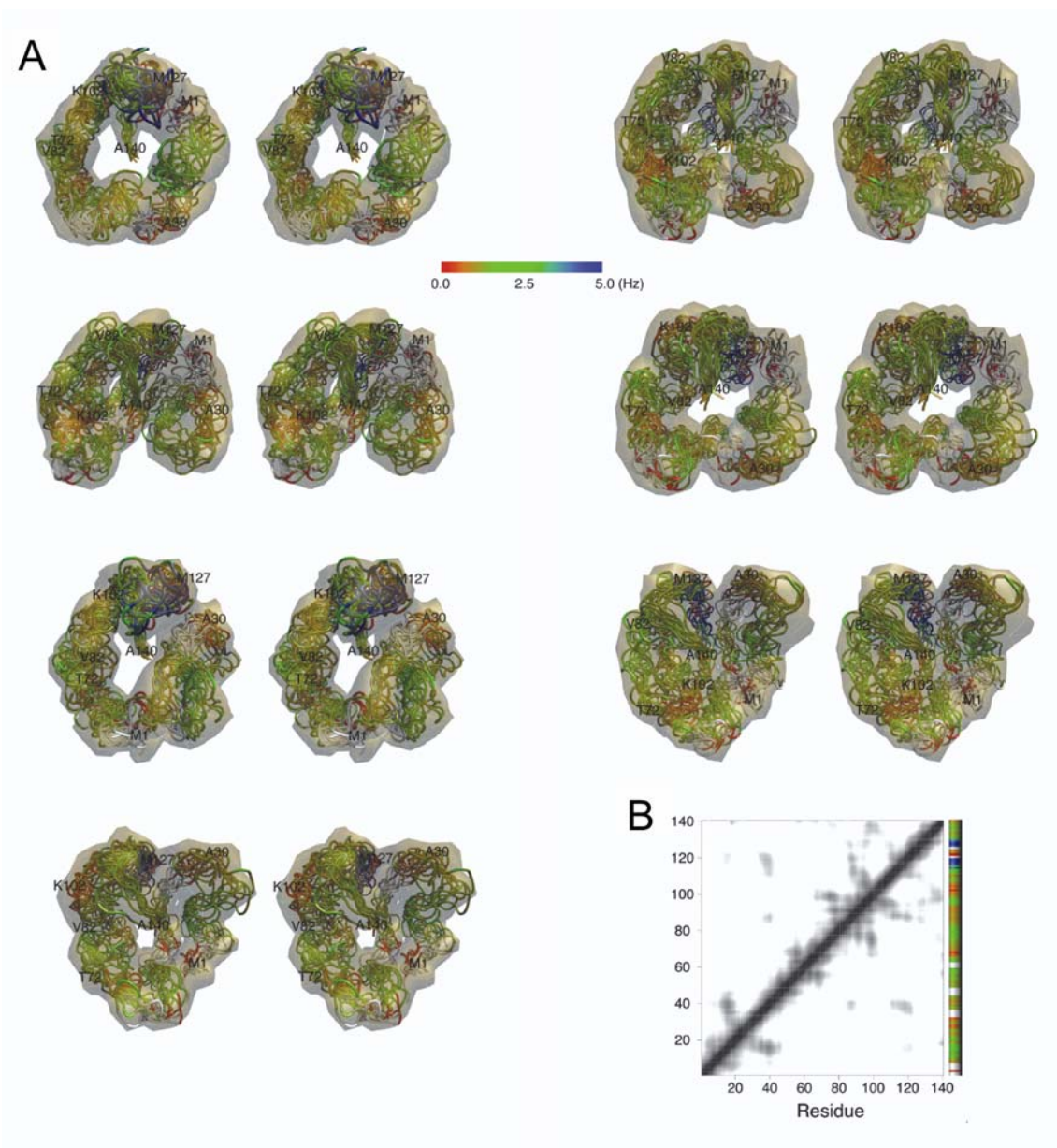
**Figure 4.12. Structural models for native state conformations of αS.** Representation of the native state of αS calculated from paramagnetic relaxation enhancement data. **A**. Shown are the seven most populated clusters containing 80, 75, 46, 39, 25, 24 and 20 structures representing 50 % of all calculated conformations. The ten lowest energy structures of each cluster within an atomic density map (Schwieters and Clore, 2002) calculated from all conformations contained in each cluster are shown. Residual dipolar couplings were mapped onto the structures with the use of a continuous color scale. **B**. Average contact map for the centre structures of the seven most populated clusters representing 50% of all calculated conformations. A continuous grey scale from 3 Å (black) to 22 Å (white) is used. Residual dipolar couplings as a function of residue number are indicated by a color bar ranging from 0 Hz (red) to 5 Hz (blue).

The calculated structures represent temporal and distance-averages over an ensemble of conformations, and thus may combine structural features that may not necessarily coexist

in a given molecule and at a given time. In particular, calculated structures are overly compact due to the $r^{-6}$ distance dependence of paramagnetic broadening.

Favorable long-range interactions were extracted by an average contact map calculated from the centre structures of these seven clusters representing 50% of 630 calculated structures (Figure 4.12B). The most important interaction is a hydrophobic cluster that comprises the C-terminal part of the highly hydrophobic NAC region (residues 85-95) and the C-terminus (residues 110-130), probably mediated by $Met^{116}$, $Val^{118}$, $Tyr^{125}$ and $Met^{127}$. Within the C-terminal domain residues 120 to 130 contact residues 105 to 115, and the region about residue 120 also interacts with the N-terminus about residue 20.

The influence of the chosen computational strategy was tested by additional structure calculations using Rosetta (Figure 4.13B), in which hydrophobic burial and strand pairing as well as satisfaction of PRE restraints were favored (Simons et al., 1997; Bowers et al., 2000).
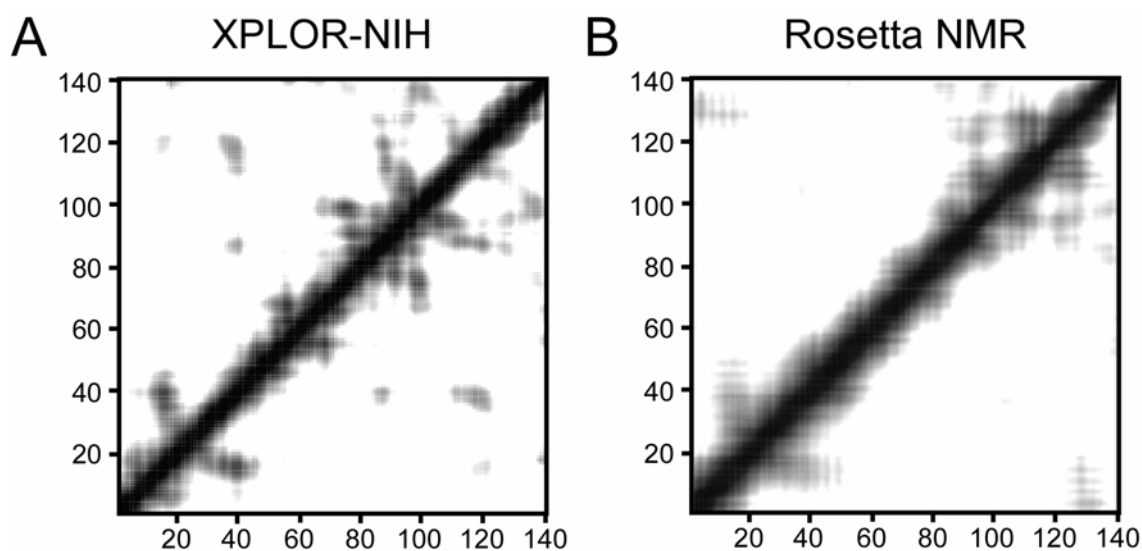


**Figure 4.13. Contact maps for the native state conformations of αS.** Comparison of the computational strategy on determining PRE derived structures. The average contact maps for the centre structures of the seven most populated clusters calculated with XPLOR-NIH (**A**) and RosettaNmr (**B**) are shown. The seven clusters comprise 50 %(**A**) and 80% (**B**) of all calculated structures. A continuous grey scale from 3 Å (black) to 22 Å (white) is used.

These interactions presumably seem to inhibit spontaneous αS oligomerization and are compatible with the influence in fibrillation exerted by methionine oxidation, tyrosine nitration and phosphorylation of $Ser^{129}$ (Fujiwara et al., 2002; Norris et al., 2003). Furthermore, shielding of the hydrophobic NAC region explains why the C-terminal acidic tail functions as a solubilizing domain for αS (Souza et al., 2000) and truncated αS is more amyloidogenic than the full-length protein (Crowther et al., 1998). The compact state of

native αS also involves a turn in the N-terminus of the molecule (residues 20 to 30). This turn favors an ensemble of structures in which domain I, identified by RDCs (Figure 4.6), folds back onto domain II, a conformation that could be stabilized by the partial α-helical character of domain I (Bussell and Eliezer, 2001). Dipolar couplings provide further support for key features visible in the calculated structures. Turn regions are mainly associated with small RDCs indicative of increased flexibility (e.g. residues 26-32), whereas more extended parts correspond to regions with large dipolar couplings (e.g. residues 72-82). The largest RDCs are located in the most compact structural region (residues 110-130) (Figure 4.6).

### 4.5. Polyamine binding releases long-range interactions in αS.

To address the functional relevance of these long-range, intramolecular interactions, we performed the same set of experiments as performed for the native state of the protein, but now for the previously examined conditions favoring aggregation, namely polycation binding, increased temperature and reduced pH.

The polycation spermine is a naturally occurring polyamine that increases the kinetic efficiency of αS aggregation by 105 due to a specific interaction with the C-terminus of the protein (Fernandez et al., 2004). There was a general change in the PRE profiles of the three Cys-containing mutants upon addition of spermine. In particular the PRE effects of residues 18 to 60 (A18C mutant) were considerably reduced (Figure 4.14A), demonstrating that binding of polyamines to the C-terminal domain causes a release of the N-terminus and suggesting an opening of the αS structure. This phenomenon is also consistent with the intensity increases of NMR signals of residues 22 to 93 resulting from polyamine binding (Figure 4.3) (Fernandez et al., 2004).

For the A90C mutant, binding of spermine led to a minimization of paramagnetic broadening in the C-terminus, achieving a profile similar to that of the denatured state in 8 M urea (Figures 4.10E vs. Figure 4.13B). According to the A140C data, the presence of spermine also reduced the compactness of the region between residues 110 to 125 (Figure 4.13C). Broadening in other regions of the protein reflects the increased flexibility of the C-terminus and residual N-terminus/C-terminus interaction.
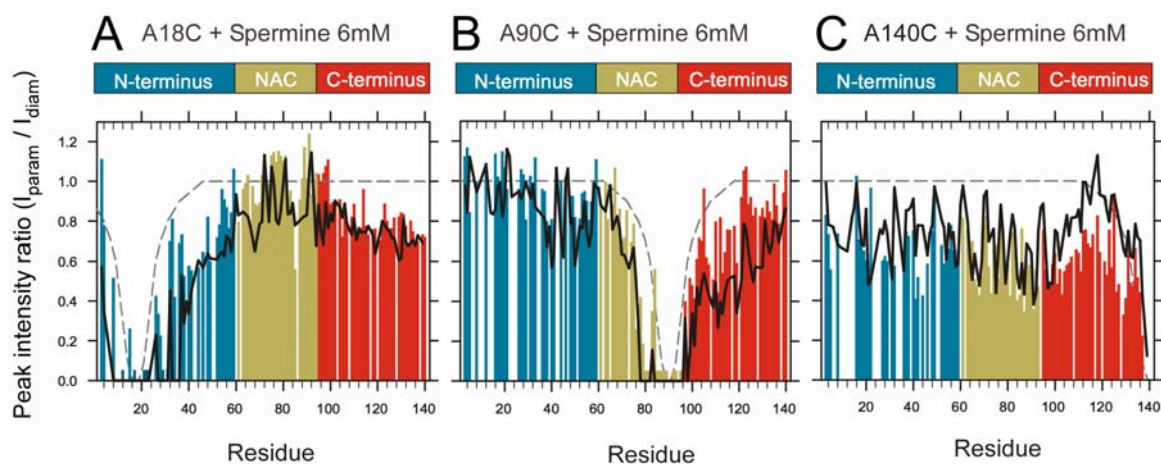
**Figure 4.14. PRE on polyamine-liganded spin-labeled αS.** Intensity ratios between paramagnetic and diamagnetic states ($I_{param}/I_{diam}$) for amide resonance peaks corresponding to A18C (**A**), A90C (**B**) and A140C (**C**) cysteine mutants of αS labeled with MTSL and in the presence of 6mM Spermine (+4). Colored bars correspond to the intensity ratios measured in the experiment and are compared with the profile corresponding to the same mutants of αS in the absence of the polycation (bold black line). Dashed grey lines indicate paramagnetic effects expected for a random coil polypeptide with the paramagnetic tag in the same position as the αS mutant.

In line with these findings, the large RDCs observed for the C-terminus of the protein were reduced in the presence of polyamines (Figure 4.15). Greater polyamine charge – putrescine (+2) < spermidine (+3) < spermine (+4) – correlated with a stronger reduction in $^1D_{NH}$ values, as well as with an enhancement of fibrillation (Fernandez et al., 2004).

In addition, binding of spermine to the C-terminus reduced RDCs for residues 12 to 26 by about 60 % indicating a long-range effect with the N-terminus, in agreement with intensity increases of NMR signals of residues 22 to 93 upon from polyamine binding (Fernandez et al., 2004). Such a decrease was not observed upon addition of urea, pointing to an electrostatic interaction between the negatively charged C- and the positively charged N-terminus. The persistent paramagnetic broadening in the C-terminus for the A18C mutant (Figure 4.13D) indicates that the N-terminus/C-terminus interaction is not abolished upon addition of polyamines but only weakened, and that RDCs and PREs possess different sensitivities to the strength of long-range interactions.
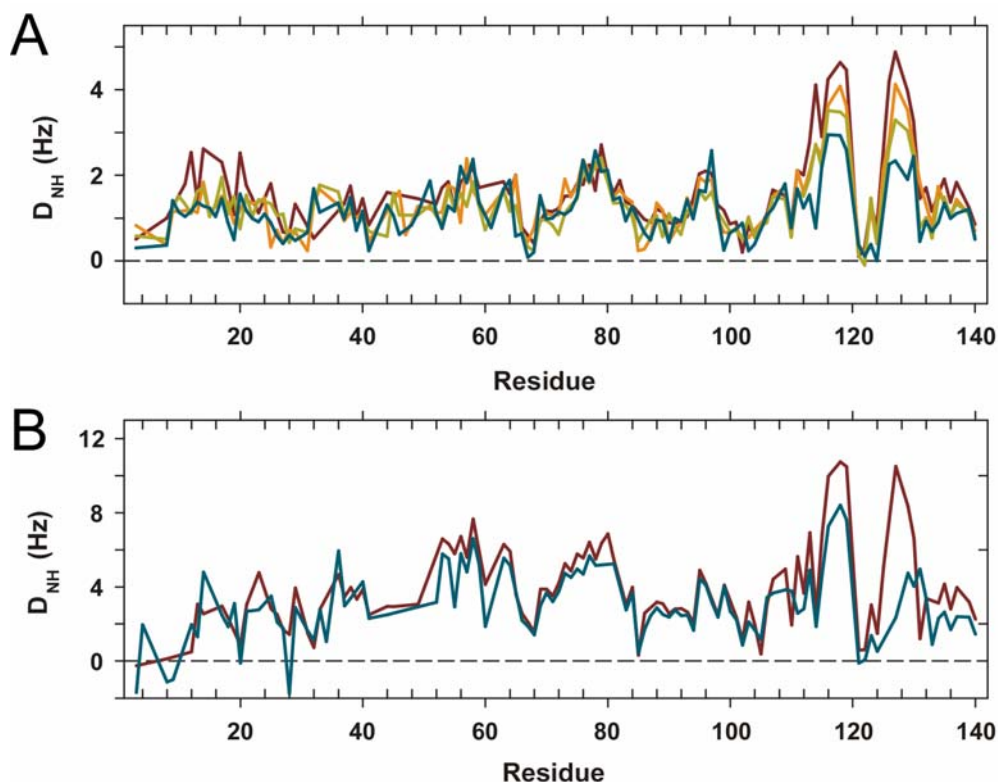
**Figure. 4.15. Residual dipolar couplings in polyamine-bound αS. A**. $^1D_{NH}$ dipolar couplings measured on αS aligned with 5 mg/ml Pf1 phage solution in buffer A (dark red), and in the presence of 3 mM putrescine (+2) (orange), 3 mM spermidine (+3) (green) and 3 mM spermine (+4) (cyan). **B**. RDCs measured for in 5 % $C_8E_5$/octanol mixture for αS alone (dark red) and in the presence of 3mM spermine (+4) (cyan).

We further investigated whether hydrodynamic properties of the protein were affected upon polyamine binding, as suggested by the PRE profiles. By means of pulse-field gradient NMR it is possible to estimate the diffusion coefficient of polypeptides, and thus derive their hydrodynamic radius (Rh) by comparison with standards of known size (Wilkins et al., 1999). Empirical relationships have been derived by using these method, which relate the length of a polypeptide chain protein with its hydrodynamic radii at folded ($R_n = 4.75 \times N^{0.29}$ Å) and unfolded ($R_d = 2.21 \times N^{0.57}$ Å) states. Thus, according to its 140 amino acids, the expected size for a collapsed state of αS would be 18 Å, while the completely unfolded state would reach 34 Å.

Our determinations, showed on figure 4.16, demonstrated that αS populates relatively compact conformations at physiological pH (Rh of 29.3 Å), and that it radius increases upon addition of 100 mM NaCl (Rh of 31.9 Å), which is in accordance with a ~ 2-3 fold increase on the rate of aggregation of αS in the presence of salt (Hoyer et al., 2002; Hoyer et al., 2004).
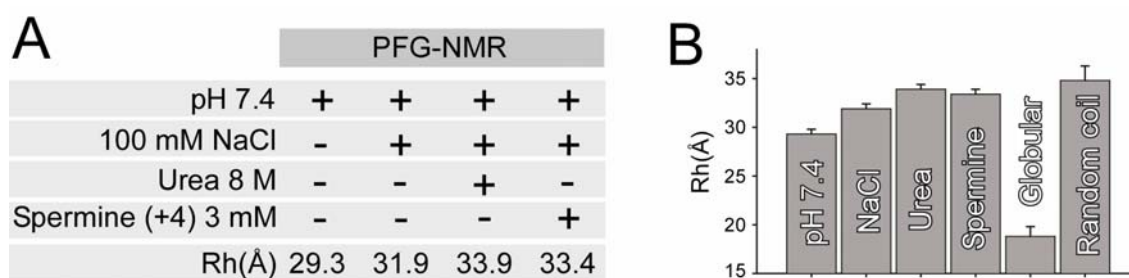
**Figure 4.16. PFG-NMR measurement of hydrodynamic properties of αS under different solution conditions. A**. Hydrodynamic radius (Rh) of αS was measured by PFG-NMR under the following conditions: pH 7.4, 100 mM NaCl, urea 8M and spermine 3mM. **B**. Comparison of Rh determinations for αS with the dimensions expected for a globular protein or a random coil polypeptide of 140 residues. Errors in the determination are within 2%.

Upon polyamine binding we evidenced a significant increase in the apparent size of the conformations populated by αS (Rg of 33.4 Å), dimensions similar to those determined for the urea denatured state of the protein (Rg of 33.9 Å). This suggests that upon conditions that significantly impair long range interactions there is a concurrent increase in the hydrodynamic dimensions of the ensemble of conformations populated by αS. This could be rationalized in terms of adoption of more extended structures, as probed by PREs (Figures 4.11 and 4.14) and due to an increment on the dynamics of the backbone of the polypeptide chain, as probed by RDCs (Figures 4.6 and 4.15).

Taking together, these data demonstrate that long-range interactions involving the C-terminus and the NAC region, presumably of hydrophobic nature, as well as with the N-terminus, acting via electrostatic interactions, protect αS from oligomerization. Docking of polycations to the C-terminus destabilizes these interactions. The high free energy of the extended conformation, in which the hydrophobic NAC region is exposed to the solvent, would favor the association of monomers, thereby increasing the extent of both the nucleation and propagation steps of aggregation (Fernandez et al., 2004).

**4.6. The residual structure of native αS is lost at elevated temperatures**.

The rate of fibrillation increases when αS is incubated at increasing temperatures (Uversky et al., 2001b), and we have already hints that suggest a re-distribution of the ensembles of conformations at higher temperatures, as amide resonances of αS are strongly affected, and several cross-peaks, in particular those corresponding to the central region of the protein are vanished from the spectrum (Figure 4.2 and 4.17A). We therefore measured RDCs and PREs

on αS at high temperatures in order to characterize the features of the conformers populated at this condition.

A comparison of RDCs measured at 15 °C and 37 °C showed a strong perturbation of the polypeptide backbone upon increment of the temperature (Figure 4.17C). Due to the lack of adequate signal-to-noise ratio, few data points were able to be sampled at the N-terminus and NAC region. Nevertheless it was observed that couplings at the NAC region were reduced, while a decrease in the coupling values for both sub-domains of the C-terminus was evidenced. Measurement of RDCs at higher temperatures (47 °C) were attempted, but were not suited due to the high aggregation tendency of protein combined with the long acquisition times required for the experiment (~ 20 h). However, this result correlated well with further evidence obtained from PRE studies on the A90C mutant. At 37 °C the paramagnetic effect on the C-terminus was only slightly perturbed at 15 °C, while at 47 °C, virtually no paramagnetic broadening remained for resonances beyond residue 105 (Figure 4.17.B).

It can be concluded that at 37 °C the ensemble of conformations that is populated display a more loose long range interaction between the NAC region and the C-terminus, according to the RDC data, although is not completely abolished, as reported by the PRE data. As the temperature is increased further, the C-terminus of αS adopts a fully extended conformation, similar to the one achieved upon addition of denaturant or polycation. It is noteworthy that are 37 °C the changes in RDCs are already evident, but the PRE broadening remains unchanged. This result is in agreement with the proposal that destabilization of long-range interactions initially releases the stiffness of the polypeptide chain (as probed by the decrease in RDCs) followed by an opening of the tertiary structure (as monitored by PRE effects). We further conclude that RDCs provide a very powerful tool for probing structural transitions in unfolded proteins.
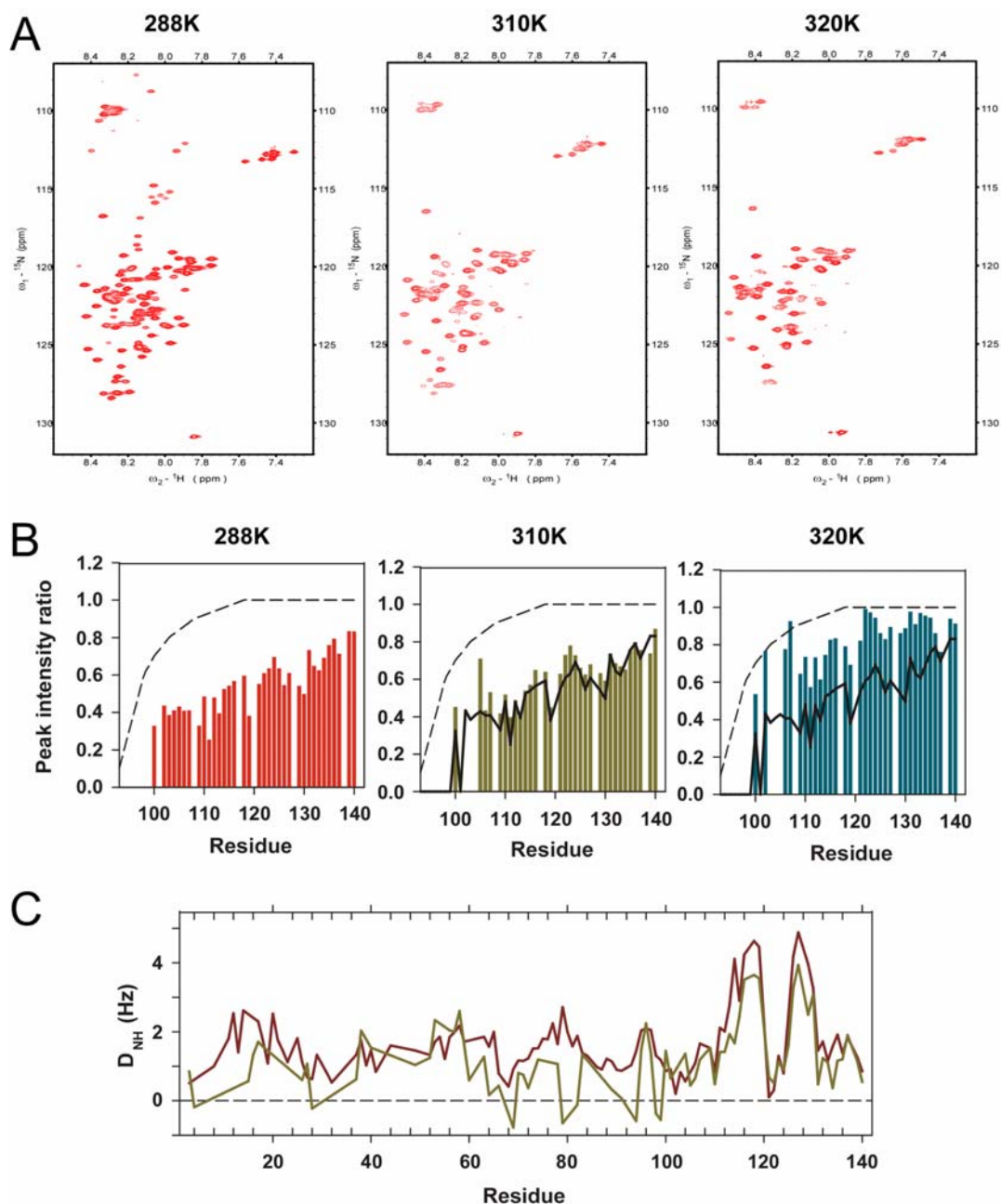
**Figure 4.17. Temperature-induced structural changes in αS. A**. 1H-15N HSQC spectra for αS acquired at 15 °C (288 K), 37 °C (310 K) and 47 °C (320 K). **B**. PRE effect on amide protons for MTSL labeled αS A90C, at increasing temperatures 15 °C (288 K, red bars), 37 °C (310 K, green bars) and 47 °C (320 K, blue bars). At 37 °C and 47 °C the PRE effect at 15 °C is depicted for comparison in bold black line. Dashed grey lines indicate paramagnetic effects expected for a random coil polypeptide with the paramagnetic tag in the same position as the αS mutant. **C**. RDCs profile for αS aligned in 5 mg/ml Pf1 at 15 °C (dark red) and at 37 °C (dark yellow).

**4.7. αS populates a native-like destabilized conformation at pH 6.5.**

The last condition earlier evidenced to cause changes in the intensity of signals and with polyamines and temperature may have consequences in the redistribution of the ensemble of αS conformers is pH. A strong reduction in the pH of the solution was reported by our group to have drastic consequences on the aggregation of the protein (Hoyer et al., 2002). We further studied the effect of such slight decrease in the pH of the solution in the aggregation properties of the protein. As evidenced on figure 4.18, there was a significant reduction in the half time for aggregation at pH 6.5 when compared with pH 7.5 (~ 40 h at pH 6.5 vs. ~ 58 h at pH 7.4). No differences in the lag times for aggregation were observed (~ 20 h for both conditions), but a 2-fold increase in the $k_{app}$ (rate constant for monomer addition) was calculated, suggesting that αS at pH 6.5 is incorporated into fibrils more rapidly than at pH 7.4.
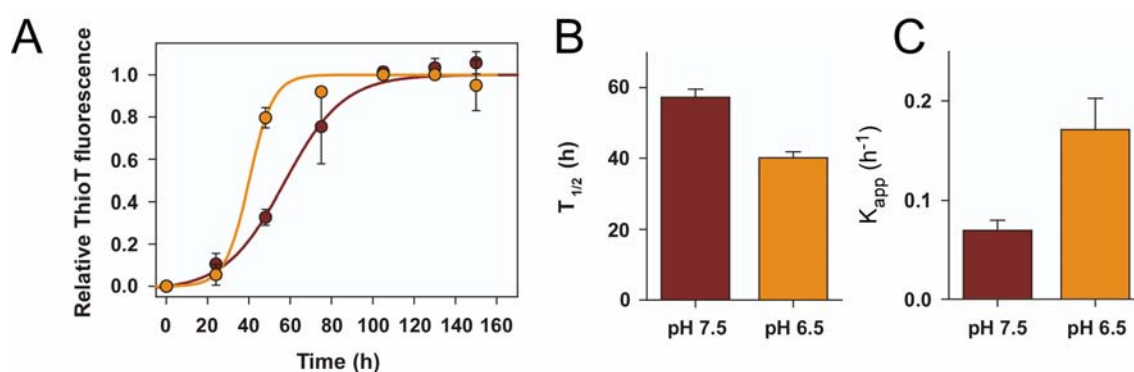


**Figure 4.18. αS at pH 6.5 aggregates faster than a pH 7.4.** Aggregation assay for αS at pH 6.5 and 7.4. **A**. Normalized ThioT traces for αS aggregation at pH 6.5 (orange) and 7.4 (dark red) in the presence of 100 mM NaCl (protein concentration is 100 μM). **B**. Half time for aggregation for traces shown on A. **C**. Apparent rate constant for monomer addition derived from the traces shown in A.

Chemical shifts perturbations are exclusively localized to two defined regions surrounding residues 3 and residues 50 (Figure 4.19). The first zone could be attributed to changes in the protonation state of the terminal amine group, while the second one is unambiguously due to changes in the side chain of the sole histidine residue of the protein. N-terminal amines should have a higher pKa, thus another possibility is that the changes detected are only due to His protonation and long range interactions between the N-terminus and His50, i.e. such that hydrogen bonds nets cause the perturbations. This would have strong consequences on the ensemble of conformations and may account for the changes in

aggregation propensity. It would be interesting to probe whether natural ligands of His residues, namely metal cations are able to bind to αS and cause changes in fibrillation.
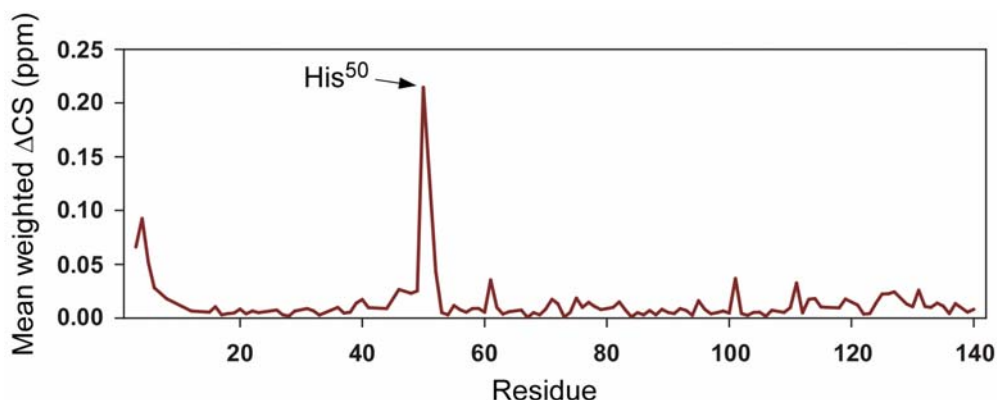


**Figure 4.19. Amide chemical shift perturbations upon pH reduction in αS.**
Plot of mean weighted $^{1}$H-$^{15}$N chemical shift differenced between αS at pH 6.5 and 7.4.

In order to easily probe a general property of the ensemble, we first measure the hydrodynamic properties of the protein by PFG-NMR at pH 6.5 and 100 mM NaCl. No change on the Rh of the protein was found when compared with pH 7.4 and 100 mM NaCl (Rh of 31.9 ± 0.3 Å at pH 7.4 and Rh of 32.0 ± 0.5 Å at pH 6.4). Thus the ensemble is not perturbed significantly upon changes in pH.

Due to the absence of hydrodynamic changes we discarded the use of PRE to evaluate this condition, and solely employed RDCs to search for slight conformational changes on the protein. The RDCs profile of the protein at pH 6.5 is correlated with the one measured at pH 7.4, although it shows, in general, a reduction in the values of the couplings and an inversion in the sign of the RDCs for the very N-terminus (Figure 4.20). The reduced couplings over the whole polypeptide chain are likely caused by a slight decrease in the alignment properties of either the protein or the anisotropic phase. However local changes are observed for the first sub-domain of the C-terminus, where reduction of the couplings would be indicative of a reduction in the strength of the long range contacts, similarly to what was observed at 37 °C. The inversion of the sign of the couplings suggests the presence of turns or that helical conformations are readily populated (Mohana-Borges et al., 2004).
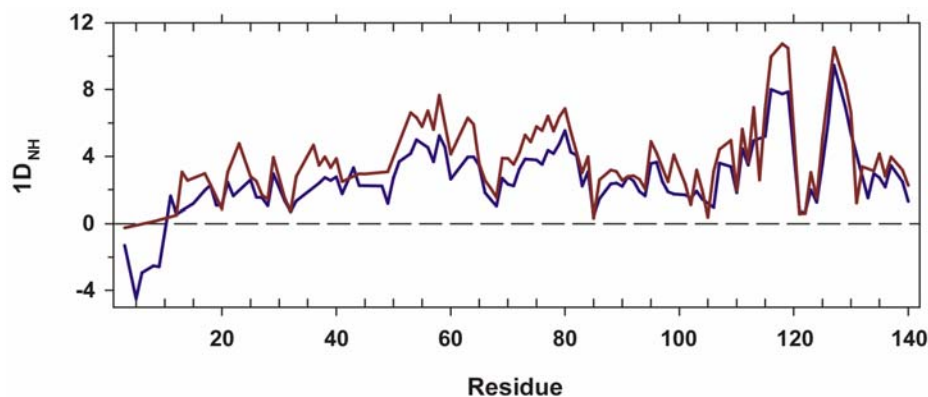
**Figure 4.20. RDCs profile for αS at pH 6.5.** $^{1}D_{NH}$ dipolar couplings measured on αS aligned with 5 % $C_8E_5$/octanol mixture for αS at pH 7.4 (dark red) and at pH 6.5 (dark blue).

Overall these results suggest that that the ensemble of conformations populated at pH 6.5 is not particularly different to the one populated at 7.4, but may favor the partition towards a defined sub-set of conformations that readily aggregates. A characteristic of these conformers populated at slight low pH is a perturbed local structure at the very N-terminus and on the region surrounding the His[50] residue, and the mechanism for an increased aggregation my not necessarily involve an impairment of long range tertiary contacts, as probed by RDCs.

## 5. Results. Chapter II: "PD-linked familial mutants of αS have a destabilized conformation".

Two missense mutations in the *αS* gene have been identified as causes of early on-set PD. The changes of Ala[30] to Pro and Ala[53] to Thr lead to an increase in the tendency to form toxic oligomeric species, and in particular the Ala[53] to Thr substitution increases the rate of fibril formation (Conway et al., 2000). Previous low and high resolution spectroscopic characterizations of these two proteins had not provided a structural rationale for such differential behavior. Thus we applied our set of NMR techniques to study the characteristics of the ensemble of conformations populated by these two proteins.

### 5.1. Conformations of familial mutants of αS studied by heteronuclear 2D NMR.

The HSQC spectra of both A30P and A53T genetic mutants did not differ significantly from the spectra of the *wt* αS protein, aside from the immediate surroundings of the mutated residues (Figure 5.1).
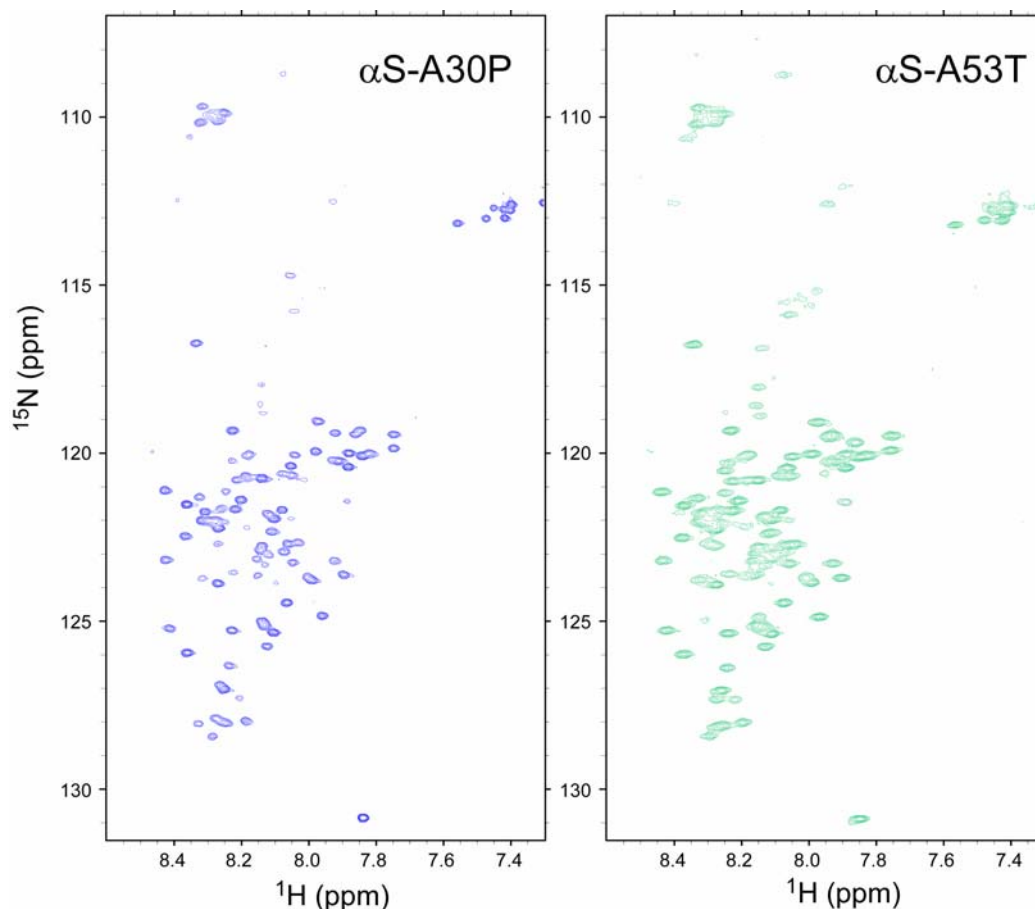


**Figure 5.1. ¹H-¹⁵N HSQC spectra of αS genetic mutants.** ¹⁵N-labeled A30P

and A53T protein variants of αS were subjected to 2D heteronuclear NMR. Both HSQC spectra show, besides the surrounding point of mutation, no significant perturbations in chemical shifts when compared with the wt protein.

However, some slight changes in the intensity of the signals were evident, in particular for the A30P mutant. As shown on figure 5.2, when compared with the *wt* protein (dark red), the amide cross-peaks for the A30P protein (cyan) showed a reduced intensity of the N-terminal resonances (from residue 20 to 70) and an increased intensity of the resonances corresponding to the C-terminus (amino acids 112 until 130). For A53T (green), the changes were minor, and only in evidence at the N-terminus (from residue 20 to 60).
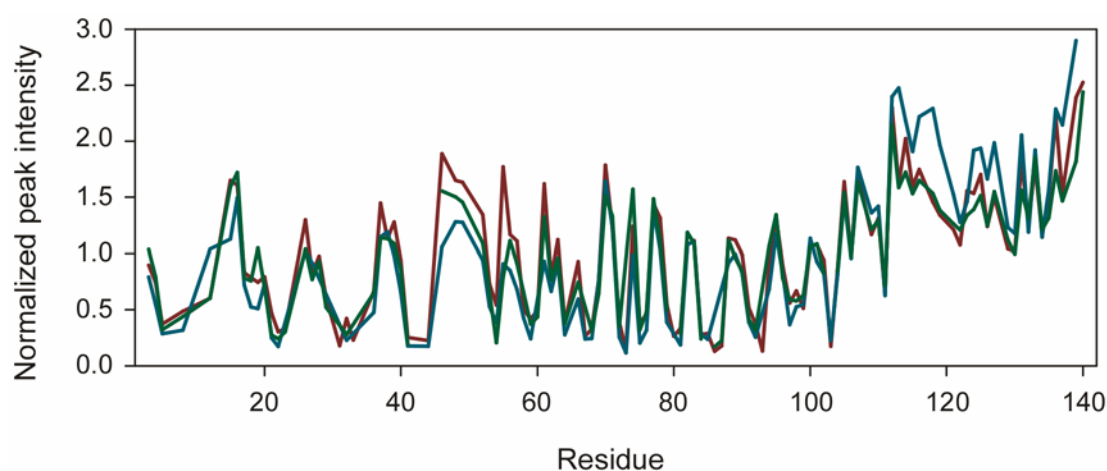


**Figure 5.2. Intensity plots for HSQC-amide cross-peaks of *wt* αS and its genetic mutants.** Normalized peak intensity, relative to signal average, for HSQC-derived amide resonances corresponding to αS wt (dark red), αS A30P (cyan) and αS A53T (green). Average peak intensities were employed for normalization due to changes at the C-terminus of the A30P mutant.

A comparison of these results in terms of the findings described on chapter 1 for different conditions that alter the ensemble of conformations populated by αS, reveal some similarities. The slight decrease of intensities of the N-terminal resonances for both mutants is similar to that observed under high temperature conditions for *wt* αS (Chapter 1, Figure 4.1).

Furthermore, when we recorded HSQC spectra for *wt* αS at 15 °C and 25 °C, for the same sample in the same conditions, there was an overall reduction of the intensity of peaks from the N-terminal and NAC regions (Figure 5.3A, 5.3B). The normalized peak intensity profile for the spectra recorded at 25 °C was very similar to that evidenced for the A30P mutant, and also displayed lower intensity of resonances in the region comprising residues 20 to 60, as with both the A30P and A53T αS variants (Figure 5.3C).
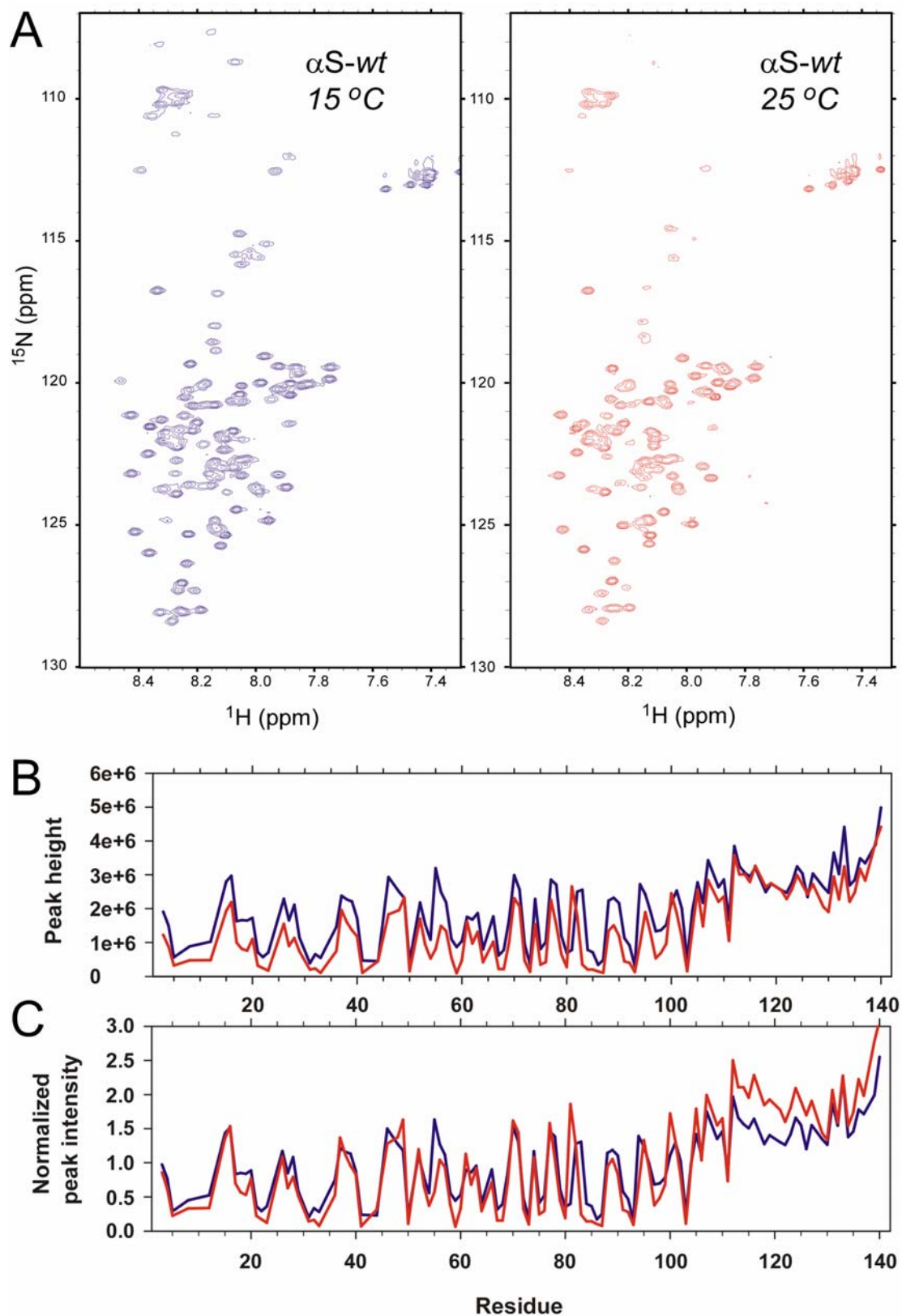
**Figure 5.3. Intensity changes on the HSQC spectrum of *wt* αS at 298 K. A.** HSQC spectra of *wt* αS show a slight reduction in peak intensity upon raising the temperature from 15 °C to 25 °C, similarly to the effect evidenced on αS genetic mutants. **B**. Profile of intensities of amide crosspeaks for αS *wt* at 15 °C (blue) and 25

°C (red) obtained from the spectra shown on A. **C**. normalized peak intensity, relative to average, corresponding to the spectra shown on A. In blue are shown the values for αS *wt* at 15 °C and in red those corresponding to 25 °C.

This kind of NMR determinations does not seem to be capable of determining differences between the ensemble of conformations populated by the A30P and A53T mutants and the *wt* protein. The overall signatures of the HSQC spectrum are conserved, i.e. peaks still clustering by residue nature, a narrow spread of signals in the $^1$H dimension is observed, and there are no chemical shifts perturbations between the native and mutant proteins. However, a detailed characterization of the profile of intensity of the signals provides some indication of a slight perturbation of the ensemble of conformers, similarly to the changes observed in the protein when the temperature is raised from 15 °C to 25 °C. Thus, there exists a small but finite probability that a redistribution of conformers in the ensemble may take place in the native soluble state of the A30P genetic mutants, and to a lesser extent with the A53T variant. Such preferential partition would likely be towards those conformers with increased amyloidogenic properties.

We consequently hypothesized whether such small perturbations in the ensemble of conformers would be observable by the suit of experiments that have been successful in probing residual structure and long range interactions in *wt* αS, and decided to employ paramagnetic relaxation enhancement and residual dipolar couplings to study the native soluble state of both αS-A30P and αS-A53T.

## 5.2 The A30P and A53T familial mutations perturb tertiary interactions in the native state of αS.

We have shown in chapter 1 how PRE of nuclear spin relaxation based on nitroxide spin labels is a very powerful technique for observing long range interactions in the native state of αS.

Due to the attachment of a nitroxide radical to a Cys residue in the protein, a distance-dependent broadening of NMR signals extends as far as 20 Å, permitting the characterization of the ensemble of conformations that are populated. As αS lacks cysteine, three different double mutants, containing variable single Ala to Cys replacements, were constructed for both the A30P and A53T mutant αS, mirroring the *wt* αS variants studied in chapter 1. Thus we evaluated the PRE effect on MTSL-labeled αS A30P-A18C, A30P-A90C, A30P-A140C mutants, as well as A53T-A18C, A53T-A90C, A53T-A140C variants (Figure 5.4A).
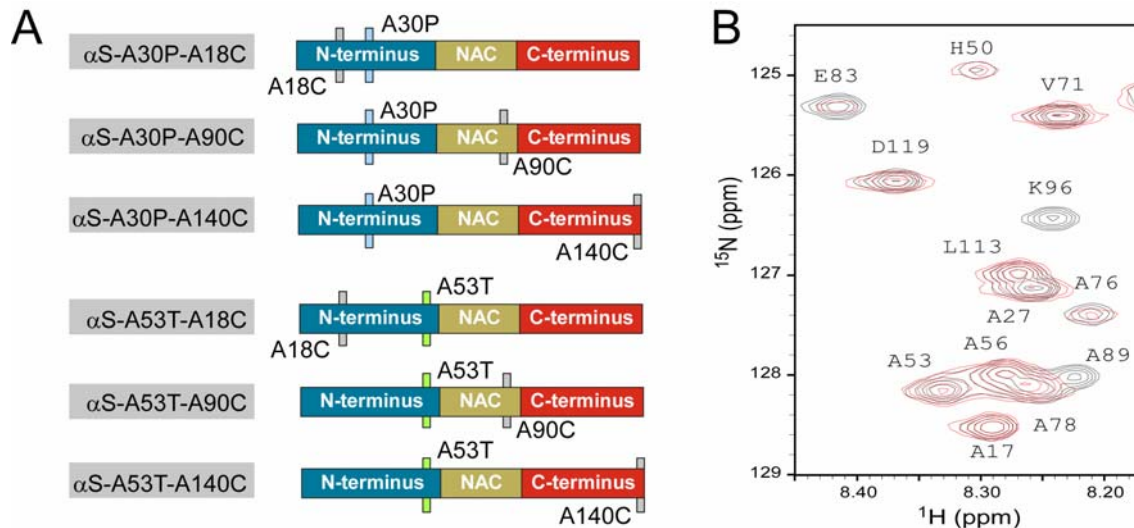
**Figure 5.4 Constructs studied on the PRE-based characterization of familial mutants of αS. A.** Double mutants of αS, containing the A30P or A53T mutations and a variable Cys replacement (A18C, A90C or A140C) were constructed in order to provide attachment sites for nitroxide labels. **B**. Overlapped slices from two ${}^{1}$H-${}^{15}$N HSQC spectra acquired on αS-A30P-A90C in the absence (diamagnetic) (black) and presence (paramagnetic) (red) of the nitroxide spin label MTSL.

The profiles derived from the PRE experiments on αS familial mutants are largely similar to those obtained on the *wt* protein, but some particular differences were observed (Figure 5.5). In the A18C spin labeled mutant αS, intensity ratios between the paramagnetic and the diamagnetic states ($I_{param}/I_{diam}$) as low as 0.5 were observed in the C-terminus, similar to that of *wt* αS (Chapter 1). In contrast, the relaxation enhancement of residues 40-60 decreased by about 20 % for both missense mutants compared to the *wt* protein (Figures 5.5A, 5.5D). The reduced paramagnetic broadening of residues 40-60 suggests that the compaction of the N-terminal region is slightly reduced in mutant αS, in agreement with recent Trp fluorescence energy transfer measurements (Lee et al., 2004).

The attachment of the spin label MTSL to residue 90 greatly attenuated NMR signals of amino acids in the C-terminus of A30P mutant αS with peak intensity ratios in the range of 0.5 to 0.9 (Figure 5.5B). This result indicates that the C-terminal domain of A30P αS is very compact, as had been observed previously for *wt* αS (Chapter 1) and also holds for the A53T mutant (Figure 5.5E).

When the spin label was attached to residue 140 in the *wt* protein, the NMR signals of residues located in the NAC region were considerable broadened, providing support for a back-folding of the C-terminus on this region in *wt* αS (Chapter 1). Such a long-range interaction was not observed in either the A30P or A53T mutants as the broadening effect

exerted by the spin labeled was similar to the expected for a random coil polypeptide (Figures 5.5C, 5.5F).
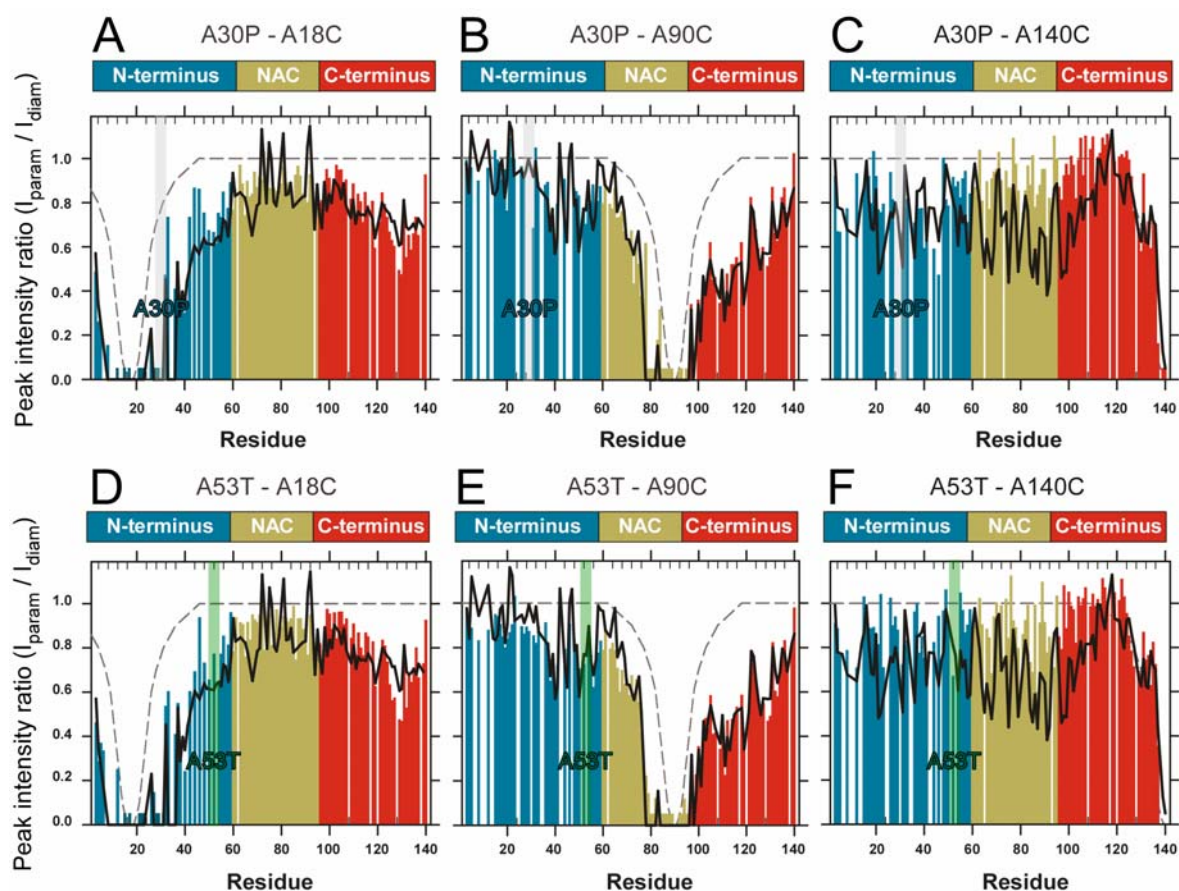


**Figure 5.5**. **PRE profiles in Parkinsonism-linked mutant αS.** Intensity ratios ($I_{param}/I_{diam}$) of the resonance peaks in $^1$H-$^{15}$N HSQC spectra in the presence (paramagnetic) and absence (diamagnetic) of the spin label MTSL at 15 °C. Dashed lines indicate intensity ratios simulated for a random coil polypeptide. Decreases in peak intensity ratios that occur far from the site of spin labeling (>10 residues) are indicative of intramolecular long-range contacts between the spin label and distant areas of sequence. Intensity ratios for A30P/A18C (**A**), A30P/A90C (**B**), A30P/A140C (**C**), A53T/A18C (**D**), A53T/A90C (**E**) and A53T/A140C αS (**F**). Solid lines indicate the intensity ratios observed for *wt* αS.

We further addressed the relative strength of the long range interactions present in mutant αS by measuring PREs on urea denatured spin-labeled proteins. Of note in the case of the *wt* A18C variant was the persistence of residual long-range contacts between the N- and C-terminus in 8 M urea (Chapter 1). Both the A30P and A53T A18C-labelled variants displayed the absence of such persistent long range interactions under strong denaturing conditions, likely populating a fully random coil conformation (Figure 5.6A, 5.6B). The A90C variants, as expected, did not display significant differences between the *wt* and mutant

proteins due to the fact that in this particular case the profiles of the three proteins correlate well with the expected for a completely unfolded polypeptide (Figure 6.6C, 6.6D).
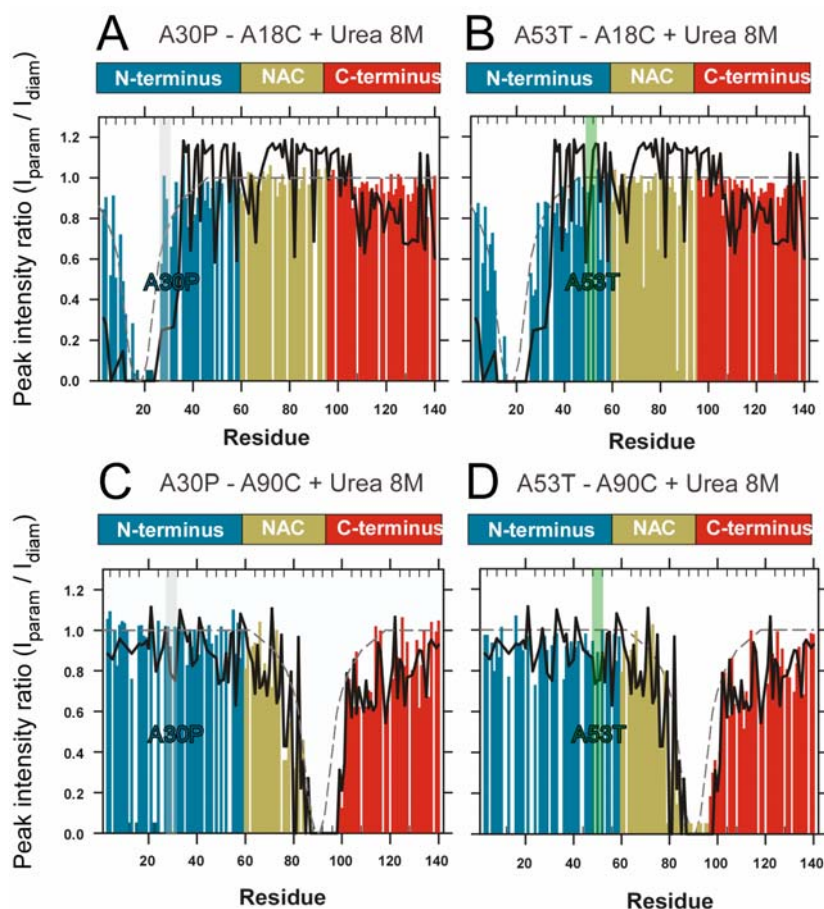


**Figure 5.6. PRE profiles in urea denatured αS mutants.** Intensity ratios of the resonance peaks in $^1$H-$^{15}$N HSQC spectra in the presence (paramagnetic) and absence (diamagnetic) of the spin label MTSL at 15 °C acquired in the presence of 8 M urea as denaturing agent . Dashed lines indicate intensity ratios simulated for a random coil polypeptide. **A**. A30P-A18C. **B**. A53T-A18C. **C**. A30P-A90C. **D**. A53T/A90C. Solid lines indicate the intensity ratios observed for the correspondent Cys-containing mutant of *wt* αS in Urea 8 M. The A140C mutant was not particularly useful in studying the chemically denatured state of the *wt* protein and thus the genetic mutant variants on that position were not studied under urea 8 M.

If we consider the relative perturbation under chemical denaturant as a signature of the strength of the tertiary interactions preserving the native unfolded state, we could hypothesize that the A30P and A53T mutations provoke a partition in the ensemble conformations that are populated by the protein towards conformers with higher free energy. The increased population of such conformers is likely to facilitate misfolding and self-oligomerization, as occur with both mutant proteins.

## 5.3. A30P and A53T mutations destabilize αS.

Residual dipolar couplings are exquisitely sensitive to bond vector orientation and can be measured in a weakly aligned protein, for which the large internuclear dipolar interactions no longer average to zero (Bax and Grzesiek, 1993). As we reported in Chapter 4, RDCs identified five different domains in *wt* αS with different degrees of residual structure, in some cases long-range-coded (domain I: residues 1-28; domain II: residues 33-65; domain III: residues 70-88; domain IV: residues 95-105; and domain V: the C-terminus). In particular, RDCs probed a hydrophobic core comprising the C-terminus and domain III and IV, which resulted to be a native gatekeeper for avoiding αS aggregation. We intended to measure this NMR-derived parameter in order to obtain further evidence for differences between the backbone conformations populated by both mutant proteins.

RDCs in PD-linked mutant αS were first observed by dissolving A30P and A53T αS mutants in a dilute liquid crystalline phase of 5% $C_8E_5$/octanol. No significant differences in the chemical shifts of spectra in $C_8E_5$/octanol and free in solution were observed, suggesting that the anisotropic phase did not appreciably perturb the ensemble of αS conformations. In general reduced couplings were observed for many residues in both genetic mutants when compared with *wt* αS (Figure 5.7). Since both variant are just single point mutations, and due to the conservation of solution and conditions of anisotropic phase preparation, the differences are not ascribed to variations in protein alignment, rather are likely caused by changes at the level of the conformations sampled by these proteins with respect to the *wt*.
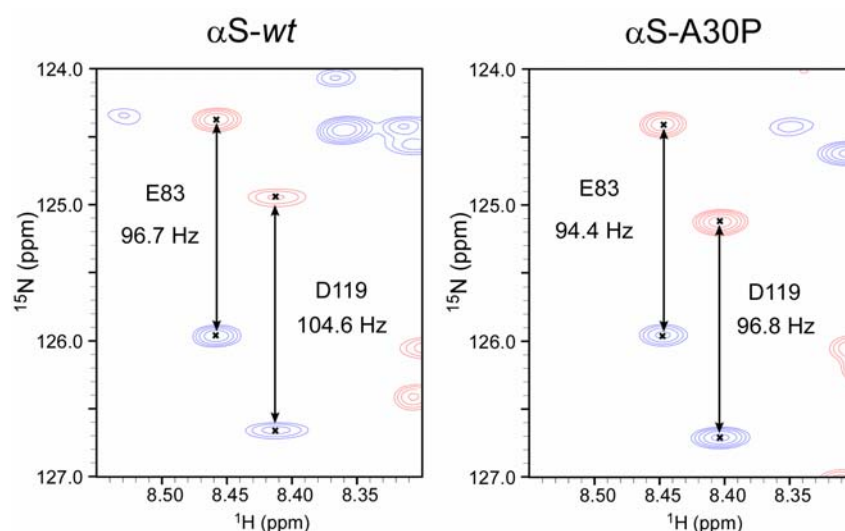


**Figure 5.7. RDCs in αS genetic mutants.** Region of the $^1H^{15}N$- in phase-anti phase (IPAP)-HSQC spectrum corresponding to αS *wt* (*left*) and αS A30P (*right*) aligned in 5% $C_8E_5$/octanol mixture, showing the $^1D_{NH}$ couplings for Glu$^{83}$ (E83) and

Asp[119] (D119). The upfield doublet components (anti-phase) are indicated in red, while the downfield components (in-phase) in blue.

RDCs in A30P and A53T mutant αS were predominantly positive with regions displaying relatively large RDCs separated by residues with RDCs close to zero (Figure 5.8A, 5.8B), and slightly negative couplings were observed for some residues.
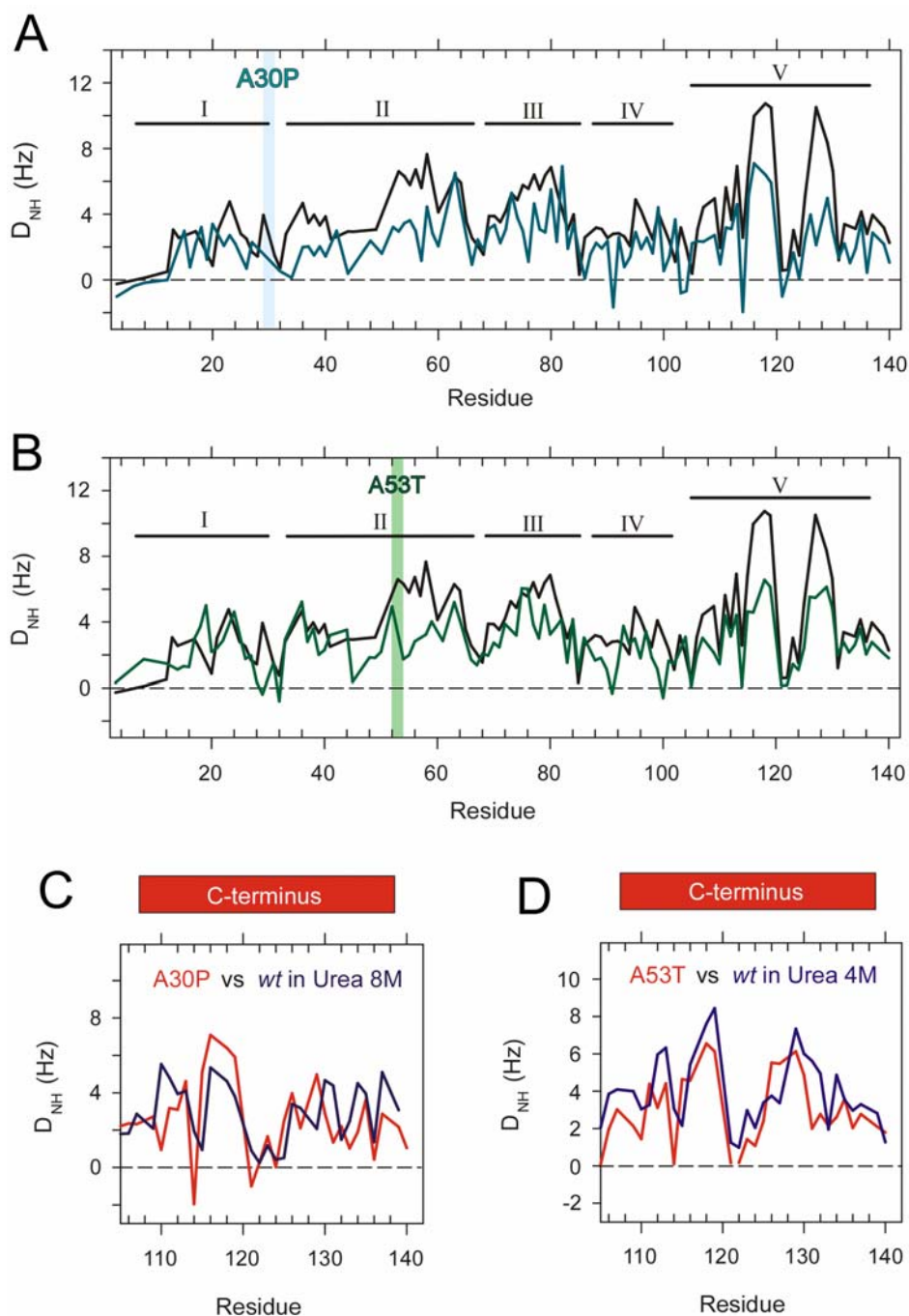


**Figure 5.8. Residual dipolar couplings in mutant αS.** Backbone N-H dipolar couplings, $^1D_{NH}$, were measured in A30P and A53T mutant αS oriented in a 5% $C_8E_5$/octanol mixture at 15 °C. Non-zero dipolar couplings are indicative of structural

and motional restrictions of the protein backbone. **A.** $D_{NH}$ profile for A30P αS (blue) and *wt* αS (black) in buffer A. **B.** $D_{NH}$ profile for A53T αS (green) and *wt* αS (black) in buffer A. **C.** $D_{NH}$ couplings in the C-terminus of A30P αS in buffer A (red) and of *wt* αS in buffer A + 8 M urea (dark blue). **D.** $D_{NH}$ couplings in the C-terminus of A53T αS in buffer A (red) and of *wt* αS in buffer A + 4 M urea (blue). RDC domains identified in *wt* αS (domain I: residues 1-28; domain II: residues 33-65; domain III: residues 70-88; domain IV: residues 95-105; and domain V: the C-terminus) (Chapter 4) are indicated.

Despite the reduced values, the profiles corresponding to the mutant dipolar couplings correlate well with the RDC domain pattern of the *wt* protein. However, some differences were observed in particular domains. In contrast to *wt* αS, the RDCs for domain II (residues 50-62) and domain III (residues 70-94) were strongly reduced. In the C-terminal domain, the magnitudes of RDCs were comparable to those in the rest of the protein, as opposed to the RDC profile of *wt* αS, in which the values were almost twice as high. Rather the dipolar couplings of A30P αS were similar to those of *wt* αS in the presence of 8 M urea (Figure 5.8C), whereas the magnitude of RDCs of A53T αS was comparable to that of *wt* αS in the presence of 4 M urea (Figure 5.8D). Furthermore the profile of urea denatured A30P mutant is similar to *wt* αS, but still differs from the pattern observed in native solution conditions (Figure 5.9A).

In the vicinity of both missense mutations, the dipolar couplings were considerably reduced, suggesting an increased mobility in these regions. For the A30P mutation, the increased flexibility is in agreement with the reduced heteronuclear $^{15}$N $R_1^{\rho}$ relaxation rates of backbone amide groups and a reduced helical propensity for domain I (residues 18-31) (Bussell and Eliezer, 2001).

In line with the alteration of long-range interactions by PD-linked mutations, as suggested previously by PRE measurements, RDCs also evidenced a very strong reduction of couplings in the hydrophobic NAC region and at the C-terminal domain of mutant αS. These results point toward a reduced shielding of the hydrophobic NAC region by the C-terminus in the A30P and A53T mutant αS.

As an important control of those experiments, the couplings for A18C αS, a non-amyloidogenic mutant of αS with an unaltered time course of aggregation (Chapter 1), were nearly identical to that of *wt* αS (Figure 5.9B).
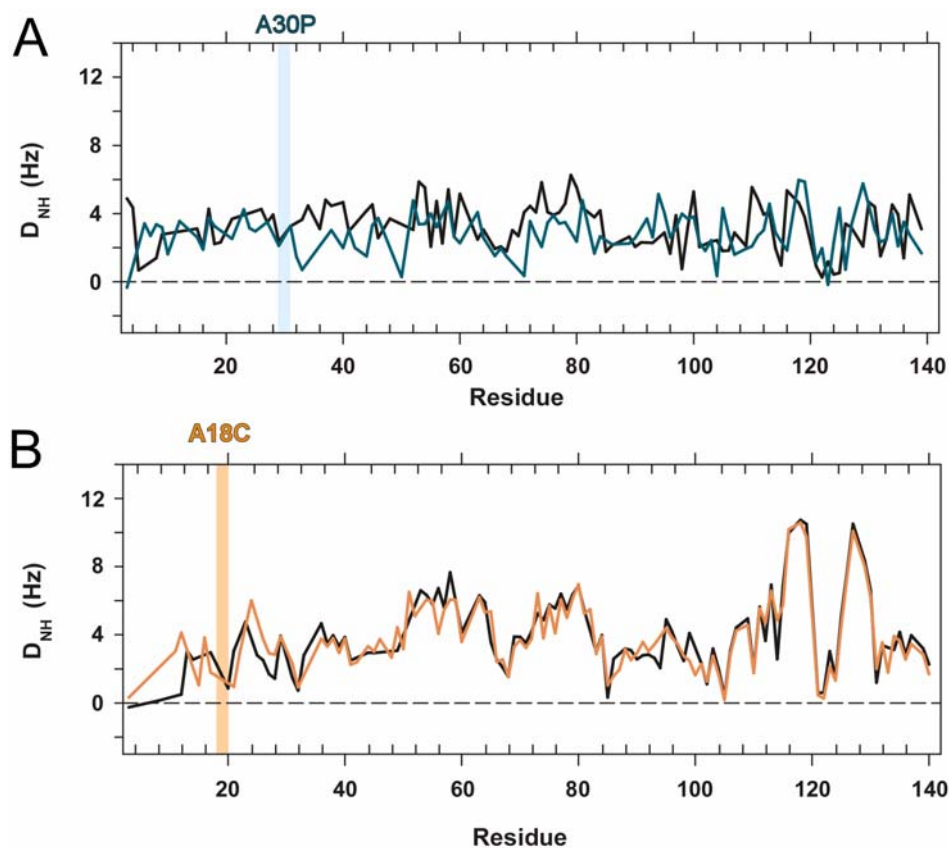
**Figure 5.9. Control data for residual dipolar couplings in PD-linked mutant αS.** Backbone N-H dipolar couplings, $D_{NH}$, were measured in αS variants oriented in a 5% C8E5/octanol mixture at 15 °C. **A.** $D_{NH}$ profile of A30P αS (blue) and *wt* αS (black) both in buffer A + 8 M urea. **B.** $D_{NH}$ profile of A18C αS (orange), a non-amyloidogenic mutant of αS with an unaltered time course of aggregation, and *wt* αS (black) both in buffer A.

In addition, the results presented in figure 5.8 were reproduced in Pf1 phages as a second alignment medium (Figure 5.10A, 5.10B), confirming in general our findings. There was, as well, an overall reduction of the RDCs values for the polypeptide chain, confirming that the populated conformers differ. However, the strong reduction of the couplings observed for the C-terminus in $C_8E_5$/octanol phase was shown in Pf1 media as a mild reduction, similarly to what we evidence upon raising the temperature on the *wt* protein, and confirming the reduced strength of long range interactions.

We further measured RDCs at higher temperature for the A30P mutant, in order to determine whether there was a difference between both proteins at physiological conditions. When the temperature was raised to 37 °C we still spotted the reduced value of C-terminal dipolar couplings suggesting that the destabilizing effect of the genetic mutations is also significant at physiological conditions (Figure 5.10C).
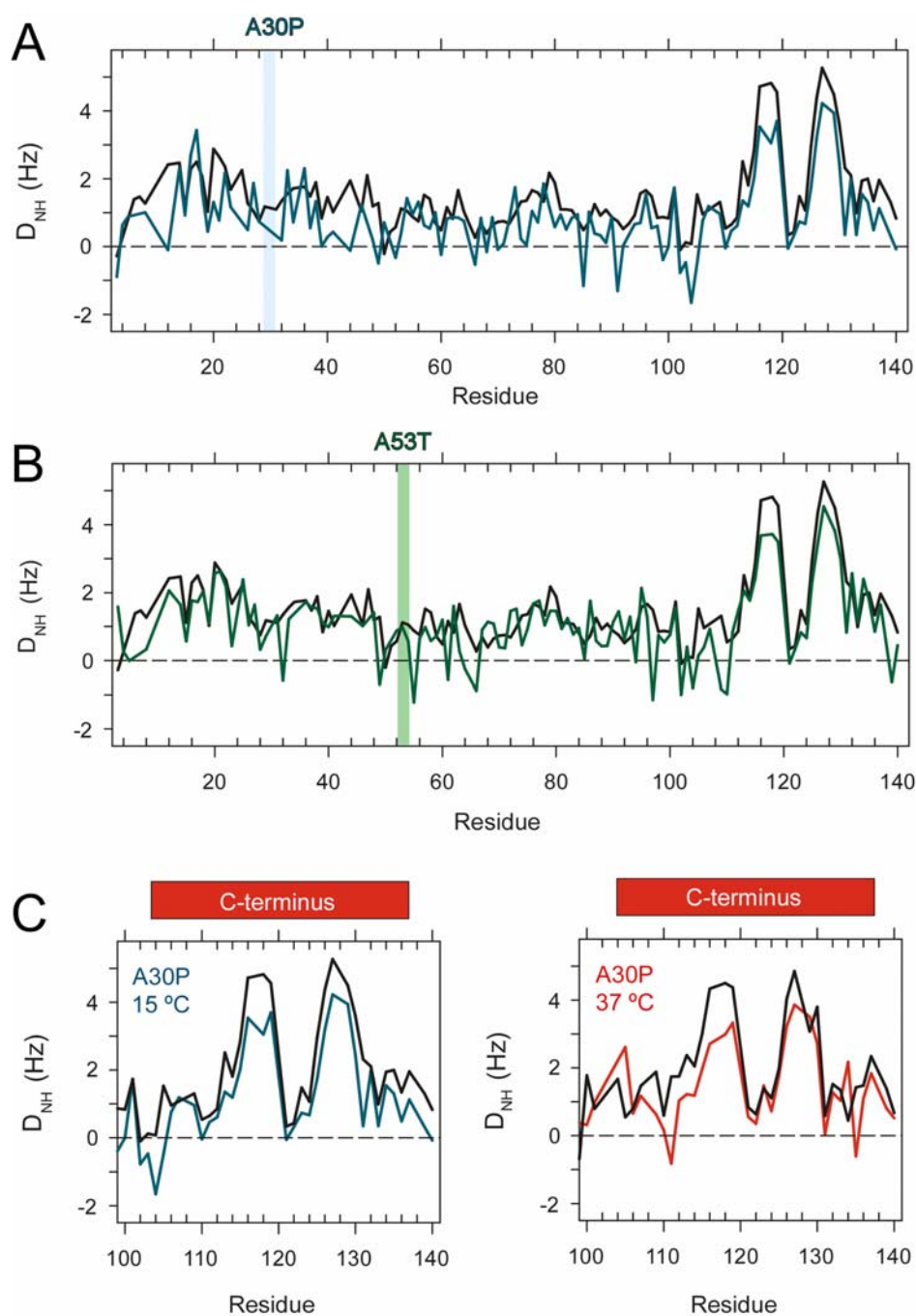
**Figure 5.10. Residual dipolar couplings in mutant αS oriented in Pf1 bacteriophage.** A. D$_{NH}$ profile for A30P αS (blue) and *wt* αS (black). B. D$_{NH}$ profile for A53T αS (green) and *wt* αS (black). C. D$_{NH}$ profile for the residues corresponding to the C-terminus of A30P αS (blue and red) and *wt* αS (black) at 15 °C (left panel) and 37 °C (right panel).

## 5.4. Synergistic long range interactions occur in the native state of αS.

In chapter 1 we identified two types of long range interactions in the native state of αS, a hydrophobic cluster between the NAC region and key residues at the C-terminus, and an interaction between the N-terminus and C-terminus. Despite the reduction of the shielding on

the NAC region, a strong paramagnetic broadening exerted by a spin label attached to either residue 18 or 90 on the C-terminal domain of the protein remained (Figure 5.5A, 5.5B, 5.5D and 5.5E), suggesting that long-range interactions are not completely abolished in the A30P and A53T αS mutants. The remaining long range N-terminal/C-terminal interaction is predicted to be of electrostatic nature, due to the high positive net charge of the N-terminus and the high negative net charge of the C-terminus.

To further disclose which interactions are affected upon mutation, we investigated the hydrodynamic properties of the ensemble of conformations populated by both mutants employing pulse-field gradient (PFG) NMR. In order to probe the sole effect of the genetic mutations in the ensemble of conformations, the PFG-NMR experiments were measured in the absence of salt, which has been found to extend αS conformations (Chapter 1).

As observed in figure 5.11, an unexpected finding from the hydrodynamic characterization of the αS genetic mutants was that both A30P and A53T proteins display a smaller Rh than the *wt* protein (~ 29 Å for A30P and A53T, and 30.5 Å for wt αS). This result is in line with the PRE findings on the tagged-αS A18C showing a slight increase of the paramagnetic broadening centered on position 130. Conversely, in both mutant proteins a dissociation of the C-terminus from the NAC region, as probed by the 140C position, was evidenced, suggesting an extend conformation. However, the C-terminus still remains compact, as shown on the PRE profiles of the mutant A90C variants.
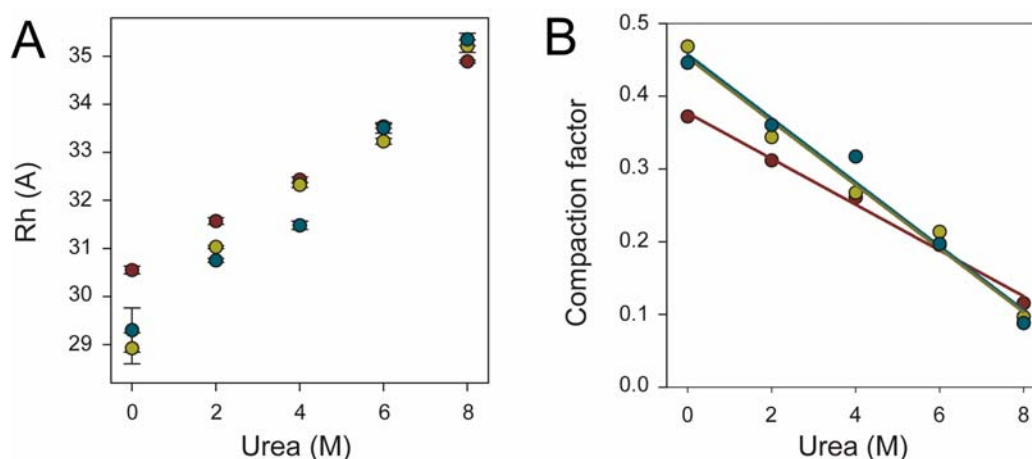


**Figure 5.11. Changes on hydrodynamic properties upon denaturant addition for *wt* and mutant αS. A.** Changes in Rh upon urea titration of *wt* αS (dark red), A30P (blue) and A53T (dark yellow) genetic mutants. **B**. Calculation of changes in compaction factors upon urea titration for the measurements in A. Linear fits for the variation of compaction factor *vs.* urea addition are shown in bold lines.

Another interpretation of these results would suggest that the N-terminus and the NAC region compete for long range interactions with the C-terminus. Thus, the NAC/C-terminal hydrophobic interaction may disfavor the electrostatic N-terminal/C-terminal interaction, and in the absence of such hydrophobic cluster, the electrostatic interaction would prevail and favor a collapsed ensemble.

If the native state of the *wt* protein features both interactions, we could assume with a certain degree of confidence that the NAC/C-terminal contact is strongly perturbed in both genetic mutants. Thus we should be able to dissect the contributions of each interaction by comparing how urea destabilizes the ensemble for both *wt* and mutant proteins. When we measured stepwise the variation of Rh upon urea addition we observed that all the three proteins reached almost the same extended conformation at the last concentration of urea probed (~ 35 Å at 8 M urea).

Although the proteins displayed an almost linear dependence of compaction vs. urea addition, the manner in which the mutants achieved their chemically unfolded state differed from that of the *wt* protein. Considering that the protein would be 100% compact at an ideal, empirically determined, globular state, and that it would be 0% compact at an equally ideal, also empirically derived, chemically unfolded state, we can calculate compaction factors for each state of the ensemble (Wilkins et al., 1999). Thus the compactness of the mutants would be ~ 45% in the absence of urea, and would decrease to 9% upon addition of 8 M, while for the *wt* protein it would change from 37 % to 11 % under the same conditions. The A30P and A53T mutants extended as well as denatured with a pseudo-rate of 4.4% per mole of urea added, whereas the value for *wt* protein was only 3.1% per mole of urea. These results imply that *wt* αS is more resistant to the addition of denaturant than the mutant variants, suggesting a synergistic effect for both types of long range interactions despite their inherently antagonistic character.

Furthermore, since the mutant proteins still extended as urea was added, the mere absence of the hydrophobic cluster is not likely to trigger the unfolding of the protein, and rather a combined impairment of both long range interactions would be required, likely the scenario upon polyamine binding.

## 5.5. Competition of electrostatic and hydrophobic interactions in the native state of αS.

To further probe the strength of distant N- and C-terminal electrostatic interactions in the A30P and A53T mutants upon destabilization of the long-range hydrophobic cluster, we sought to determine the affinities of these proteins for the polycation spermine. The rationale

was that if electrostatic contacts are modulated, one should perceive a change in the affinity of the protein for the polycations.

When we titrated αS A30P and A53T mutants with spermine we observed a general effect of the polycation on the amide resonances of the protein. Both the chemical shift perturbations and the changes in the intensity of the signals observed for *wt* αS (Fernandez et al., 2004) were reproduced for the A30P and A53T mutants (Figure 5.12). The chemical shifts perturbations were also localized at the C-terminus of the protein, with the principal changes centered on the stretch comprising residues 124 to 135, similar to the *wt* protein, and thus permitting a comparison of the binding affinities for the three proteins.
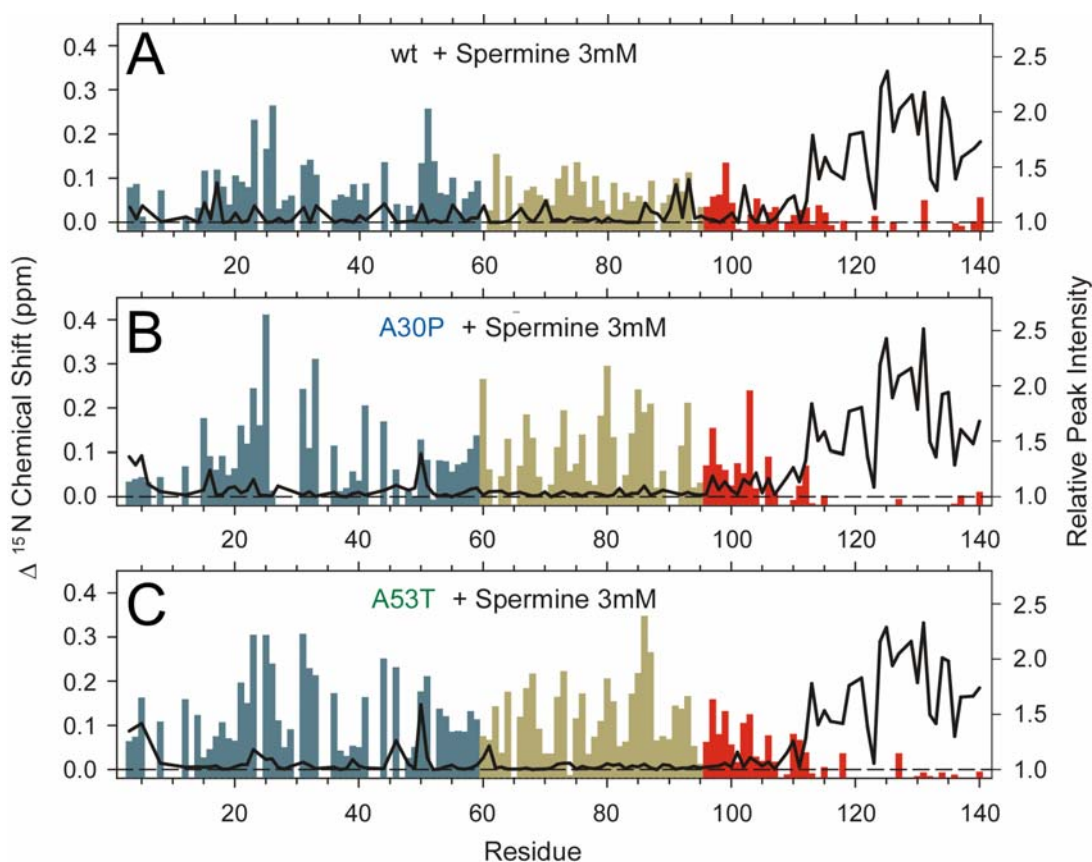


**Figure 5.12. Binding of spermine to mutant αS is similar as to the *wt* protein.** Comparison between polyamine binding to wt and mutant αS. Upon spermine binding (3mM) to αS, changes in $^{15}$N chemical shifts (bold black line) and in peak intensities (colored bars) are visible, reflecting formation of a complex between the negatively charged C-terminus of the protein and the polycation. **A**. αS-*wt*. **B**. αS-A30P. **C**. αS-A53T.

If the protein is in fast exchange with the ligand, due to the conformational average sampled by the timescale of the NMR measurement, the chemical shifts of those residues directly implicated in the binding event should gradually change from 0 until a maximum

upon saturation. Thus one may employ the HSQC-based titration experiments to evaluate the dissociation constants (*Kd*) of the formation of the protein-ligand complex.

The determinations of the *Kd* for the A30P and the A53T proteins is shown in figure 5.13. A global analysis, assuming a single *Kd* but independent maximal chemical shifts perturbations for each residue evaluated, determined that both mutant variants have ~ half the affinity for spermine than the *wt* protein (1.3 mM and 1.23 mM for A30P and A53T, respectively, vs. 0.61 mM for αS *wt*).
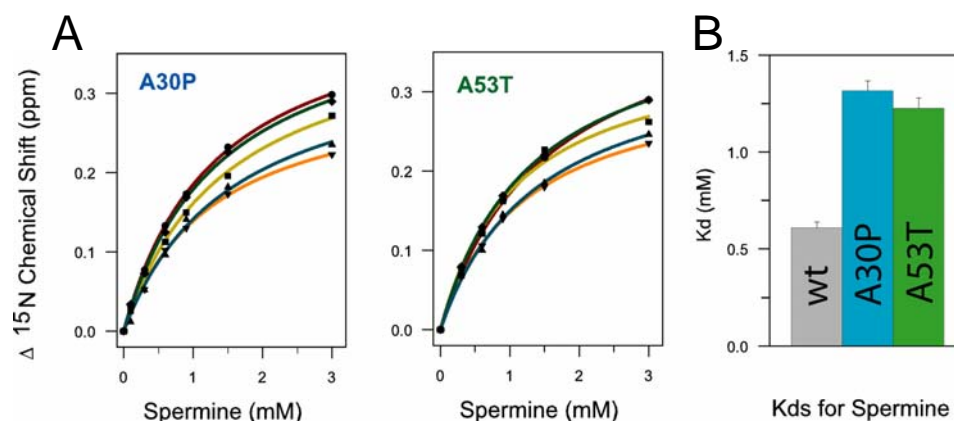


**Figure 5.13. Determination of dissociation constants for spermine-mutant αS complexes.** Kd for the binding of the polycation spermine (+4) to both A30P and A53T αS proteins were determined by titration experiments based on $^1$H-$^{15}$N-HSQC NMR spectra. **A**. $^{15}$N chemical shifts difference as a function of total concentration of ligand for αS-A30P (left) and αS-A53T (right). Residues are as follows: Ala[124] (dark red), Glu[126] (orange), Met[127] (light green), Ser[129] (dark green), Asp[135] (cyan). **B**. Comparison of *Kds* for spermine-αS complexes determined by this procedure. The values are $0.61 \pm 0.03$ mM for αS-*wt*, $1.31 \pm 0.05$ mM for αS-A30P, and $1.23 \pm 0.06$ mM for αS-A53T. Protein concentration was 100 μM in all the cases.

This result would suggest that the N-terminal and the polycation compete for the negatively charged C-terminal, and that the composite influence of the electrostatic interactions reduce the affinity of the protein for the polycation. The net charge of the N-terminal domain is + 4, equivalent to a single molecule of spermine. The 100 μM of N-terminus in solution was considerable lower than the high excess of polycation present in the sample in great excess. Thus if competition were the sole cause of the affinity change, the *Kd* of the N-terminus/C-terminus complex would have to be ~ 10 times lower than for the polyamine/C-terminus complex. This could be explained in terms of the high local concentration effect that the charges at the N-terminus are expected to exert since they are directly attached to the C-terminus through the polypeptide chain and are not subject to diffusion or exchange as the polyamine molecules do.

In the previous we must consider that there is a second effect that may additionally regulate the affinity of the C-terminus to the polycation, namely the residual structure of the C-terminus, which is indeed perturbed in the mutants, as revealed by the RDCs.

In order to explore the possibility that residual structure at the C-terminus regulates binding to polyamines, we studied the spermine binding characteristics of a peptide comprising residues 105 to 136 derived from the C-terminus of $\alpha$S. As probed by RDCs this peptide populates unfolded conformations with diminished residual structure when compared with the full length protein (Chapter 1), and thus is an excellent probe for evaluating polyamine binding in the absence of both long range interactions.

Upon titration with spermine the peptide displayed essentially a similar dose-dependent shift of the resonances, although the saturating chemical shifts perturbations for the evaluated residues were 50% to 80% higher than the values displayed by the full length protein. The stronger chemical shift perturbation in the peptide could be due to the absence of conformational restrictions imposed by the full length polypeptide chain.

However, the resulting *Kd* for the peptide/spermine complex was ~ 1 mM, approximately 80% higher than the 0.6 mM determined for the *wt* protein. These findings support the notion that the lost of residual structure at the C-terminus is able to modulate binding to ligands, which may also have consequences for other protein-protein interactions.
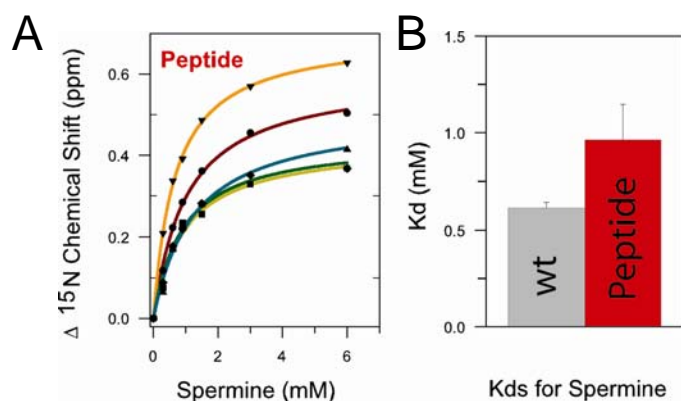


**Figure 5.11. Determination of dissociation constants for spermine- $\alpha$S C-terminal peptide complex.** A titration experiment for spermine binding to the C-terminal peptide of $\alpha$S ($\alpha$S$_{105-136}$) was carried out to determine the *Kd* for the formation of the complex. $^1$H-$^{15}$N-HSQC NMR spectra were acquired at a constant concentration of peptide (1 mM) and different concentration of polycation. **A**. $^{15}$N chemical shifts difference as a function of total concentration of ligand for $\alpha$S-C-terminal peptide. Residues are as follows: Ala$^{124}$ (dark red), Glu$^{126}$ (orange), Met$^{127}$ (light green), Ser$^{129}$ (dark green), Asp$^{135}$ (cyan). **B**. Comparison of *Kds* for complexes of spermine-$\alpha$S (0.61 $\pm$ 0.03 mM) and for spermine-$\alpha$S-C-terminal peptide (1.0 $\pm$ 0.2 mM).

If we now compare the whole picture, the doubling in *Kd* of the mutant protein/spermine complex can be attributed to the loss of residual structure and from the strengthen of electrostatic long range interactions. Assuming a linear combination of both effects we can estimate that the competition between the N-terminus and the polyamine for the negative charges at the C-terminus would account for ~ 20 % increase in the *Kd*. Thus there is an increment in the effectiveness of the N-terminal/C-terminal interaction upon reduction of the long range hydrophobic interaction.
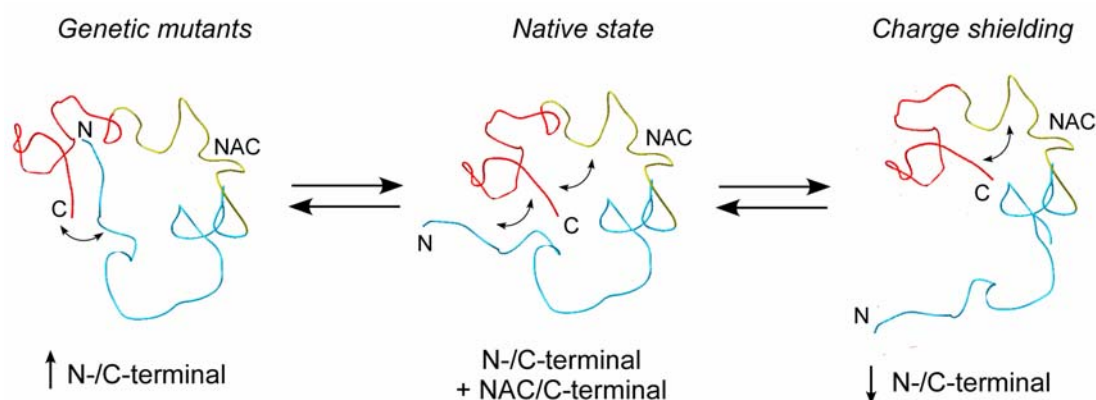


**Figure 5.12. Synergistic long range interactions in αS**. Proposed scheme for the occurrence of long-range interactions in αS. The ensemble of conformations populated by native αS (center) accounts for long-range interactions involving the N-terminus (blue), the NAC region (yellow) and the C-terminus (red) of the protein. The presence of genetic mutations (right) abolishes the hydrophobic NAC/C-terminus interaction, while charge shielding (right) as the presence of salt or low pH cause reduction of the electrostatic N-/C-terminus interaction.

In conclusion, dipolar couplings demonstrate that the intricate network of long-range interactions is perturbed in PD-linked mutant αS, such that the protein is more flexible and able to sample conformations somewhat more collapsed that the *wt* protein. Due to the preferential interaction with the N-terminus, the C-terminus would not be favored to interact with the NAC region, and the hydrophobic residues of this latter domain would be exposed to the solvent, increasing the free energy of the ensemble of conformations. Thus the A30P and A53T mutant αS may overcome more easily the energetic barrier for self-association, leading to an increased tendency to oligomerize (Conway et al., 2000).

## 6. Results. Chapter III: "Structural characterization of the PD-associated protein β-Synuclein."

The protein β-synuclein (βS) is, together with γS, the second and third discovered members of the synuclein family of proteins. βS is highly homologous to αS, co-localizing in presynaptic nerve terminals (Buchman et al., 1998). However, in pathological conditions such as Parkinson's disease (PD) or dementia with Lewy bodies (DLB), βS has a protective role, impeding αS aggregation, both *in vitro* and *in vivo* (Hashimoto et al., 2001; Uversky et al., 2002). It has been suggested that a disruption of a critical balance between αS and βS abundance may be required for neurodegeneration to occur (Rockenstein et al., 2001; Hashimoto et al., 2004), and indeed it has been proposed that a direct interaction between αS and βS is responsible for the inhibitory effect to take place, albeit such a phenomenon has not been documented (Park and Lansbury, 2003).

As determined by CD spectroscopy βS populate unfolded states in aqueous solution (Uversky et al., 2002), and adopt alpha helical conformations upon binding to lipid vesicles (Park and Lansbury, 2003), identically to αS. Conversely, βS and αS differ in their ability to assemble into amyloid-like fibrils, given that βS does not readily aggregate as αS under physiological conditions (Uversky et al., 2002). These differences can be reconciled by consideration of the absence in βS of a hydrophobic 11 amino acid stretch important for αS fibrillation (Figure 6.1) (Giasson et al., 2001).



```
        |            |            |            |            |            |
αS    1 MDVFMKGLSKAKEGVVAAAEKTKQGVAEAAGKTKEGVLYVGSKTKEGVVH   50
βS    1 MDVFMKGLSMAKEGVVAAAEKTKQGVTEAAEKTKEGVLYVGSKTREGVVQ   50

αS   51 GVATVAEKTKEQVTNVGGAVVTGVTAVAQKTVEGAGSIAAATGFVKKDQL  100
βS   51 GVASVAEKTKEQASHLGGAVFSG----------AGNIAAATGLVKREEF    89

αS  101 GKN---EEGAPQEGILEDMPVDPD---NEAYEM-PSEEGYQDYEPEA  140
βS   90 PTDLKPEEVA-QEAAEEPLIEPLMEPEGESYEDPPQEE-YQEYEPEA  134
```

**Figure 6.1. Alignment of αS and βS amino acid sequence.** Comparison of the amino acid sequences of αS and βS. Alignment privileged amino acid conservation on αS RDCs domains (Chapter 1), so no gap penalty was imposed. Shaded in grey are amino acids that differ between both proteins**.**

Interestingly, it was recently reported that βS can also assemble into β-sheet rich oligomers or adopt fibrilar structures under extreme conditions (Yamin et al., 2005). The capacity of βS to fibrillate appears to be determined by the presence of imperfect KTKEGV

repeats in the N-terminal domain of the protein, which is more than 90% homolog to αS (Yamin et al., 2005).

In order to shed more light into the mechanisms regulating αS fibrillation is thus mandatory to inspect βS for sequence determinants of such behavior, similarly to what we determined for αS in chapter 1. No high resolution spectroscopic study had been previously performed on βS, such that nothing was known about the characteristics of the conformations populated by this protein. Such information would be very valuable for a comparative assessment of the hierarchy of tertiary interactions impeding αS oligomerization, or as a prelude for identifying structural determinants able to reverse αS aggregation.

In this chapter we describe the first characterization of βS by means of high resolution NMR spectroscopy. First we applied a set of triple resonance experiments in order to assign the resonances of the protein, and to determine its secondary structure propensities and backbone dynamics. We further studied the protein by techniques optimized for the evaluation of unfolded states of polypeptides, namely RDCs and PRE, and compared those determinations with the measurement of $^3J_{HNH\alpha}$ couplings, reporters of $\phi$ torsion angles. A thorough comparison with its neurotoxic homolog αS provides clues for the understanding of the aggregation behavior of the latter protein.

## 6.1 Backbone assignment of βS.

As a first step towards the characterization of the structure and dynamics of βS, we had to assign the NMR resonances corresponding to the backbone of the protein, since there were no previous reports on NMR experiments on this particular protein. Conventional three-dimensional HNCO, HN(CA)CO, HNCACB and CBCA(CO)NH spectra (Ikura et al., 1990) were successfully recorded on a $^{13}C$-$^{15}N$ labeled βS sample, but assignment was difficult just relying on this experiments. Due to the unfolded nature of βS a limited dispersion of resonances was observed, demanding the use of non-standard three-dimensional experiments, as the HNN pulse-sequence (Panchal et al., 2001) in order to unequivocally assign the resonances. Further obstacles arose from the presence of imperfect KTKEGV repeats but could be circumvent with the strategy applied (table 6.1).

As observed in the $^1H$-$^{15}N$ HSQC spectrum shown on figure 6.2, amide cross-peaks of βS are localized into regions according to the residue nature. Together with the narrow chemical shift dispersion in the $^1H$ dimension, resembling the one of αS (chapter 1) and

denatured ubiquitin (Peti et al., 2001), these observations demonstrate the unfolded nature of βS in solution.
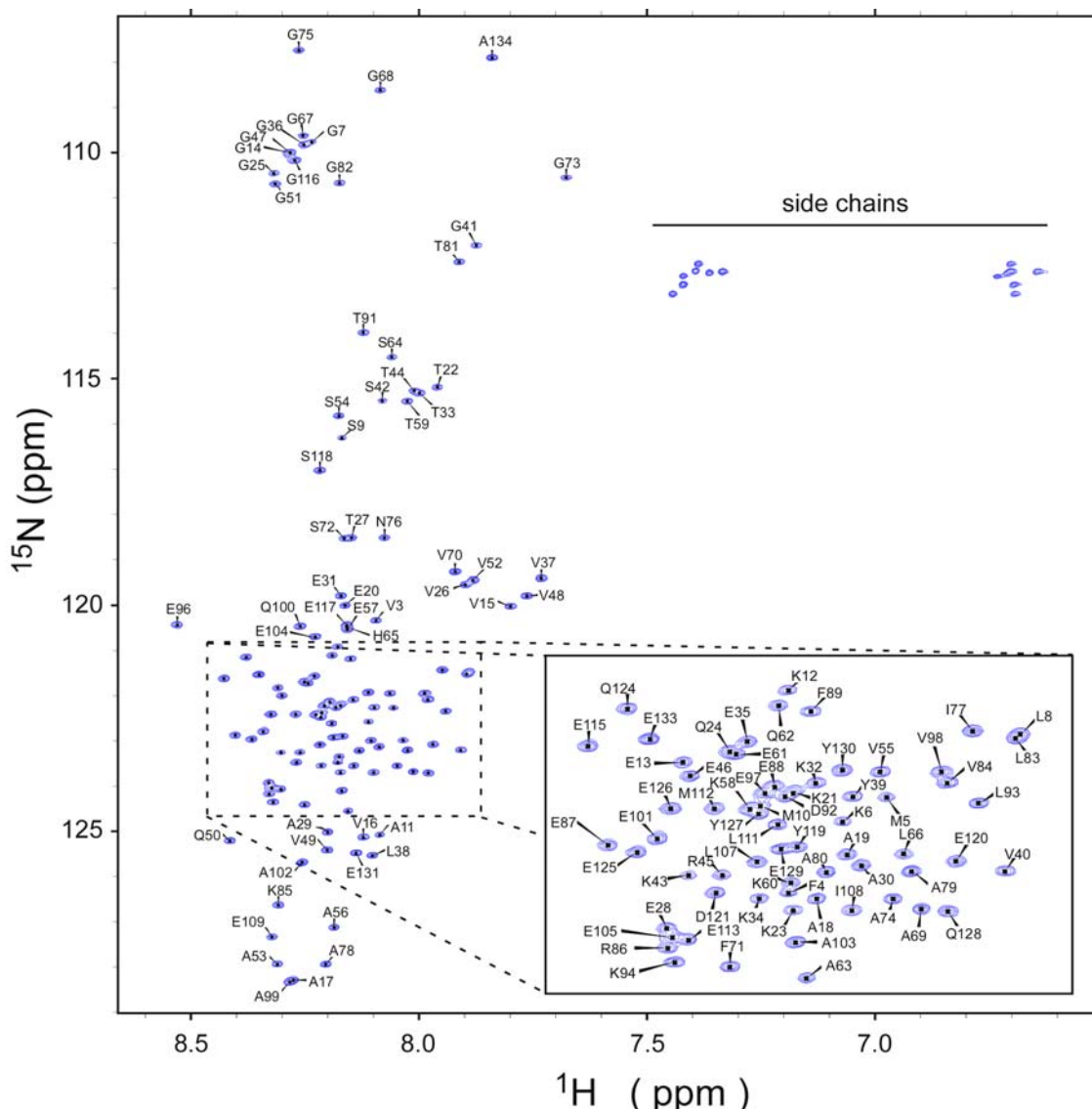


**Figure 6.2. Assignment of the $^{1}$H-$^{15}$N HSQC spectrum of βS.** Employing a combinations of triple resonance experiments it was feasible the assignment of the backbone resonances corresponding to βS. Shown is here an assigned $^{1}$H-$^{15}$N HSQC spectrum were the resonances corresponding to the amide N-H bond are detected. Conditions were pH 6.5, NaCl 100 mM.

Despite signal overlap we were able to assign 126 from 128 non proline residues, failing only to observe resonances corresponding to the very first and second amino acids, due to rapid exchange. Thus 98% of the chemical shifts corresponding to $^{1}$H, $^{15}$N, $^{13}$Cα, $^{13}$Cβ and $^{13}$C´atoms from the backbone of βS were determined.

Interestingly all the amide cross-peaks occurring in the HSQC spectrum display closely similar intensities, suggesting that conformational exchange does not occur under this condition of pH and temperature. The conditions employed to study βS were pH 6.5 and 100 mM NaCl, and when compared with the spectrum of αS measured at the same conditions, some differences are evident. As observed in figure 6.3, the pattern of intensity for amide resonances corresponding to βS is nearly flat (red line), except for short stretches of residues centered on amino acids 8 and 44. Differences with αS (blue line) where observed at Thr, Ser and Val residues.
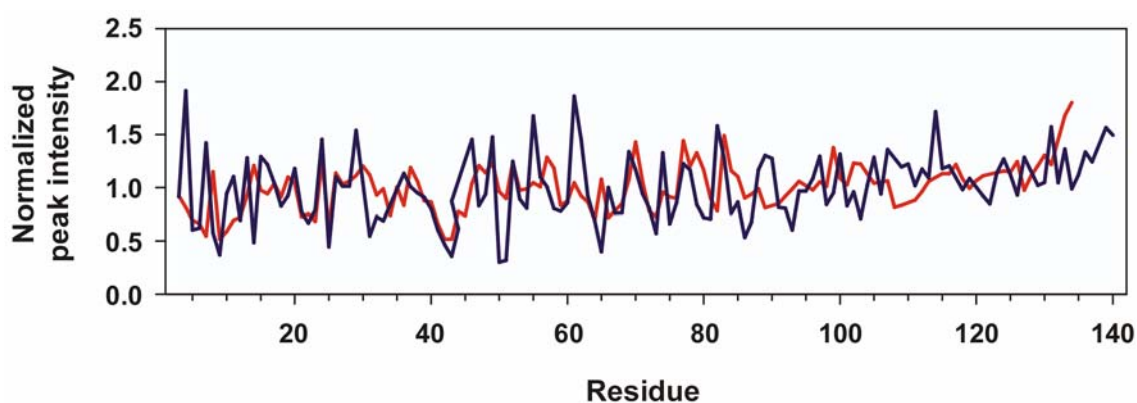


**Figure 6.3. Intensity ratios for amide resonances in βS compared with αS.** Profile for the normalized intensity ratio (respect to average signal), corresponding to βS (red line) and αS (blue line) at pH 6.5.

In order to further compare the intensity profiles of βS with αS, we measure an HSQC spectrum of βS at pH 7.4 (Figure 6.4A). As shown on figure 6.4B, under these conditions βS appears to behave similarly to αS, and features a reduced intensity of several resonances at the N-terminus of the protein. Thus amide exchange rates are also defining the intensity of peaks at the N-terminal region of βS.
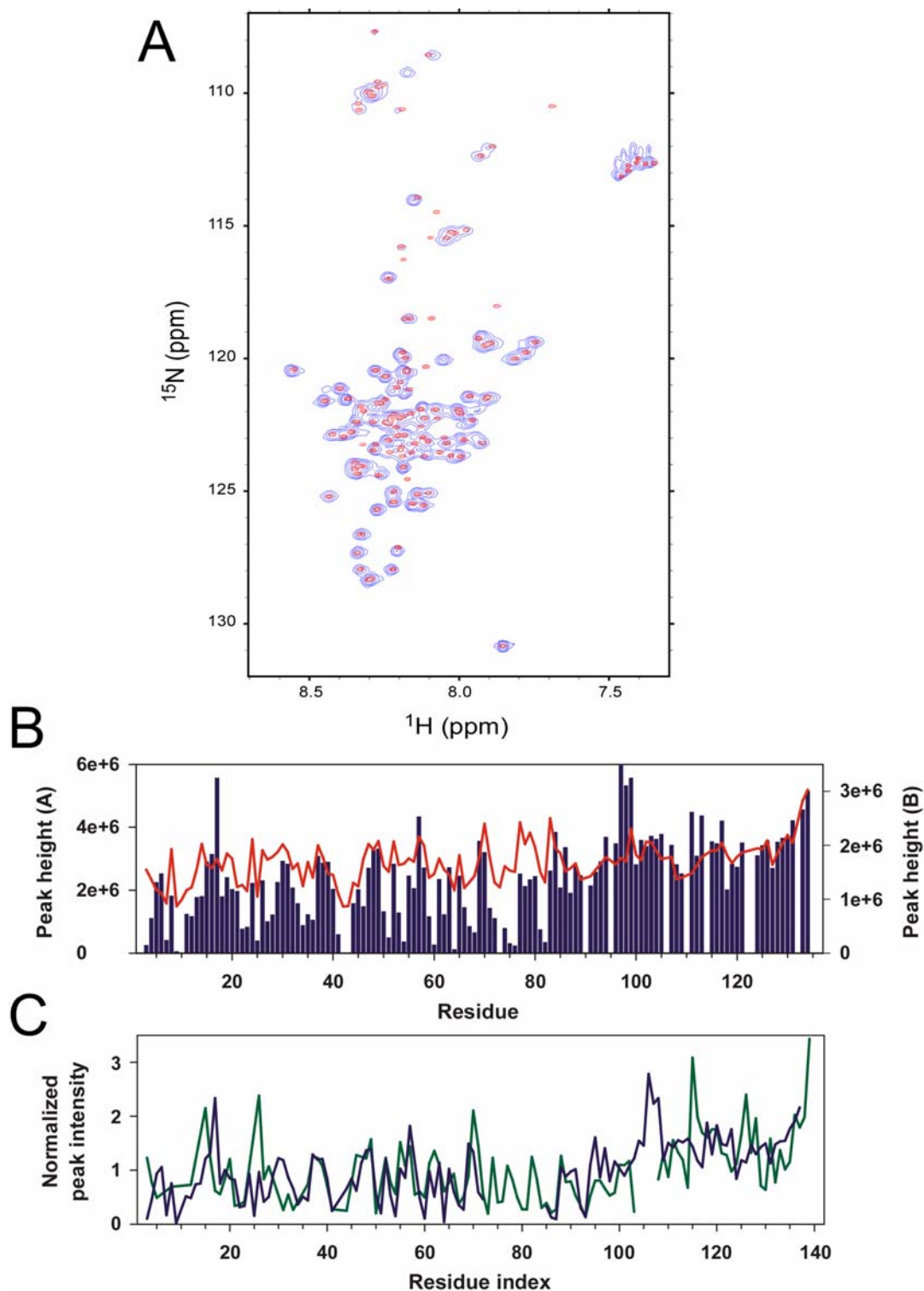
**Figure 6.4. Amide resonances of βS at pH 7.4**. **A**. ^{1}H-^{15}N HSQC spectrum of βS measured at pH 7.4 and 100 mM NaCl (blue), overlapped with a spectrum measured at pH 6.5 and 100 mM NaCl (red). The spectrum in blue was acquired at 600 MHz while the spectrum in red at 900 MHz (cryoprobe), and thus the differences in line widths. **B**. Intensity plots of the spectrums shown on A for βS at pH 7.4 (blue bars, A) and pH 6.5 (red line, B), scaled to the peak intensity of the residue A[134]. **C**. Normalized peak intensity for βS (blue line) and αS (green line) at pH 7.4, relative to average peak height.

In order to obtain a general characterization on the ensemble of conformations populated by the protein, we measured the hydrodynamic properties of βS. Employing PFG NMR we found that, although being 6 residues shorter, βS possess an Rh almost 0.5 Å longer than αS (Figure 6.4).
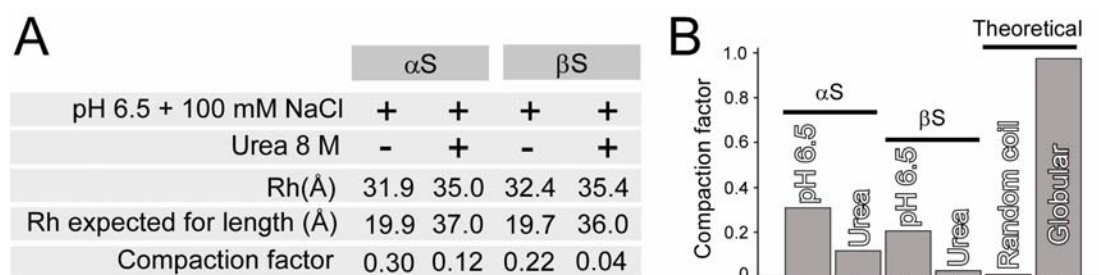


**Figure 6.4. Hydrodynamic properties of βS. A.** Measurement of Rh by PFG-NMR for αS and βS under different solution conditions. The expected Rh for length are calculated based on empirical determinations on native and unfolded proteins (Wilkins, 1999, Biochemistry), and as described in the methods section. **B**. Plot of compaction factors derived in A.

The degree of unfolding of the two proteins can be compared through calculation of their compaction factors, which relates the measured Rh with empirical estimations of the minimum and maximum values expected for the length of the polypeptide chain (Wilkins et al., 1999). Thus, at the studied conditions, αS possess a compaction factor of 0.3, higher than the 0.22 value determined for βS. This predicts that βS is considerably more extended than αS, which has been already observed by SAXS (Uversky et al., 2002). Furthermore, by measuring the Rh at strong denaturing conditions, we determined that at 8 M urea βS adopts a completely unfolded conformation (compaction factor of 0.04), while αS still is still slightly collapsed (compaction factor of 0.12). This supports the findings of small persistence of residual long range interactions between the N- and C-terminus of αS at 8 M urea, as probed by PRE (Chapter 1), and suggests that βS may not feature such stabilizing interactions, adopting readily random coil conformations.

**6.2. Propensity to form secondary structure in βS is suggested by chemical shift analysis.**

In the preceding section we have found differences and similarities between αS and βS, but still both proteins are considerably unfolded as judge by $^1$H and $^{15}$N resonance dispersion. Triple resonance NMR experiments are well suited to provide information about the backbone of an unfolded protein on a residue-specific basis. Thus, local propensities for

structures that are preferentially sampled by the backbone of such highly dynamic systems may be derived from the determination of the NMR chemical shifts for backbone Hα, Cα and C′ atoms, as well as side-chain Cβ atoms (Dyson and Wright, 2004). In particular Hα, Cα and C′ chemical shifts are suitable for determining secondary structure propensies by subtracting the values corresponding to the empirically determined random coil shifts (Wishart and Sykes, 1994).

As shown in figure 6.5, significant deviations in chemical shifts occur for backbone regions in βS. Consistent negative deviations for Hα shifts suggest that the whole polypeptide chain populates conformations with slight helical nature (Figure 6.5A). Positive deviations in Cα and C′ shifts, indicative of α-helical propensies, were exclusively observed at the N-terminus of the protein, where the stretch comprising residues 56 to 66 showed the strongest propensity to adopt such conformations.

Negative deviations from random coil shifts are indicative of β-sheet or extended structures, and were evidenced at the whole C-terminus of βS, surprising result in view of the occurrence of 8 proline residues on this region. The restrictions imposed by these amino acids, known to impede β-sheet formation, would then favor adoption of extended polyproline II conformations in βS, consistently with the helical preference determine by Hα deviations (McCarney et al., 2005). Backbone chemical shift analysis fail to differentiate polyproline II from β-sheet, which largely overlap in the Ramachandran space.
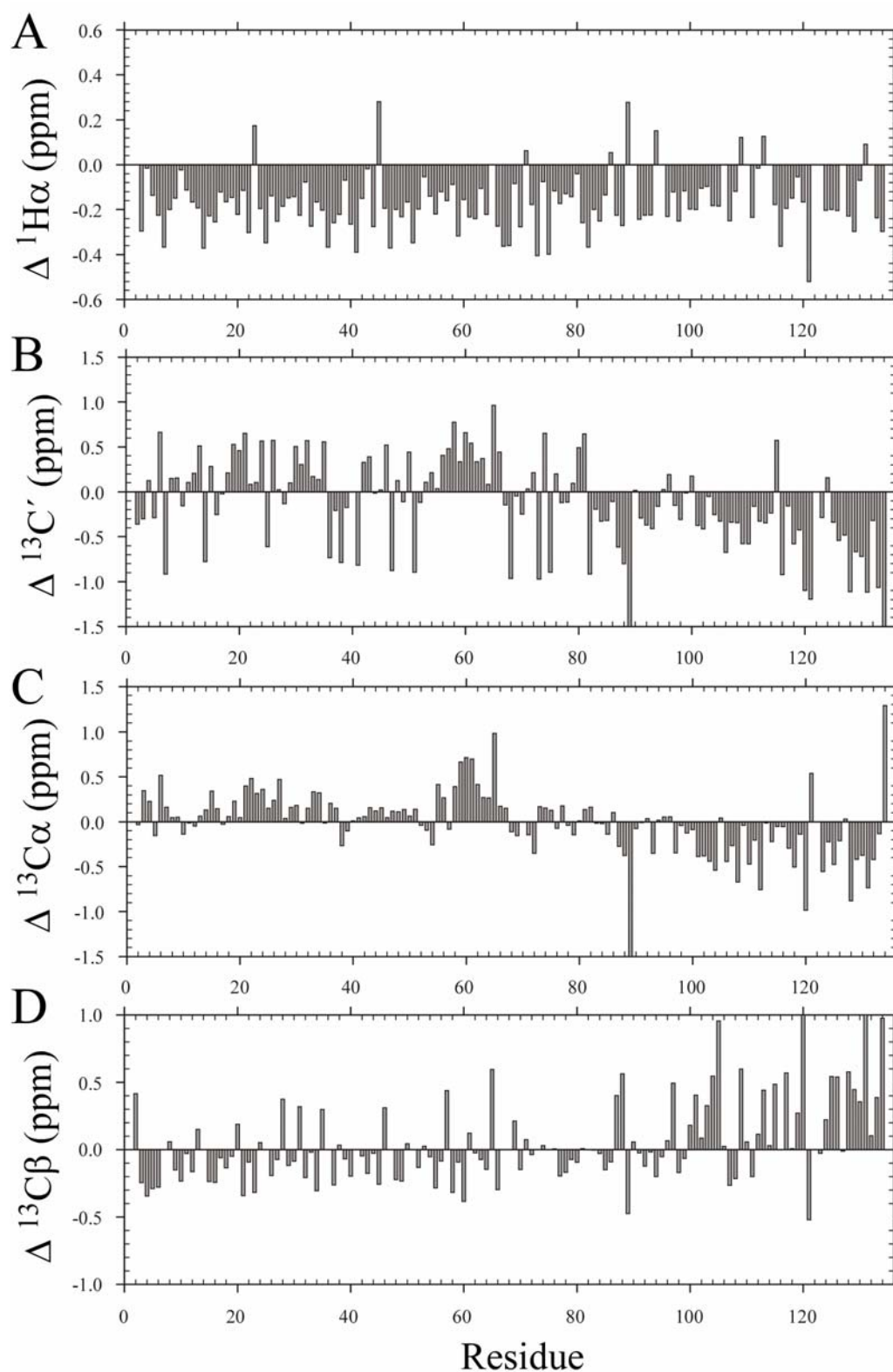
**Figure 6.5. Chemical shifts deviations for the backbone of βS.** Measured chemical shift values for backbone atoms of βS were subtracted from random coil values and the result differences are plotted. **A**. Hα proton. **B**. Carbonyl carbon. **C**. Cα carbon. **D**. Cβ carbon.

Mean weighted chemical shift differences taking in account Cα and C′ deviations from random coil values showed a strong dependence between residual secondary structure in βS and interactions with the solvent. As depicted in figure 6.6, hydrophilic regions on the N-terminus of the protein displayed propensity to adopt α-helical conformation, while hydrophobic regions reflected a tendency to populate conformations with residual β-sheet character, likely providing a minimized interaction with the polar solvent.
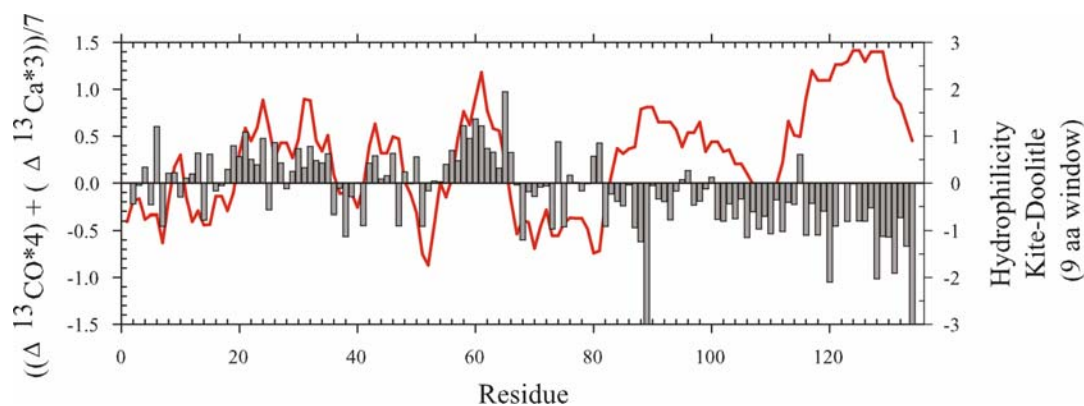


**Figure 6.6. Mean weighted chemical shifts correlate with hydrophilicity in βS.** Correlation between combined and weighted carbonyl and Cα carbon chemical shifts differences (grey bars), and hydrophilicity by Kite-Doolitle method (red line, 9 residue window).

The correlation with the solvent is lost for the C-terminus of the protein, starting on residue 80. Due to the high net charge of this region (-16), a strong hydrophilicity was predicted, but the chemical shift analysis indicates an overall tendency to populate restricted conformations with β-sheet propensity. As stated before, the occurrence of 8 proline residues discourages such residual structure on this region and we interpret this observation as a tendency to adopt polyproline II conformations. The helical nature of this particular structure would thus be in accordance with the hydrophilic properties of the C-terminus and with a strong protein-solvent interaction.

For αS, only Cα chemical shift differences with random coil values have been reported (Bussell and Eliezer, 2001). When compared with those that we measured in βS, a strong correlation at the N-terminus is observed (Figure 6.7), due to the high homology of both domains. However, almost the whole stretch of residues between amino acids 8 to 50 displays in βS (blue line) a reduced propensity to adopt secondary helical structure compared with αS (red line). The opposite is seen around position 60, where βS shows high propensity to form helical structures which are small in αS. This is likely to be due to the absence of

hydrophobic residues in the beginning of the central domain of βS, favoring solvent-side chains interactions.
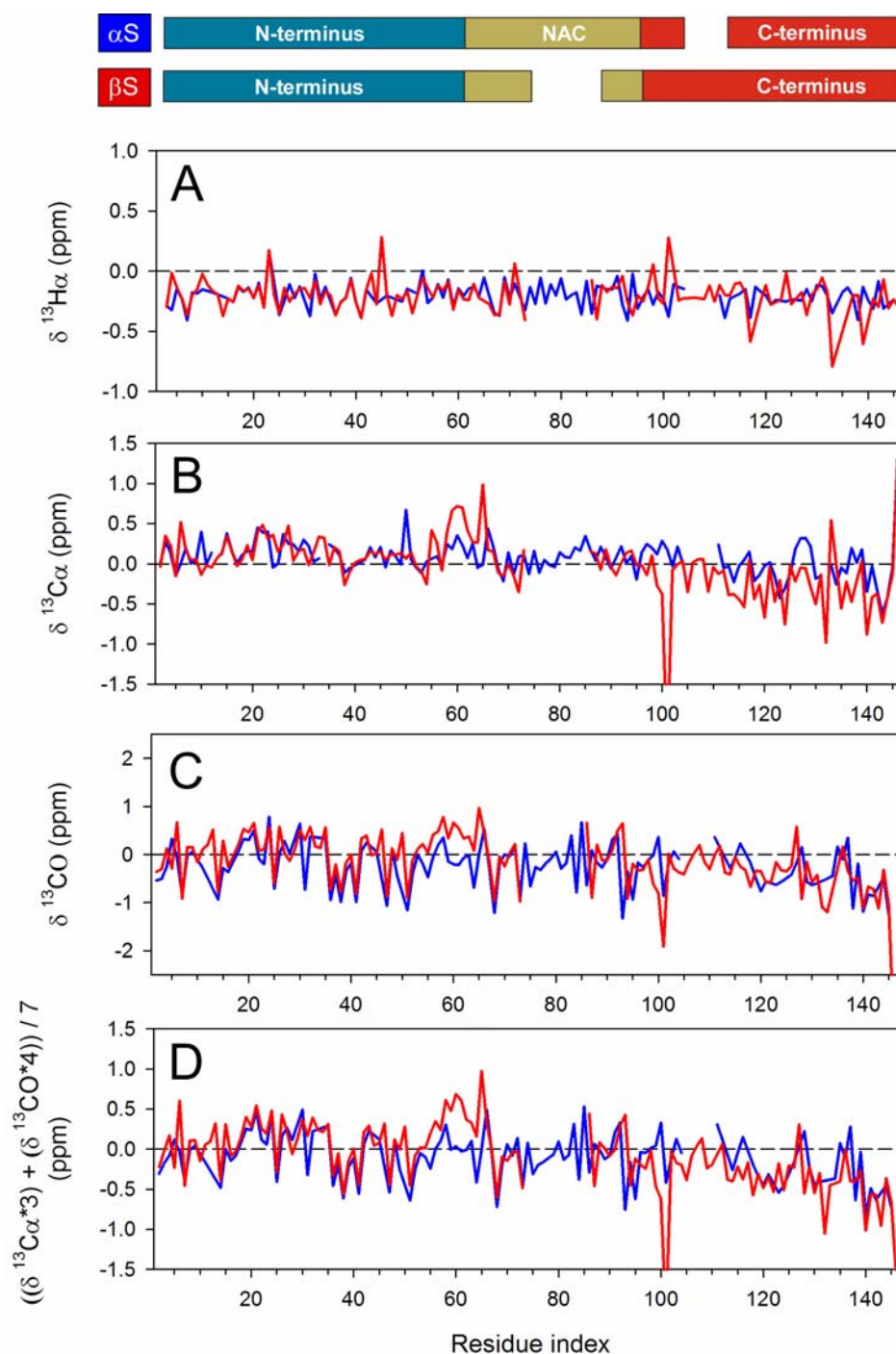


**Figure 6.7. Comparison of secondary chemical shift deviations for αS and βS.** Deviations of measured chemical shifts from the expected random coil values provide hints on the nature of the secondary structure sampled by the backbone of a protein. For Cα (**B**), CO (**C**) and mean weighted carbon chemical shift (**D**) positive deviations are indicative of α-helices, while negative deviations suggest β-sheet or extended conformations. In the case of Hα (**A**), an inverse relationship is valid. In red is

shown βS and in blue αS, both measured at pH 6.5 and 100 mM NaCl. Protein sequences are aligned according to the lack of NAC region in βS and the shorter C-terminus in αS (top scheme).

The correlation is lost at the C-terminus of the protein, with βS showing an overall propensity towards extended conformations, while in αS few scattered residues show such characteristic. Although both proteins possess a highly negatively charged C-terminus, βS possess 3 more negative residues featuring an increased number of aspartic residues instead of the glutamic ones found in αS. In addition, βS has 8 Pro residues on this domain, 3 more than αS, which could sustain extended conformations as polyproline II.

**6.3. NMR relaxation evidences fast dynamics in βS.**

In order to provide more insights into the unfolded nature of the protein we characterized the dynamics of the polypeptide chain by measuring $T_1$, $T_2$ and heteronuclear NOEs for backbone resonances in βS. These standard determinations are very useful for determining order parameters in folded proteins, which are related to the motional restrictions associated with domains with defined secondary structure.

As observed in figure 6.8, measurement of $R_1$ and $R_2$ rates for βS amide cross-peaks displayed a bell-shaped profile characteristic of unstructured polypeptides. For $R_1$ a mean value of 1.4 $s^{-1}$ was observed (Figure 6.8A), while the average $R_2$ value was 3.0 $s^{-1}$ (Figure 6.8B), rates very similar to the ones reported for other native unfolded polypeptides as the HIV-1 Tat protein or the histone mRNA binding protein SLBP (Thapar et al., 2004; Shojania and O'Neil, 2006a). Minor deviations centered on residues 42, 60 and 110 were evidenced, suggesting slower dynamics for these regions in the ns-ps timescale. These determined values clearly indicated that rapid internal motion exists for most amides, consistent with the protein being mostly unfolded.

In addition, steady-state heteronuclear NOEs were measured for βS and ranged in the region ± 0.2, indicative of the absence of restricted dynamics in the ns-ps timescales (Figure 6.7C). Nevertheless two stretches of residues with high NOEs were evidenced centered on positions 60 and 90, likely reflecting minor degrees of dynamic restrictions in such timescale.

When compared with αS, some particular differences can be noted. The average $R_1$ for αS ranges on ~ 2 $s^{-1}$, significantly higher than the mean value in βS (1.4 $s^{-1}$) (Bussell and Eliezer, 2001). Similarly, the $R_2$ mean value for αS is higher than for βS (3.8 $s^{-1}$ vs 3.0 $s^{-1}$), and only displays a cluster with high $R_2$ at position 44. What is preserved between both

proteins is the NOE pattern which for αS ranges also on the ± 0.2 region. The lower $R_1$ and $R_2$ values are in line with the higher unfolded nature of βS respect αS.
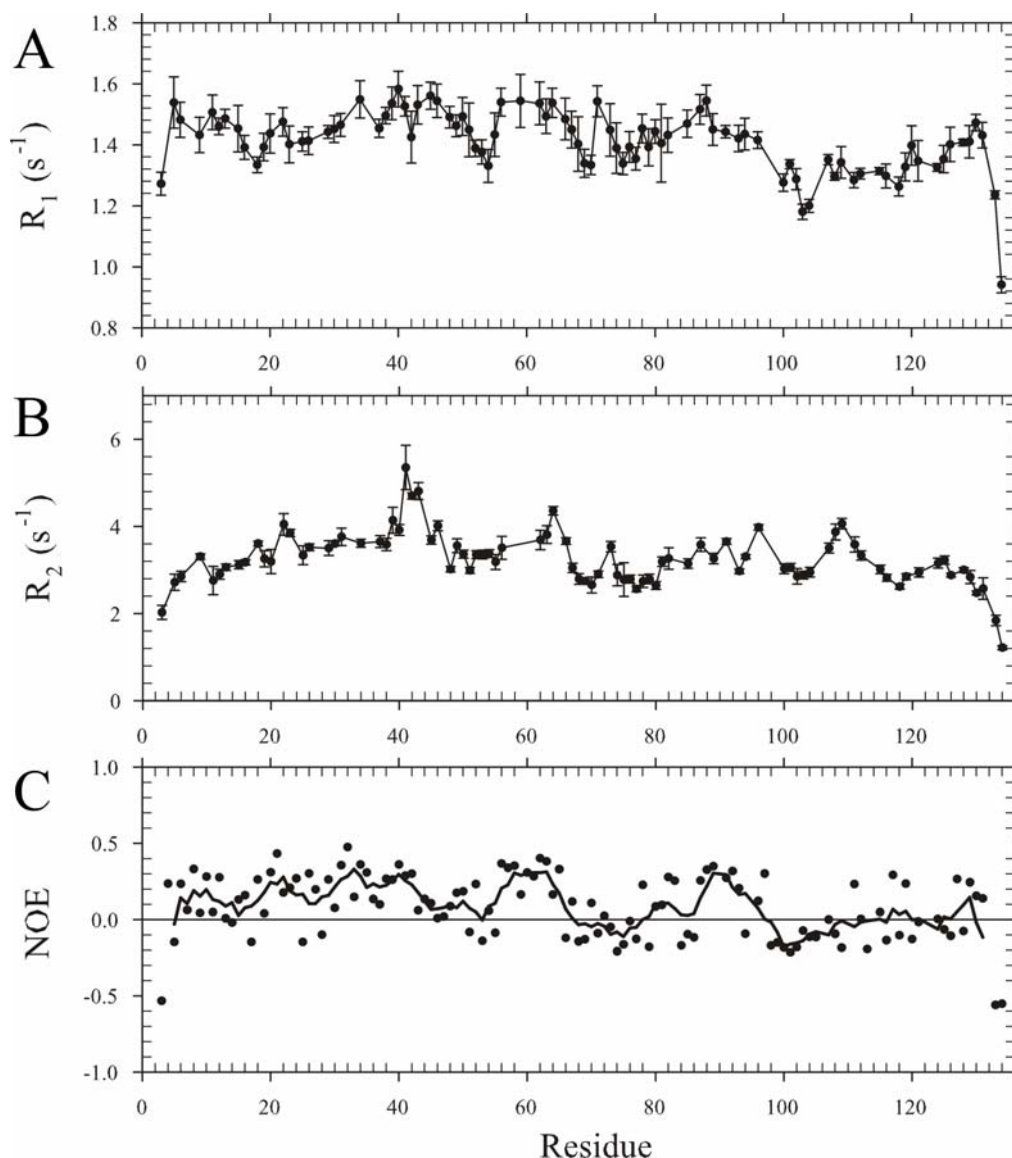


**Figure 6.8. NMR-relaxation profiles for βS. A.** Longitudinal relaxation rates (R1). **B.** Transverse relaxation rates (R2). **C.** Heteronuclear NOEs with a 5 residue average window.

## 6.4. Residual structure in βS probed by dipolar couplings.

It has been shown throughout the previous chapters how residual dipolar couplings were a very powerful NMR parameter to study the unfolded state of αS. However, interpretation of RDCs in random coil polypeptides has been a subject of debate, but now it is widely accepted that they report on the degree of residual structure and the persistent length of segments in the chain (Louhivuori et al., 2003; Louhivuori et al., 2004). Thus small couplings would be indicative of a poor degree of preferred orientations by the segment, while high RDCs values

would arise from conformational restrictions and residual structure. We have previously applied this technique to study the native unfolded state of αS and found long range interactions and residual structure at the C-terminus of the protein important for impeding protein aggregation (Chapter 1).

When $^1D_{NH}$ dipolar couplings were measured in βS aligned in Pf1 phages as anisotropic media, we observed predominantly positive couplings similar to what was described for αS (Figure 6.10A). A particular feature of βS is that the whole C-terminus of the protein shows RDC values that on average are 2 times higher than the N-terminus. These small couplings in the N-terminal domain are indicative of the flexible nature of this region, in line with the relaxation rates that we determined. On the other hand, the high couplings measured for the entire stretch of 30 residues at the C-terminus suggest a significant amount of residual structure, not detected by measurement of relaxation but inferred from the chemical shift analysis, and supporting the occurrence of polyproline II conformations.
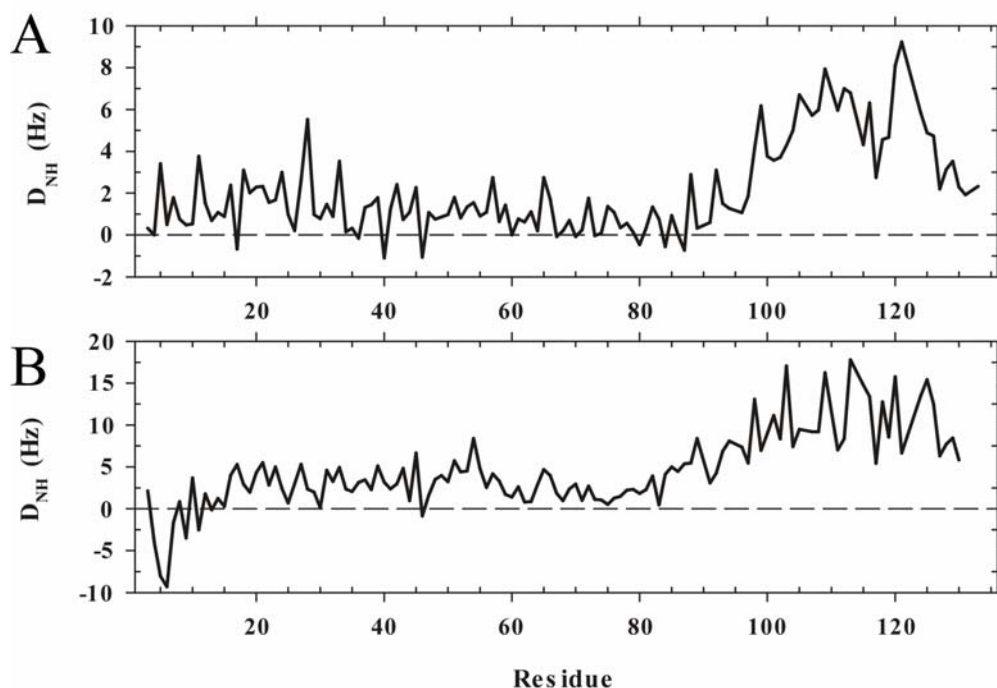


**Figure 6.10. Residual dipolar coupling in βS. A.** RDCs profile for βS aligned in Pf1 (5mg/ml). **B.** Pattern of RDCs for βS aligned in 5% $C_8E_5$/octanol.

Importantly, the main features of the RDCs pattern were reproduced in a second alignment media, a PEG/alcohol mixture (Figure 6.10B).

The high values of RDCs at the C-terminus of the protein are reminiscent of the profile obtained for αS. In αS the RDCs reported long range-induced residual structure as

two clusters with particularly high values of $^1D_{NH}$ correlating with couplings in the NAC region. When compared with βS (Figure 6.11), it is noteworthy the sole presence of high couplings at the C-terminus, which are not restricted but rather extended to the whole domain.
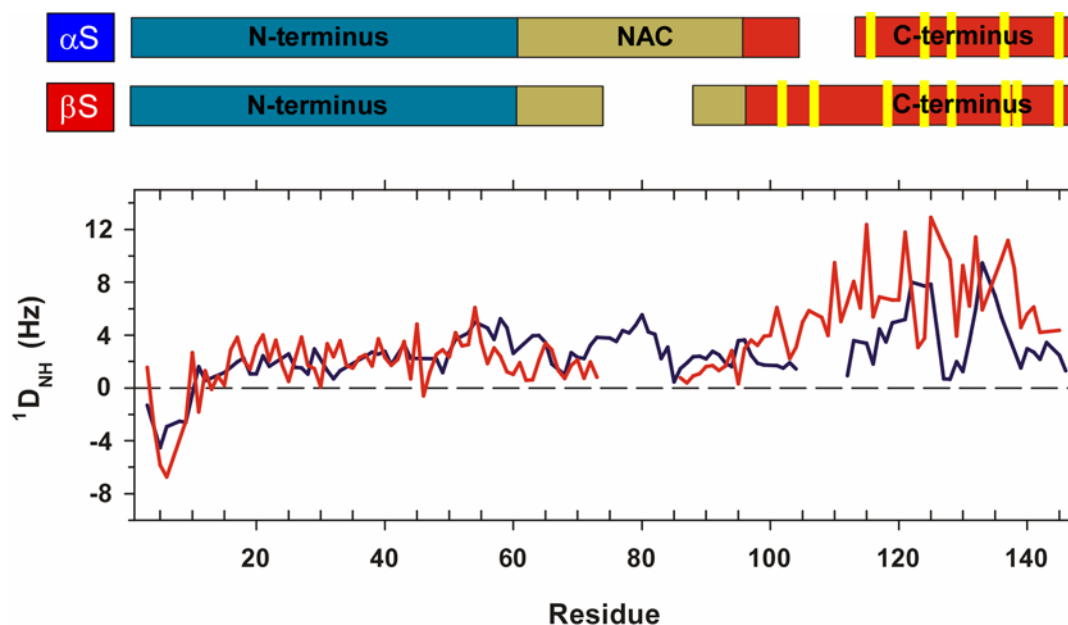


**Figure 6.11. Comparison of RDCs between αS and βS.** Overlay of RDCs profiles for αS (blue) and βS (red) measured in C8E5/octanol as alignment media. Sample condition was pH 6.5 and 100 mM NaCl in both cases.

The question underlying these findings is whether βS, although being highly unfolded, still has long range interactions, or whether in this case the RDCs are probing a locally-encoded residual structure. Due to the absence of the NAC region, feasible long-range contacts to occur in βS would involve the positively charged N-terminus and the negatively charged C-terminus, as seen in the case of αS.

## 6.5. Residual structure in βS is locally encoded.

In order to dissect local and non-local contributions to the conformational restrictions observed at the C-terminus of βS, we sought to evaluate the occurrence of long range interactions in this protein. In a similar fashion as used to reveal long range contacts in αS (Chapter 1), we employed paramagnetic resonance enhancement by nitroxide spin labels to study the conformations populated by βS in solution.

When we placed the paramagnetic reporter at the N-terminus of the protein (position 18th) the broadening effect was only local but more pronounced that the one expected for a

random coil polypeptide, suggesting a minor degree of compactness of this region (Figure 6.12). Similarly, when the spin label was placed at the center of the protein (position 79th), a strong paramagnetic effect was extended towards the N-terminus of the protein but not towards the C-terminus, reflecting the occurrence of local compaction but the absence of long-range contacts.
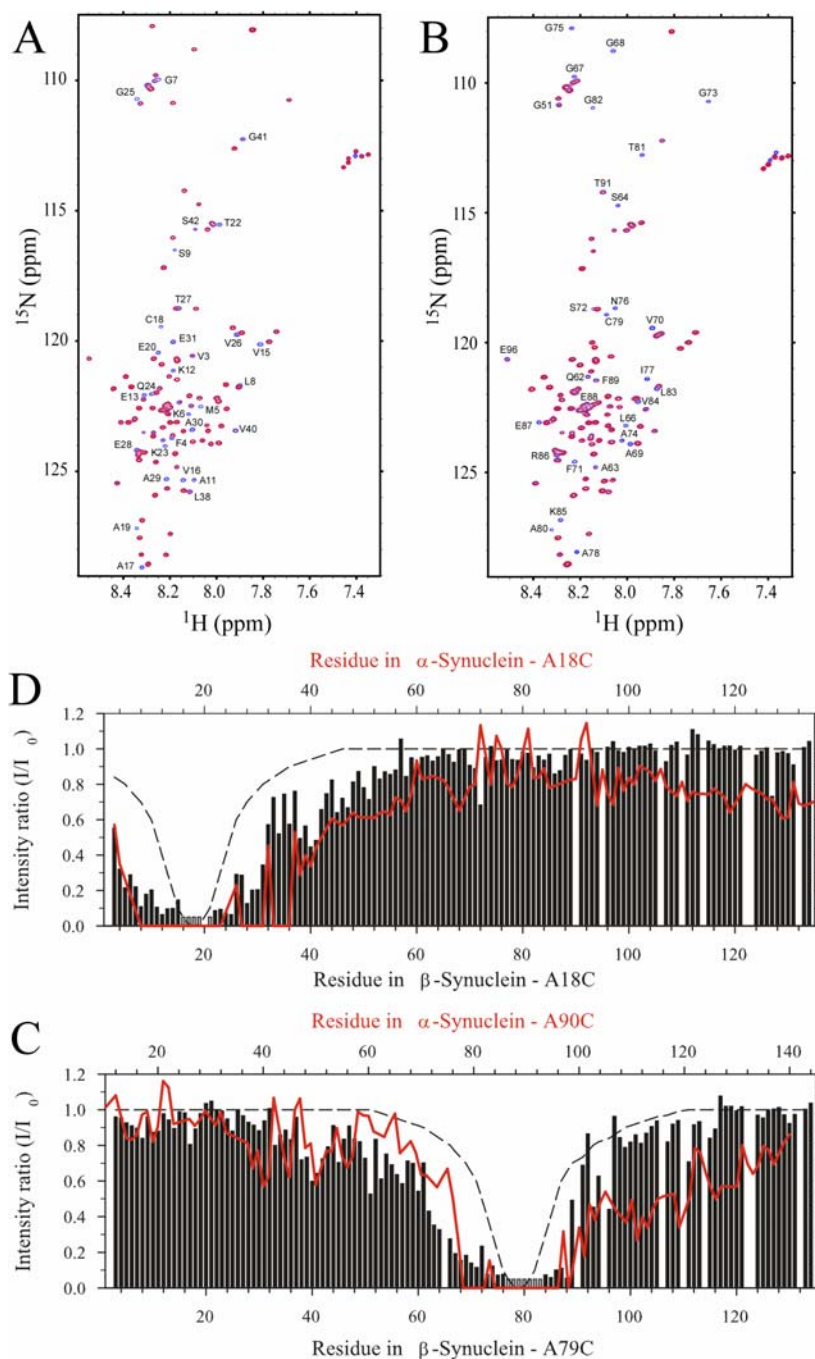


**Figure 6.12. Paramagnetic relaxation enhancement in βS.** Two Cys-containing mutants of βS (A18C and A79C) were constructed in order to provide attachment sites for the paramagnetic tag MTSL. **A**. Overlay of the HSQC spectra measured in the presence (red) and absence (blue) of MTSL attached to position 18.

Note how affected resonances are broadened beyond detection. **B**. Same as A, but for the MTSL tag placed on position 79. **C**. Profile of intensity ratios for resonance peaks between the paramagnetic (MTSL) and diamagnetic (no MTSL) states for βS-A18C protein (black bars). In red, the intensity ratios for the mirrored mutant in αS (αS-18C) are overlaid for comparison. The expected profile for a random coil polypeptide, with the paramagnetic tag placed at the same position, is depicted in grey dashed line. **D**. The same as C, but for βS-A19C (black bars) and αS-A90C (red line).

The paramagnetic labeling at 18th and 79th positions in βS mirror the 18th and 90th positions employed in the study of αS, which allowed us to perceive long range contacts between the N- and C-terminus of the protein and a compaction at the C-terminus aid by an interaction with the central hydrophobic stretch, respectively (Chapter 1). In βS neither long range interactions nor C-terminal compaction was observed, which may be due to the lack of the hydrophobic region in the middle of the protein. Thus residual structure at the C-terminus of βS is exclusively the result of local conformational restrictions. In addition, these results in βS provide additional confirmation to the key role that the central hydrophobic region of αS plays on the formation of the long range interactions with the C-terminus.

## 6.6. Polyproline II structure is evidenced at the C-terminus of βS.

Local structure in unfolded polypeptides has been attributed to the presence of a significant amount of polyproline II (PII) helical extended conformations, even for sequences of low proline content (McCarney et al., 2005). This observed tendency to adopt PII helix is attributed to the tendency of the backbone to preferentially populate $\phi$, $\psi$ angles in the lowest, broadest energy levels, situated in the upper left quadrant of the Ramachandran space, where β-sheet and PII helices occur (Dyson and Wright, 2002).

To further search for factors that could explain the chemical shift patterns and the RDCs profile obtained for βS, we measured $^3J_{HNHA}$ scalar couplings which report on the $\phi$ torsion angle of a given residue. Thus small $^3J_{HNHA}$ couplings (3 to 5 Hz) correspond to helical conformations, where high couplings are indicative of sheet conformations (8 to 11 Hz) (Dyson and Wright, 2002). As shown on figure 6.13, the $^3J_{HNHA}$ scalar coupling profile for βS demonstrates that the whole polypeptide backbone is preferentially sampling coil and helical conformations, with no single residue displaying coupling values higher than 8. The average coupling value of ~ 5.5 is reduced in comparison with the value of ~ 7 found for other unfolded polypeptides (Smith et al., 1996; Shojania and O'Neil, 2006a).
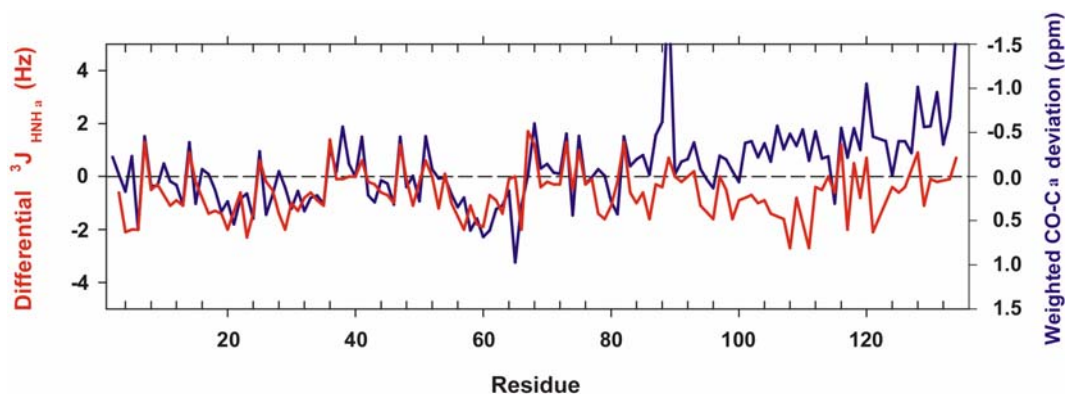
**Figure 6.13. ³J$_{HNH\alpha}$ profile for βS.** The measurement of three-bond scalar coupling between the amide proton and the Cα proton is indicative of the φ torsion angle that the amino acid is preferentially sampling. The secondary ³J$_{HNH\alpha}$ profile (coil values substracted from experimental values) for βS (red) is compared with the weighted deviation between carbonyl and Cα carbons (blue), indicative of secondary structure propensities for the polypeptide backbone.

The low ³J$_{HNHA}$ scalar couplings are easily rationalized for the N-terminal half of the protein (up to residue 80), by correlating with the determined chemical shift deviation, suggesting a sampling of conformations with a slight preference for α-helices. The correlation is lost in the C-terminus, where Cα and C´ deviations suggest populations of extended, β-sheet like, conformations, while Hα and ³J$_{HNHA}$ couplings demonstrate that these residues preferentially sample helical conformations. The backbone conformation reconciling such features is the PII structure, which preserves helical-like features sampling an extended space (Dyson and Wright, 2002). The PII residual structure at the C-terminus of βS is also suggested by the presence of 8 Pro residues, 2 of them consecutive, which do not particularly favor sampling β-sheet conformations, but may easily adopt PII structure.

Additional support for claiming the finding of PII instead of α-helices, could be inferred from the RDCs pattern. While β-sheet and PII conformations align the NH bond vector perpendicular to the principal axis to the chain direction, α-helices align it parallel (Mohana-Borges et al., 2004). This effect will provoke, in the manner that we determined the RDCs, dipolar couplings to be positive for β-sheets and PII structures, and negative for α-helices. We did observe strong positive coupling for the whole C-terminus, supporting the preferential sampling of residual PII conformations. In line with these findings we detected negative RDCs for the first 10 residues of the protein (aligned in C8E5, Figure 6.12B), but failed to detect such conformational restriction in the rest of the N-terminus, where couplings were very small, similar to what is expected for a random coil ensemble (Louhivuori et al.,

2004). These data do not support the existence of a population of conformers with a consistent α-helical content at the N-terminus, suggesting rather a highly dynamic conformational sampling, likely modulated by solvent-side chains interactions.

The $^3J_{HNHA}$ scalar couplings measured for αS (Figure 6.14) were also consistent with the unfolded nature of the protein, with a mean value of ~ 8 Hz, slightly higher than the average value of ~ 7 Hz, found in unfolded polypeptides. When compared with the previous result, the overall smaller couplings on βS are readily evident. Interestingly, the C-terminus of αS, despite having 5 Pro residues and a similarly high negative net charge as βS, does not populate PII structure, as suggested by the higher $^3J_{HNHA}$ couplings.
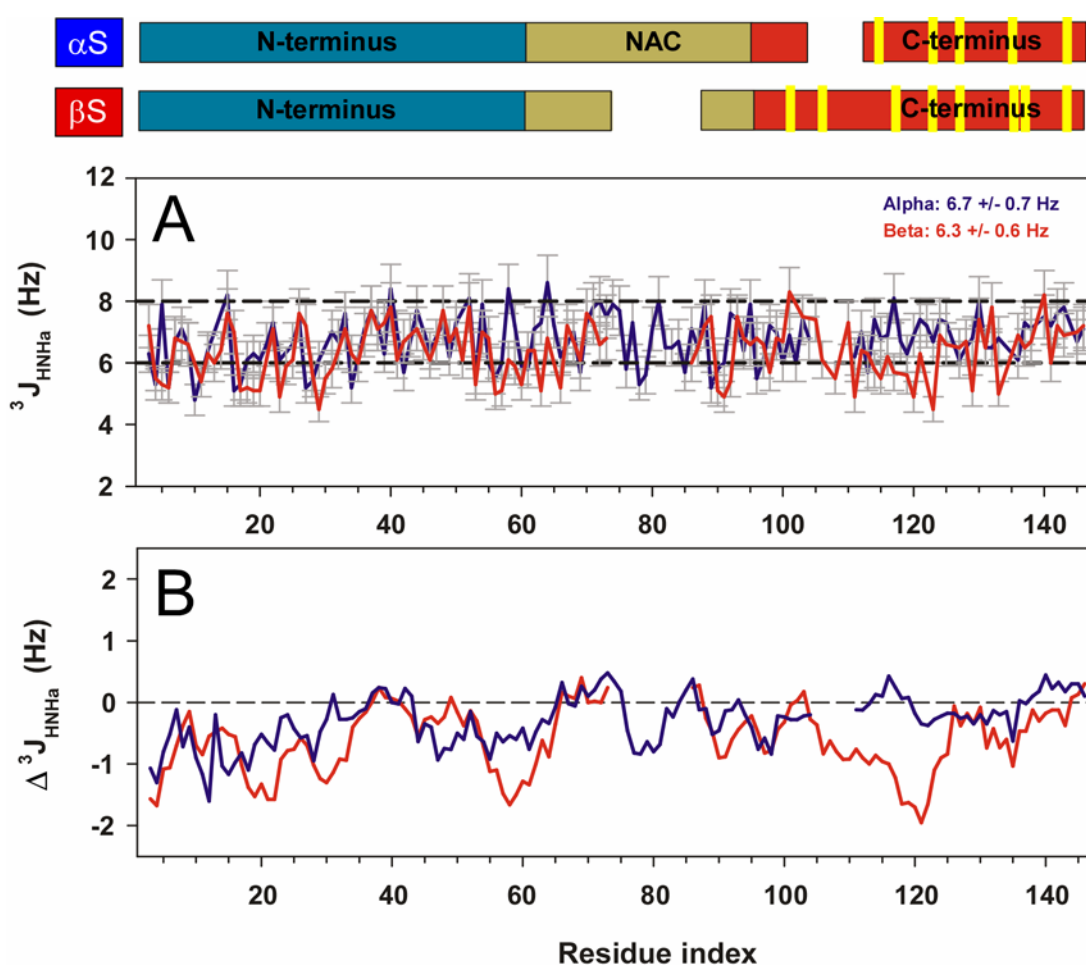


**Figure 6.14. Comparison of $^3J_{HNH\alpha}$ couplings for αS and βS. A.** Overlay plot of three-bond scalar coupling between amide proton and Cα proton for αS (blue) and βS (red). **B**. Comparison of secondary $^3J_{HNH\alpha}$ profile (coil values substracted from experimental values) for αS (blue) and βS (red), over a 5 residue window, indicative of the differences in the conformations sampled by both polypeptide chains. Sample condition was pH 6.5 and 100 mM NaCl in both cases.

The $^3J_{HNHA}$ values reported here for αS were measured at pH 7.4 while the ones in βS were measured at pH 6.5. This could be a reason why some differences for the couplings at the N-terminus of both homologous proteins were observed for this highly conserved domain. However, as RDCs probed in αS, only minor changes were determined on the protein upon a slight reduction in the pH, which are centered on the very N-terminus. The structural features of the C-terminus domain of αS remained unperturbed, and thus a comparison with βS is possible.

In summary we have demonstrated in this chapter that βS is a natively unfolded protein that populates an ensemble of extended conformations. The N-terminal half of the protein does not possess significant amount of residual structure, and interacts strongly with the aqueous solvent. Conversely, the C-terminal half populates conformations with significant residual PII extended structure. Furthermore, these studies also helped us to understand the role of residual structure and long range interactions in the native state of αS.

## 7. Results. Chapter IV: "Structural basis of metal binding to α-synuclein".

An increasing number of studies indicate that transition metals, in their di- and trivalent ionic form, are capable of accelerating the aggregation process of various pathologic proteins, as Aβ, prion proteins, β2-microglobulin and αS (Sayre et al., 1999). In the case of αS, it was shown that Cu(II) was the most effective ion in promoting αS oligomerization (Paik et al., 1999). Later on, a systematic analysis of the effect of various metal ions revealed that Al(III), Fe(III) and Cu(II) efficiently accelerate αS fibrillation *in vitro*, whereas Fe(II) and Mn(II) presumably form stable complexes with the protein as they quench tyrosine fluorescence (Uversky et al., 2001c; Golts et al., 2002).

Neither the structural characterization of the binding sites for metal ions, nor the identification of the amino acids involved in the interaction have been reported up to date. We thus sought to employ high-resolution spectroscopic techniques to establish the role of metal ions in αS fibrillation at the molecular resolution currently available for other amyloid diseases.

We chose Cu(II) as the first metal ion to characterize, since it was reported to effectively accelerate αS aggregation (Paik et al., 1999), and because it seems to be a common denominator under many amyloid diseases as AD and Prion diseases, among others (Sayre et al., 1999). In addition, the paramagnetic nature of the metal ion allowed us to employ high resolution techniques, as NMR to map the binding interfaces, and electron paramagnetic resonance (EPR) spectroscopy to study the ligand contribution to the complex. After assessing the structural determinants of Cu(II) binding to αS we performed a comparative study of other divalent paramagnetic ions in order to determine the hierarchy of metal-protein complex formation.

### 7.1. Cu(II) binding to αS promotes protein aggregation

The above-mentioned reports on the effects of transition metal ions on αS fibrillation were performed at mM concentrations, far greater than those normally occurring in tissues, which are ~ 20 μM (Brown et al., 1997), such that the physiological relevance of these effects is still open to question. Performing experiments under more physiological conditions provide more relevant indications as to whether metal binding may or may not be a relevant event in the aggregation of αS *in vivo*.

We monitored the time course of αS aggregation in the presence of $CuCl_2$ at 37 °C by the Thioflavin-T fluorescence assay. Addition of 40 to 200 μM Cu(II) decreased the

characteristic lag time for aggregation of the unliganded protein in a manner dependent on Cu(II) concentration (Figure 7.1A). An inverse relationship was found between $t_{1/2}$ and Cu(II) concentration, but no major changes were observed in the rate of monomer addition ($k_{app}$).
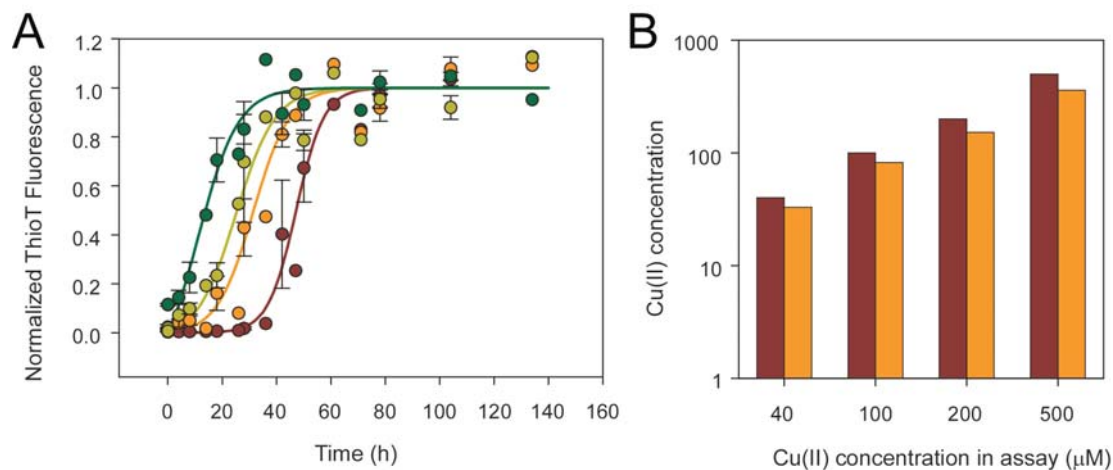


**Figure 7.1. Aggregation kinetics αS aggregation in the presence of copper**. **A**. 0 (dark red), 40 (orange), 100 (dark yellow) and 200 μM of Cu(II) (green) were added to 100 μM αS, and the protein was incubated at 37 °C with continuous stirring. Solid lines represent fits according to the αS aggregation model. The fits yielded the following parameters: $k_{app}$ (h$^{-1}$) = 0.19 ± 0.03, 0.15 ± 0.05, 0.14 ± 0.05, 0.14 ± 0.01 and $t_{1/2}$ (h) = 47 ± 5, 31 ± 4, 25 ± 3, 11 ± 3 (in order of increasing Cu(II) concentration). B. PAR assay of Cu(II) content in αS fibrils obtained in the aggregation assay shown in A.

We determined whether Cu(II) was incorporated into the fibrils to any significant degree, and we found that 70-90% of the Cu(II) added to the aggregation assay was incorporated into the protein aggregates (Figure 7.1B). Notably, even when 5 equivalents of Cu(II) were added, more than 4 equivalent were found in the fibrils, suggesting the presence of several binding sites for the metal.

Since solution conditions strongly perturb the morphology of the resulting αS fibrils (Hoyer et al., 2002), it was necessary to assess whether the metal incorporation had any particular influence on the aggregated protein. A morphological analysis by electron microscopy of the fibrils formed upon incubation with 40 to 200 μM Cu(II) revealed fibrilar structures qualitatively similar to those obtained in the absence of the metal ion (Figure 7.2). This suggests that the Cu(II)-bound aggregating-prone protein populates misfolded conformations that are on-pathway intermediates of fibrillation.
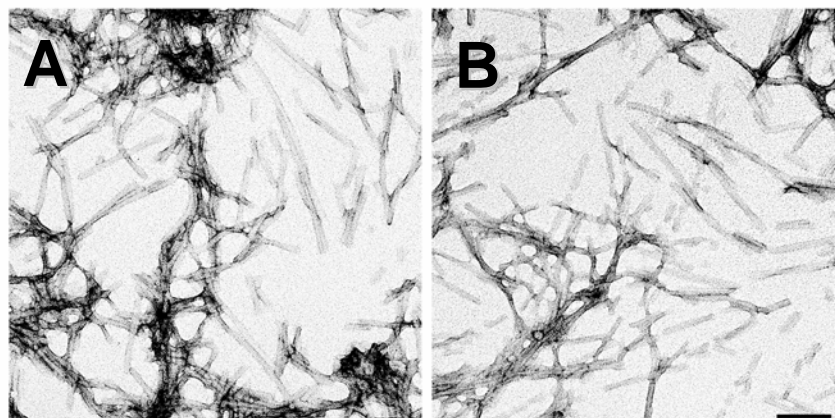
**Figure 7.2. Morphology of αS fibrils grew in the presence of copper.**
Electron microscopy images of αS aggregates obtained without Cu(II) (**A**) or in the presence of 100 µM Cu(II) (**B**). Scale bars, 100 nm.

## 7.2. Quantitative assessment of Cu(II) binding to αS.

Besides the notorious effect of Cu(II) on the aggregation of αS, it was of interest to determine the affinity of the protein for the metal, in order to assess the possibility that the complex occurs *in vivo*. We obtained initial estimates of the dissociation constant for Cu(II) binding to αS by equilibrium dialysis. By equilibrating a metal-free αS solution against buffer containing 1 µM or 10 µM Cu(II), and measuring the increment of metal inside the protein compartment, we estimated Cu(II):protein ratios of 0.9 and 1.4 after dialysis. Thus, αS is able to bind more than one equivalent of Cu(II) with dissociation constants <1 µM and >10 µM.
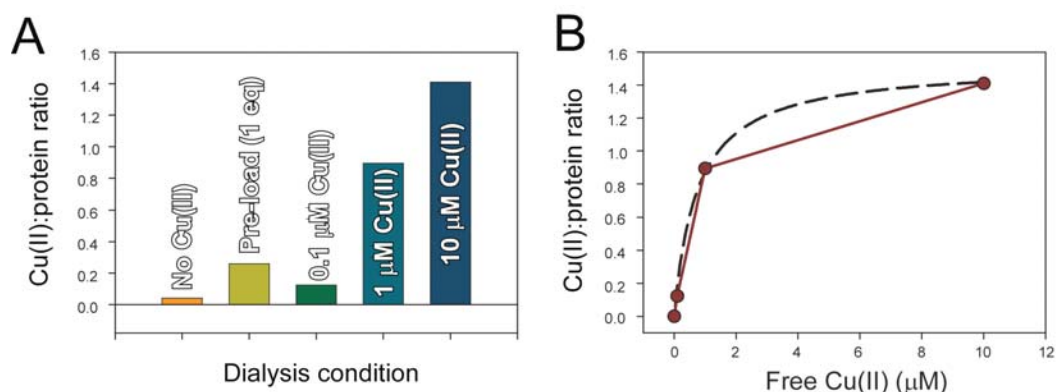


**Figure 7.3. Equilibrium dialysis of the complex αS-Cu(II). A.** αS was subjected to equilibrium dialysis experiments. Free (orange) or Cu(II) preloaded (dark yellow) protein was extensively dialyzed against buffer free of metal, and ~ 0.3 eq of metal were found attached to the protein. Similarly, free protein was dialyzed against buffer containing 0.1 µM (green), 1µM (cyan) or 10 µM (blue) of Cu(II) and the amount of metal liganded by the protein was measured. In all the cases protein concentration was 300 µM. **B.** Cu(II) binding to αS estimated by equilibrium dialysis suggest two sites of binding one with high affinity ($K_{d1}$ < 1 µM and $K_{d2}$ > 10 µM).

When a solution of αS containing one equivalent of Cu(II) was dialyzed against a metal-free buffer, a Cu(II):protein ratio of 0.26 was obtained, demonstrating both the reversibility and high affinity of the Cu(II)-αS complexes.

Formation of Cu(II) complexes often leads to energetic transitions in the metal that can be efficiently studied spectroscopically. We monitored Cu(II) binding by visible electronic absorption and CD spectroscopy, performing titrations of αS with increasing concentrations of metal. At sub-stoichiometric Cu(II):αS ratios, a single visible absorption band appeared in the electronic spectra at ~ 620 nm, saturating at one equivalent with $\varepsilon = 70$ $M^{-1}$ $cm^{-1}$, typical of a Cu(II) d-d transition (Figure 7.4.A).

The absorption maximum ($\lambda_{max}$) is sensitive to the identity of the metal ligands and can be used as an indication of the number of nitrogen ligands bound to the Cu(II) ion (Bryce and Gurd, 1966). The visible absorption spectrum of the Cu(II)-αS complex is characteristic of two or three nitrogen coordination in a type (II) square-planar or distorted tetragonal arrangement. Beyond one equivalent of Cu(II), the visible absorption band increased in intensity and shifted toward lower energy. Subtraction of the spectrum recorded with one equivalent of Cu(II) revealed an absorption band with a maximum at 720 nm, likely reflecting the incorporation of a second Cu(II) ion into a different coordination environment.
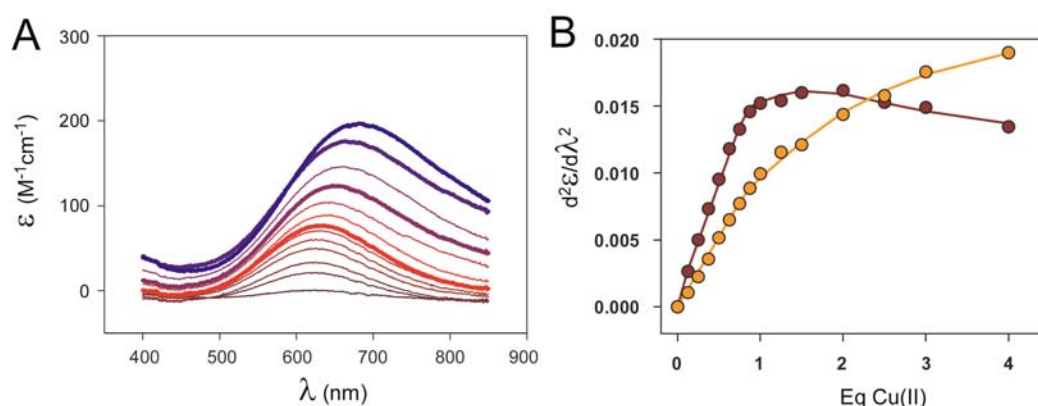


**Figure 7.4. Absorption spectroscopy of Cu(II)-αS complexes. A.** Ligand field region of the spectra. Bold lines highlight the spectra at 1, 2, 3 and 4 equivalents of Cu(II). **B**. Direct titration of αS with Cu(II). Concentration dependence of the second derivative absorbance at 620 nm (dark red) and 660 nm (orange). Solid lines show the result of the simultaneous fit of both sets of data points as described in the text.

Analysis of the second derivatives ($\partial^2 E / \partial \lambda^2$) of the spectra yielded quantitative information. The plot of this quantity at 620 nm showed discontinuities in the binding curve at one and two molar equivalents of Cu(II) (Figure 7.4B). However, the absorbance curves

recorded up to four equivalents of Cu(II) did not saturate. Thus, we fit the data according to a model incorporating complexes of Cu(II) in three classes of independent, non-interactive binding sites per αS molecule: (1) a high affinity site ($K_{d1}$); (2) a lower affinity site ($K_{d2}$); and (3) a class of non-specific $n$ sites with very low affinity ($K_{d3}/n$).

The molar derivative absorbance signal [$(\partial^2 E/\partial\lambda^2)$] corresponding to the above scheme is given by

$$\Delta\left(\frac{\partial^2 E}{\partial\lambda^2}\right) = \sum_{k=1}^{3} \alpha_k \delta_k \qquad [1]$$

where $\alpha_k$ and $\delta_k$ are the relative fractional concentration and the molar difference absorbance second-derivative, respectively, associated with formation of the Cu(II) complex(es) at site $k$.

Analysis according to these models yielded the following dissociation constants: $K_{d1}$ = 120 ± 160 nM, $K_{d2}$ = 36 ± 36 μM and $K_{d3}/n$ = 470 ± 80 μM. Despite the large numerical uncertainties associated with these quantities, due to the high concentration of the protein required to achieve accurately measurable signals ([αS]$_{tot}$ >> $K_{d1,2}$), their relative order of magnitude was well established.

The CD spectra of αS complexed with Cu(II) showed a positive band in the d-d region (~ 600 nm) and a negative band at 300 nm (Figure 7.5A). The latter can be assigned to a charge transfer transition (c.t.) between the metal center and an imidazole group ($\pi_1$ N$_{im}$–Cu c.t., 280-345 nm) or a deprotonated peptide nitrogen (N–Cu c.t., 295-315 nm) (Daniele et al., 1996).
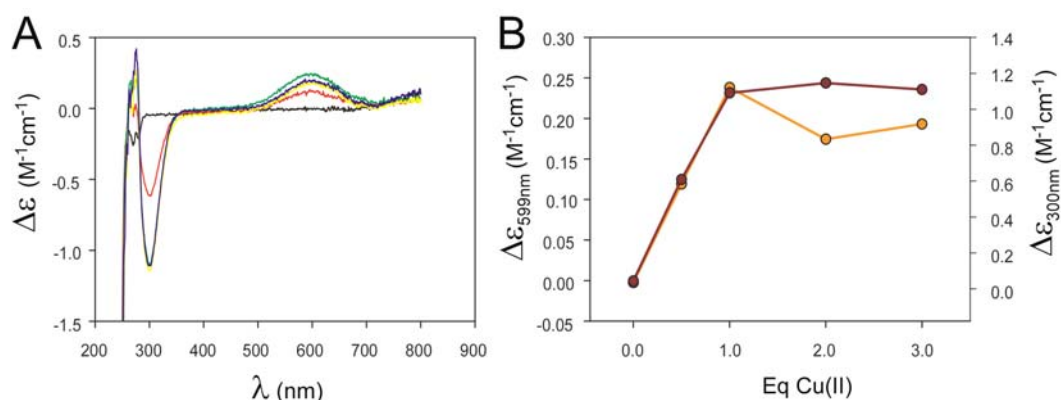


**Figure 7.5. Absorption spectroscopy of Cu(II)-αS complexes. A.** CD spectra of wild type αS corresponding to 0 (black), 0.5 (red), 1 (green), 2 (blue) and 3 (yellow) equivalents of Cu(II) added to the protein. **B**. ΔE values at 300 nm (dark red) and at 599 nm (orange) vs. Cu(II) concentration. Protein concentration was 300 μM.

The CD band at 300 nm saturated with one equivalent of added Cu(II) (Figure 7.5B). In contrast, the intensity of the CD band at 600 nm increased up to one equivalent of Cu(II), decreased upon further addition up to two equivalents of Cu(II), and remained constant at higher Cu(II) concentrations. We conclude that the c.t. band is associated with the highest affinity Cu(II) binding site. The decrease in ellipticity at 600 nm observed with more than one equivalent of Cu(II) probably reflects the development of a negative band associated with formation of the second Cu(II) complex.

### 7.3. Dissecting domain contributors to Cu (II) binding to αS.

In order to evaluate the contributions of different regions of the protein to Cu(II) binding we divided the αS molecule in two, constructing an αS C-terminal deletion mutant ($\alpha S_{1-108}$) and an N-terminal deletion mutant ($\alpha S_{95-137}$). We studied the association of Cu(II) to both mutants by UV-Vis and CD spectrophotometric titrations.

As observed in figure 7.6, both polypeptides bind Cu(II) in a different manner. While the absorption spectrum of the Cu(II)-$\alpha S_{1-108}$ complex was similar to that of the wild-type protein, the ligand field absorption band in the spectra of $\alpha S_{95-137}$ was considerably red-shifted. These results suggest that the high affinity Cu(II) binding site is located at the N-terminus of the protein.
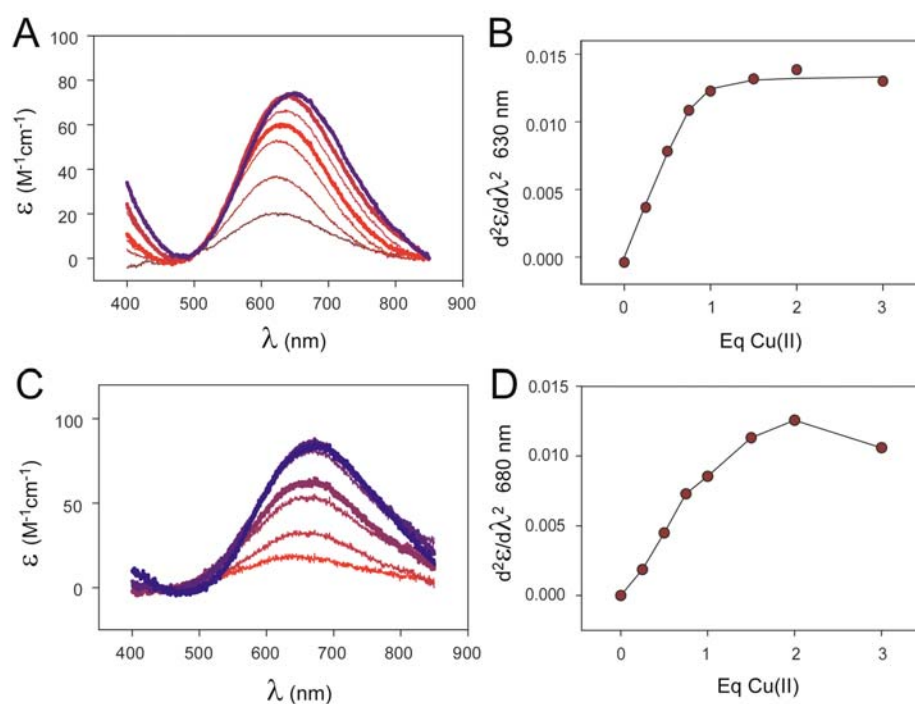


**Figure 7.6. UV-Vis spectroscopy of Cu(II) binding to $\alpha S_{1-108}$ and $\alpha S_{95-137}$.**
The contributions to different regions of the protein to the binding of Cu(II) was studied

on deletions mutants of the protein. **A, B.** $\alpha S_{1-108}$ titration with Cu(II) shows the evolution of a peak at 630 nm which saturates at 1 equivalent of metal added. **C, D.** Conversely, titration of $\alpha S_{95-137}$ shows a band evolving at 680 nm and saturating at 2 equivalents of metal added. In all the cases protein concentration was 300 $\mu$M.

The CD spectra of both truncated species displayed even stronger differences. The Cu(II)-$\alpha S_{1-108}$ complex closely matched that of the full length $\alpha S$, from which we conclude that the geometry and position of the ligand set observed in the whole protein is highly conserved in the $\alpha S_{1-108}$ fragment (Figure 7.7A).

Conversely, the truncated form $\alpha S_{95-137}$ showed an intense negative band in the visible region at ~700 nm ($\Delta\varepsilon_{700} = -0.5$ M$^{-1}$ cm$^{-1}$) and a positive band centered at 324 nm, assigned to a $^-$N–Cu c.t (Figure 7.7B). Indeed, a negative band was foreseen upon titration of full length $\alpha S$ by an excess of metal, suggesting that the second affinity binding site in the protein may be located at the C-terminus.
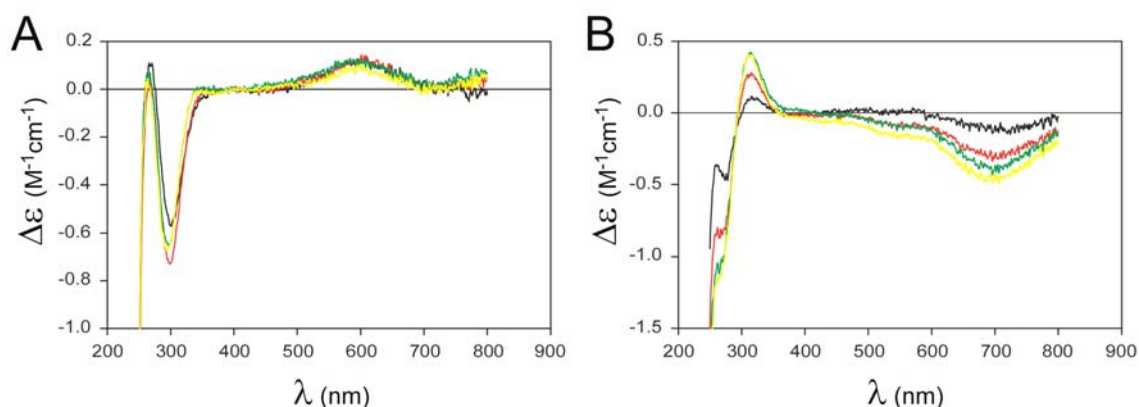


**Figure 7.7. CD spectroscopy of Cu(II) binding to $\alpha S_{1-108}$ and $\alpha S_{95-137}$.** Domain contributions to copper binding in $\alpha S$ could be determined by the CD spectrum of the deletion mutant-Cu(II) complexes. The CD spectra of $\alpha S_{1-108}$ (**A**) and $\alpha S_{95-137}$ (**B**) are shown. Spectra correspond to 0.5 (black), 1 (red), 2 (green) and 3 (yellow) equivalents of Cu(II) added to the proteins. Protein concentrations were 200 $\mu$M ($\alpha S_{1-108}$) and 150 $\mu$M ($\alpha S_{95-137}$).

These results establish the hierarchical contributions of regions in the polypeptide to metal binding. While Cu(II) binding to the N-terminal fragment mirrors the CD spectra of the Cu(II):$\alpha S$ complex, the metal complex with the C-terminal fragment is not able to recreate any of the Cu(II) binding sites of $\alpha S$.

## 7.4. Mapping Cu(II) binding interfaces in $\alpha S$ by heteronuclear NMR.

Due to the paramagnetic nature of Cu(II), we could explore the details of Cu(II) binding to $\alpha S$ by NMR spectroscopy. Similarly to the paramagnetic effect that we exploited with

nitroxide spin labels in the previous chapters, the electron spin relaxation from the Cu(II) ion provokes differential broadening of the amide resonances linked to the paramagnetic center. Thus, through-bond or through-space interactions (up to ~ 10Å) will cause a reduction in the intensity of the peaks in the NMR spectrum, providing means for mapping the metal binding interfaces in the protein.

We first recorded a series of $^1$H-$^{15}$N HSQC spectra of 100 μM αS at pH 6.5 in the presence of increasing concentrations of Cu(II) (0-60 μM) and determined the extent of paramagnetic broadening by evaluating the ratio of peak intensities in the presence ($I_{para}$) and absence ($I_{diam}$) of the metal ion. As shown on figure 7.8, significant changes in cross-peak intensities occurred in well-defined regions of αS.
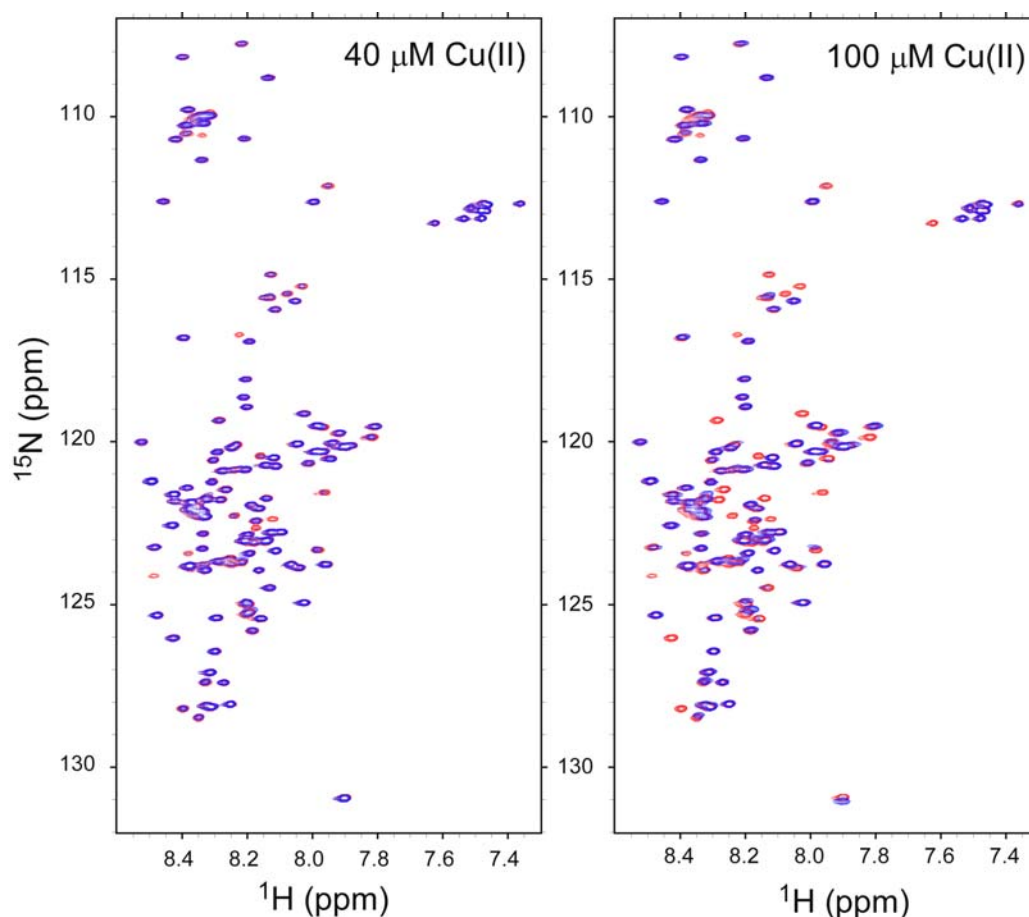


**Figure 7.8. NMR spectra of Cu(II) binding to αS**. Overlaid $^1$H-$^{15}$N-HSQC spectra of αS(100 μM) in the absence (red) and presence of 40 μM Cu(II) (blue, left) and 100 μM Cu(II) (blue, right).

The strongest broadening effects at 20 μM Cu(II) were centered on the amide group of His50 in the N-terminal region, whereas little or no broadening was observed for the amide groups of residues located in the NAC region or belonging to the C-terminal domain (Figure

7.9A). Thus, the N-terminal region was the most affected by Cu(II) binding under this condition.

The broadening was further pronounced at 40-60 µM Cu(II), as reflected in values of $I_{para}/I_{diam} < 0.2$ for the resonances corresponding to residues 3-9 and 49-52 (Figure 7.9B, 7.9C). Residues 15-45 were also involved to a lesser extent, but significant changes were evidenced at the C-terminal region, the strongest effect centered on Asp[121]. Interestingly, the amide resonances assigned to the NAC region remained unaltered, even at higher Cu(II) concentrations. All NMR spectral changes induced by Cu(II) were abolished upon EDTA addition, confirming the reversibility of Cu(II) binding.
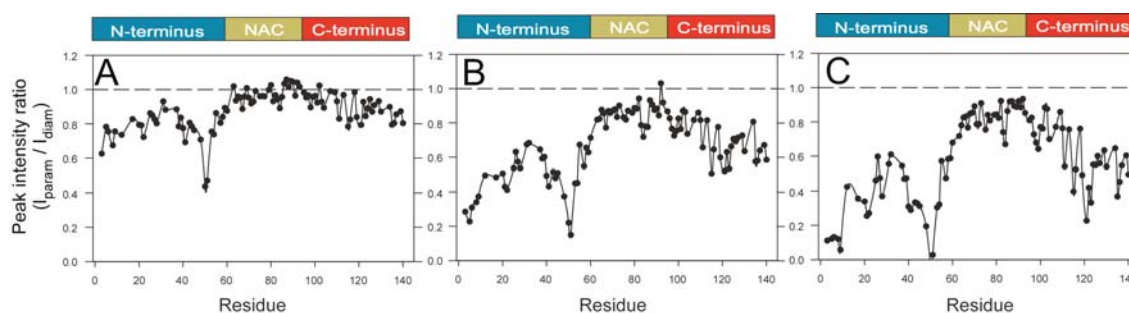


**Figure 7.9. Cu(II) binding to αS investigated by NMR.** $I_{para}/I_{diam}$ profiles corresponding to 100 µM αS at pH 6.5. **A**. 20 µM Cu(II). **B**. 40 µM Cu(II). **C**. 60 µM Cu(II).

The NMR titration experiment showed that the residues encompassing His50 were the most perturbed, suggesting that the imidazole ring plays a critical role in anchoring the Cu(II) ion to the N-terminal domain. In order to prove this assertion we tested whether modification of the sole His residue in αS by DEPC affects Cu(II) binding to the protein.

Exposure to DEPC shifted the paramagnetic influence of Cu(II) from the N-terminal to the C-terminal domain (Figure 7.10A), manifested by substantial changes in cross-peak intensities at Cu(II) concentrations as low as 20 µM. The strongest effects were centered on the amide group of Asp[121], whereas resonances in the NAC domain remained unaffected under these conditions. The decrease in intensity of the signals corresponding to residues 49-52 was likely due to residual Cu(II) coordination capability of His50, e.g. through the imidazole N atom unmodified by DEPC. In summary, Cu(II) binding to DEPC-treated αS clearly shows the existence of two different copper binding interfaces in the protein, one at the N-terminus and another at the C-terminus.
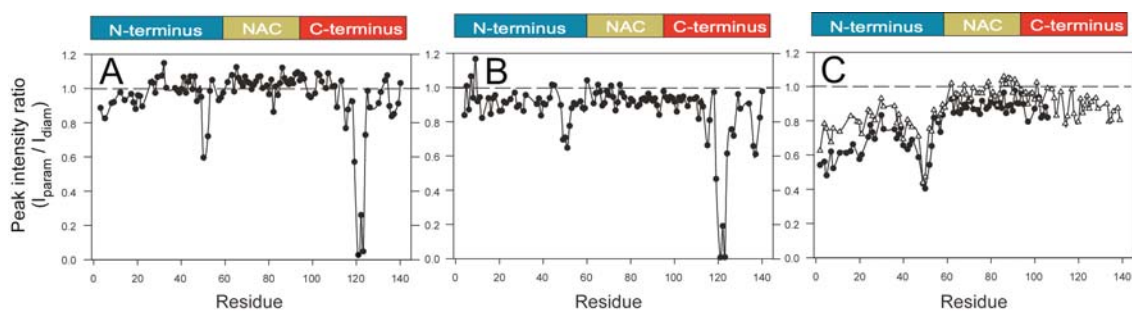
**Figure 7.10. Modulation of copper binding to αS studied by NMR.** Peak intensity ratios corresponding to Cu(II) binding to modified and C-terminal truncated αS. **A** DEPC-modified αS, 20 μM Cu(II). **B**. 20 μM Cu(II), pH 5.0. **C**. Wild type (Δ) and 1-108 (•) αS, 20 μM Cu(II).

Because protonation of His50 should reduce Cu(II) binding, we determined the pH dependence of Cu(II) binding to αS in the range of 5.0-6.5 (Figure 7.11). The $I_{para}/I_{diam}$ profile measured at pH 5.0 and 20 μM Cu(II) is shown in figure 7.10B. The strongest broadening effects corresponded to the C-terminal domain, again centered on Asp121, with a smaller effect evident in the N-terminal domain, located at His50. The cross-peaks of residues in the NAC region remained insensitive to Cu(II) at pH 5.0.
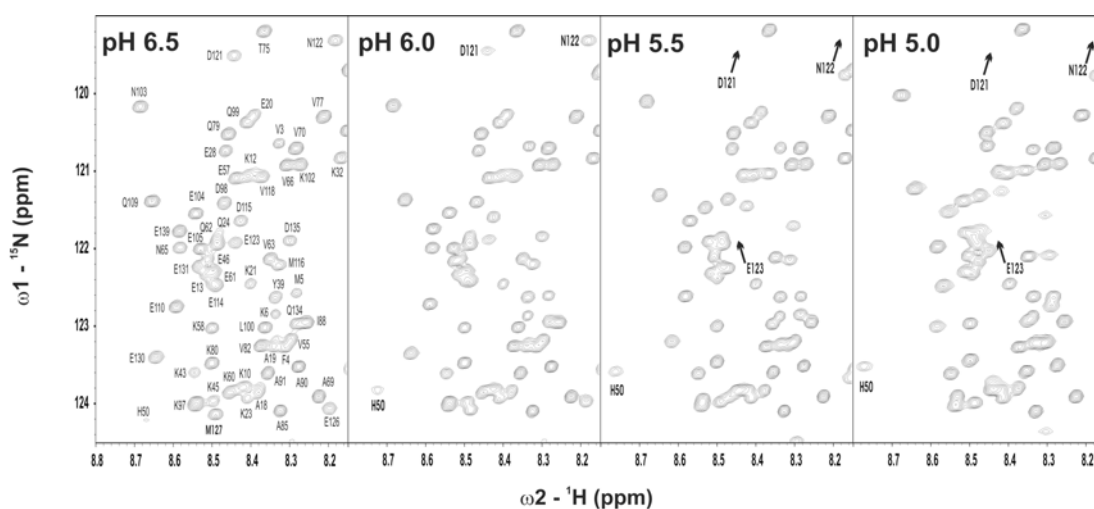


**Figure 7.11. Protonation of His[50] modulates Cu(II) binding to αS.** pH titration of 100 μM αS in the presence of 40 μM Cu(II). Selected regions of the $^1H$-$^{15}N$ HSQC spectra are shown, and the most affected signals by the binding of Cu(II) are identified.

It is noteworthy that even when the most affected cross-peaks in the N-terminal region were severely broadened under conditions favoring Cu(II) binding (pH 6.5); signals were still detected at 40-60 μM Cu(II) (Figure 7.9B, 7.9C). In contrast, upon DEPC modification or protonation of His50, Cu(II) concentrations as low as 20 μM were sufficient

to broaden beyond detection the resonances of the most affected residues in the C-terminal region (Figure 7.10A, 7.10B). This behavior presumably reflects differences in the exchange dynamics and residence times of the two Cu(II) binding sites in αS and supports the assignment of the N-terminal region as the high affinity interface.

The interaction of the C-terminal truncated species of the protein with Cu(II) was studied with the aim of understanding further the structural contribution of the C-terminus to the overall binding process. The $I_{para}/I_{diam}$ profiles for αS1-108 in the concentration range of 0-60 μM of Cu(II) were almost identical to those obtained with wild-type αS (Figure 7.10C), confirming that the binding of Cu(II) to the N-terminal region of αS is independent of the presence of the C-terminus.

Conditions that were effective in triggering αS aggregation were shown previously to induce changes in the general properties of the ensemble populated by the protein (Chapter 1). In addition, mM concentrations of metal ions have shown to cause a reduction in the radio of gyration ($R_g$) of the protein, and effect that was attributed to the formation of a partially folded intermediate (Uversky et al., 2001b; Uversky et al., 2001c). We sought evidence for the formation of metal-induced misfolded intermediates of αS by determining the hydrodynamic properties of the αS-Cu(II) complexes employing PFG-NMR. Measurement of Rh for αS (100 μM) in the absence and presence of Cu(II) (40 to 200 μM) did not provide evidences of a partially collapsed intermediate or an extended species. While the values observed for the protein in its native state (Rh of 32.0 Å) were consistent with previous determinations (Morar et al., 2001; Uversky et al., 2001b) no changes were detected upon addition of Cu(II) (Rh of 32.1 Å), suggesting that the interaction neither affects the size of native αS ensemble nor causes a significant collapse to a more compact conformation.

## 7.5. Cu(II) coordination in the complex with α-synuclein studied by EPR.

The 9-GHz-EPR spectrum of the αS-Cu(II) complex at pH 6.5 was characteristic of Type 2 Cu(II) proteins (Väängård, 1972) (Figure 7.12A). The spectrum of the DEPC-modified αS-Cu(II) complex presented similar characteristics but some differences were evident (Figure 7.12C). The Cu(II) complexes between the modified and unmodified protein differed qualitatively in that the spectrum of the former extended to a significantly lower field and lacked an over-shoot line in the $g_\perp$ region. The Cu(II) hyperfine splittings and $g$-values in the low-field, parallel region were $A_{//} = 186$ and $176 \times 10^{-4}$ cm$^{-1}$, and $g_{//} = 2.223$ and 2.316 ($g_\perp \sim$ 2.05 and 2.06), for the unmodified and modified protein, respectively.
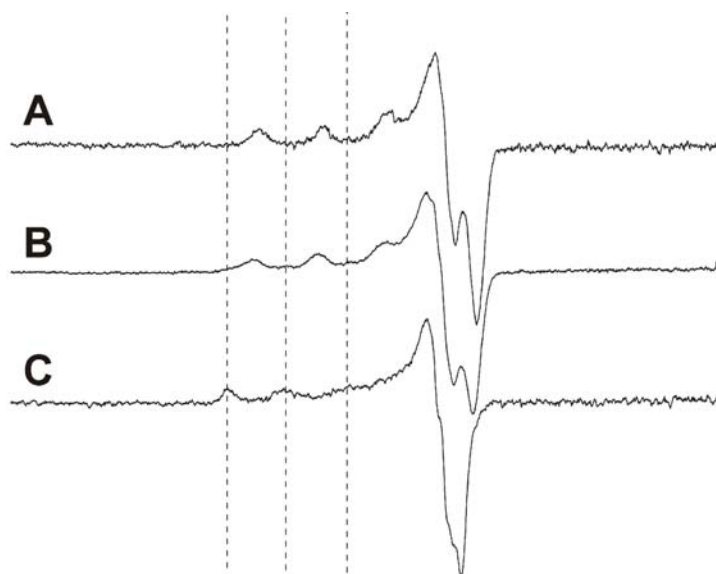
**Figure 7.12. EPR spectroscopy of Cu(II) binding to αS**. 9-GHz EPR spectra of Cu(II) bound to αS (1:1 molar ratio). **A**. pH 6.5. **B**. pH 5.0. **C.** DEPC-modified at pH 6.5. In all the measurements T = 77 K. Centre field = 0.297 T; scan width = 0.2 T; ν = 9.146 GHz. Dotted vertical lines correspond to the three lower hyperfine lines in the DEPC-modified sample.

The Cu(II) EPR spectrum of the unmodified protein at pH 5.0 (Figure 7.12B) resembled that of the unmodified protein at pH 6.5, but also clearly contained a weaker spectral component corresponding to the DEPC-modified protein (Figure 7.12*C*). The appearance of the latter, lower affinity, component agrees fully with the NMR results at pH 5.0.

Figure 7.13 provides a plot of $A_{//}$ vs. $g_{//}$ for various small-molecule Cu(II)-complexes, using data from the literature showing the dependence of these parameters on the type of ligands in the complexes (Peisach and Blumberg, 1974; Sakaguchi and Addison, 1979). The EPR data from Cu(II) bound to unmodified αS at pH 6.5 correlated rather well with those for Cu(II)-complexes with 2 nitrogen and 2 oxygen ligands ($N_2O_2$), whereas in the case of αS with modified histidine, the EPR parameters were indicative of four oxygen ligands ($O_4$).
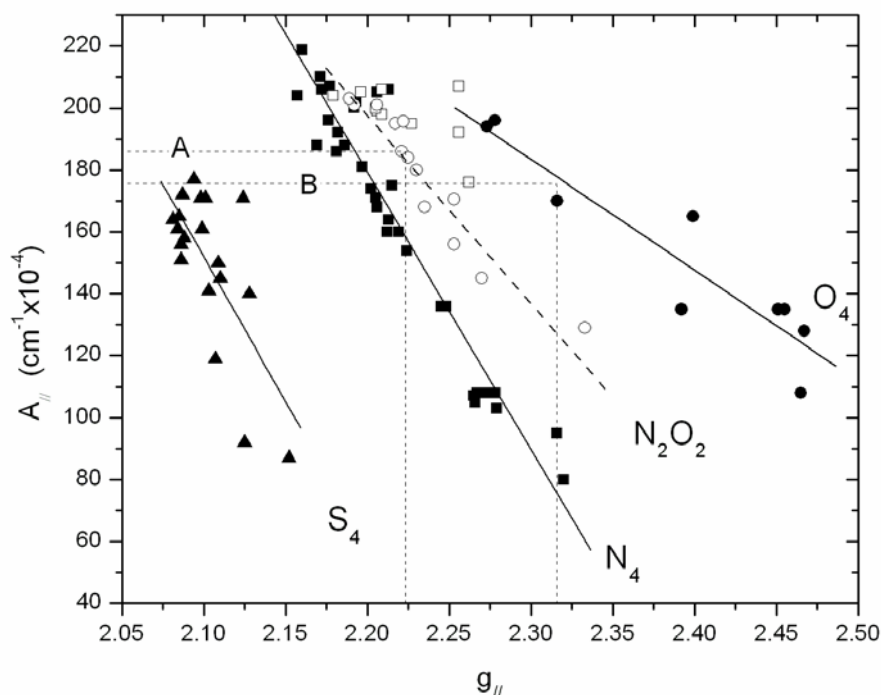
**Figure 7.13. Correlation diagram between A$_{//}$ and g$_{//}$ in the EPR spectra of Cu(II) complexes with different ligands.** The labels correspond to ■ four nitrogen ligands (N$_4$), ● four oxygen ligands (O$_4$), ▲ four sulphur ligands (S$_4$), ○ two nitrogen and two oxygen ligands (N$_2$O$_2$), □ imidazyl-type N$_4$ ligands. References to original data are in(Peisach and Blumberg, 1974; Sakaguchi and Addison, 1979). Dashed horizontal and vertical lines indicate the parameters for Cu(II) bound to native (**A**) and chemically modified (**B**) AS at pH 6.5.

## 7.6. Paramagnetic metal ions bind to αS with different affinities.

In the previous sections we have assessed the structural features of Cu(II) binding to αS, given that this metal is strongly bound by the protein, causing an increase on its fibrillation rate. In order to establish the hierarchy of metal-αS interaction, we comparatively studied the role of other paramagnetic metal ions on αS aggregation.

We have previously shown that 40 μM of Cu(II) were effective in accelerating the aggregation of αS (100 μM). To determine whether other divalent cations as Mn(II), Fe(II), Co(II) or Ni(II) could directly affect fibril formation of αS under similar conditions, we monitored the kinetics of aggregation of αS in the presence of 100 μM Mn(II), Co(II), Ni(II) and Fe(II), monitored by the standard Thioflavin-T fluorescence assay (Figure 7.14). We additionally employed Cu(II) as a control for the assay. The characteristic $t_{1/2}$ for aggregation of αS was reduced from ~ 65 h to ~ 30 h in the presence of 100 μM Cu(II) (Figure 7.14). Instead, no fibrils were observed in the presence of the other divalent metal ions during the

firsts 30 h, indicating that these cations have a minimal or no stimulatory effect on αS fibrillation under these conditions.
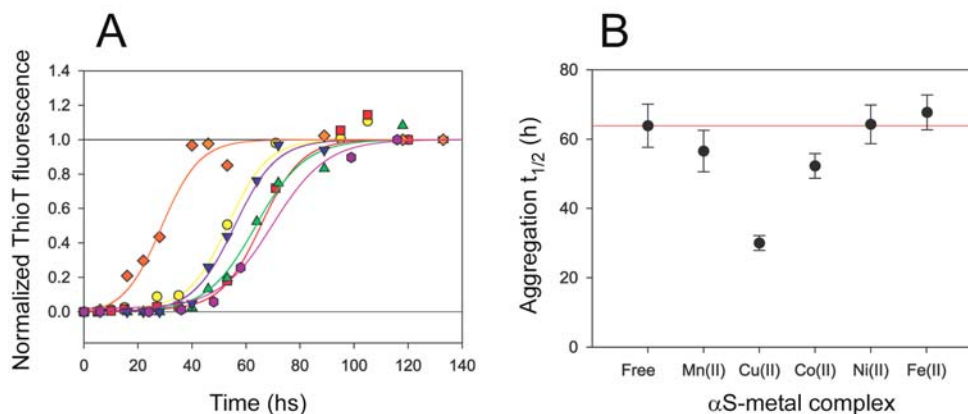


**Figure 7.14. Aggregation kinetics of αS in the presence of divalent metal cations. A.** 100 μM αS in Buffer A (▲), 100 μM Cu(II) (◆), 100 μM Co(II) (●), 100 μM Mn(II) (▼), 100 μM Ni(II) (■), 100 μM Fe(II) (⬣). Solid lines represent fits to the Equation 1 as described in the methods section. **B**. Plot of $t_{1/2}$ (h) values obtained for each metal ion from the fitting procedure in **A**. Control (64 ± 7), Cu(II) (30 ± 2), Ni(II) (64 ± 6), Co(II) (53 ± 4), Mn(II) (57 ± 6) and Fe(II) (67 ± 5). Error bars correspond to standard errors of five independent experiments. Line corresponds to the value obtained for wt αS.

In order to assess whether the absence of fibrillation enhancement by the other divalent metal ions might be linked to a reduced affinity for the protein, we estimated the dissociation constants of the various αS-metal(II) complexes by equilibrium dialysis (Figure 7.14). In contrast to the Kd evidenced for Cu(II) using this technique ($K_d$ < 1 μM), the dissociation constants estimated for Mn(II), Fe(II), Co(II), and Ni(II) were all in the 1-2 mM range.
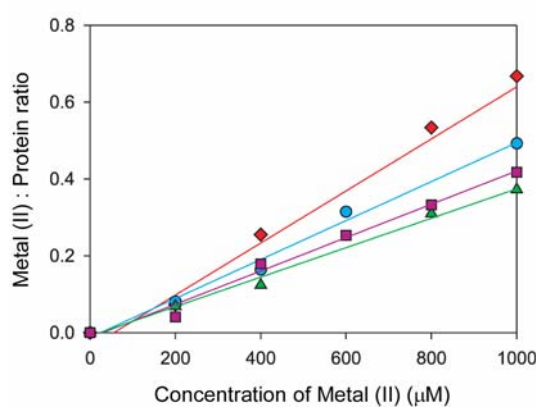


**Figure 7.15. Equilibrium dialysis for metal(II)-αS complexes.** Equilibrium dialysis plots characterizing the binding of divalent metal ions to αS. Mn(II) (■), Co(II)

(•), Fe(II) (♦), Ni(II) (▲). The $K_d$ values estimated for Fe(II), Mn(II), Co(II), and Ni(II) are all in the 1-2 mM range.

These results demonstrate that under the low concentrations of metal ions used in the aggregation experiments, the degree of occupancy of the metal binding sites in αS was significant only for Cu(II).

**7.7. NMR characterization of the interaction between divalent metal ions and αS.**

Although scarcely populated under the conditions assayed, the αS-metal(II) complexes could be extensively characterized by NMR due to the paramagnetic nature of the metal ions studied. The range of αS-metal(II) affinities estimated indicates that the metal complexes determined here must have lifetimes substantially shorter than that with Cu(II) at the N-terminus of αS. This implies that the resonances of the nuclei close to the paramagnetic ions can be more dramatically affected than those in a tight complex (*e.g.*, αS-Cu(II)) due to paramagnetic exchange broadening (Bertini et al., 2003). This effect serves as a sensitive indicator of the location of the metal ions in the protein structure, and has been successfully applied in the characterization of transient metal-protein interactions by NMR (Bertini et al., 2003).

Changes in the ^{1}H NMR spectra of the side chains of a protein are sensitive probes for detecting metal binding and defining the binding interface. (Viles et al., 1999; Belosi et al., 2004; Jones et al., 2004; Syme et al., 2004; Valensin et al., 2004; Gaggelli et al., 2005) The ^{1}H NMR spectra of αS in $D_2O$ showed well-resolved clusters of resonances in the 7.0-8.0 ppm range, comprising the side chains of different aromatic residues: His (aa50), Phe (aa4, aa94) and Tyr (aa39, aa125, aa133, aa136) (Figure 7.16A). The distribution of these residues throughout the αS sequence provides excellent probes for exploring the binding features of metal ions to αS.

Addition of 50 µM Cu(II) to αS caused the selective disappearance of the His[50] peak (Figure 7.16B), whereas further addition of Cu(II) (100 µM) revealed the disruption of the fine scalar-coupling structure of Tyr signals and the disappearance of resonances in the Phe region (Figure 7.16C). This pattern fully agrees with our previous finding, showing the preferential binding of Cu(II) at the N-terminus (indicated here by the disappearance of His[50] and resonances attributed to Phe[4]) and the low affinity effects on the C-terminus due to exchange broadening (showed by the broadening of Tyr resonances).
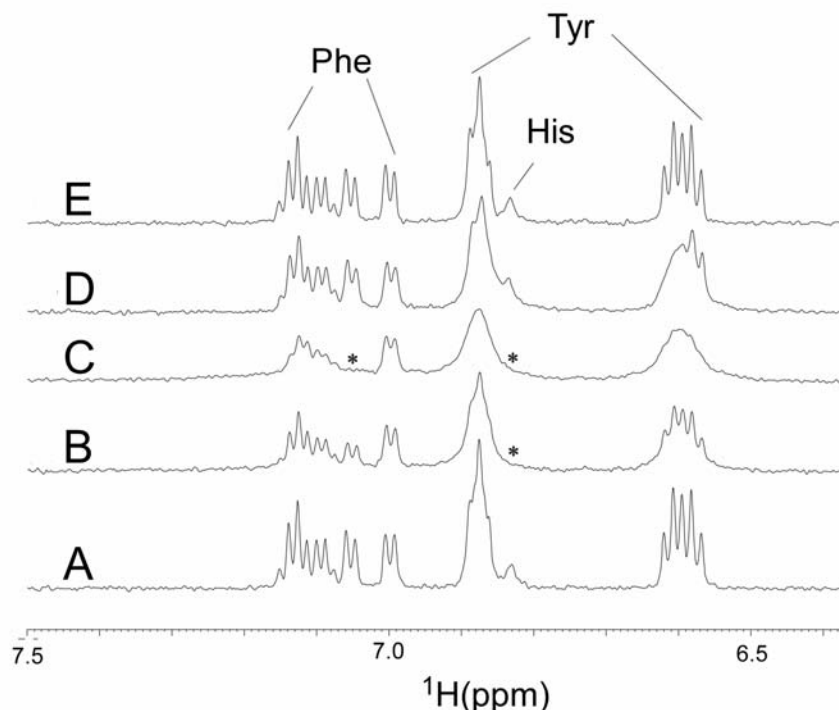
**Figure 7.16. $^{1}$H NMR spectra of aromatic side-chains of αS in the presence of divalent metal ions.** Spectra were registered at 15°C in D$_2$O of samples containing 100 μM αS (A), 50 μM Cu(II) (B), 100 μM Cu(II) (C), 100 μM Mn(II) (D), 100 μM Fe(II) (E). The asterisk (*) indicates peaks broadened beyond detection.

As shown in Figure 7.14D, the presence of 100 μM Mn(II) caused the selective line broadening of Tyr signals, likely reflecting the preference of this metal ion for the C-terminus. The remaining sharp signals in the cluster centered at 6.6 ppm belong to Tyr [39], as revealed by the 1D spectrum of the C-truncated species (αS 1-108) (data not shown). The spectral features of the 1D $^{1}$H NMR of αS in the presence of 100 μM Fe(II) remained almost unperturbed (Figure 7.16E), as was also the case with 100 μM Co(II) and Ni(II).

To shed light on the structural basis determining the affinity of αS by metal ions, the specific regions for metal binding to αS were mapped by two-dimensional heteronuclear NMR spectroscopy. We first recorded a series of $^{1}$H-$^{15}$N HSQC spectra of αS (100 μM) in the presence of increasing levels of Mn(II). Sub-stoichiometric concentrations of Mn(II) were necessary to avoid an excessive broadening of the signals and to minimize chemical exchange effects. Significant changes in cross-peaks intensities were observed under these conditions, being restricted to residues located in the C-terminal region of αS (Figure 7.17).
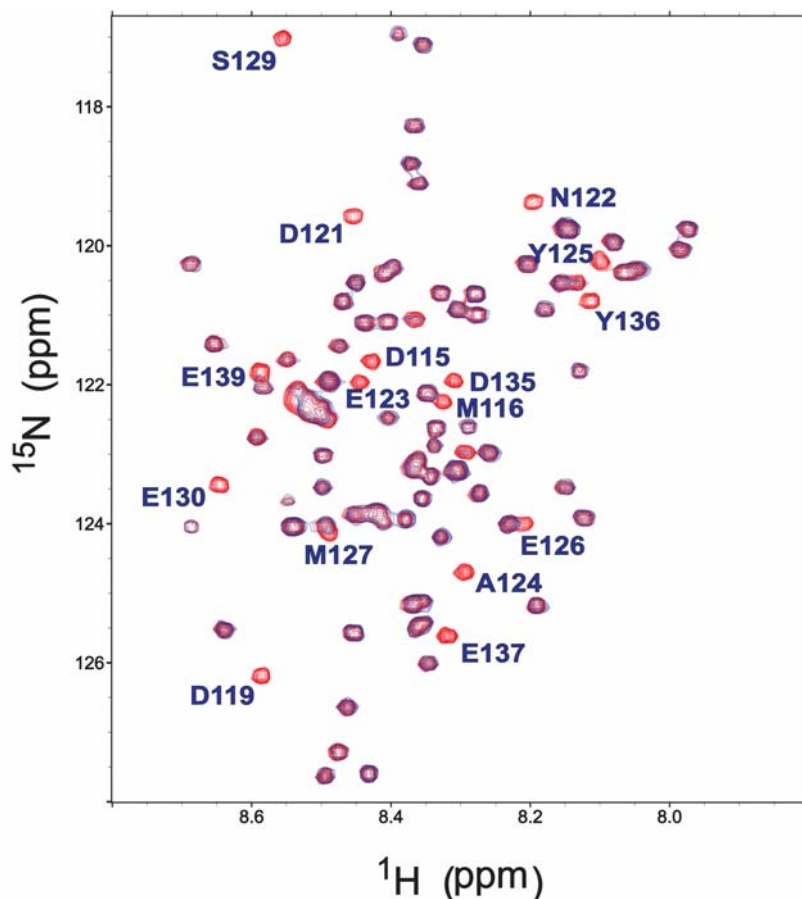
**Figure 7.17. ¹H-¹⁵N HSQC spectra of αS in the presence of Mn (II).**
Overlaid contour plots of the ¹H-¹⁵N HSQC spectra of 100 μM αS in buffer B, at 15°C, in the absence (red) and presence (blue) of 100 μM Mn(II). Amino acid residues broadened beyond detection are identified.

The strongest broadening effects at 10-20 μM Mn(II) corresponded to amide groups of residues Asp[121], Asn[122] and Glu[123], indicating that this site is the most populated under these conditions (Figure 7.18A). The paramagnetic effect was further pronounced and generalized at 40-100 μM Mn(II) (Figure 7.18B, 7.18C), possibly reflecting the transient population of secondary sites. Interestingly, the amide resonances assigned to residues located in the N-terminus or belonging to the NAC region remained unaltered even at high Mn(II) concentrations.
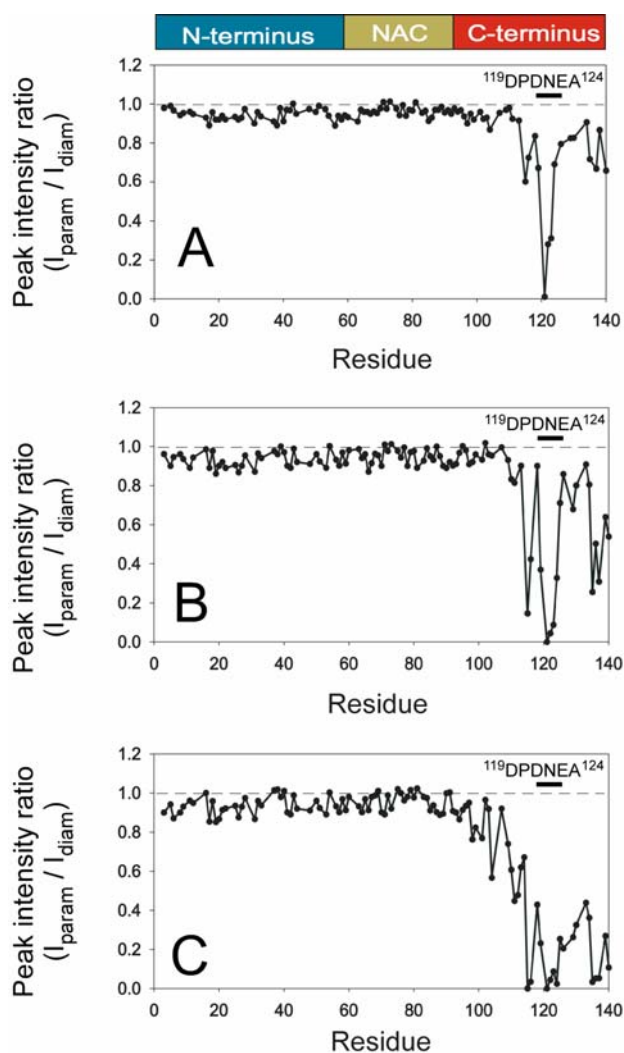
**Figure 7.18. Paramagnetic broadening caused by binding of Mn(II) to αS.**
*I/I*$_0$ profiles of the backbone amide groups of αS in the presence of divalent metal ions.
$^1$H-$^{15}$N HSQC spectra of 100 μM αS in Buffer B, at 15°C were registered upon addition of 15 μM Mn(II) (**A**), 40 μM Mn(II) (**B**), 100 μM Mn(II) (**C**). N-terminal region (residues 1-60), NAC region (residues 61-95), C-terminal region (residues 96-140) are highlighted.

Titration of αS with Fe(II), Co(II) and Ni(II) showed effects qualitatively similar to those caused by low levels of Mn(II), in that resonances of residues Asp121, Asn122 and Glu123 in the C-terminus were severely affected (Figure 7.19A, 7.19B). However, no generalized line broadening was induced at the C-terminus by added 100 μM metal ion; overall the spectra remained sharper and the effects were well localized in the 121-123 region. Since the affinities estimated for the αS-metal(II) complexes are similar, the different degree of broadening must be reflecting the magnitude of the electron spin relaxation times ($\tau_S$) of each paramagnetic metal ion (Mn(II) ~ 10$^{-8}$ s, whereas Fe(II), Co(II) and Ni(II) ~ 10$^-$

$^{11}$–$10^{-13}$s) (Bertini and Luchinat, 1996) The cross-peaks of residues located in the NAC region remained insensitive to Fe(II), Co(II) and Ni(II) even at metal:αS ratios of 10:1, whereas a paramagnetic effect centered on His50 was clearly observed for [Fe(II)], [Co(II)] ≥ 500 μM (Figure 7.19D-7.19F).
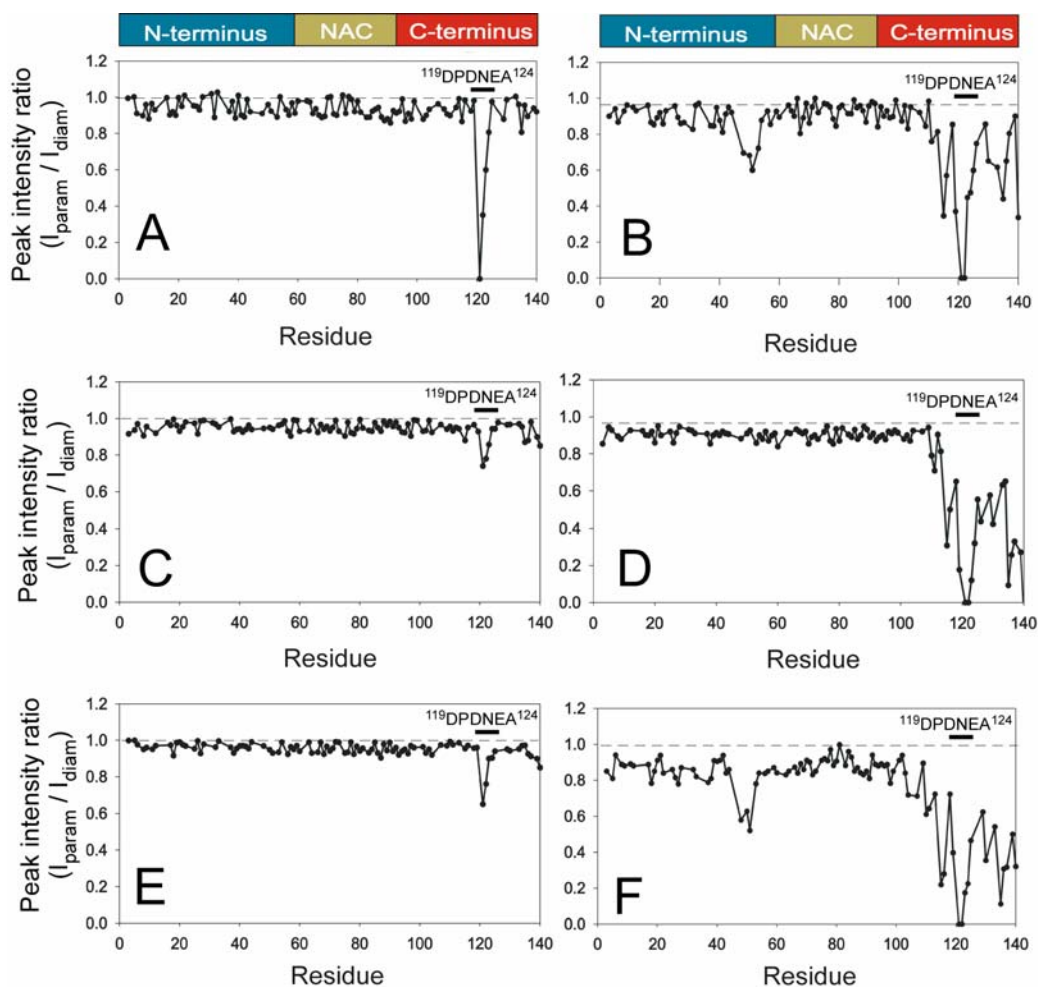


**Figure 7.19. Binding of Fe(II), Co(II) and Ni(II) to αS.** $I/I_0$ profiles of the backbone amide groups of αS in the presence of divalent metal ions. $^1$H-$^{15}$N HSQC spectra of 100 μM AS in Buffer B, at 15°C were registered upon addition of (**A**) 100 μM Co(II), (**B**) 1000 μM Co(II), (**C**) 100 μM Ni(II), (**D**) 1000 μM Ni(II), (**E**) 100 μM Fe(II)), (**F**) 1000 μM Fe(II). N-terminal region (residues 1-60), NAC region (residues 61-95), C-terminal region (residues 96-140) are highlighted.

An estimation of the binding affinity of Mn(II) to αS was independently obtained by NMR. Determining the paramagnetic relaxation enhancement, $R_{1p}$, induced by low sub-stoichiometric levels of metal at different concentrations of protein provides a valuable tool to assess the dissociation constant of the complex (Bertini and Luchinat, 1996). A plot of $1/R_{1p}$ against $C_{αS}$ for Asp$^{121}$, Asn$^{122}$ and Glu$^{123}$ resonances gives a straight line (Figure 7.20),

from which a dissociation constant of ~ 1 mM was obtained. This determination confirms the findings from equilibrium dialysis experiments.
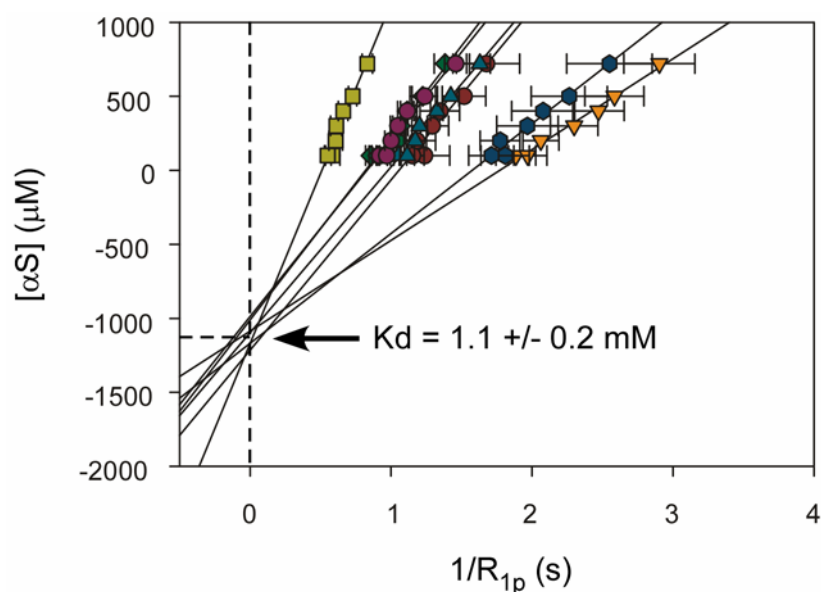


**Figure 7.20. Paramagnetic relaxation enhancement induced by Mn.** An independent estimation of the affinity constant of the complex αS-Mn(II) was obtained by measurement of the paramagnetic relaxation enhancement cause by the metal at different protein concentrations. Residues at the C-terminal are Asp[115] (red), Asp[119] (orange), Asp[121] (dark yellow), Asn[122] (green), Glu[123] (light blue), Ala[124] (dark blue), Asp[135] (violet).

*Discussion*

## 8. Discussion

### 8.1. Auto-inhibitory long range interactions in the native state of αS.

The protein α-synuclein (αS) is implicated in the deposition of pertinacious aggregates in many neurodegenerative disorders, including Parkinson´s disease. αS is expressed in high levels in the *substantia nigra* of healthy individuals, and locus triplication, point mutations, or as yet elusive environmental conditions are able to cause the self-association of the protein in the form of toxic oligomers and amyloid like fibrilar structures (Cookson, 2005). What is intriguing from the biophysical point of view, is that αS belongs to the class of natively unfolded proteins with no apparent ordered secondary structure detectable by far-UV CD, FTIR or NMR spectroscopy (Uversky, 2003). Thus, it is not evident how this protein is able to avoid self-association and amyloid deposition in the neuronal cytoplasm.

The challenge of this thesis work has been to rationalize in structural terms the inactive state of the soluble, unstructured protein, searching how the enhancement of aggregation is achieved by point mutations, ligand binding or changes in solution conditions. However, the conformational flexibility inherent to natively unfolded proteins places them beyond the reach of classical structural biology, and a special set of NMR-based experiments had to be implemented in order to study the native soluble state of αS, namely paramagnetic relaxation enhancement and residual dipolar couplings.

When we employed paramagnetic relaxation enhancement from site-directed spin-labeling, we were able to detect a complex network of long range interactions involving an N- to C-terminal contact plus a shielding of the hydrophobic central NAC region by the C-terminus. Experiments conducted under chemical denaturation suggest that the contacts between the NAC region and the C-terminus are of hydrophobic nature. On the contrary, the interaction between the positively charged N-terminus and the acidic C-terminus are electrostatic in origin. Furthermore, distance restraints were obtained from the paramagnetic experiments and an ensemble of conformations was obtained for the native state of αS (Figure 8.1.).

The model that we present here can be interpreted as either an ensemble of unfolded structures, where each structure is satisfying the experimental data, or as an ensemble of unfolded structures where as an average the ensemble satisfy the experimental data (Teilum et al., 2002). Despite these uncertainties, it is evident from our experiments and structure calculations that αS is not a random coil as was described before, but rather populates a

defined set of conformations that, despite lacking secondary structure, are stabilized by long range tertiary contacts.
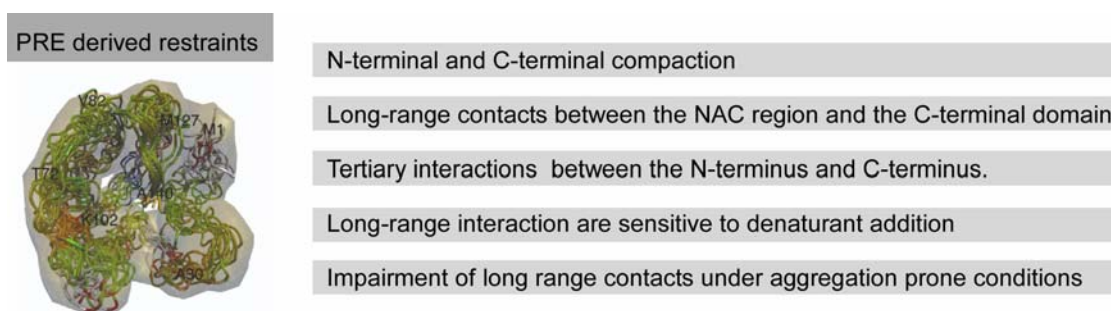


**Figure 8.1. Summary of structural features in the ensemble of αS conformations derived by PRE.** The native state of αS, although deprived of persistent secondary structure, should not be viewed as a random coil, rather specific long range (tertiary) contacts promote population of compact conformations, which aid the protein to remain soluble.

We attempted to determine the importance of these long range contacts in maintaining the protein in its soluble state by assaying different conditions known to enhance self-association and aggregation of the protein. We observed a significant impairment of long range interactions upon addition of a natural polycation, spermine, which specifically bind to the C-terminus of the protein. This effect was evidenced as a retirement of the C-terminus from the NAC region, causing a solvent exposure of the central hydrophobic domain. Similarly, raising the temperature to 47 °C caused a release of this protective effect. In the case of the polyamine-bound αS we further obtained evidenced that the hydrodynamic shape of the ensemble was increased, supporting the achievement of a more extended conformation.

Furthermore, when we studied the A30P or A53T familial mutants of αS, known to cause early on-set PD, likely due to an increased oligomerization propensity, we also observed a slight perturbation of the key long range interaction between the C-terminus and the NAC region. However, strong N-terminal and C-terminal compactions remain unaltered in these proteins, and a slight increase of the electrostatic interaction is suggested. Thus, the general shape of the ensemble of conformations populated by the mutants is somewhat collapsed respect the *wt* protein.

Interestingly, this mechanism of losing key tertiary contacts rendering a more unfolded state is proposed as the trigger mechanism for the misfolding of proteins that account for defined secondary structure (Jahn and Radford, 2005). The similar situation that

is found in our studies for αS would imply that even for natively unfolded proteins, the general mechanisms proposed for amyloid formation are still applicable.

Examination of the homologous protein βS, which lacks the central NAC region and consequently does not readily oligomerize, did not evidence long range interactions. Neither electrostatic N- to C-terminal contacts nor C-terminal compaction occur in βS, as probed by the PRE strategy. This is in line with the determination of the size of the ensemble, which showed to be considerably more expanded than αS. While the positively charged N-terminus of αS and βS is almost identical, the very acidic C-terminus is highly divergent and more negatively charged in βS, thus electrostatic long-range interactions would be favored. The absence of such contacts could be then rationalized either by the requirement of the flip-back of the C-terminus on the NAC region for the electrostatic interaction to occur or by particular conformational states adopted by the domains imply in the interaction which disfavors such contacts. Since in the genetic mutants we evidenced persistent electrostatic interactions in the absence of the hydrophobic core, it is very likely that conformational restrictions at the C-terminus of βS are responsible for inhibiting the formation of such interactions. As discussed afterwards, we found at the C-terminus of βS a strong amount of polyproline II (PII) extended conformations which opposes to the compact and flexible nature of the C-terminus in αS.

At the same time our studies were reported, a similar work on αS was published by the Dobson laboratory (Dedmon et al., 2005). The authors employed the same PRE-based strategy to investigate the nature of the ensemble of conformations populated by αS, arriving to the same conclusions as the one presented in this work. They investigated 5 different Cys-containing mutants and obtained by restrained molecular dynamic simulations an ensemble of conformations which reproduces the compact dimensions experimentally observed in the protein. A close comparison of their contact map with ours shows a striking correlation, validating our studies, and supporting the occurrence of tertiary interactions in αS.

Spin-labeling techniques have been previously employed in the study of the unfolded states of otherwise normally folded proteins, but have never been used in natively unfolded proteins. From the methodological point of view, this study represents the first of such application of long range restraints to determine a low resolution model of a natively unfolded protein. The number of intrinsically unstructured proteins is growing rapidly (Uversky et al., 2000), and it is becoming clear that these proteins participate in a vast range of biochemical processes (Dyson and Wright, 2005). We thus believe that our results will

encourage future high resolution structural studies of dynamic ensembles of interconverting conformers.

## 8.2. Residual structure in the ensemble of conformers populated by αS.

Residual dipolar couplings measured in a weakly aligned protein are excellent reporters of residual structure and conformational restrictions in the unfolded states of proteins (Shortle and Ackerman, 2001; Fieber et al., 2004; Mohana-Borges et al., 2004). In contrast to the bell-like smooth distribution of dipolar couplings that is expected for a random coil polypeptide chain (Louhivuori et al., 2003), a particular distribution of predominantly positive RDCs was observed for αS. Five different domains could be identified in the protein, consistently with previous biophysical studies, and linker regions with couplings close to zero could be rationalized by the occurrence of residues with small side chains (Ala-Gly linkers) (Mohana-Borges et al., 2004). This local higher flexibility of the polypeptide backbone effectively decouples the five domains, and they would exhibit concerted motions, suggesting that they may also align independently (Figure 8.2.).
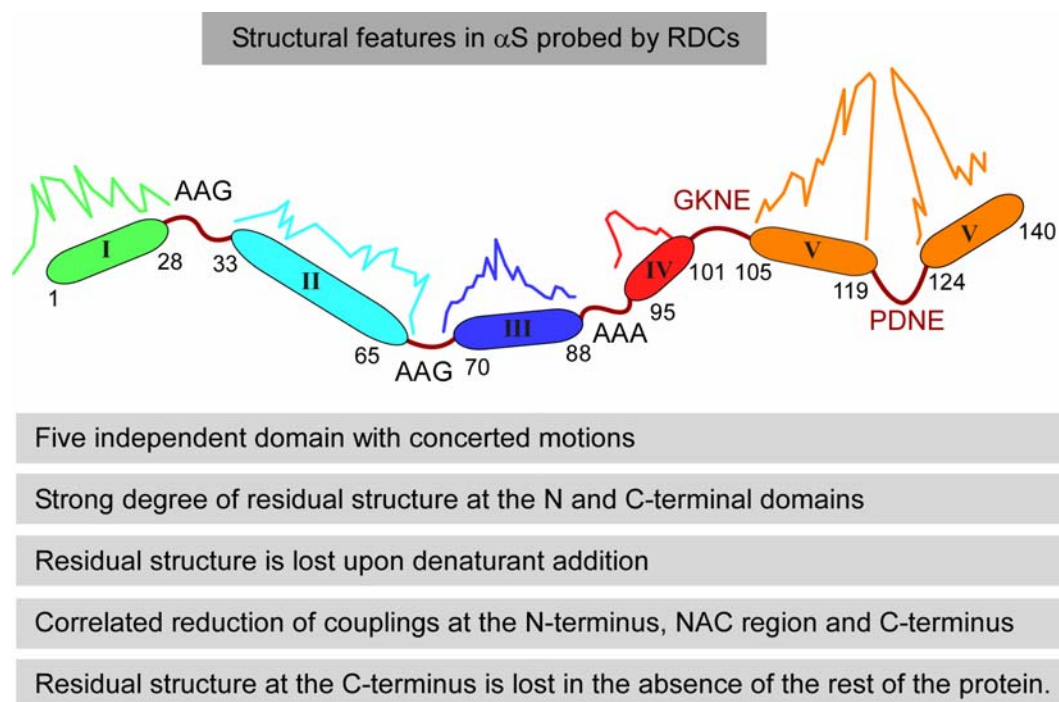


**Figure 8.2. RDCs probe residual structure and long range interactions in αS.** The N-terminus is subdivided into two regions with similar RDCs (domain I: residues 1-28; domain II: residues 33-65) with a linker sequence showing couplings close to zero (residues 28-32). The NAC domain (residues 61-95) exhibits large couplings about its central core, is flanked by two regions with reduced RDCs (residues 66-70 and 88-92) and is followed by a fourth domain (IV) comprising residues 95-101.

The C-terminus (domain V) displays exceptionally large couplings with two major peaks for residues 115 to 119 and 125 to 129.

Steric hindrance between residues, limiting the conformational space that the torsion angle is allowed to sample, was probed by RDCs, suggesting that this parameter is sensitive to conformational restrictions (Louhivuori et al., 2004). The model suggests that high RDCs in unfolded polypeptides would be displayed by regions with residual structure, since they adopt a defined alignment, which does not average out in the ensemble of conformations. In our measurements, the highly acidic C-terminus of αS exhibited very large dipolar couplings, which in principle could be associated with side-chain-side-chain repulsion and to the occurrence of proline residues. However, chemical denaturation of the protein decreased the RDC values in this region, and studies of a C-terminal peptide showed couplings of a magnitude similar to the rest of the protein. Suggesting that the residual structure is not locally encoded rather is a consequence of long range contacts. This fully agrees with the results obtained employing spin labels, showing that the C-terminus is involved in tertiary contacts.

RDCs also probed the impairment of long range interactions in αS upon conditions that trigger protein oligomerization. Polyamine binding and increased of temperature were shown to cause reduction of couplings at the C-terminus of the protein, demonstrating that the residual structure in the C-terminus is key to ensure the population of native conformations.

Notably, RDCs resulted to be excellent reporters of the differences between the conformations populated by the αS genetic mutants, respect the *wt* protein. The measurement of RDCs in the A30P and A53T mutants of αS shows that these point mutations cause a great perturbation of the long range interactions that are responsible of maintaining the protein in an auto-inhibited soluble state. Higher couplings at the C-terminus, distant from the site of the mutation, are consistently reduced, which supports the absence of the NAC-C-terminus interaction, already observed in by PREs. A similar effect for key point mutations has been recently observed by RDCs on the denatured state of acyl-coenzyme A binding protein (ACBP) at pH 2.3. Fieber and colleagues (Fieber et al., 2004) showed that a reduction in RDCs for certain residues in the Ile[27]Ala mutant of ACBP is correlated with the abolishment of long range interaction between two distant domains, already evidenced by other means. Further evidence for single point mutations affecting long range hydrophobic interactions in non-native states was obtained in a study of denatured lysozyme at pH 2 (Klein-

Seetharaman et al., 2002). The Trp62Gly substitution breaks up a long range hydrophobic core that stabilizes the unfolded state of lysozyme, as was evaluated by NMR transverse relaxation rates.

Therefore valuable residue-specific information on the composition of the ensemble of conformations that are populated by the natively unfolded αS can be obtained easily analyzing the variations of RDCs profiles of the protein. This methodology is, up to now, the only experimental set up where slight changes at the level of the αS monomer are able to be detected, and may constitute an essential tool for screening during the development of therapeutic drugs for PD.

## 8.3. Dissecting the nature of long range interactions probed by RDCs in αS

As mentioned before, in folded proteins RDCs report on the orientation of internuclear vectors relative to a global molecular alignment tensor (Bax, 2003). In unfolded states of polypeptides they are believed to provide information about the degree of orientation that the internuclear vector adopts, with respect to the orientation of the persistence length fragment in which the residue is immersed (Dyson and Wright, 2004). Thus, RDCs are suggested to be valuable reporters of both local and long-range conformational propensities, and indeed they have proved to be exquisitely sensitive in the study of αS conformations. However, the true nature of what RDCs are able to detect is somehow still unclear, and thus it is instructive to comment on how the studies of the αS system may help to shed more light on this issue.

At the starting of this thesis work, the application of RDCs for unfolded proteins had just been introduced. Almost 5 years ago, much of a debate was started when Shortle explained the unexpected observation of RDCs in chemically denatured staphylococcal nuclease as evidence of the persistence of secondary structure, contrary to the expectation of vanishingly weak couplings due to conformational averaging (Shortle and Ackerman, 2001). Theoretical studies by Annila refuted that explanation stating that conformational restrictions on the backbone of the polypeptide chain were sufficient to give non-vanishing RDCs (Louhivuori et al., 2003; Louhivuori et al., 2004), and later, experimental data from the Poulsen and Wright laboratories conclusively demonstrated the ability of RDCs to probe conformational propensities in chemically denatured proteins (Mohana-Borges et al., 2004). However, it has not been until very recently that ensemble-averaged computer simulations provided conclusive evidence on the nature of RDCs in unfolded states of proteins.

In order to understand the origin of conformational restrictions probed by RDCs, Sosnick and collegues (Jha et al., 2005a) generated an unfolded state ensemble by using a self-avoiding statistical coil model that was based on backbone conformational frequencies in a coil library, a subset of the Protein Data Bank (Jha et al., 2005b). This ensemble of unfolded chains is shown to predict the experimental RDCs in chemically denatured apomyoglobin, ubiquitin, staphylococcal nuclease and eglin C, while retaining the global conformation of the unfolded state (Rg). The authors found that local structural propensities, in particular extended β and PII conformations, contributed strongly to the RDC signal (Jha et al., 2005a).

Blackledge and colleagues (Bernado et al., 2005b), independently generated a statistical ensemble of coil conformations and calculated averaged RDCs over the entire population. Each conformer from the ensemble was built sequentially using randomly selected φ/ψ pairs drawn from a database of amino acid specific conformations present in loop regions of high-resolution X-ray structures, and a simple volume-exclusion model was added to avoid steric overlap. RDCs were calculated for each NH vector of the conformer and $D_{NH}$ from each site were then averaged over 50000 conformers to ensure convergence. The authors successfully reproduced RDCs from the native unfolded domain of protein PX and the chemically unfolded states of apomyoglobin and staphylococcal nuclease. The outcome of this study is that non-vanishing RDCs will be expected for polypeptides sampling randomly the Ramachandran space, and suggest that RDCs are an interpretable structural signature of the unfolded state (Bernado et al., 2005b).

A collaboration with the Blackledge laboratory allowed us to apply this strategy on the RDCs studies of αS (Bernado et al., 2005a). An ensemble of conformers was generated for αS and RDCs were calculated for the protein aligned in C8E5/octanol anisotropic media (Figure 8.3.A). The range and fine structure of RDCs in αS were reproduced for the central part of the protein (residues 30 to 110) suggesting local conformational restrictions caused by random sampling of residue-specific φ/ψ distributions (Bernado et al., 2005b). However, the ensemble failed to reproduce the high couplings at the N- and C-terminus of the protein. When a long-range interaction constraint between the N-and C-terminus was imposed to the creation of the ensemble, a remarkably close agreement with the experimental value was obtained in the RDCs calculations (Figure 8.3.B). Variations in long-range contacts were assayed, but the closest match remained to be in the N- to C-terminal contact. The results indicate that the proposed contact is present in the native ensemble of conformations

populated by αS in solution, although they do not exclude the presence of other contacts within the same conformer. Indeed, imposing as constraints simultaneous contacts between the C-terminal domain and N-terminal and NAC regions provides an ensemble that fits the data almost as closely ($\chi^2 = 59$).



| Segment | 41-60 | 61-80 | 81-100 | 101-120 | 121-140 |
|---------|-------|-------|--------|---------|---------|
| 1-20    | 141   | 117   | 120    | 89      | 55      |
| 21-40   |       | 129   | 119    | 99      | 71      |
| 41-60   |       |       | 132    | 140     | 118     |
| 61-80   |       |       |        | 143     | 156     |
| 81-100  |       |       |        |         | 181     |
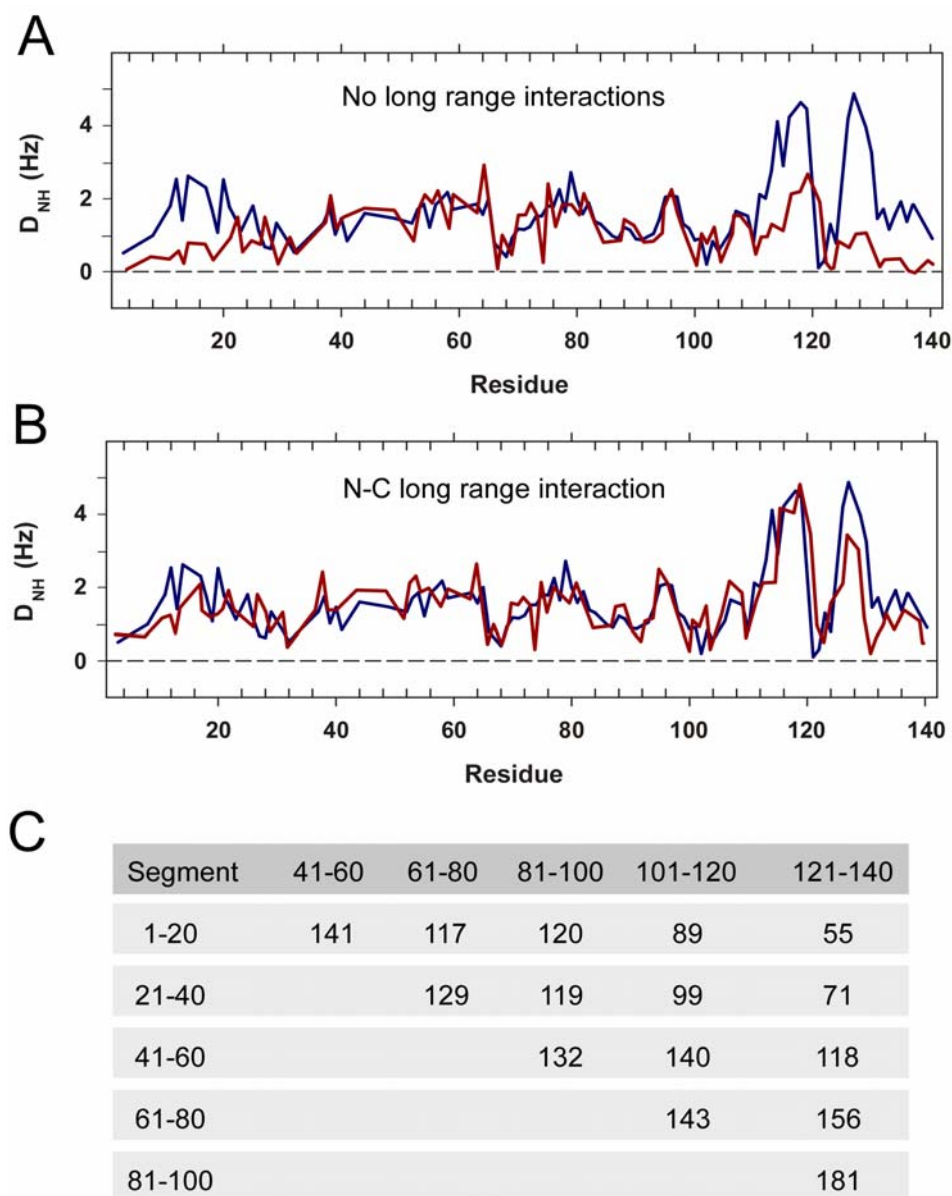
**Figure 8.3. Long range order in αS probed by ensemble-averaged simulations of RDCs. A , B.** Ensemble-averaged RDCs simulated (red) without long-range contacts (red, A) and when long range contacts between the N-terminus and C-terminus are set as restraints (red, B). In blue the experimental RDCs measure in Pf1 phages as alignment media are shown. Simulated data are scaled to maximize fit in the region 22-112. **C.** Effect of long-range contacts on capacity of conformational ensembles to reproduce experimental RDCs from αS. Figures denote $\chi^2 = \Sigma(D_{ij,\text{calc}} - D_{ij,\text{meas}})^2$ that compares experimental RDCs measured in αS aligned in Pf1 phage with calculated averages over 50000 conformers having long-range contacts ($<15$ Å)

between Cβ in the specified ranges. Adjacent domains are equivalent to ensembles with no specified contact shown in A ($\chi^2$= 129) and are not shown.

This theoretical approach is therefore complementary to the PRE-based detection of long-range contacts in αS, and unequivocally shows that tertiary interactions are present in the native state of αS. We are working currently in an atomic resolution complementation to this alignment prediction strategy, which may deliver more precise detail on the conformations populated by αS, and comparison with the ensemble of conformers that we previously generated by PRE will further provide valuable insights.

Intriguingly, when we measured RDCs in the homologous protein βS, which lacks the central hydrophobic domain and does not evidence tertiary interactions as the one present in αS, we observed that the C-terminus of this protein also displayed high couplings. However, in contrast to the profile obtained for αS, high couplings in βS were exclusively located at that region, which has previously displayed a strong tendency to populate extended conformations with the PII signature. The occurrence of 8 Pro residues and the contribution of electrostatic repulsion between negatively charged side chains (net charge of -16) favor the adoption of extended conformations at the C-terminus. Thus, in this particular case, RDCs probe locally encoded conformational restrictions in the ensemble of conformations populated by the natively unfolded protein βS.

Taken together these data supports the novel interpretation of RDCs as simultaneous reporters of long-range structural order and local conformational sampling in an ensemble of rapidly interconverting conformations.

## 8.3. RDCs probe slow conformational dynamics in αS

NMR spectroscopy is uniquely suited for studying dynamical processes in proteins such as intramolecular motions. Movements in the range of the rotational correlation time of the molecule (~ ns) can be efficiently studied employing $^{15}$N spin relaxation. On the other hand, motions in the order of micro to milliseconds require the use of other experimental approaches. Slow time scales are of particular interest because functionally important biological processes, including enzyme catalysis, signal transduction, ligand binding, protein folding and allosteric regulation, among others are expected to occur in this time range (Mittermaier and Kay, 2006). Thus, motions up to millisecond time scales can be detected using CPMG relaxation dispersion methods (Palmer et al., 2001), as recently evidenced for folding intermediates of the Fyn SH3 domain (Korzhnev et al., 2004). However, these

measurements are very time consuming. Another alternative for characterizing slow dynamics are RDCs, which also  report on averages over longer time scales (up to the millisecond range) and therefore encode key information for understanding protein motions in the submicro- to millisecond range (Figure 8.4) (Bouvignies et al., 2005; Lakomek et al., 2006).
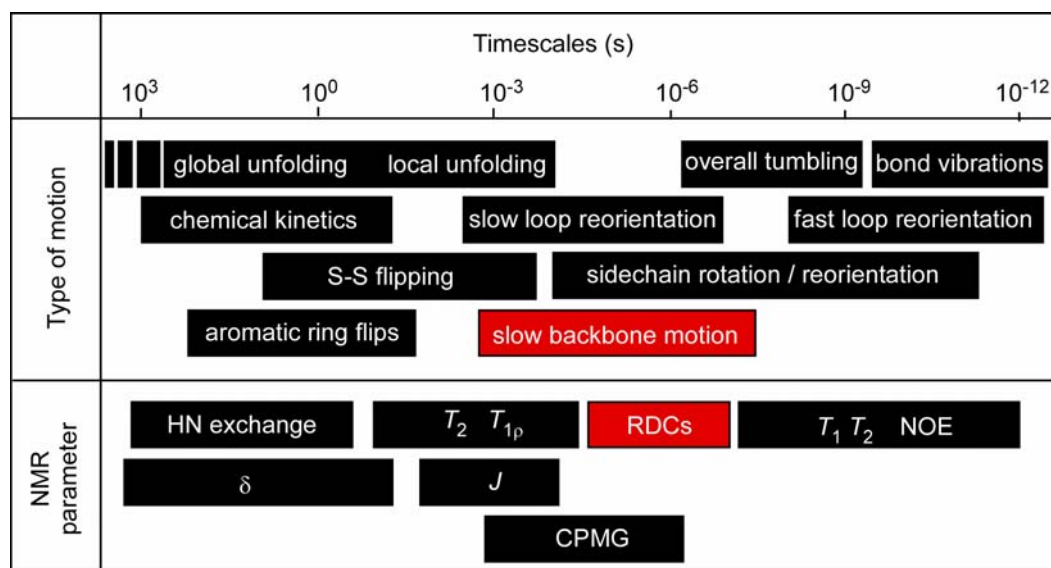


**Figure 8.4. NMR parameters employed to detect motions in proteins.** Almost all different types of motions that may occur in proteins can be efficiently studied by means of NMR spectroscopy.

RDCs report on time and ensemble-averaged conformations and therefore can be used to characterize both the structure and dynamics of unfolded proteins. When we employed RDCs to characterize the ensemble of rapid interconverting conformations of αS, we found a high degree of conformational restriction present at the C-terminus of the protein. Measurement of RDC in αS under the presence of chemical denaturants, on a C-terminal peptide and on A30P and A53T mutants demonstrated that this residual structure was not locally encoded, but rather was caused by a precise contribution of long-range interactions, which were further confirmed by ensemble-averaged computer simulations. Such conformational restrictions were not evidenced by ^{15}N relaxation time measurements, showing that αS was indeed very flexible. Furthermore, these measurement did not indicate any major long-range effects upon A30P and A53T replacements (Bussell and Eliezer, 2001). As ^{15}N relaxation is sensitive to motions in the order of pico- to nanoseconds, we conclude that RDCs probe slow motions (μs-ms time scale) in the conformations populated by αS.

Transverse relaxation rates have been also used previously to probe long-range interactions within the unfolded state of proteins (Klein-Seetharaman et al., 2002). $^{15}$N relaxation time measurements of αS did not provide evidence for long-range interactions and only a very slight increase in $R_2$ relaxation rates for residue 20 and 122 was observed, supporting our findings (Bussell and Eliezer, 2001). Thus, it is particularly interesting that the intrinsic structure present in αS restricts motions slower than the overall correlation time of the protein, but faster than the millisecond motions probed by $R_2$ measurements. This timescale is precisely the one in which secondary structures form during protein folding (Kubelka et al., 2004). Moreover, this suggests that the conditions that trigger αS oligomerization, in particular the PD-linked mutations, strongly increase structural fluctuations on this time scale, reducing the energetic barrier required for self association (Figure 8.5).
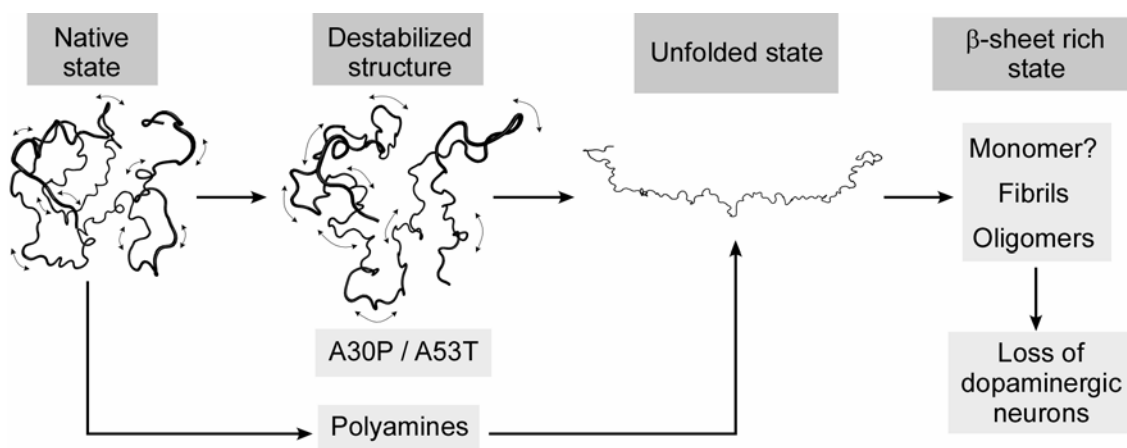


**Figure 8.5. Proposed scheme for the increased neurotoxicity of αS genetic mutants.** In this study we demonstrated that the two familial Parkinson´s disease associated mutants A30P and A53T perturb the long range interactions essential for the native state of αS. Long range interactions characterize the auto-inhibited native state of αS, maintaining the protein in a soluble innocuous state. Mutant αS can overcome more easily the energetic barrier for self-association, leading to an increased tendency to oligomerize. Polyamine binding and high temperature, conditions that *in vitro* enhance αS aggregation, induce a completely unfolded structure. Therefore we propose that redistribution of the ensemble of αS conformers, such that the highly amyloidogenic NAC region becomes exposed to the solvent and β-sheet rich conformations are adopted more easily, represents the common mechanism for both genetically linked and environmentally induced αS oligomerization in Parkinson's disease.

In the case of βS, our studies on the backbone dynamics probed by $^{15}$N longitudinal and transverse relaxation rates show the bell-shaped pattern expected for a random coil

polypeptide, and only suggest slight conformational restrictions at residues 40 to 45. However, chemical shift deviations and $^3J_{HNH\alpha}$ couplings in the C-terminus are suggestive of a strong propensity for populating extended conformations, likely PII, opposite to the rest of the protein where solvent interactions dictate the conformational propensity. When we measured RDCs for backbone NH in βS it was evident that residual structure was present at the whole domain, which, as mentioned before, in this case was not due to long range interactions. This suggest a bias in the random sampling of residue-specific $\phi,\psi$ distributions for the C-terminus of βS, causing restricted motions occurring in the μs-ms timescale only detected by RDCs.

## 8.4. Stabilization of auto inhibitory interactions in αS may inhibit amyloid protein deposition.

There is a whole body of biochemical evidence supporting the occurrence of the auto inhibitory long range interactions that we have identified in αS. Shielding of the hydrophobic central region of the protein by the C-terminal domain explains why this acidic tail functions as a chaperone-like solubilizing domain (Souza et al., 2000). It also provides a reason for the fact that C-terminally truncated αS is more amyloidogenic than the full-length protein (Crowther et al., 1998), an event that has been documented *in vivo*, and has been suggested to trigger disease states  (Li et al., 2005).

Posttranslational modifications are also known to occur at specific sites of the C-terminus of αS, triggering aggregation of the protein. Influence in fibrillation has been reported to be exerted by methionine oxidation, tyrosine nitration and phosphorylation of Ser[129] (Fujiwara et al., 2002; Norris et al., 2003). The effect of this modifications seems to be related to the formation of stable oligomeric species, in line with the proposed facilitation of αS self association upon loss of residual structure. It could be particularly interesting to evaluate modified αS with the set of NMR experiments that we have optimized.

Furthermore, the compaction of both the N- and C-termini coupled to a flip-back of the C-terminus over the central region of the protein explains why the hydrodynamic radius of αS corresponds to that of a completely unfolded polypeptide chain in the presence of 8 M urea, but, as we determined is considerably smaller in the native state. *In vivo*, the native compaction is likely to be further stabilized by the strong excluded volume effects associated with macromolecular crowding. Indeed, αS has recently been shown to remain natively unfolded in the bacteria cytoplasm, by in-vivo NMR measurements (McNulty et al., 2006a).

It is thus very likely that these long-range interactions that we identified *in vitro* play a central role *in vivo*.

We conclude that the release of intrinsic structure in the αS monomer is *a* or *the* key step that triggers oligomerization and aggregation. That is, the achievement of the fully unfolded state renders the hydrophobic patches of the NAC region accessible, and the N-terminus fully extended, such that the protein is able to adopt β-sheet conformations conducive to aggregation. The high free energy of the extended conformation, in which the hydrophobic NAC region is exposed to the solvent, would favor the association of monomers, thereby increasing the extent of both the nucleation and propagation steps of aggregation. It follows that alterations in the energetic barriers to achieve this conformational transition would affect the deposition rate of αS aggregates *in vivo* and thus the evolution of disease. From the therapeutic point of view, it could be foreseen that the reinforcement of these native, auto-inhibitory, long-range interactions in αS may constitute a logical functional target for new pharmacological agents designed to impede or even reverse aggregate formation in Parkinson's disease.

## 8.5. Redistribution of the ensemble of αS conformers may underlie toxic gain-of-function in A30P and A53T genetic mutants.

Similarly to the posttranslational modifications evidenced for the *wt* protein, several biological and biochemical properties underlying the toxic gain-of-function of the familial mutants A30P and A53T of αS can now be rationalized in terms of the different intrinsic structural features of these proteins (Table 8.2). Recently, it was proposed that the generation and accumulation of C-terminal truncated αS may involve cleavage between residues 119 to 123, phenomenon that was enhanced in mice models upon expression of mutant αS (Li et al., 2005). These findings may be explained by the results of the present study. Although the truncation site is far from the A30P and A53T missense mutations, the destabilization of αS tertiary structure may allow proteases to degrade the αS C-terminus more efficiently.

This destabilization may also be the source for the increased affinity of lysosomal chaperone-mediated autophagy (CMA) receptors for mutant αS, recognizing the sequence $_{95}$VKKDQ$_{99}$ present in the C-terminus of αS, and thereby causing an impairment in protein catabolism (Cuervo et al., 2004). Regarding self-association, an increased tendency to form dimers, oligomers and annular protofibrils has been evidenced for both PD-linked mutants (Conway et al., 2000; Lashuel et al., 2002a; Krishnan et al., 2003), which may as well be

explained in terms of our findings. The decreased shielding of the highly hydrophobic NAC region due to the reduction of long-range interactions, would allow A30P and A53T mutant αS to preferentially expose this region to the solvent, facilitating self-association.

| Characteristics associated with the increased neurotoxicity of A30P and A53T | |
| --- | --- |
| Biological features | Reduced cell viability in cell culture models (1)<br>Increased inhibition of proteasomal activity (2)<br>Impaired protein degradation via CMA (3)<br>Enhanced in vivo C-terminal truncation (4) |
| Biochemical features | Facilitated formation of dimers (5)<br>Acceleration of oligomerization (6)<br>Presence of annular protofibrills (7)<br>Rapid fibrillation (only A53T) (8)<br>Higher vesicle permeabilization activity (9) |
| Structural features | Perturbed autoinhibitory long range interactions<br>Increased backbone flexibility in the nano to microsecond time scale<br>Increased exposure of NAC region |

**Table 8.1. Distinctive features of αS-mediated pathogenesis correlate with the properties of A30P and A53T mutants.** References are as follows: (1) (Dev et al., 2003), (2) (Stefanis et al., 2001; Tanaka et al., 2001), (3) (Cuervo et al., 2004), (4) (Li et al., 2005), (5) (Krishnan et al., 2003), (6) (Conway et al., 2000), (7) (Lashuel et al., 2002a), (8) (Conway et al., 2000), (9) (Volles and Lansbury, 2002).

Thus, the redistribution of the structural ensemble of the A30P and A53T αS mutants potentiates oligomerization and modulates binding to ligands, proteases and receptors. This effect may account for the toxic gain-of-function of familial Parkinsonism-linked mutant αS. Conformationally altered αS may constitute a general molecular mechanism underlying the induction of PD by environmental and genetic conditions. Thus, agents specifically designed to stabilize the native state of αS may also prove useful in impeding or reversing its pathologic aggregation in familial forms of Parkinson's disease.

## 8.6. Characterization of the structural basis of metal-αS complexes.

The neurobiology of metal ions has attracted growing interest by virtue of their link to major neurological syndromes. Divalent metal ions, especially Cu(II), Fe(II) and Mn(II), are considered as risk factors for PD based on clinical and epidemiological studies (Sayre et al., 1999). The simplest mechanism proposed involves a direct effect of the metal ions on the aggregation of αS (Uversky et al., 2001c). In this study, we found that Cu(II), but not Mn(II),

Co(II), Ni(II) or Fe(II), are effective in accelerating the aggregation of αS at low μM concentrations, likely found *in vivo*. Differences between Cu(II) and the other divalent ions studied relate to the primary site of binding and to the different ranges of affinities estimated for the formation of metal-αS complexes (Table 8.2). These findings lead to a new conceptual scheme defining the hierarchy of metal-αS interactions which reflects both biological and structural effects, the latter resulting from the nature of the coordinating moieties of the protein, as discussed below.

| | Aggregation and affinity | | Primary binding sites | |
|---|---|---|---|---|
| Complex | t1/2 (h) | Kd(mM) | Motifs | Domain |
| Free | 64 ± 7 | - | - | - |
| Cu(II) | 30 ± 2 | ~ 0.1 [a] | [1]MDVFMKGLS[9] [48]VAHGV[52] | N-terminal |
| Other metals | 61 ± 7 | ~ 1000 [b] | [119]DPDNEA[124] | C-terminal |

**Table 8.2. Effects of binding of divalent metal ions to αS.** Synopsis of results derived from aggregation assays and affinity determinations for binding of Cu(II) and other divalent metal ions (Fe(II), Mn(II), Ni(II) and Co(II)) to αS.

According to the analysis of Thio-T traces of metal-induced αS fibrillation, Cu(II) promotes nucleation of αS but does not affect the growth phase, suggesting that the Cu(II)-bound form of αS is more prone to nucleate than the unliganded protein, a feature observed previously for polyamine complexes (Fernandez et al., 2004). The presence of Cu(II) in the fibrils indicates that the protein aggregates in its copper-bound form. Interestingly, Cu(II) does not affect the structural features inherent to the spontaneous aggregation of αS, inasmuch as copper-induced fibrils exhibit the same morphology as those formed in the absence of the cation.

Previous studies suggested that αS was able to bind between five to ten copper ions with a $K_d$ of ~ 50 μM (Paik et al., 1999; Lee et al., 2003). We showed here that the protein tightly binds only two Cu(II) ions per monomer with dissociation constants in the 0.1-50 μM range. More Cu(II) ions can be ligated by the protein, but with significantly lower affinity and probably via non-specific electrostatic interactions with charged amino acid side groups located at the C-terminus. We found that at sub-stoichiometric levels Cu(II) mainly interacts with residues located in the N-terminal region of αS, contrary to previous results suggesting

that Cu(II) was exclusively bound to the negatively charged C-terminal region (Paik et al., 1999; Uversky et al., 2001c). In the light of our findings, we believe that the observation of the N-terminal binding site for Cu(II) was masked in the previous studies due to a bias in the experimental setup designed to observe rapid oligomerization of αS. The high metal:protein ratios employed (5 to 10 molar excess, 0.5 mM Cu(II) concentration), and the SDS-PAGE methodology chosen to evidence αS self-interaction, requiring the addition of a coupling reagent for stabilizing the oligomers, could have impaired the observation of the high affinity binding site, in favor of the more numerous lower affinity bindings sites.

Different clusters of residues at the N-terminus are clearly simultaneously affected by Cu(II) binding, with aa3-9 and aa49-52 showing the strongest effect, whereas aa20-24 and aa39-44 were less affected. The broadening effect of a type II Cu(II) site on the amide resonances reaches ~11 Å from the Cu(II) location (Bermel et al., 2003). Thus, a decrease in intensity of a resonance does not necessarily indicate the direct participation of the corresponding residue in the coordination of the metal ion. Nevertheless, upon modification of His[50] by DEPC, the entire N-terminus of the protein loses the ability to interact with the metal, demonstrating the role of this residue as the anchor for Cu(II) binding and suggesting the involvement of the affected regions in the formation of a single Cu(II) binding interface. This finding also correlates with the Cu(II) coordination environment described by EPR, characterized by two N and two O ligand atoms. His[50] provides one nitrogen ligand, implying that the source of the other nitrogen comes either from the amide backbone or the N-terminal $NH_2$ group. The oxygen ligands could be provided by water molecules or/and backbone carbonyls from the peptide.

Our results ascribed the second, lower affinity, binding motif for Cu(II) in αS to the C-terminus. The affected region comprises residues 110-140, which also constitute the primary binding site for the polycationic polyamines (Fernandez et al., 2004). However, as demonstrated upon modification or protonation of the His[50], the Cu(II)-αS interaction within this interface is initially highly localized around residues 119-123, the spectral features of which are most affected. Thus, we conclude that Asp[119], Asp[121], Asn[122] and Glu[123] likely represent the ligand set for the second metal ion. Correspondingly, EPR spectroscopy indicates that the Cu(II) atom bound to DEPC-modified AS has four oxygen donors, suggesting the involvement of carboxylates as major contributors for metal binding.

After this study was published, two reports have provided complementary evidence showing that the first ten N-terminal residues of αS are able to bind Cu(II) (Kowalik

(Kowalik-Jankowska et al., 2005) in the absence of the His[50] residue, and suggesting that this amino acid may be involved on a second high affinity site also located at the N-terminus (Sung et al., 2006). It is possible that in our experiments unspecific DEPC modification of the N-terminus at pH 6.5, or its protonation at pH 5, may have occurred simultaneously to His[50] modifications, masking the distinction of two binding sites. However, DEPC is highly specific to His residues, and the N-terminus should be fully protonated at pH lower than 7 (pKa > 8.0). We do not disfavor the ability of the sole N-terminus to bind Cu(II), but its is possible, due to the highly flexible nature of the polypeptide backbone, that binding of Cu(II) to the N-terminus of αS does not involve a single binding interface, rather is dynamic and may accommodate different ligand sets. In the absence of the His residue, another side chain may provide the N contribution (a Lys fro example) preserving the ability of the protein to bind the metal. EPR and affinity determinations on a His50 mutant αS protein are going to provide more insights into the mechanism of Cu(II) binding .

Since elucidation of the residue specific effects might be central to an understanding of the mechanism of metal induced fibrilogenesis of αS, we also performed experiments aimed at correlating Cu(II) binding and destabilization of the αS monomer structure. The invariance of the chemical shifts of the backbone amide groups and of the hydrodynamic properties of αS indicate the absence of significant conformational changes or the induction of a partially misfolded species. Thus, in the presence of Cu(II), the formation of a complex between Cu(II) and αS, rather than the induction of a partially folded structure, would represent the critical step in the early stage of fibrillation of the protein. However, the central question as of what constitutes the basis for the enhancement of aggregation by Cu(II) binding could still be related to a perturbation of N-terminal long range interactions, similarly to what occurs upon protonation of the N-terminus and His[50] upon reducing the pH in αS.

Another possibility, similar to what has been reported for the amyloid β-peptide and prion protein, is that αS is also highly susceptible to metal-catalyzed oxidation, a reaction that induces extensive oligomerization and precipitation of these proteins (Paik et al., 1999; Requena et al., 2001). Since metal catalyzed oxidation of proteins is a highly selective, site-specific process that occurs primarily at protein sites with transition metal-binding capacity (Stadtman and Oliver, 1991), one can hypothesize that copper binding to the N-terminus of αS renders the protein a relatively easy target (*e.g.* for oxidative damage) and that the ensuing damage might lead *in vivo* to a cascade of structural alterations promoting the generation of a pool of αS molecules more prone to aggregate.

The NMR analysis of the rest of αS-metal(II) complexes indicated that the divalent metal ions studied bind preferentially to the C-terminal domain of αS in its native state. We conclude that a common, multiple binding site for metal ions exists in the region comprising residues 110-140, which also constitutes the binding interface for polycationic polyamines (Fernandez et al., 2004). Exploiting the different degree of paramagnetism of the metal ions or using substoichiometric metal to protein ratios we identified the primary site for metal ion coordination. The metal interaction was localized on residues Asp[121], Asn[122] and Glu[123], the spectral features of the former being the most affected. This picture is very similar to that determined for the αS-Cu(II) complexes formed at low pH, a condition favoring Cu(II) binding to the C-terminus

A coordination site formed mostly by carboxylate moieties is in agreement with the modest affinity constants observed for metal binding to the C-terminus of αS, and thus the high levels of metal ions, except Cu(II), required to induce the aggregation of αS (Uversky et al., 2001c). Some studies propose that the mechanism for metal αS induced aggregation could involve exclusively binding to the negatively charged carboxylates in the C-terminal region, leading to masking of the electrostatic repulsion and the collapse to a partially-folded conformation (Paik et al., 1999; Uversky et al., 2001c). Although the NMR experiments performed at up to 1 mM concentrations of metal ions did not reveal the formation of such an intermediate, our results support a mechanism of metal-induced aggregation *in vitro* sharing common features for the divalent metal ions Mn(II), Fe(II), Co(II) and Ni(II); yet indicating that this process differs significantly from that induced by Cu(II).

It is also instructive to relate the metal binding to αS with other structural features characterizing the αS system. The identification of a similar binding interface for divalent metal ions in the C-terminus of αS suggest a common mode of binding dictated largely by electrostatic interactions. Under these circumstances, the metal ions would more likely interact with carboxylate groups clustered in the protein sequence. This might be the case with the Asp[121] binding site, which is surrounded by the aspartic and glutamic acids Asp119, Glu[123] and Glu[126]. A qualitatively similar effect would be expected for the cluster of residues around Asp[135], comprising Glu[130], Glu[131], Glu[137] and Glu[139]. Instead, a noticeable difference was observed in the metal binding capabilities of the two regions. These discrepancies can be reconciled by comparing the RDC profiles for αS with the $I_{para}/I_{diam}$ profiles obtained in the presence of low sub-stoichiometric levels of metal ions. As shown in figure 8.4, a clear

correlation is observed between the selective broadening induced by the binding of divalent metal ions to the C-terminus and the intrinsic residual structure identified in that region.
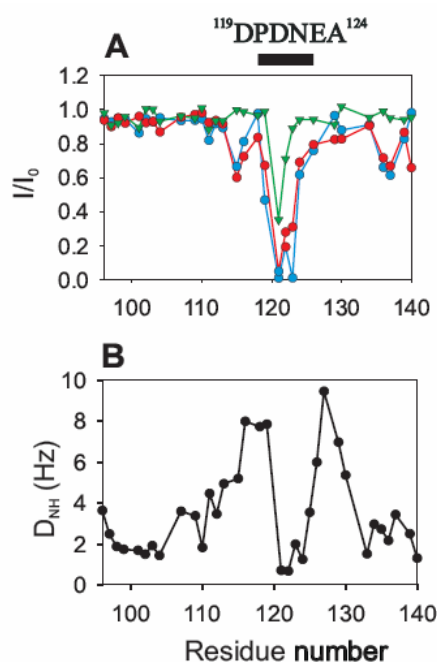


**Figure 8.4. Binding of divalent metals to the C-terminus of αS correlates with the residual structure of that domain. A**. Ipara/Idiam profiles for 100 μM αS, pH 6.5, in the presence of 15 μM Mn(II) (red circle) and 40 μM Co(II) (green triangle). At pH 5.0, Cu(II) binding is also located preferentially at the C-terminus(15 mM Cu(II), blue). B. RDCs profile for the C-terminus of αS at pH 6.5 aligned in C8E5/octanol.

The strong correlation between the location of the primary metal binding site and the dynamic and structural properties inherent to the C-terminal domain suggest that the presence of a specific spatial organization about residues 121-123 might result in a particular orientation of the coordination moieties favoring metal binding to this region. Thus, we propose that binding of metal ions to the C-terminus of αS is not driven exclusively by electrostatic interactions but is mostly determined by the intrinsic conformation of this domain. Complementary experiments on αS-metal complexes under conditions where long-range interactions and residual structure are impaired, i.e. under 8 M urea or with A30P or A53T mutations, will be needed to prove this hypothesis.

This view is consistent with recent biochemical and structural studies revealing a role for dynamic and conformational restrictions at the C-terminus in controlling abnormal αS cleavage and degradation *in vivo*. It was recently shown that the generation and accumulation of C-terminal truncated AS might be involved in the initiation and progression of αS aggregation *in vivo* (Li et al., 2005). *In vitro* studies have shown endoproteolytic cleavage of

αS by proteosomes at Asp[119]-Pro[120] and cleavage of αS by calpain I at Asn[122]-Glu[123] (Liu et al., 2003; Mishizen-Eberz et al., 2003; Li et al., 2005). In particular, the Asp-Pro peptide bonds are known to be very labile, (Segalas et al., 1995) and thus the presence of a specific spatial organization in this region might act to protect the sole Asp-Pro bond in αS from cleavage. We observe substantial differences in the degree of broadening induced by metal ions on the amide backbone cross peaks of residues Aps[119] and Asp[121], located within the [119]DPDNEA[124] fragment, which could reveal a certain degree of hindrance necessary to maintain the [119]Asp-Pro[120] bond in a non-cleavable conformation.

**8.7. Cu(II) binding is a biological link among amyloid diseases.**

The fact that Cu(II) can promote αS aggregation efficiently at physiologically relevant concentrations, and the identification of a binding interface in the N-terminus where Cu(II) binds with the highest affinity, constitute important findings of this work and support the notion of PD as a metal-associated neurodegenerative disorder. At this juncture a tighter link with other amyloid-related disorders such as Alzheimer's disease and prion disease can be sought, based on these new insights into the structural basis of copper interactions with αS. The key factors of AD and prion diseases are the amyloid precursor protein (APP) and prion protein (PrP), respectively.

As shown in table 8.3, the principal feature of Cu(II) binding to APP, PrP and αS is the presence of His residues acting as anchoring sites and allowing coordination with other nitrogen, oxygen or sulfur donors in 2N1O1S, 2N2O or 3N1O arrangements. In all cases, the proteins bind one copper atom per site. Interestingly, the affinity of Cu(II) for these proteins is in the low or sub-micromolar range, a fact that may have important biological implications. Even if the intracellular Cu(II) pools are regulated by binding to ligands (i.e., metallothioneins) of various affinities, the coordination of Cu(II) by these ligands is labile and subject to fluctuations.

| | AD | | Prion disease | PD |
|---|---|---|---|---|
| Protein/peptide | APP | Aβ* | PrP † | αS |
| Ligand donor set | 2N1O1S | 3N1O | 3N1O / 2N2O | 2N2O |
| Coordination‡ | T | DT | S / DT | S / DT |
| Anchoring residue | His | His | His | His |
| Kd ( M) | ~ 0.01 | 0.3 - 4 | 0.1-10 | ~ 0.1 |
| Stoichiometry | 1 : 1 | 1 : 1 | 1 : 1 | 1 : 1 |
| References | (1, 2) | (3-6) | (7-11) | This work |

**Table 8.3. Structural and binding properties of high affinity Cu(II) sites in amyloidogenic proteins involved in Alzheimer's disease, Prion disease and Parkinson's disease.** * $Aβ_{1-40}$, $Aβ_{1-42}$, [†] Reported data correspond to the octarepeat binding motif. [‡] Coordination geometry: T (tetrahedral); S (square-planar); DT (distorted tetragonal). References are as follows: 1, (Hesse et al., 1994); 2, (Barnham et al., 2003); 3, (Atwood et al., 1998); 4, (Garzon-Rodriguez et al., 1999); 5, (Huang et al., 1999); 6, (Karr et al., 2004); 7, (Hornshaw et al., 1995); 8, (Brown et al., 1997); 9, (Viles et al., 1999); 10, (Aronoff-Spencer et al., 2000); 11, (Garnett and Viles, 2003).

It is likely that the concentrations of Cu(II) in neurons and glia are sufficient to contribute to potential abnormal interaction with proteins such as αS, under certain stress circumstances. Furthermore, although the metabolic pathways of extracellular Cu(II) are poorly understood, Cu(II) levels as high as 15 μM can be envisioned (Hartter and Barnea, 1988), sufficiently high to form complexes with extracellular targets implicated in disease such as amyloid-β peptide (Aβ). Although more studies are needed to explore other biological aspects of Cu(II)-αS interactions, the structural features emerging from this work indicate that perturbations in copper metabolism may constitute a more widespread element in neurodegenerative disorders than has been recognized previously.

# *Conclusions*

## 9. Conclusions

The major outcome of this thesis work concerns the description of the ensemble of conformers populated by the Parkinson's disease associated protein αS, and the study of the destabilizing effect caused by genetic and environmental factors promoting self-oligomerization and amyloid-like protein deposition. The following conclusions have been derived from the results presented here:

- The protein αS, although deprived of defined secondary structure, is not a random coil, but rather populates compact conformations stabilized by long range interactions.

- Two types of long-range tertiary contacts are found in αS, a hydrophobic core between the central NAC region and the C-terminus, and electrostatic interactions between the N- and C-terminus.

- Genetically-linked and environmentally-induced pathological states of αS are characterized by the impairment of long-range interactions rendering exposure of the central hydrophobic NAC region and facilitating self oligomerization.

- The homologous protein βS, which lacks the central NAC region, does not display long range interaction and populates more extended unfolded conformations, yet with a high content of residual structure at the C-terminus.

- αS possesses a high affinity Cu(II) binding site at the N-terminus of the protein, and interactions with the metal cation at low micromolar concentrations cause aggregation of the protein, suggesting that impairment of Cu(II) homeostasis is a common feature of amyloid disorders such as Alzheimer's or Prion diseases.

- From the methodological point of view, our data represent the first study of a natively unstructured protein by means of PREs, suggesting that this approach may also be valid for the study of such highly dynamic systems.

- In addition, the measurement of RDCs in αS and βS was shown to be sensitive both to restricted slow motions (μs timescale) and long-range interactions, as complementary probed by ensemble averaged computer-derived structures. This result categorizes RDCs as highly suitable for studying the complex conformational states of natively unfolded polypeptides.

# References

# 10. References

Abeliovich, A., Schmitz, Y., Farinas, I., Choi-Lundberg, D., Ho, W. H., Castillo, P. E., Shinsky, N., Verdugo, J. M., Armanini, M., Ryan, A*., et al.* (2000). Mice lacking alpha-synuclein display functional deficits in the nigrostriatal dopamine system. *Neuron 25*, 239-252.

Ackerman, M. S., and Shortle, D. (2002). Molecular alignment of denatured states of staphylococcal nuclease with strained polyacrylamide gels and surfactant liquid crystalline phases. *Biochemistry 41*, 3089-3095.

Alexandrescu, A. T., and Kammerer, R. A. (2003). Structure and disorder in the ribonuclease S-peptide probed by NMR residual dipolar couplings. *Protein Sci. 12*, 2132-2140.

Anfinsen, C. B. (1973). Principles that govern the folding of protein chains. *Science 181*, 223-230.

Antony, T., Hoyer, W., Cherny, D., Heim, G., Jovin, T. M., and Subramaniam, V. (2003). Cellular polyamines promote the aggregation of alpha-synuclein. *J. Biol. Chem. 278*, 3235-3240.

Aronoff-Spencer, E., Burns, C. S., Avdievich, N. I., Gerfen, G. J., Peisach, J., Antholine, W. E., Ball, H. L., Cohen, F. E., Prusiner, S. B., and Millhauser, G. L. (2000). Identification of the Cu2+ binding sites in the N-terminal domain of the prion protein by EPR and CD spectroscopy. *Biochemistry 39*, 13760-13771.

Atwood, C. S., Moir, R. D., Huang, X. D., Scarpa, R. C., Bacarra, N. M. E., Romano, D. M., Hartshorn, M. K., Tanzi, R. E., and Bush, A. I. (1998). Dramatic aggregation of Alzheimer A beta by Cu(II) is induced by conditions representing physiological acidosis. *J. Biol. Chem. 273*, 12817-12826.

Auvinen, M., Paasinen, A., Andersson, L. C., and Holtta, E. (1992). Ornithine decarboxylase activity is critical for cell transformation. *Nature 360*, 355-358.

Baldwin, R. L. (2002). A new perspective on unfolded proteins. *Adv. Protein. Chem. 62*, 361-367.

Barnham, K. J., McKinstry, W. J., Multhaup, G., Galatis, D., Morton, C. J., Curtain, C. C., Williamson, N. A., White, A. R., Hinds, M. G., Norton, R. S*., et al.* (2003). Structure of the Alzheimer's disease amyloid precursor protein copper binding domain: A regulator of neuronal copper homeostasis. *J. Biol. Chem. 278*, 17401-17407.

Battiste, J. L., and Wagner, G. (2000). Utilization of site-directed spin labeling and high-resolution heteronuclear nuclear magnetic resonance for global fold determination of large proteins with limited nuclear overhauser effect data. *Biochemistry 39*, 5355-5365.

Bax, A. (2003). Weak alignment offers new NMR opportunities to study protein structure and dynamics. *Protein Sci. 12*, 1-16.

Bax, A., and Grzesiek, S. (1993). Methodological Advances in Protein Nmr. *Acc. Chem. Res. 26*, 131-138.

Bax, A., Griffey, R. H., and Hawkins, B. L. (1983). Correlation of proton and N-15 chemical-shifts by multiple quantum NMR. *J. Mag. Res. 55*, 301-315.

Bax, A., Ikura, M., Kay, L. E., Torchia, D. A., and Tschudin, R. (1990). Comparison of different modes of 2-Dimensional reverse-correlation NMR for the study of proteins. *J. Mag. Res. 86*, 304-318.

Belosi, B., Gaggelli, E., Guerrini, R., Kozlowski, H., Luczkowski, M., Mancini, F. M., Remelli, M., Valensin, D., and Valensin, G. (2004). Copper binding to the neurotoxic peptide PrP106-126: Thermodynamic and structural studies. *Chembiochem. 5*, 349-359.

Bence, N. F., Sampat, R. M., and Kopito, R. R. (2001). Impairment of the ubiquitin-proteasome system by protein aggregation. *Science 292*, 1552-1555.

Bermel, W., Bertini, I., Felli, I. C., Kummerle, R., and Pierattelli, R. (2003). 13C direct detection experiments on the paramagnetic oxidized monomeric copper, zinc superoxide dismutase. *J. Am. Chem. Soc. 125*, 16423-16429.

Bernado, P., Garcia de la Torre, J., and Pons, M. (2004). Macromolecular crowding in biological systems: hydrodynamics and NMR methods. *J. Mol. Recognit. 17*, 397-407.

Bernado, P., Bertoncini, C. W., Griesinger, C., Zweckstetter, M., and Blackledge, M. (2005a). Defining long-range order and local disorder in native alpha-synuclein using residual dipolar couplings. *J. Am. Chem. Soc. 127*, 17968-17969.

Bernado, P., Blanchard, L., Timmins, P., Marion, D., Ruigrok, R. W., and Blackledge, M. (2005b). A structural model for unfolded proteins from residual dipolar couplings and small-angle x-ray scattering. *Proc. Natl. Acad. Sci. U. S. A. 102*, 17002-17007.

Bertini, I., and Luchinat, C. (1996). NMR of Paramagnetic Substances, Vol 150 (The Netherlands: Elsevier Science S.A).

Bertini, I., Gelis, I., Katsaros, N., Luchinat, C., and Provenzani, A. (2003). Tuning the affinity for lanthanides of calcium binding proteins. *Biochemistry 42*, 8011-8021.

Bodenhausen, G., and Ruben, D. J. (1980). Natural abundance 15N NMR by enhanced heteronuclear spectroscopy. *Chem. Phys. Lett. 69*, 185-189.

Bolin, K. A., Pitkeathly, M., Miranker, A., Smith, L. J., and Dobson, C. M. (1996). Insight into a Random Coil Conformation and an Isolated Helix: Structural and Dynamical Characterisation of the C-Helix Peptide from Hen Lysozyme. *J. Mol. Biol. 261*, 443-453.

Booth, D. R., Sunde, M., Bellotti, V., Robinson, C. V., Hutchinson, W. L., Fraser, P. E., Hawkins, P. N., Dobson, C. M., Radford, S. E., Blake, C. C., and Pepys, M. B. (1997). Instability, unfolding and aggregation of human lysozyme variants underlying amyloid fibrillogenesis. *Nature 385*, 787-793.

Bouvignies, G., Bernado, P., Meier, S., Cho, K., Grzesiek, S., Bruschweiler, R., and Blackledge, M. (2005). Identification of slow correlated motions in proteins using residual dipolar and hydrogen-bond scalar couplings. *Proc. Natl. Acad. Sci. U. S. A. 102*, 13885-13890.

Bowers, P. M., Strauss, C. E., and Baker, D. (2000). De novo protein structure determination using sparse NMR data. *J. Biomol. NMR. 18*, 311-318.

Braun, S., Kalinowski, H.-O., and Berger, S. (1999). 150 and More Basic NMR Experiments: A Practical Course, 2nd edn (Weinheim: Wiley-VCH).

Brown, D. R., and Kozlowski, H. (2004). Biological inorganic and bioinorganic chemistry of neurodegeneration based on prion and Alzheimer diseases. *J. Chem. Soc. Dalton Trans.*, 1907-1917.

Brown, D. R., Qin, K., Herms, J. W., Madlung, A., Manson, J., Strome, R., Fraser, P. E., Kruck, T., von Bohlen, A., Schulz-Schaeffer, W.*, et al.* (1997). The cellular prion protein binds copper in vivo. *Nature 390*, 684-687.

Bryce, G. F., and Gurd, F. R. N. (1966). Visible spectra and optical rotatory properties of cupric ion complexes of L-histidine-containing peptides. *J. Biol. Chem. 241*, 122-129.

Bucciantini, M., Giannoni, E., Chiti, F., Baroni, F., Formigli, L., Zurdo, J., Taddei, N., Ramponi, G., Dobson, C. M., and Stefani, M. (2002). Inherent toxicity of aggregates implies a common mechanism for protein misfolding diseases. *Nature 416*, 507-511.

Buchman, V. L., Hunter, H. J., Pinon, L. G., Thompson, J., Privalova, E. M., Ninkina, N. N., and Davies, A. M. (1998). Persyn, a member of the synuclein family, has a distinct pattern of expression in the developing nervous system. *J. Neurosci. 18*, 9335-9341.

Buchner, J. (1996). Supervising the fold: functional principles of molecular chaperones. *FASEB J. 10*, 10-19.

Bukau, B., and Horwich, A. L. (1998). The Hsp70 and Hsp60 chaperone machines. *Cell 92*, 351-366.

Bush, A. I. (2000). Metals and neuroscience. *Curr. Opin. Chem. Biol. 4*, 184-191.

Bush, A. I., Masters, C. L., and Tanzi, R. E. (2003). Copper, beta-amyloid, and Alzheimer's disease: tapping a sensitive connection. *Proc. Natl. Acad. Sci. U. S. A. 100*, 11193-11194.

Bussell, R., Jr., and Eliezer, D. (2001). Residual structure and dynamics in Parkinson's disease-associated mutants of alpha-synuclein. *J. Biol. Chem. 276*, 45996-46003.

Bussell, R., Jr., and Eliezer, D. (2003). A structural and functional role for 11-mer repeats in alpha-synuclein and other exchangeable lipid binding proteins. *J. Mol. Biol. 329*, 763-778.

Bussell, R., Jr., Ramlall, T. F., and Eliezer, D. (2005). Helix periodicity, topology, and dynamics of membrane-associated alpha-synuclein. *Protein Sci. 14*, 862-872.

Calamai, M., Chiti, F., and Dobson, C. M. (2005). Amyloid Fibril Formation Can Proceed from Different Conformations of a Partially Unfolded Protein. *Biophys. J. 89*, 4201-4210.

Castellani, R. J., Siedlak, S. L., Perry, G., and Smith, M. A. (2000). Sequestration of iron by Lewy bodies in Parkinson's disease. *Acta. Neuropathol. 100*, 111-114.

Caughey, B., and Lansbury, P. T. (2003). Protofibrils, pores, fibrils, and neurodegeneration: separating the responsible protein aggregates from the innocent bystanders. *Annu. Rev. Neurosci. 26*, 267-298.

Chandra, S., Chen, X. C., Rizo, J., Jahn, R., and Sudhof, T. C. (2003). A broken alpha-helix in folded alpha-synuclein. *J. Biol. Chem. 278*, 15313-15318.

Chandra, S., Gallardo, G., Fernandez-Chacon, R., Schluter, O. M., and Sudhof, T. C. (2005). Alpha-synuclein cooperates with CSPalpha in preventing neurodegeneration. *Cell 123*, 383-396.

Chandra, S., Fornai, F., Kwon, H. B., Yazdani, U., Atasoy, D., Liu, X., Hammer, R. E., Battaglia, G., German, D. C., Castillo, P. E., and Sudhof, T. C. (2004). Double-knockout mice for alpha- and beta-synucleins: effect on synaptic functions. *Proc. Natl. Acad. Sci. U. S. A. 101*, 14966-14971.

Chen, P. E., Specht, C. G., Morris, R. G., and Schoepfer, R. (2002). Spatial learning is unimpaired in mice containing a deletion of the alpha-synuclein locus. *Eur. J. Neurosci. 16*, 154-158.

Chiti, F., Stefani, M., Taddei, N., Ramponi, G., and Dobson, C. M. (2003). Rationalization of the effects of mutations on peptide and protein aggregation rates. *Nature 424*, 805-808.

Choi, W., Zibaee, S., Jakes, R., Serpell, L. C., Davletov, B., Crowther, R. A., and Goedert, M. (2004). Mutation E46K increases phospholipid binding and assembly into filaments of human alpha-synuclein. *FEBS Lett. 576*, 363-368.

Chung, K. K., Zhang, Y., Lim, K. L., Tanaka, Y., Huang, H., Gao, J., Ross, C. A., Dawson, V. L., and Dawson, T. M. (2001). Parkin ubiquitinates the alpha-synuclein-interacting protein, synphilin-1: implications for Lewy-body formation in Parkinson disease. *Nat. Med. 7*, 1144-1150.

Ciechanover, A. (2005). Proteolysis: from the lysosome to ubiquitin and the proteasome. *Nat. Rev. Mol. Cell. Biol. 6*, 79-87.

Ciechanover, A., and Brundin, P. (2003). The ubiquitin proteasome system in neurodegenerative diseases: sometimes the chicken, sometimes the egg. *Neuron 40*, 427.

Clayton, D. F., and George, J. M. (1998). The synucleins: a family of proteins involved in synaptic function, plasticity, neurodegeneration and disease. *Trends Neurosci. 21*, 249-254.

Clayton, D. F., and George, J. M. (1999). Synucleins in synaptic plasticity and neurodegenerative disorders. *J. Neurosci. Res. 58*, 120-129.

Conway, K. A., Harper, J. D., and Lansbury, P. T. (1998). Accelerated in vitro fibril formation by a mutant alpha-synuclein linked to early-onset Parkinson disease. *Nat. Med. 4*, 1318-1320.

Conway, K. A., Rochet, J. C., Bieganski, R. M., and Lansbury, P. T., Jr. (2001). Kinetic stabilization of the alpha-synuclein protofibril by a dopamine-alpha-synuclein adduct. *Science 294*, 1346-1349.

Conway, K. A., Lee, S. J., Rochet, J. C., Ding, T. T., Williamson, R. E., and Lansbury, P. T., Jr. (2000). Acceleration of oligomerization, not fibrillization, is a shared property of both alpha-synuclein mutations linked to early-onset Parkinson's disease: implications for pathogenesis and therapy. *Proc. Natl. Acad. Sci. 97*, 571-576.

Cookson, M. R. (2005). The biochemistry of Parkinson's disease. *Annu. Rev. Biochem. 74*, 29-52.

Cordier, F., Dingley, A. J., and Grzesiek, S. (1999). A doublet-separated sensitivity-enhanced HSQC for the determination of scalar and dipolar one-bond J-couplings. *J. Biomol. NMR. 13*, 175-180.

Crowther, R. A., Jakes, R., Spillantini, M. G., and Goedert, M. (1998). Synthetic filaments assembled from C-terminally truncated alpha-synuclein. *FEBS Lett. 436*, 309-312.

Cuervo, A. M., Stefanis, L., Fredenburg, R., Lansbury, P. T., and Sulzer, D. (2004). Impaired degradation of mutant alpha-synuclein by chaperone-mediated autophagy. *Science 305*, 1292-1295.

Cummings, C. J., Mancini, M. A., Antalffy, B., DeFranco, D. B., Orr, H. T., and Zoghbi, H. Y. (1998). Chaperone suppression of aggregation and altered subcellular proteasome localization imply protein misfolding in SCA1. *Nat. Genet. 19*, 148-154.

Daniele, P. G., Prenesti, E., and Ostacoli, G. (1996). Ultraviolet-circular dichroism spectra for structural analysis of copper(II) complexes with aliphatic and aromatic ligands in aqueous solution. *J. Chem. Soc. Dalton Trans.*, 3269-3275.

Davidson, W. S., Jonas, A., Clayton, D. F., and George, J. M. (1998). Stabilization of alpha-synuclein secondary structure upon binding to synthetic membranes. *J. Biol. Chem. 273*, 9443-9449.

Davis, R. L., Shrimpton, A. E., Holohan, P. D., Bradshaw, C., Feiglin, D., Collins, G. H., Sonderegger, P., Kinter, J., Becker, L. M., Lacbawan, F.*, et al.* (1999). Familial dementia caused by polymerization of mutant neuroserpin. *Nature 401*, 376-379.

Dawson, T. M., and Dawson, V. L. (2003). Molecular pathways of neurodegeneration in Parkinson's disease. *Science 302*, 819-822.

Dedmon, M. M., Lindorff-Larsen, K., Christodoulou, J., Vendruscolo, M., and Dobson, C. M. (2005). Mapping long-range interactions in alpha-synuclein using spin-label NMR and ensemble molecular dynamics simulations. *J. Am. Chem. Soc. 127*, 476-477.

Delaglio, F., Grzesiek, S., Vuister, G. W., Zhu, G., Pfeifer, J., and Bax, A. (1995). NMRPipe: a multidimensional spectral processing system based on UNIX pipes. *J. Biomol. NMR. 6*, 277-293.

Der-Sarkissian, A., Jao, C. C., Chen, J., and Langen, R. (2003). Structural organization of alpha-synuclein fibrils studied by site-directed spin labeling. *J. Biol. Chem. 278*, 37530-37535.

Dev, K. K., Hofele, K., Barbieri, S., Buchman, V. L., and van der Putten, H. (2003). Part II: alpha-synuclein and its molecular pathophysiological role in neurodegenerative disease. *Neuropharmacology 45*, 14-44.

Dill, K. A., and Chan, H. S. (1997). From Levinthal to pathways to funnels. *Nat. Struct. Mol. Biol. 4*, 10.

Ding, T. T., Lee, S. J., Rochet, J. C., and Lansbury, P. T., Jr. (2002). Annular alpha-synuclein protofibrils are produced when spherical protofibrils are incubated in solution or bound to brain-derived membranes. *Biochemistry 41*, 10209-10217.

Dinner, A. R., Sali, A., Smith, L. J., Dobson, C. M., and Karplus, M. (2000). Understanding protein folding via free-energy surfaces from theory and experiment. *Trends. Biochem. Sci. 25*, 331-339.

Dobson, C. M. (2003). Protein folding and misfolding. *Nature 426*, 884-890.

Dobson, C. M. (2004). Principles of protein folding, misfolding and aggregation. *Semin. Cell. Dev. Biol. 15*, 3-16.

Dobson, C. M., and Karplus, M. (1999). The fundamentals of protein folding: bringing together theory and experiment. *Curr. Opin. Struct. Biol. 9*, 92-101.

Dumoulin, M., Canet, D., Last, A. M., Pardon, E., Archer, D. B., Muyldermans, S., Wyns, L., Matagne, A., Robinson, C. V., Redfield, C., and Dobson, C. M. (2005). Reduced global cooperativity is a common feature underlying the amyloidogenicity of pathogenic lysozyme mutations. *J. Mol. Biol. 346*, 773-788.

Dyson, H. J., and Wright, P. E. (2002). Insights into the structure and dynamics of unfolded proteins from nuclear magnetic resonance. *Adv. Protein. Chem. 62*, 311-340.

Dyson, H. J., and Wright, P. E. (2004). Unfolded proteins and protein folding studied by NMR. *Chem. Rev. 104*, 3607-3622.

Dyson, H. J., and Wright, P. E. (2005). Intrinsically unstructured proteins and their functions. *Nat. Rev. Mol. Cell. Biol. 6*, 197-208.

Eaton, W. A., Munoz, V., Thompson, P. A., Henry, E. R., and Hofrichter, J. (1998). Kinetics and Dynamics of Loops, alpha-Helices, beta-Hairpins, and Fast-Folding Proteins. *Acc. Chem. Res. 31*, 745-753.

El-Agnaf, O. M., Nagala, S., Patel, B. P., and Austen, B. M. (2001). Non-fibrillar oligomeric species of the amyloid ABri peptide, implicated in familial British dementia, are more potent at inducing apoptotic cell death than protofibrils or mature fibrils. *J. Mol. Biol. 310*, 157-168.

El-Agnaf, O. M., Jakes, R., Curran, M. D., Middleton, D., Ingenito, R., Bianchi, E., Pessi, A., Neill, D., and Wallace, A. (1998). Aggregates from mutant and wild-type alpha-synuclein proteins and NAC peptide induce apoptotic cell death in human neuroblastoma cells by formation of beta-sheet and amyloid-like filaments. *FEBS Lett. 440*, 71-75.

Eliezer, D., Kutluay, E., Bussell, R., Jr., and Browne, G. (2001). Conformational properties of alpha-synuclein in its free and lipid-associated states. *J. Mol. Biol. 307*, 1061-1073.

Farrow, N. A., Zhang, O. W., Szabo, A., Torchia, D. A., and Kay, L. E. (1995). Spectral Density-Function Mapping Using N-15 Relaxation Data Exclusively. *J. Biomol. NMR 6*, 153-162.

Fernandez-Escamilla, A. M., Rousseau, F., Schymkowitz, J., and Serrano, L. (2004). Prediction of sequence-dependent and mutational effects on the aggregation of peptides and proteins. *Nat. Biotechnol. 22*, 1302-1306.

Fernandez, C. O., Hoyer, W., Zweckstetter, M., Jares-Erijman, E. A., Subramaniam, V., Griesinger, C., and Jovin, T. M. (2004). NMR of alpha-synuclein-polyamine complexes elucidates the mechanism and kinetics of induced aggregation. *EMBO J. 23*, 2039-2046.

Fersht, A. (1999). Structure and Mechanism in Protein Science: A Guide to Enzyme Catalysis and Protein Folding (New York: W H Freeman & Co.).

Fezoui, Y., and Teplow, D. B. (2002). Kinetic studies of amyloid beta-protein fibril assembly. Differential effects of alpha-helix stabilization. *J. Biol. Chem. 277*, 36948-36954.

Fieber, W., Kristjansdottir, S., and Poulsen, F. M. (2004). Short-range, long-range and transition state interactions in the denatured state of ACBP from residual dipolar couplings. *J. Mol. Biol. 339*, 1191-1199.

Fitzkee, N. C., and Rose, G. D. (2004). Reassessing random-coil statistics in unfolded proteins. *Proc. Natl. Acad. Sci. U. S. A. 101*, 12497-12502.

Flory, P. J. (1969). Statistical Mechanics of Chain Molecules (New York: Wiley).

Forno, L. S. (1996). Neuropathology of Parkinson's disease. *J. Neuropathol. Exp. Neurol. 55*, 259-272.

Fujiwara, H., Hasegawa, M., Dohmae, N., Kawashima, A., Masliah, E., Goldberg, M. S., Shen, J., Takio, K., and Iwatsubo, T. (2002). alpha-Synuclein is phosphorylated in synucleinopathy lesions. *Nat. Cell. Biol. 4*, 160-164.

Gaggelli, E., Bernardi, F., Molteni, E., Pogni, R., Valensin, D., Valensin, G., Remelli, M., Luczkowski, M., and Kozlowski, H. (2005). Interaction Of The Human Prion PrP(106-126) Sequence With Copper(II), Manganese(II), And Zinc(II): NMR and EPR Studies. *J. Am. Chem. Soc. 127*, 996-1006.

Galvin, J. E., Uryu, K., Lee, V. M. Y., and Trojanowski, J. Q. (1999). Axon pathology in Parkinson's disease and Lewy body dementia hippocampus contains alpha -, beta -, and gamma -synuclein. *Proc. Natl. Acad. Sci. U. S. A. 96*, 13450-13455.

Garnett, A. P., and Viles, J. H. (2003). Copper binding to the octarepeats of the prion protein. Affinity, specificity, folding, and cooperativity: insights from circular dichroism. *J. Biol. Chem. 278*, 6795-6802.

Garzon-Rodriguez, W., Yatsimirsky, A. K., and Glabe, C. G. (1999). Binding of Zn(II), Cu(II), and Fe(II) ions to Alzheimer's A beta peptide studied by fluorescence. *Bioorg. Med. Chem. Lett. 9*, 2243-2248.

Giasson, B. I., and Lee, V. M. (2001). Parkin and the molecular pathways of Parkinson's disease. *Neuron 31*, 885-888.

Giasson, B. I., and Lee, V. M. (2003). Are ubiquitination pathways central to Parkinson's disease? *Cell 114*, 1-8.

Giasson, B. I., Murray, I. V., Trojanowski, J. Q., and Lee, V. M. (2001). A hydrophobic stretch of 12 amino acid residues in the middle of alpha-synuclein is essential for filament assembly. *J. Biol. Chem. 276*, 2380-2386.

Gillespie, J. R., and Shortle, D. (1997a). Characterization of long-range structure in the denatured state of staphylococcal nuclease. I. paramagnetic relaxation enhancement by nitroxide spin labels. *J. Mol. Biol. 268*, 158-169.

Gillespie, J. R., and Shortle, D. (1997b). Characterization of long-range structure in the denatured state of staphylococcal nuclease. II. Distance restraints from paramagnetic relaxation and calculation of an ensemble of structures. *J. Mol. Biol. 268*, 170-184.

Goddard, T. D., and Kneller, D. G. SPARKY 3 (San Francisco: University of California).

Goedert, M. (2001). Alpha-synuclein and neurodegenerative diseases. *Nat. Rev. Neurosci. 2*, 492-501.

Goldberg, M. S., and Lansbury, P. T., Jr. (2000). Is there a cause-and-effect relationship between alpha-synuclein fibrillization and Parkinson's disease? *Nat. Cell. Biol. 2*, E115-119.

Golts, N., Snyder, H., Frasier, M., Theisler, C., Choi, P., and Wolozin, B. (2002). Magnesium inhibits spontaneous and iron-induced aggregation of alpha-synuclein. *J. Biol. Chem. 277*, 16116-16123.

Gomes-Trolin, C., Nygren, I., Aquilonius, S. M., and Askmark, H. (2002). Increased red blood cell polyamines in ALS and Parkinson's disease. *Exp. Neurol. 177*, 515-520.

Gosavi, N., Lee, H. J., Lee, J. S., Patel, S., and Lee, S. J. (2002). Golgi fragmentation occurs in the cells with prefibrillar alpha-synuclein aggregates and precedes the formation of fibrillar inclusion. *J. Biol. Chem. 277*, 48984-48992.

Griffiths-Jones, S. R., Sharman, G. J., Maynard, A. J., and Searle, M. S. (1998). Modulation of intrinsic phi,psi propensities of amino acids by neighbouring residues in the coil regions of protein structures: NMR analysis and dissection of a beta-hairpin peptide. *J. Mol. Biol. 284*, 1597-1609.

Haass, C., and Steiner, H. (2001). Protofibrils, the unifying toxic molecule of neurodegenerative disorders? *Nat. Neurosci. 4*, 859-860.

Hammarstrom, P., Jiang, X., Hurshman, A. R., Powers, E. T., and Kelly, J. W. (2002). Sequence-dependent denaturation energetics: A major determinant in amyloid disease diversity. *Proc. Natl. Acad. Sci. U. S. A. 99 Suppl 4*, 16427-16432.

Hansen, M. R., Mueller, L., and Pardi, A. (1998). Tunable alignment of macromolecules by filamentous phage yields dipolar coupling interactions. *Nat. Struct. Biol. 5*, 1065-1074.

Harper, J. D., Wong, S. S., Lieber, C. M., and Lansbury, P. T. (1997). Observation of metastable Abeta amyloid protofibrils by atomic force microscopy. *Chem. Biol. 4*, 119-125.

Harper, J. D., Wong, S. S., Lieber, C. M., and Lansbury, P. T., Jr. (1999). Assembly of A beta amyloid protofibrils: an in vitro model for a possible early event in Alzheimer's disease. *Biochemistry 38*, 8972-8980.

Hartl, F. U., and Hayer-Hartl, M. (2002). Molecular chaperones in the cytosol: from nascent chain to folded protein. *Science 295*, 1852-1858.

Hartter, D. E., and Barnea, A. (1988). Brain tissue accumulates 67copper by two ligand-dependent saturable processes. A high affinity, low capacity and a low affinity, high capacity process. *J. Biol. Chem. 263*, 799-805.

Hashimoto, M., Rockenstein, E., Mante, M., Mallory, M., and Masliah, E. (2001). beta-Synuclein inhibits alpha-synuclein aggregation: a possible role as an anti-parkinsonian factor. *Neuron 32*, 213-223.

Hashimoto, M., Hsu, L. J., Xia, Y., Takeda, A., Sisk, A., Sundsmo, M., and Masliah, E. (1999). Oxidative stress induces amyloid-like aggregate formation of NACP/alpha-synuclein in vitro. *Neuroreport 10*, 717-721.

Hashimoto, M., Rockenstein, E., Mante, M., Crews, L., Bar-On, P., Gage, F. H., Marr, R., and Masliah, E. (2004). An antiaggregation gene therapy strategy for Lewy body disease utilizing beta-synuclein lentivirus in a transgenic model. *Gene Ther. 11*, 1713-1723.

Hesse, L., Beher, D., Masters, C. L., and Multhaup, G. (1994). The beta A4 amyloid precursor protein binding to copper. *FEBS Lett. 349*, 109-116.

Hornshaw, M. P., McDermott, J. R., Candy, J. M., and Lakey, J. H. (1995). Copper binding to the N-terminal tandem repeat region of mammalian and avian prion protein: structural studies using synthetic peptides. *Biochem. Biophys. Res. Commun. 214*, 993-999.

Hoyer, W., Cherny, D., Subramaniam, V., and Jovin, T. M. (2004). Impact of the Acidic C-Terminal Region Comprising Amino Acids 109-140 on alpha-Synuclein Aggregation in Vitro. *Biochemistry 43*, 16233-16242.

Hoyer, W., Antony, T., Cherny, D., Heim, G., Jovin, T. M., and Subramaniam, V. (2002). Dependence of alpha-synuclein aggregate morphology on solution conditions. *J. Mol. Biol. 322*, 383-393.

Huang, X., Cuajungco, M. P., Atwood, C. S., Hartshorn, M. A., Tyndall, J. D., Hanson, G. R., Stokes, K. C., Leopold, M., Multhaup, G., Goldstein, L. E., *et al.* (1999). Cu(II) potentiation of alzheimer abeta neurotoxicity. Correlation with cell-free hydrogen peroxide production and metal reduction. *J. Biol. Chem. 274*, 37111-37116.

Ikura, M., Kay, L. E., and Bax, A. (1990). A Novel-Approach For Sequential Assignment Of H-1, C-13, And N-15 Spectra Of Larger Proteins - Heteronuclear Triple-Resonance 3-Dimensional Nmr-Spectroscopy - Application To Calmodulin. *Biochemistry 29*, 4659-4667.

Jahn, T. R., and Radford, S. E. (2005). The Yin and Yang of protein folding. *FEBS J. 272*, 5962-5970.

Jahn, T. R., Parker, M. J., Homans, S. W., and Radford, S. E. (2006). Amyloid formation under physiological conditions proceeds via a native-like folding intermediate. *Nat. Struct. Mol. Biol. 13*, 195-201.

Jenner, P., and Olanow, C. W. (1998). Understanding cell death in Parkinson's disease. *Ann. Neurol. 44*, S72-84.

Jensen, P. H., Nielsen, M. S., Jakes, R., Dotti, C. G., and Goedert, M. (1998). Binding of alpha-synuclein to brain vesicles is abolished by familial Parkinson's disease mutation. *J. Biol. Chem. 273*, 26292-26294.

Jha, A. K., Colubri, A., Freed, K. F., and Sosnick, T. R. (2005a). Statistical coil model of the unfolded state: resolving the reconciliation problem. *Proc. Natl. Acad. Sci. U. S. A. 102*, 13099-13104.

Jha, A. K., Colubri, A., Zaman, M. H., Koide, S., Sosnick, T. R., and Freed, K. F. (2005b). Helix, sheet, and polyproline II frequencies and strong nearest neighbor effects in a restricted coil library. *Biochemistry 44*, 9691-9702.

Jin, T., Gu, Y., Zanusso, G., Sy, M., Kumar, A., Cohen, M., Gambetti, P., and Singh, N. (2000). The chaperone protein BiP binds to a mutant prion protein and mediates its degradation by the proteasome. *J. Biol. Chem. 275*, 38699-38704.

Jo, E., McLaurin, J., Yip, C. M., St George-Hyslop, P., and Fraser, P. E. (2000). alpha-Synuclein membrane interactions and lipid specificity. *J. Biol. Chem. 275*, 34328-34334.

Johnson, B. A., and Blevins, R. A. (1994). NMRVIEW: a computer program for the visualization and analysis of NMR data. *J. Biomol. NMR. 4*, 603-614.

Johnston, J. A., Ward, C. L., and Kopito, R. R. (1998). Aggresomes: a cellular response to misfolded proteins. *J. Cell. Biol. 143*, 1883-1898.

Jones, C. E., Abdelraheim, S. R., Brown, D. R., and Viles, J. H. (2004). Preferential Cu2+ coordination by His96 and His111 induces beta-sheet formation in the unstructured amyloidogenic region of the prion protein. *J. Biol. Chem. 279*, 32018-32027.

Jones, J. A., Wilkins, D. K., Smith, L. J., and Dobson, C. M. (1997). Characterisation of protein unfolding by NMR diffusion measurements. *J. Biomol. NMR 10*, 199-203.

Karr, J. W., Kaupp, L. J., and Szalai, V. A. (2004). Amyloid-beta binds Cu2+ in a mononuclear metal ion binding site. *J. Am. Chem. Soc. 126*, 13534-13538.

Kayed, R., Head, E., Thompson, J. L., McIntire, T. M., Milton, S. C., Cotman, C. W., and Glabe, C. G. (2003). Common structure of soluble amyloid oligomers implies common mechanism of pathogenesis. *Science 300*, 486-489.

Keck, S., Nitsch, R., Grune, T., and Ullrich, O. (2003). Proteasome inhibition by paired helical filament-tau in brains of patients with Alzheimer's disease. *J. Neurochem. 85*, 115-122.

Kerner, M. J., Naylor, D. J., Ishihama, Y., Maier, T., Chang, H. C., Stines, A. P., Georgopoulos, C., Frishman, D., Hayer-Hartl, M., Mann, M., and Hartl, F. U. (2005). Proteome-wide analysis of chaperonin-dependent protein folding in Escherichia coli. *Cell 122*, 209-220.

Kiefhaber, T., Rudolph, R., Kohler, H. H., and Buchner, J. (1991). Protein aggregation in vitro and in vivo: a quantitative model of the kinetic competition between folding and aggregation. *Biotechnology (N.Y.) 9*, 825-829.

Kim, T. D., Paik, S. R., and Yang, C. H. (2002). Structural and functional implications of C-terminal regions of alpha-synuclein. *Biochemistry 41*, 13782-13790.

Kim, T. D., Paik, S. R., Yang, C. H., and Kim, J. (2000). Structural changes in alpha-synuclein affect its chaperone-like activity in vitro. *Protein Sci. 9*, 2489-2496.

Kitada, T., Asakawa, S., Hattori, N., Matsumine, H., Yamamura, Y., Minoshima, S., Yokochi, M., Mizuno, Y., and Shimizu, N. (1998). Mutations in the parkin gene cause autosomal recessive juvenile parkinsonism. *Nature 392*, 605-608.

Klein-Seetharaman, J., Oikawa, M., Grimshaw, S. B., Wirmer, J., Duchardt, E., Ueda, T., Imoto, T., Smith, L. J., Dobson, C. M., and Schwalbe, H. (2002). Long-Range Interactions Within a Nonnative Protein. *Science 295*, 1719-1722.

Koo, E. H., Lansbury, P. T., Jr., and Kelly, J. W. (1999). Amyloid diseases: abnormal protein aggregation in neurodegeneration. *Proc. Natl. Acad. Sci. U. S. A. 96*, 9989-9990.

Koradi, R., Billeter, M., and Wuthrich, K. (1996). MOLMOL: A program for display and analysis of macromolecular structures. *J. Mol. Graphics 14*, 51-55.

Korzhnev, D. M., Salvatella, X., Vendruscolo, M., Di Nardo, A. A., Davidson, A. R., Dobson, C. M., and Kay, L. E. (2004). Low-populated folding intermediates of Fyn SH3 characterized by relaxation dispersion NMR. *Nature 430*, 586-590.

Kowalik-Jankowska, T., Rajewska, A., Wisniewska, K., Grzonka, Z., and Jezierska, J. (2005). Coordination abilities of N-terminal fragments of alpha-synuclein towards copper(II) ions: a combined potentiometric and spectroscopic study. *J. Inorg. Biochem. 99*, 2282-2291.

Krishnan, S., Chi, E. Y., Wood, S. J., Kendrick, B. S., Li, C., Garzon-Rodriguez, W., Wypych, J., Randolph, T. W., Narhi, L. O., Biere, A. L., *et al.* (2003). Oxidative dimer formation is the critical rate-limiting step for Parkinson's disease alpha-synuclein fibrillogenesis. *Biochemistry 42*, 829-837.

Kruger, R., Kuhn, W., Muller, T., Woitalla, D., Graeber, M., Kosel, S., Przuntek, H., Epplen, J. T., Schols, L., and Riess, O. (1998). Ala30Pro mutation in the gene encoding alpha-synuclein in Parkinson's disease. *Nat. Genet. 18*, 106-108.

Kubelka, J., Hofrichter, J., and Eaton, W. A. (2004). The protein folding 'speed limit'. *Curr. Opin. Struc. Biol. 14*, 76-88.

Kuzmic, P. (1996). Program DYNAFIT for the analysis of enzyme kinetic data: Application to HIV proteinase. *Anal. Biochem. 237*, 260-273.

Lakomek, N. A., Carlomagno, T., Becker, S., Griesinger, C., and Meiler, J. (2006). A thorough dynamic interpretation of residual dipolar couplings in ubiquitin. *J. Biomol. NMR 34*, 101-115.

Lambert, M. P., Viola, K. L., Chromy, B. A., Chang, L., Morgan, T. E., Yu, J., Venton, D. L., Krafft, G. A., Finch, C. E., and Klein, W. L. (2001). Vaccination with soluble Abeta oligomers generates toxicity-neutralizing antibodies. *J. Neurochem. 79*, 595-605.

Lansbury, P. T., Jr. (1999). Evolution of amyloid: what normal protein folding may tell us about fibrillogenesis and disease. *Proc. Natl. Acad. Sci. U. S. A. 96*, 3342-3344.

Lashuel, H. A., Hartley, D., Petre, B. M., Walz, T., and Lansbury, P. T., Jr. (2002a). Neurodegenerative disease: Amyloid pores from pathogenic mutations. *Nature 418*, 291.

Lashuel, H. A., Petre, B. M., Wall, J., Simon, M., Nowak, R. J., Walz, T., and Lansbury, P. T., Jr. (2002b). Alpha-synuclein, especially the Parkinson's disease-associated mutants, forms pore-like annular and tubular protofibrils. *J. Mol. Biol. 322*, 1089-1102.

Lee, E. N., Lee, S. Y., Lee, D., Kim, J., and Paik, S. R. (2003). Lipid interaction of alpha-synuclein during the metal-catalyzed oxidation in the presence of Cu2+ and H2O2. *J. Neurochem. 84*, 1128-1142.

Lee, J. C., Langen, R., Hummel, P. A., Gray, H. B., and Winkler, J. R. (2004). alpha-synuclein structures from fluorescence energy-transfer kinetics: Implications for the role of the protein in Parkinson's disease. *Proc. Natl. Acad. Sci. U.S.A. 101*, 16466-16471.

Leroy, E., Boyer, R., Auburger, G., Leube, B., Ulm, G., Mezey, E., Harta, G., Brownstein, M. J., Jonnalagada, S., Chernova, T.*, et al.* (1998). The ubiquitin pathway in Parkinson's disease. *Nature 395*, 451-452.

Li, W., West, N., Colla, E., Pletnikova, O., Troncoso, J. C., Marsh, L., Dawson, T. M., Jakala, P., Hartmann, T., Price, D. L., and Lee, M. K. (2005). Aggregation promoting C-terminal truncation of alpha-synuclein is a normal cellular process and is enhanced by the familial Parkinson's disease-linked mutations. *Proc. Natl. Acad. Sci. U. S. A. 102*, 2162-2167.

Lietzow, M. A., Jamin, M., Jane Dyson, H., and Wright, P. E. (2002). Mapping Long-range Contacts in a Highly Unfolded Protein. *J. Mol. Biol. 322*, 655-662.

Lindahl, E., Hess, B., and van der Spoel, D. (2001). GROMACS 3.0: a package for molecular simulation and trajectory analysis. *J. Mol. Model. 7*, 306-317.

Lindorff-Larsen, K., Kristjansdottir, S., Teilum, K., Fieber, W., Dobson, C. M., Poulsen, F. M., and Vendruscolo, M. (2004). Determination of an ensemble of structures representing the denatured state of the bovine acyl-coenzyme a binding protein. *J. Am. Chem. Soc. 126*, 3291-3299.

Liu, C. W., Corboy, M. J., DeMartino, G. N., and Thomas, P. J. (2003). Endoproteolytic activity of the proteasome. *Science 299*, 408-411.

Lotharius, J., and Brundin, P. (2002). Pathogenesis of Parkinson's disease: dopamine, vesicles and alpha-synuclein. *Nat. Rev. Neurosci. 3*, 932-942.

Louhivuori, M., Fredriksson, K., Paakkonen, K., Permi, P., and Annila, A. (2004). Alignment of chain-like molecules. *J. Biomol. NMR 29*, 517-524.

Louhivuori, M., Pääkkönen, K., Fredriksson, K., Permi, P., Lounila, J., and Annila, A. (2003). On the Origin of Residual Dipolar Couplings from Denatured Proteins. *J. Am. Chem. Soc. 125*, 15647-15650.

Lovell, M. A., Robertson, J. D., Teesdale, W. J., Campbell, J. L., and Markesbery, W. R. (1998). Copper, iron and zinc in Alzheimer's disease senile plaques. *J. Neurol. Sci. 158*, 47-52.

Maier, T., Ferbitz, L., Deuerling, E., and Ban, N. (2005). A cradle for new proteins: trigger factor at the ribosome. *Curr. Opin. Struct. Biol. 15*, 204-212.

Makin, O. S., and Serpell, L. C. (2005). Structures for amyloid fibrils. *FEBS J. 272*, 5950-5961.

Mandal, P. K., and Majumdar, A. (2004). A comprehensive discussion of HSQC and HMQC pulse sequences. *Conc. Mag. Res. A 20A*, 1-23.

Manning-Bog, A. B., McCormack, A. L., Li, J., Uversky, V. N., Fink, A. L., and Di Monte, D. A. (2002). The herbicide Paraquat causes up-regulation and aggregation of alpha-synuclein in mice: Paraquat and alpha-synuclein. *J. Biol. Chem. 277*, 1641-1644.

Margerum, D. W., and Banks, C. V. (1954). Spectrophotometric Determination of Iron in Vanadium, Chromium, Manganese, Nickel, and Zinc - 1,10-Phenanthroline Rate Phenomena. *Anal. Chem. 26*, 200-202.

Mayer, T. U., Braun, T., and Jentsch, S. (1998). Role of the proteasome in membrane extraction of a short-lived ER-transmembrane protein. *EMBO J. 17*, 3251-3257.

Mayor, U., Guydosh, N. R., Johnson, C. M., Grossmann, J. G., Sato, S., Jas, G. S., Freund, S. M., Alonso, D. O., Daggett, V., and Fersht, A. R. (2003). The complete folding pathway of a protein from nanoseconds to microseconds. *Nature 421*, 863-867.

McCall, K. A., and Fierke, C. A. (2000). Colorimetric and fluorimetric assays to quantitate micromolar concentrations of transition metals. *Anal. Biochem. 284*, 307-315.

McCarney, E. R., Kohn, J. E., and Plaxco, K. W. (2005). Is there or isn't there? The case for (and against) residual structure in chemically denatured proteins. *Crit. Rev. Biochem. Mol. Biol. 40*, 181-189.

McNaught, K. S., and Jenner, P. (2001). Proteasomal function is impaired in substantia nigra in Parkinson's disease. *Neurosci. Lett. 297*, 191-194.

McNaught, K. S., Shashidharan, P., Perl, D. P., Jenner, P., and Olanow, C. W. (2002). Aggresome-related biogenesis of Lewy bodies. *Eur. J. Neurosci. 16*, 2136-2148.

McNaught, K. S. P., Olanow, C. W., Halliwell, B., Isacson, O., and Jenner, P. (2001). Failure of the Ubiquitin-Proteasome System in Parkinson's disease. *Nat. Rev. Neurosci. 2*, 589.

McNulty, B. C., Young, G. B., and Pielak, G. J. (2006a). Macromolecular crowding in the Escherichia coli periplasm maintains alpha-synuclein disorder. *J. Mol. Biol. 355*, 893-897.

McNulty, B. C., Tripathy, A., Young, G. B., Charlton, L. M., Orans, J., and Pielak, G. J. (2006b). Temperature-induced reversible conformational change in the first 100 residues of alpha-synuclein. *Protein Sci. 15*, 602-608.

Mishizen-Eberz, A. J., Guttmann, R. P., Giasson, B. I., Day, G. A., 3rd, Hodara, R., Ischiropoulos, H., Lee, V. M., Trojanowski, J. Q., and Lynch, D. R. (2003). Distinct cleavage patterns of normal and pathologic forms of alpha-synuclein by calpain I in vitro. *J. Neurochem. 86*, 836-847.

Mittermaier, A., and Kay, L. E. (2006). New tools provide new insights in NMR studies of protein dynamics. *Science 312*, 224-228.

Mohana-Borges, R., Goto, N. K., Kroon, G. J. A., Dyson, H. J., and Wright, P. E. (2004). Structural characterization of unfolded states of apomyoglobin using residual dipolar couplings. *J. Mol. Biol. 340*, 1131-1142.

Morar, A. S., Olteanu, A., Young, G. B., and Pielak, G. J. (2001). Solvent-induced collapse of alpha-synuclein and acid-denatured cytochrome c. *Protein Sci. 10*, 2195-2199.

Morrison, L. D., and Kish, S. J. (1995). Brain polyamine levels are altered in Alzheimer's disease. *Neurosci. Lett. 197*, 5-8.

Mouradian, M. M. (2002). Recent advances in the genetics and pathogenesis of Parkinson disease. *Neurology 58*, 179-185.

Murray, I. V., Giasson, B. I., Quinn, S. M., Koppaka, V., Axelsen, P. H., Ischiropoulos, H., Trojanowski, J. Q., and Lee, V. M. (2003). Role of alpha-synuclein carboxy-terminus on fibril formation in vitro. *Biochemistry 42*, 8530-8540.

Nakagawa, T., Zhu, H., Morishima, N., Li, E., Xu, J., Yankner, B. A., and Yuan, J. (2000). Caspase-12 mediates endoplasmic-reticulum-specific apoptosis and cytotoxicity by amyloid-beta. *Nature 403*, 98-103.

Narayanan, V., and Scarlata, S. (2001). Membrane binding and self-association of alpha-synucleins. *Biochemistry 40*, 9927-9934.

Nichols, M. R., Moss, M. A., Reed, D. K., Lin, W. L., Mukhopadhyay, R., Hoh, J. H., and Rosenberry, T. L. (2002). Growth of beta-amyloid(1-40) protofibrils by monomer elongation and lateral association. Characterization of distinct products by light scattering and atomic force microscopy. *Biochemistry 41*, 6115-6127.

Norris, E. H., Giasson, B. I., Ischiropoulos, H., and Lee, V. M. Y. (2003). Effects of oxidative and nitrative challenges on alpha-synuclein fibrillogenesis involve distinct mechanisms of protein modifications. *J. Biol. Chem. 278*, 27230-27240.

Ohnishi, S., Lee, A. L., Edgell, M. H., and Shortle, D. (2004). Direct demonstration of structural similarity between native and denatured eglin C. *Biochemistry 43*, 4064-4070.

Ottiger, M., Delaglio, F., and Bax, A. (1998). Measurement of J and Dipolar Couplings from Simplified Two-Dimensional NMR Spectra. *J. Magn. Res. 131*, 373-378.

Paik, S. R., Shin, H. J., and Lee, J. H. (2000). Metal-catalyzed oxidation of alpha-synuclein in the presence of Copper(II) and hydrogen peroxide. *Arch. Biochem. Biophys. 378*, 269-277.

Paik, S. R., Shin, H. J., Lee, J. H., Chang, C. S., and Kim, J. (1999). Copper(II)-induced self-oligomerization of alpha-synuclein. *Biochem. J. 340*, 821-828.

Pall, H. S., Blake, D. R., Gutteridge, J. M., Williams, A. C., Lunec, J., Hall, M., and Taylor, A. (1987). Raised Cerebrospinal-Fluid Copper Concentration in Parkinsons-Disease. *Lancet 330*, 238-241.

Palmer, A. G., Kroenke, C. D., and Loria, J. P. (2001). Nuclear magnetic resonance methods for quantifying microsecond-to-millisecond motions in biological macromolecules. *Methods Enzymol. 339*, 204-238.

Palmer, A. G., Cavanagh, J., Wright, P. E., and Rance, M. (1991). Sensitivity Improvement In Proton-Detected 2-Dimensional Heteronuclear Correlation Nmr-Spectroscopy. *J. Mag. Res. 93*, 151-170.

Panchal, S. C., Bhavesh, N. S., and Hosur, R. V. (2001). Improved 3D triple resonance experiments, HNN and HN(C)N, for HN and 15N sequential correlations in (13C, 15N) labeled proteins: application to unfolded proteins. *J. Biomol. NMR 20*, 135-147.

Pappu, R. V., Srinivasan, R., and Rose, G. D. (2000). The Flory isolated-pair hypothesis is not valid for polypeptide chains: Implications for protein folding. *Proc. Nat. Acad. Sci. U. S. A. 97*, 12565-12570.

Park, J. Y., and Lansbury, P. T., Jr. (2003). Beta-synuclein inhibits formation of alpha-synuclein protofibrils: a possible therapeutic strategy against Parkinson's disease. *Biochemistry 42*, 3696-3700.

Park, S. M., Jung, H. Y., Kim, T. D., Park, J. H., Yang, C. H., and Kim, J. (2002a). Distinct roles of the N-terminal-binding domain and the C-terminal-solubilizing domain of alpha-synuclein, a molecular chaperone. *J. Biol. Chem. 277*, 28512-28520.

Park, S. M., Jung, H. Y., Chung, K. C., Rhim, H., Park, J. H., and Kim, J. (2002b). Stress-induced aggregation profiles of GST-alpha-synuclein fusion proteins: role of the C-terminal acidic tail of alpha-synuclein in protein thermosolubility and stability. *Biochemistry 41*, 4137-4146.

Peisach, J., and Blumberg, W. E. (1974). Structural implications derived from the analysis of electron paramagnetic resonance spectra of natural and artificial copper proteins. *Arch. Biochem. Biophys. 165*, 691-708.

Perrin, R. J., Woods, W. S., Clayton, D. F., and George, J. M. (2000). Interaction of human alpha-Synuclein and Parkinson's disease variants with phospholipids. Structural analysis using site-directed mutagenesis. *J. Biol. Chem. 275*, 34393-34398.

Perrin, R. J., Woods, W. S., Clayton, D. F., and George, J. M. (2001). Exposure to long chain polyunsaturated fatty acids triggers rapid multimerization of synucleins. *J. Biol. Chem. 276*, 41958-41962.

Peti, W., Smith, L. J., Redfield, C., and Schwalbe, H. (2001). Chemical shifts in denatured proteins: resonance assignments for denatured ubiquitin and comparisons with other denatured proteins. *J. Biomol. NMR. 19*, 153-165.

Plakoutsi, G., Bemporad, F., Calamai, M., Taddei, N., Dobson, C. M., and Chiti, F. (2005). Evidence for a mechanism of amyloid formation involving molecular reorganisation within native-like precursor aggregates. *J. Mol. Biol. 351*, 910-922.

Plaxco, K. W., Simons, K. T., and Baker, D. (1998). Contact order, transition state placement and the refolding rates of single domain proteins. *J. Mol. Biol. 277*, 985-994.

Poirier, M. A., Li, H., Macosko, J., Cai, S., Amzel, M., and Ross, C. A. (2002). Huntingtin spheroids and protofibrils as precursors in polyglutamine fibrilization. *J. Biol. Chem. 277*, 41032-41037.

Polymeropoulos, M. H., Lavedan, C., Leroy, E., Ide, S. E., Dehejia, A., Dutra, A., Pike, B., Root, H., Rubenstein, J., Boyer, R*., et al.* (1997). Mutation in the alpha-synuclein gene identified in families with Parkinson's disease. *Science 276*, 2045-2047.

Prestegard, J. H., Bougault, C. M., and Kishore, A. I. (2004). Residual dipolar couplings in structure determination of biomolecules. *Chem. Rev. 104*, 3519-3540.

Pujato, M., Bracken, C., Mancusso, R., Cataldi, M., and Tasayco, M. L. (2005). pH dependence of amide chemical shifts in natively disordered polypeptides detects medium-range interactions with ionizable residues. *Biophys. J. 89*, 3293-3302.

Ramachandran, G. N., Ramakrishnan, C., and Sasisekharan, V. (1963). Stereochemistry of polypeptide chain configurations. *J. Mol. Biol. 7*, 95-99.

Requena, J. R., Groth, D., Legname, G., Stadtman, E. R., Prusiner, S. B., and Levine, R. L. (2001). Copper-catalyzed oxidation of the recombinant SHa(29-231) prion protein. *Proc. Natl. Acad. Sci. U.S.A. 98*, 7170-7175.

Rochet, J. C., Conway, K. A., and Lansbury, P. T., Jr. (2000). Inhibition of fibrillization and accumulation of prefibrillar oligomers in mixtures of human and mouse alpha-synuclein. *Biochemistry 39*, 10619-10626.

Rockenstein, E., Hansen, L. A., Mallory, M., Trojanowski, J. Q., Galasko, D., and Masliah, E. (2001). Altered expression of the synuclein family mRNA in Lewy body and Alzheimer's disease. *Brain Res. 914*, 48-56.

Rückert, M., and Otting, G. (2000). Alignment of Biological Macromolecules in Novel Nonionic Liquid Crystalline Media for NMR Experiments. *J. Am. Chem. Soc. 122*, 7793-7797.

Sakaguchi, U., and Addison, A. W. (1979). Spectroscopic and redox studies of some copper (II) complexes with biomimetic donor atoms - implications forprotein copper centers. *J. Chem. Soc. Dalton Trans.*, 600-608.

Sayre, L. M., Perry, G., and Smith, M. A. (1999). Redox metals and neurodegenerative disease. *Curr. Opin. Chem. Biol. 3*, 220-225.

Schapira, A. H., Gu, M., Taanman, J. W., Tabrizi, S. J., Seaton, T., Cleeter, M., and Cooper, J. M. (1998). Mitochondrial dysfunction in neurodegenerative disorders. *Ann. Neurol. 44*, S89-98.

Schmid, D., Baici, A., Gehring, H., and Christen, P. (1994). Kinetics of molecular chaperone action. *Science 263*, 971-973.

Schroder, M., and Kaufman, R. J. (2005). The mammalian unfolded protein response. *Annu. Rev. Biochem. 74*, 739-789.

Schubert, U., Anton, L. C., Gibbs, J., Norbury, C. C., Yewdell, J. W., and Bennink, J. R. (2000). Rapid degradation of a large fraction of newly synthesized proteins by proteasomes. *Nature 404*, 770-774.

Schulman, B. A., Kim, P. S., Dobson, C. M., and Redfield, C. (1997). A residue-specific NMR view of the non-cooperative unfolding of a molten globule. *Nat. Struct. Biol. 4*, 630-634.

Schwieters, C. D., and Clore, G. M. (2002). Reweighted atomic densities to represent ensembles of NMR structures. *J. Biomol. NMR 23*, 221-225.

Schwieters, C. D., Kuszewski, J. J., Tjandra, N., and Clore, G. M. (2003). The Xplor-NIH NMR molecular structure determination package. *J. Magn. Reson. 160*, 65-73.

Segalas, I., Thai, R., Menez, R., and Vita, C. (1995). A particularly labile Asp-Pro bond in the green mamba muscarinic toxin MTX2. Effect of protein conformation on the rate of cleavage. *FEBS Lett. 371*, 171-175.

Serpell, L. C. (2000). Alzheimer's amyloid fibrils: structure and assembly. *Biochim. Biophys. Acta 1502*, 16-30.

Serpell, L. C., Berriman, J., Jakes, R., Goedert, M., and Crowther, R. A. (2000). Fiber diffraction of synthetic alpha-synuclein filaments shows amyloid-like cross-beta conformation. *Proc. Natl. Acad. Sci. U. S. A. 97*, 4897-4902.

Serrano, L. (1995). Comparison between the phi distribution of the amino acids in the protein database and NMR data indicates that amino acids have various phi propensities in the random coil conformation. *J. Mol. Biol. 254*, 322-333.

Sherer, T. B., Kim, J. H., Betarbet, R., and Greenamyre, J. T. (2003). Subcutaneous rotenone exposure causes highly selective dopaminergic degeneration and alpha-synuclein aggregation. *Exp. Neurol. 179*, 9-16.

Sherer, T. B., Betarbet, R., Stout, A. K., Lund, S., Baptista, M., Panov, A. V., Cookson, M. R., and Greenamyre, J. T. (2002). An in vitro model of Parkinson's disease: linking mitochondrial impairment to altered alpha-synuclein metabolism and oxidative damage. *J. Neurosci. 22*, 7006-7015.

Shojania, S., and O'Neil, J. D. (2006a). HIV-1 Tat is a natively unfolded protein: the solution conformation and dynamics of reduced HIV-1 Tat-(1-72) by NMR spectroscopy. *J. Biol. Chem. 281*, 8347-8356.

Shojania, S., and O'Neil, J. D. (2006b). HIV-1 Tat is a natively unfolded protein: the solution conformation and dynamics of reduced HIV-1 Tat-(1-72) by NMR spectroscopy. *J Biol Chem 281*, 8347-8356.

Shortle, D. (1996). The denatured state (the other half of the folding equation) and its role in protein stability. *FASEB J. 10*, 27-34.

Shortle, D., and Ackerman, M. S. (2001). Persistence of Native-Like Topology in a Denatured Protein in 8 M Urea. *Science 293*, 487-489.

Shults, C. W. (2006). Lewy bodies. *Proc. Natl. Acad. Sci. U. S. A. 103*, 1661-1668.

Simons, K. T., Kooperberg, C., Huang, E., and Baker, D. (1997). Assembly of protein tertiary structures from fragments with similar local sequences using simulated annealing and bayesian scoring functions. *J. Mol. Biol. 268*, 209-225.

Singleton, A. B., Farrer, M., Johnson, J., Singleton, A., Hague, S., Kachergus, J., Hulihan, M., Peuralinna, T., Dutra, A., Nussbaum, R.*, et al.* (2003). Alpha-synuclein locus triplication causes Parkinson's disease. *Science 302*, 841.

Smith, L. J., Fiebig, K. M., Schwalbe, H., and Dobson, C. M. (1996). The concept of a random coil. Residual structure in peptides and denatured proteins. *Fold. Des. 1*, R95-106.

Soulet, D., and Rivest, S. (2003). Polyamines play a critical role in the control of the innate immune response in the mouse central nervous system. *J. Cell. Biol. 162*, 257-268.

Souza, J. M., Giasson, B. I., Lee, V. M., and Ischiropoulos, H. (2000). Chaperone-like activity of synucleins. *FEBS Lett. 474*, 116-119.

Spillantini, M. G., Schmidt, M. L., Lee, V. M., Trojanowski, J. Q., Jakes, R., and Goedert, M. (1997). Alpha-synuclein in Lewy bodies. *Nature 388*, 839-840.

Stadtman, E. R., and Oliver, C. N. (1991). Metal-Catalyzed Oxidation of Proteins - Physiological Consequences. *J. Biol. Chem. 266*, 2005-2008.

Stefanis, L., Larsen, K. E., Rideout, H. J., Sulzer, D., and Greene, L. A. (2001). Expression of A53T mutant but not wild-type alpha-synuclein in PC12 cells induces alterations of the ubiquitin-dependent degradation system, loss of dopamine release, and autophagic cell death. *J. Neurosci. 21*, 9549-9560.

Stejskal, E. O., and Tanner, J. E. (1965). Spin Diffusion Measurements - Spin Echoes In Presence Of A Time-Dependent Field Gradient. *J. Chem. Phys. 42*, 288-&.

Sung, Y. H., Rospigliosi, C., and Eliezer, D. (2006). NMR mapping of copper binding sites in alpha-synuclein. *Biochim. Biophys. Acta 1764*, 5-12.

Swindells, M. B., MacArthur, M. W., and Thornton, J. M. (1995). Intrinsic phi, psi propensities of amino acids, derived from the coil regions of known structures. *Nat. Struct. Biol. 2*, 596-603.

Syme, C. D., Nadal, R. C., Rigby, S. E., and Viles, J. H. (2004). Copper binding to the amyloid-beta (Abeta) peptide associated with Alzheimer's disease: folding, coordination geometry, pH dependence, stoichiometry, and affinity of Abeta-(1-28): insights from a range of complementary spectroscopic techniques. *J. Biol. Chem. 279*, 18169-18177.

Tabor, S. (1990). Expression using the T7 RNA polymerase/promoter system (New York: Wiley-Interscience).

Tanaka, Y., Engelender, S., Igarashi, S., Rao, R. K., Wanner, T., Tanzi, R. E., Sawa, A., Dawson, V. L., Dawson, T. M., and Ross, C. A. (2001). Inducible expression of mutant alpha-synuclein decreases proteasome activity and increases sensitivity to mitochondria-dependent apoptosis. *Hum. Mol. Genet. 10*, 919-926.

Tanford, C. (1968). Protein denaturation. *Adv. Protein. Chem. 23*, 121-282.

Teilum, K., Kragelund, B. B., and Poulsen, F. M. (2002). Transient Structure Formation in Unfolded Acyl-coenzyme A-binding Protein Observed by Site-directed Spin Labelling. *J. Mol. Biol. 324*, 349-357.

Teter, S. A., Houry, W. A., Ang, D., Tradler, T., Rockabrand, D., Fischer, G., Blum, P., Georgopoulos, C., and Hartl, F. U. (1999). Polypeptide flux through bacterial Hsp70: DnaK cooperates with trigger factor in chaperoning nascent chains. *Cell 97*, 755-765.

Thapar, R., Mueller, G. A., and Marzluff, W. F. (2004). The N-terminal domain of the Drosophila histone mRNA binding protein, SLBP, is intrinsically disordered with nascent helical structure. *Biochemistry 43*, 9390-9400.

Thiruchelvam, M., Richfield, E. K., Baggs, R. B., Tank, A. W., and Cory-Slechta, D. A. (2000). The nigrostriatal dopaminergic system as a preferential target of repeated exposures to combined Paraquat and Maneb: implications for Parkinson's disease. *J. Neurosci. 20*, 9207-9214.

Tjandra, N., and Bax, A. (1997). Direct Measurement of Distances and Angles in Biomolecules by NMR in a Dilute Liquid Crystalline Medium. *Science 278*, 1111-1114.

Ulmer, T. S., and Bax, A. (2005). Comparison of structure and dynamics of micelle-bound human alpha-synuclein and Parkinson disease variants. *J. Biol. Chem. 280*, 43179-43187.

Ulmer, T. S., Bax, A., Cole, N. B., and Nussbaum, R. L. (2005). Structure and dynamics of micelle-bound human alpha-synuclein. *J. Biol. Chem. 280*, 9595-9603.

Uversky, V. N. (2002). Natively unfolded proteins: a point where biology waits for physics. *Protein Sci 11*, 739-756.

Uversky, V. N. (2003). A Protein-Chameleon: Conformational Plasticity of alpha-Synuclein, a Disordered Protein Involved in Neurodegenerative Disorders. *J. Biomol. Struct. Dyn. 21*, 211-234.

Uversky, V. N., and Fink, A. L. (2004). Conformational constraints for amyloid fibrillation: the importance of being unfolded. *Biochim. Biophys. Acta 1698*, 131-153.

Uversky, V. N., Gillespie, J. R., and Fink, A. L. (2000). Why are "natively unfolded" proteins unstructured under physiologic conditions? *Proteins 41*, 415-427.

Uversky, V. N., Li, J., and Fink, A. L. (2001a). Pesticides directly accelerate the rate of alpha-synuclein fibril formation: a possible factor in Parkinson's disease. *FEBS Lett. 500*, 105-108.

Uversky, V. N., Li, J., and Fink, A. L. (2001b). Evidence for a partially folded intermediate in alpha-synuclein fibril formation. *J. Biol. Chem. 276*, 10737-10744.

Uversky, V. N., Li, J., and Fink, A. L. (2001c). Metal-triggered structural transformations, aggregation, and fibrillation of human alpha-synuclein. A possible molecular link between Parkinson's disease and heavy metal exposure. *J. Biol. Chem. 276*, 44284-44296.

Uversky, V. N., Li, J., Souillac, P., Millett, I. S., Doniach, S., Jakes, R., Goedert, M., and Fink, A. L. (2002). Biophysical properties of the synucleins and their propensities to fibrillate: inhibition of alpha-synuclein assembly by beta- and gamma-synucleins. *J. Biol. Chem. 277*, 11970-11978.

Väängård, T. (1972). Copper Proteins, In Biological Applications of Electron Spin Resonance, H. M. Swartz, J. R. Bolton, and D. C. Borg, eds. (New York: Wiley-Interscience), pp. 411-447.

Valensin, D., Mancini, F. M., Luczkowski, M., Janicka, A., Wisniewska, K., Gaggelli, E., Valensin, G., Lankiewicz, L., and Kozlowski, H. (2004). Identification of a novel high affinity copper binding site in the APP(145-155) fragment of amyloid precursor protein. *J. Chem. Soc. Dalton Trans.*, 16-22.

Vendruscolo, M., Paci, E., Karplus, M., and Dobson, C. M. (2003). Structures and relative free energies of partially folded states of proteins. *Proc. Natl. Acad. Sci. U. S. A. 100*, 14817-14821.

Vila, M., and Przedborski, S. (2003). Targeting programmed cell death in neurodegenerative diseases. *Nat. Rev. Neurosci. 4*, 365-375.

Vila, M., Vukosavic, S., Jackson-Lewis, V., Neystat, M., Jakowec, M., and Przedborski, S. (2000). Alpha-synuclein up-regulation in substantia nigra dopaminergic neurons following administration of the parkinsonian toxin MPTP. *J. Neurochem. 74*, 721-729.

Viles, J. H., Cohen, F. E., Prusiner, S. B., Goodin, D. B., Wright, P. E., and Dyson, H. J. (1999). Copper binding to the prion protein: Structural implications of four identical cooperative binding sites. *Proc. Natl. Acad. Sci. U. S. A. 96*, 2042-2047.

Volles, M. J., and Lansbury, P. T., Jr. (2002). Vesicle permeabilization by protofibrillar alpha-synuclein is sensitive to Parkinson's disease-linked mutations and occurs by a pore-like mechanism. *Biochemistry 41*, 4595-4602.

Walsh, D. M., Lomakin, A., Benedek, G. B., Condron, M. M., and Teplow, D. B. (1997). Amyloid beta-protein fibrillogenesis. Detection of a protofibrillar intermediate. *J. Biol. Chem. 272*, 22364-22372.

Weinreb, P. H., Zhen, W., Poon, A. W., Conway, K. A., and Lansbury, P. T., Jr. (1996). NACP, a protein implicated in Alzheimer's disease and learning, is natively unfolded. *Biochemistry 35*, 13709-13715.

Wijesinha-Bettoni, R., Dobson, C. M., and Redfield, C. (2001). Comparison of the structural and dynamical properties of holo and apo bovine alpha-lactalbumin by NMR spectroscopy. *J. Mol. Biol. 307*, 885-898.

Wilkins, D. K., Grimshaw, S. B., Receveur, V., Dobson, C. M., Jones, J. A., and Smith, L. J. (1999). Hydrodynamic radii of native and denatured proteins measured by pulse field gradient NMR techniques. *Biochemistry 38*, 16424-16431.

Wishart, D. S., and Sykes, B. D. (1994). The C-13 Chemical-Shift Index - A Simple Method For The Identification Of Protein Secondary Structure Using C-13 Chemical-Shift Data. *J. Biom. NMR 4*, 171-180.

Wolynes, P. G., Onuchic, J. N., and Thirumalai, D. (1995). Navigating the folding routes. *Science 267*, 1619-1620.

Wood, S. J., Wypych, J., Steavenson, S., Louis, J. C., Citron, M., and Biere, A. L. (1999). Alpha-synuclein fibrillogenesis is nucleation-dependent. Implications for the pathogenesis of Parkinson's disease. *J. Biol. Chem. 274*, 19509-19512.

Yamin, G., Munishkina, L. A., Karymov, M. A., Lyubchenko, Y. L., Uversky, V. N., and Fink, A. L. (2005). Forcing nonamyloidogenic beta-synuclein to fibrillate. *Biochemistry 44*, 9096-9107.

Young, J. C., Agashe, V. R., Siegers, K., and Hartl, F. U. (2004). Pathways of chaperone-mediated protein folding in the cytosol. *Nat. Rev. Mol. Cell Biol. 5*, 781.

Zarranz, J. J., Alegre, J., Gomez-Esteban, J. C., Lezcano, E., Ros, R., Ampuero, I., Vidal, L., Hoenicka, J., Rodriguez, O., Atares, B*., et al.* (2004). The new mutation, E46K, of alpha-synuclein causes Parkinson and Lewy body dementia. *Ann. Neurol. 55*, 164-173.

Zhu, G., Kong, X. M., and Sze, K. H. (1998). Gradient- and sensitivity-enhanced heteronuclear multiple-quantum correlation spectroscopy. *J. Mag. Res. 135*, 232-235.

*Appendix*

## 11. Appendix

### 11.1 Fluorescence spectroscopy and microscopy to study α-synuclein fibrillation

Fluorescence spectroscopic methods offer a very suitable alternative for studying fast protein dynamics of both small and big size macromolecular complexes, many of which NMR fails to detect. Fluorescence methodologies are usually based on the alteration of the fluorescent properties of a fluorophore upon changes in the chemical constitution and/or physical properties of the solution. Thus phenomena such as fluorescence quenching, spectral shift, changes in lifetime or anisotropy are evidenced upon perturbation of the fluorophore, caused by changes in polarity of the solvent, presence of another fluorophore or increase in the molecular size of the complex. In addition, intramolecular distances can be efficiently studied by FRET, which exploits the distance dependence of near-field dipole-dipole interactions between a pair of chromophores (Lakowicz, 1999). Another method of choice is fluorescence correlation spectroscopy (FCS), which allows the determination of diffusion rates of single particles, providing insights into whether a protein is alone or part of a macromolecular complex.

Fluorescent methods with various degrees of sophistication have proven very useful in unraveling the structural characteristics of amyloid fibrils. The early use of fluorescent dyes may be tracked back to the establishment of ThioT or ANS as amyloid dyes (Nilsson, 2004). However these dyes are not specific, and provide a reduced amount of data, derivable solely from changes in fluorescence intensity, and which do not reveal what is occurring to the protein during the early stages of amyloid conversion. More information can be obtained by the use of intrinsic fluorescent probes, which report on local properties of the polypeptide chain and can be efficiently followed in time. Such fluorescent approaches are relatively easy to apply to proteins *in vitro*, by exploiting the fluorescent properties of Trp and Tyr amino acids, or by conjugating small fluorescent dyes specifically to engineered Cys residues.

Indeed, fluorescent-based methods have been employed to study protein folding and aggregation. Measurement of intramolecular distance between two fluorophores in solution by time-resolved FRET has provided data on the overall shape of the ensemble of structures populated from microseconds to milliseconds time-scale (Ratner et al., 2000). Steady-state fluorescent anisotropy methods have been of use in the case of the islet amyloid peptide (Padrick and Miranker, 2002; Koo and Miranker, 2005). More recently, residue-specific steady-state fluorescence intensity was used to characterize the amyloid core of a yeast prion

protein (Krishnan and Lindquist, 2005). However, time-resolved fluorescence methods, which have resulted very useful in providing global and residue-specific structural information in folding mechanisms (Sridevi et al., 2000; Lakshmikanth et al., 2001; Sridevi et al., 2004), have not been exploited in the study of protein aggregation. Few studies, notably one on the early oligomeric species formed by the Aβ peptide are found in the literature (Allsop et al., 2001), and the formation of amyloid protofibrils by the protein barstar has been recently studied by mapping residue-specific fluorescent dynamics (Mukhopadhyay et al., 2006).

The use of time resolved fluorescent measurements has many comparative benefits compared with steady state measurements, since much of the molecular information available from fluorescence is lost during the time average. The lifetime of the dye is modulated by the presence of different conformational states that influence the rate of decay of its fluorescent intensity. Also, the precise shape of the anisotropy decay contains information about the shape of the macromolecule, its apparent size and its flexibility. In addition, FRET can be efficiently followed by changes in the lifetime of the donor dye. Thus, in fluorescence, a great extent of the molecular information content is only available from time resolved measurements (Lakowicz, 1999).

We applied time resolved fluorescent methods to study the early structural transitions conductive to αS oligomerization, as well as the build up of such oligomeric species during protein aggregation. Placing fluorescent tags with different properties in several locations of the polypeptide chain provide probes for studying protein self-association at quasi residue-specific level. As a first approach we labeled three Cys-containing variants of αS and two of βS with commercial maleimide derivatives of the fluorescent dyes Alexa488 (Amersham) and Cy3b (Molecular Probes) (Appendix figure 1). These ten fluorescent derivatives were characterized at the soluble native monomer level by measuring of time-resolved fluorescence according to the time domain (Time-Correlated-Single-Photon-Counting, TCSPC) method. The following results and interpretations are preliminary inasmuch as time did not suffice for a complete analysis.

In time domain measurements, the sample is exited with a pulse of light of short duration, and then the time-dependent intensity is measured following the excitation pulse. Multiple (if they exist) decay times τ (tau) are derived by fitting multiple exponential functions to the decay trace. We employed for such measurements an IBH fluorimeter

equipped with Nano-LED pulse laser diode and a TCSPC device, located in the Department of Organic Chemistry, University of Buenos Aires, Argentina.
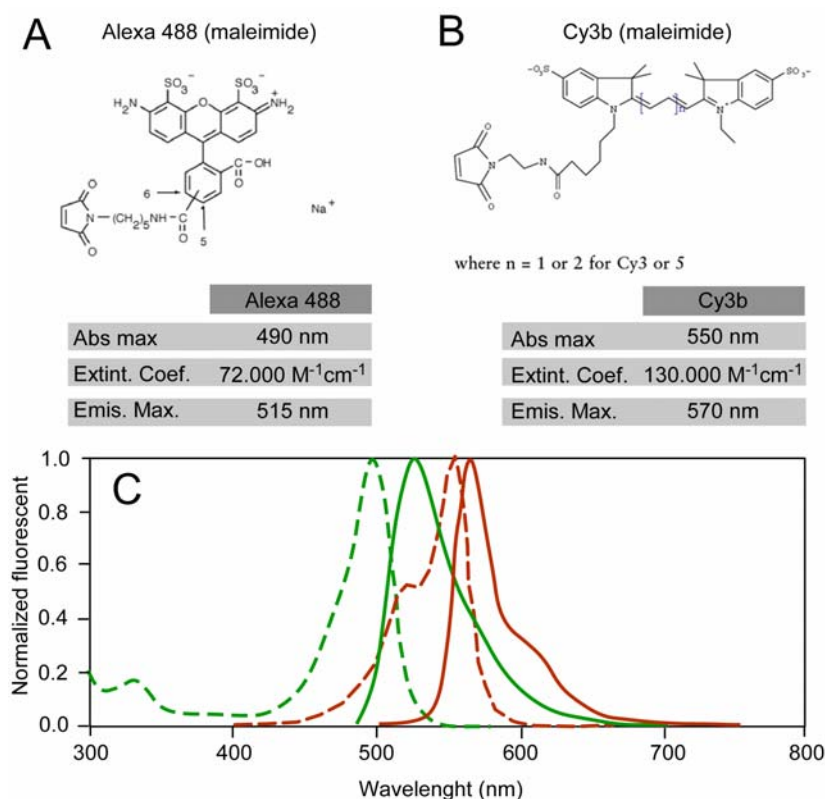


**Appendix figure 1. Properties of the fluorescent dyes employed for the study of αS and βS. A** and **B**. Structure and fluorescent-associated properties of Alexa488 (**A**) and Cy3b (**B**) on their maleimide-derivative versions. **C**. Normalized fluorescence excitation (dashed lines) and emission (bold lines) spectra for Alexa488 (green) and Cy3b (red).

Preliminary measurement of lifetimes corresponding to αS and βS labeled proteins are shown in Appendix figures 2 and 3, and the results are summarized on the Appendix table 1. In all the cases, lifetimes were fitted to a two exponential function, one corresponding to a pulse response (~ 0.5 ns) and the second corresponding to a single population of the dye (2.5 to 4 ns). This suggests that the ensemble of conformations populated by these proteins was highly homogeneous. The lifetime of the dyes attached to the proteins was in all the cases very similar to the ones in free solution (4.1 ns for Alexa 488 and 2.7 ns for Cy3b). However, some features were evident from the slight different lifetimes for the dyes at various positions. In particular the lowest lifetimes were found for the αS-A140C tagged protein, most likely reflecting the local freedom of the dye attached to the very C-terminal residue. Conversely, the longest lifetimes were observed for the αS-A90C protein, likely reflecting

the hydrophobic packing caused by long-range interactions probed by NMR-based methodologies.
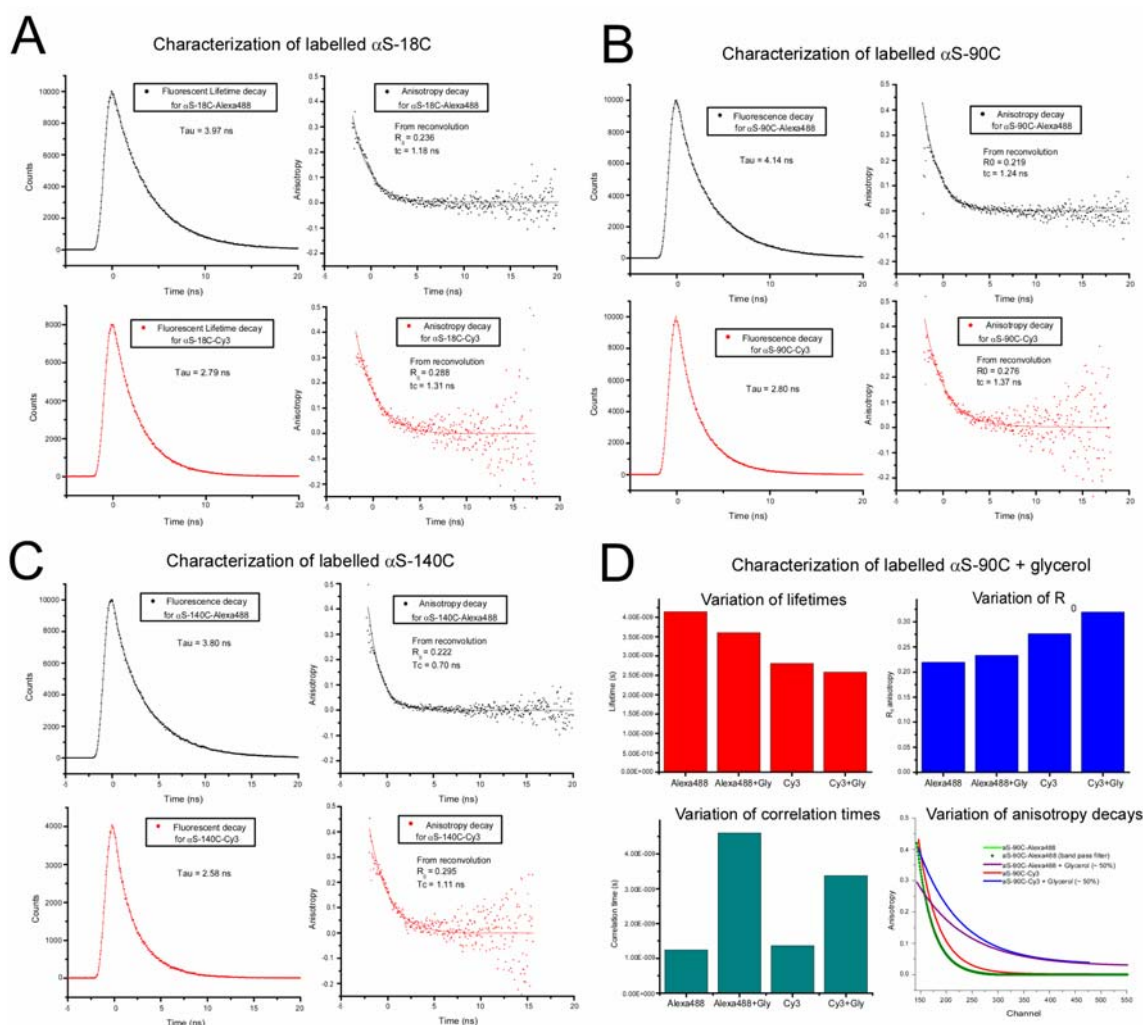


**Appendix figure 2. Lifetime fluorescent decays for fluorescently labeled αS.** Three different Cys-containing mutants of αS (A18C, A90C and A140C) were labeled with Alexa488-maleimide and Cy3b-maleimide, and their time dependent fluorescent properties were studied. **A**, **B** and **C**. Each panel shows fluorescent lifetime decays for the corresponding Alexa488 labeled (black, left) and Cy3b labeled protein (red, left), and anisotropy decays for Alexa488 labeled (black, right) and Cy3b labeled protein. **A** is for αS-A18C, **B** is for αS-A90C and **C** is for αS-A140C. **D**. Influence of the solution media on the fluorescent properties for αS-90C labeled protein. Comparison between buffer and glycerol 50% protein solutions shows the potential of anisotropy measurements for studying changes in diffusion properties of these proteins.
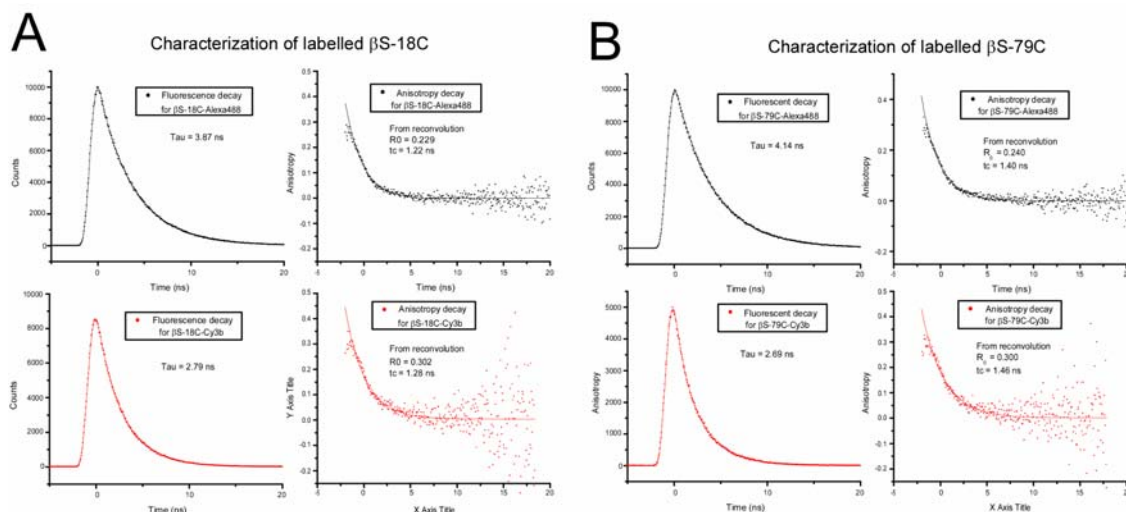
**Appendix figure 3. Lifetime fluorescent decays for fluorescently labeled βS.** The A18C (**A**) and A79C (**B**) Cys-containing mutants of βS were labeled with Alexa488-maleimide and Cy3b-maleimide, and their time dependent fluorescent properties were determined. Fluorescent lifetime decays for the corresponding Alexa488 labeled (black, left) and Cy3b labeled protein (red, left), and anisotropy decays for Alexa488 labeled (black, right) and Cy3b labeled protein.

We also performed time-dependent anisotropy measurements on the above mentioned samples. For anisotropy measurements the sample is excited with vertically polarized light and the intensity decay is measured with emission polarizers oriented along either the vertical (parallel) or the horizontal (perpendicular) axis. The anisotropy is derived from the following equation, relating the intensity decays the individual the parallel ($I_{paral}$) and perpendicular ($I_{perp}$) components (1):

$$r = \frac{I_{paral} - I_{perp}}{I_{paral} + 2\, I_{perp}} \qquad (1)$$

From the time-dependent anisotropy the correlation time of the fluorophore attached to the polypeptide chain can be derived from the Perrin equation (2) for an isotropically rotating sphere, clearly a great simplification of our system:

$$r = \frac{r_0}{1 + \dfrac{\tau}{\theta}} \qquad (2)$$

, where $r_0$ is the fundamental anisotropy (anisotropy at time 0), and $\theta$ is the rotational correlation time of the protein. By employing fluorophores with a lifetime $\tau$ similar to the expected correlation time of the protein, $\theta$ can be evaluated.

In all assayed protein derivatives, the correlation time of the fluorophore was in the order of ~1ns, much lower than the one expected to αS based on its molecular weight (5 to 6

ns). However, due to the unfolded nature and high flexibility of the polypeptide chain, one presumes that the correlation time of the fluorophore is not primarily dictated by the tumbling of the whole protein, but rather by local backbone fluctuations of the persistence length segment in which the dye is located. Thus, the very high mobility of the very end segment of αS was expected, whereas the segments corresponding to the other substitution positions displayed a lower degree of motion. In particular the 90th position in αS, and 79th position of βS, were shown to be slightly more dynamically restricted, consistent with the persistent residual structure in the vicinity of the residues revealed by NMR-residual dipolar couplings.

| Protein | Lifetime (ns) | R0 | Cor. time (ns) |
|---|---|---|---|
| αS-18C-Alexa | 3.97 | 0.236 | 1.18 |
| αS-90C-Alexa | 4.14 | 0.219 | 1.24 |
| αS-140C-Alexa | 3.80 | 0.222 | 0.70 |
| βS-18C-Alexa | 3.87 | 0.229 | 1.22 |
| βS-79C-Alexa | 3.94 | 0.240 | 1.40 |
| αS-18C-Cy3b | 2.79 | 0.288 | 1.31 |
| αS-90C-Cy3b | 2.80 | 0.276 | 1.37 |
| αS-140C-Cy3b | 2.58 | 0.295 | 1.11 |
| βS-18C-Cy3b | 2.79 | 0.302 | 1.28 |
| βS-79C-Cy3b | 2.69 | 0.300 | 1.46 |

**Appendix table 1. Time-dependent fluorescent properties for fluorescently labeled αS and βs.** Overview of the determinations of lifetime and anisotropy decays for the different variants of αS and βS at the monomeric native state.

The rationalization of the fluorescent-derived properties with the NMR-derived structural data was one of many goals of these studies. The preliminary results shown here are promising and suggest that we may be able to detect by lifetime measurement the changes in conformations populated by the unfolded polypeptide chain, and by anisotropy decays the restricted dynamics and oligomerization state of the protein during different stages of the aggregation process. In addition, the use of other fluorescent derivatives is currently under investigation in our laboratories, and will bring a whole new level in the investigation of the

biophysical properties of such protein conversions, particularly during the elusive early stages of association (oligomerization).

The integration of fluorescence spectroscopy in light microscopy adds a new dimension to microscopy, since spatial resolution information about the molecular behavior of proteins can additionally be obtained in living cells. Imaging techniques with spectral resolution in a microscope require that the proteins of interest be fluorescently tagged. This makes such studies in living cells far more complex than *in vitro*. However, it is possible to introduce into the cell an *in vitro* labeled protein, for example by microinjection. Nevertheless this procedure is highly time consuming, since each cell has to be injected individually, and the technique is not suitable for all cell lines. A far more attractive alternative strategy is to add genetically encoded fluorescent tags, as the green fluorescent protein (GFP). Biologically functional GFP fusions have been obtained for a number of proteins, and are the method of choice for studying the fate of proteins inside cells. Amyloid deposition has been studied employing such fusions. Artificial peptides and polyQ constructs have been shown to yield fluorescent aggregates in cell cultures when fused to visible fluorescent proteins (VFP) (Bence et al., 2001; Kim et al., 2002) In some cases, however, the GFP represents an excessively bulky group for the protein to which is added, in particular for small polypeptides such as αS (Figure Appendix 2A). In particular for αS, the formation of abnormal non-fluorescent aggregates deprived of fluorescence has been observed in neuronal cultures (McLean et al., 2001). Thus, monitoring αS amyloid formation in living cells has posed a formidable challenge.

To overcome the problems associated with the use of VFPs the challenge was to search for alternative genetically-encoded tags of reduced size. Such a strategy was developed by the laboratory of Roger Tsien a few years ago in the (most recent form) of a 12-mer peptide tag, containing 4 Cys residues in a defined spatial separation (CysCysXXCysCys). This so-called tetracysteine tag (TC), specifically binds organo-arsenical dyes with high affinity (Griffin et al., 2000). The tag is fused to the gene of interest and transfected cells are stained with the biarsenical dye, which is not fluorescent in solutions and becomes fluorescent upon conjugation to the TC tag. Furthermore, the TC motif is absent from natural genomes and allow specificity of the staining. We thus sought in using the strategy of small, genetically encoded, TC tags to study αS fibrillation We have succeeded in creating functional fluorescent derivatives of αS by fusing the TC sequence FLNCCPGCCMEP (Martin et al., 2005) at the C-terminus of the protein (Figure Appendix

5B). This chimera, characterized biophysically to be indistinguishable from the *wt* protein, reacts with the fluorogenic biarsenical compounds known as FlAsH and ReAsH (Figure Appendix 4), yielding fluorescent derivatives that readily aggregate (Figure Appendix 5C and 5D).
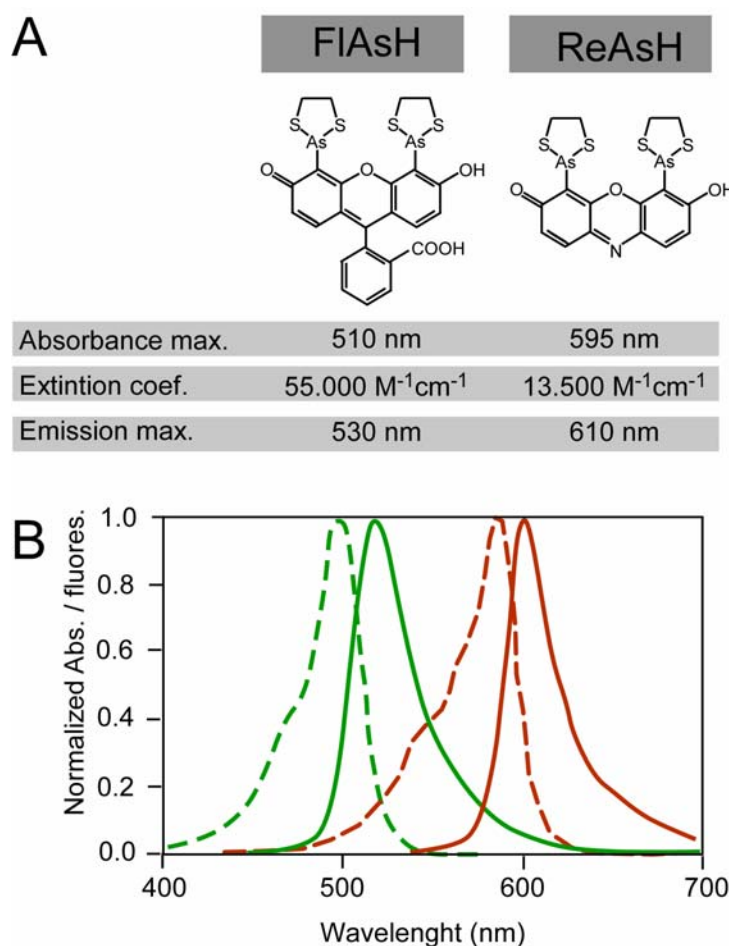


**Appendix figure 4. Properties of the FlAsH and ReAsH arsenoxide dyes employed for *in vitro* and *in vivo* studies of αS fibrillation. A**. Structure and fluorescent-associated properties of FlAsH and ReAsH. **B**. Normalized fluorescence excitation (dashed lines) and emission (bold lines) spectra for FlAsH (green) and ReAsH (red).

Monitoring αS in vivo was achieved by either microinjecting pre-labeled αS-TC-FlAsH protein or by transfecting the cells with an αS-TC-coding plasmid and staining with the cell permeable FlAsH or ReAsH dyes (Figure Appendix 2E to 2H). The intracellular distribution and aggregation of αS-TC was assessed in living cells by fluorescence microscopy, exploiting photophysical phenomena such as FRET using singly or doubly stained cells.
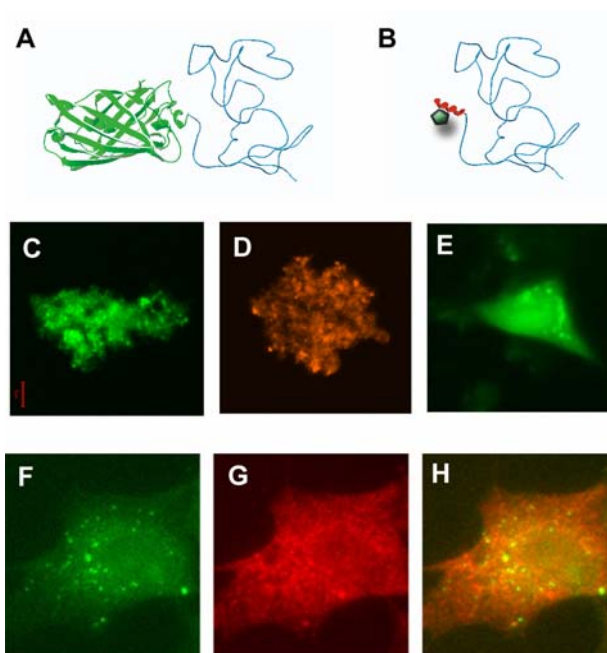
**Appendix figure 5. Fusion of a tetracysteine (TC) tag to αS shields fluorescent amyloid fibrils *in vivo*. A.** Structural model for an αS-VFP chimera. **B**. Structural model for an αS-TC chimera. **C** and **D**. αS-TC-FlAsH (**C**) and αS-TC-ReAsH (**D**) aggregates obtained in vitro. **E**. Live SHSY-5Y cell expressing the αS-TC construct and stained with FlAsH. Perinuclear αS aggregates are observed. **F**, **G** and **H**. Fixed SHSY-5Y cell expressing the αS-TC construct stained with FlAsH (**F**) and immuno-stained with an antibody anti-αS (Alexa633 conjugated secondary antibody, **G**) shows co-localization of aggregates (merged, **H**). Panels C, D, F, G and H were kindly provided by María J. Roberti (MPI-BPC and Universidad de Buenos Aires, Argentina).

Our results validate tetracysteine tags as valuable tools for direct fluorescent studies of αS fibrillation, and provide the means for investigation of protein misfolding phenomena in general. Furthermore, we foresee the potential use of our fluorescent constructs for screening procedures of therapeutic agents specific for neurodegenerative diseases.

The results shown here on αS-TC, were obtained in collaboration with María J. Roberti, a PhD student primarily responsible for the research, and a member of the group of Prof. Dr. Elizabeth Jares-Erijman of the Laboratory of Organic Chemistry, University of Buenos Aires. Some of these data have been included in the following paper submitted for publication:

- Roberti, M.J., **C.W. Bertoncini**, R. Klement, E.A. Jares-Erijman and T.M. Jovin (2006) "Shedding light on Parkinson´s disease: Tetracysteine-tagged α-synuclein, a probe for amyloid-protein formation in living cells". *Submitted*.

# References

Allsop, D., Swanson, L., Moore, S., Davies, Y., York, A., El-Agnaf, O. M., and Soutar, I. (2001). Fluorescence anisotropy: a method for early detection of Alzheimer beta-peptide (Abeta) aggregation. *Biochem. Biophys. Res. Commun. 285*, 58-63.

Bence, N. F., Sampat, R. M., and Kopito, R. R. (2001). Impairment of the Ubiquitin-Proteasome System by Protein Aggregation. *Science 292*, 1552-1555.

Griffin, B. A., Adams, S. R., Jones, J., and Tsien, R. Y. (2000). Fluorescent labeling of recombinant proteins in living cells with FlAsH. *Methods Enzymol. 327*, 565-578.

Kim, S., Nollen, E. A. A., Kitagawa, K., Bindokas, V. P., and Morimoto, R. I. (2002). Polyglutamine protein aggregates are dynamic. *Nat Cell Biol 4*, 826.

Koo, B. W., and Miranker, A. D. (2005). Contribution of the intrinsic disulfide to the assembly mechanism of islet amyloid. *Protein Sci. 14*, 231-239.

Krishnan, R., and Lindquist, S. L. (2005). Structural insights into a yeast prion illuminate nucleation and strain diversity. *Nature 435*, 765-772.

Lakowicz, J. R. (1999). Principles of Fluorescence Spectroscopy, 2nd edition edn (New York: Kluwer Academic).

Lakshmikanth, G. S., Sridevi, K., Krishnamoorthy, G., and Udgaonkar, J. B. (2001). Structure is lost incrementally during the unfolding of barstar. *Nat. Struct. Biol. 8*, 799-804.

Martin, B. R., Giepmans, B. N., Adams, S. R., and Tsien, R. Y. (2005). Mammalian cell-based optimization of the biarsenical-binding tetracysteine motif for improved fluorescence and affinity. *Nat. Biotechnol. 23*, 1308-1314.

McLean, P. J., Kawamata, H., and Hyman, B. T. (2001). α-Synuclein-enhanced green fluorescent protein fusion proteins form proteasome sensitive inclusions in primary neurons. *Neuroscience 104*, 901

Mukhopadhyay, S., Nayak, P. K., Udgaonkar, J. B., and Krishnamoorthy, G. (2006). Characterization of the formation of amyloid protofibrils from barstar by mapping residue-specific fluorescence dynamics. *J Mol Biol 358*, 935-942.

Nilsson, M. R. (2004). Techniques to study amyloid fibril formation in vitro. *Methods 34*, 151-160.

Padrick, S. B., and Miranker, A. D. (2002). Islet amyloid: phase partitioning and secondary nucleation are central to the mechanism of fibrillogenesis. *Biochemistry 41*, 4694-4703.

Ratner, V., Sinev, M., and Haas, E. (2000). Determination of intramolecular distance distribution during protein folding on the millisecond timescale. *J. Mol. Biol. 299*, 1363-1371.

Sridevi, K., Lakshmikanth, G. S., Krishnamoorthy, G., and Udgaonkar, J. B. (2004). Increasing stability reduces conformational heterogeneity in a protein folding intermediate ensemble. *J. Mol. Biol. 337*, 699-711.

Sridevi, K., Juneja, J., Bhuyan, A. K., Krishnamoorthy, G., and Udgaonkar, J. B. (2000). The slow folding reaction of barstar: the core tryptophan region attains tight packing before substantial secondary and tertiary structure formation and final compaction of the polypeptide chain. *J. Mol. Biol. 302*, 479-495.

**11.2 Backbone assignment of the native soluble state of the protein βS.**

The following data are going to be deposited on the Biological Magnetic Resonance Data Bank (http://www.bmrb.wisc.edu/) as part of the publication of the following work:

- **Bertoncini, C.W.**, R.M. Rasia, A. Binolfi, M. Zweckstetter, C. Griesinger, T.M. Jovin and C.O. Fernandez. "Solution NMR characterization of β-synuclein, a protein associated with Parkinson's disease". *In preparation.*

| Res ID | Res type | HN | N | CO | CA | CB | HA |
|--------|----------|------|---------|---------|--------|--------|-------|
| 1 | MET | n/a | n/a | n/a | n/a | n/a | n/a |
| 2 | ASP | n/a | n/a | 175.94 | 54.166 | 41.515 | n/a |
| 3 | VAL | 8.096 | 120.307 | 176 | 62.547 | 32.656 | 3.814 |
| 4 | PHE | 8.181 | 123.458 | 175.924 | 57.928 | 39.256 | 4.404 |
| 5 | MET | 8.057 | 122.25 | 176.011 | 55.246 | 32.612 | 4.183 |
| 6 | LYS | 8.113 | 122.557 | 177.265 | 56.718 | 32.822 | 4.005 |
| 7 | GLY | 8.238 | 109.692 | 173.986 | 45.262 | n/a | 3.743 |
| 8 | LEU | 7.895 | 121.5 | 177.75 | 55.146 | 42.459 | 4.151 |
| 9 | SER | 8.171 | 116.267 | 174.753 | 58.351 | 63.650 | 4.231 |
| 10 | MET | 8.216 | 122.362 | 176.144 | 55.265 | 32.666 | 4.297 |
| 11 | ALA | 8.088 | 125.065 | 177.903 | 52.485 | 19.071 | 4.077 |
| 12 | LYS | 8.181 | 120.888 | 176.805 | 56.154 | 32.937 | 4.064 |
| 13 | GLU | 8.313 | 121.804 | 177.112 | 56.663 | 30.052 | 4.047 |
| 14 | GLY | 8.286 | 109.932 | 174.123 | 45.232 | n/a | 3.738 |
| 15 | VAL | 7.798 | 119.994 | 176.582 | 62.543 | 32.664 | 3.882 |
| 16 | VAL | 8.124 | 125.116 | 176.045 | 62.347 | 32.657 | 3.855 |
| 17 | ALA | 8.279 | 128.294 | 177.778 | 52.472 | 19.039 | 4.068 |
| 18 | ALA | 8.145 | 123.532 | 178.012 | 52.558 | 18.965 | 4.025 |
| 19 | ALA | 8.107 | 122.972 | 178.327 | 52.729 | 19.052 | 4.044 |
| 20 | GLU | 8.164 | 119.972 | 177.059 | 56.647 | 30.089 | 4.018 |
| 21 | LYS | 8.174 | 122.195 | 177.25 | 56.599 | 32.759 | 4.115 |
| 22 | THR | 7.96 | 115.14 | 174.781 | 62.283 | 69.708 | 4.068 |
| 23 | LYS | 8.175 | 123.681 | 176.704 | 56.514 | 32.783 | 4.404 |
| 24 | GLN | 8.254 | 121.668 | 176.566 | 56.060 | 29.453 | 4.084 |
| 25 | GLY | 8.322 | 110.388 | 174.289 | 45.250 | n/a | 3.762 |
| 26 | VAL | 7.898 | 119.511 | 176.874 | 62.440 | 32.709 | 3.971 |
| 27 | THR | 8.15 | 118.483 | 174.723 | 62.273 | 69.728 | 4.118 |
| 28 | GLU | 8.333 | 123.909 | 176.469 | 56.637 | 30.274 | 4.055 |
| 29 | ALA | 8.203 | 125.004 | 177.899 | 52.660 | 18.982 | 4.042 |
| 30 | ALA | 8.089 | 123.112 | 178.303 | 52.683 | 19.015 | 4.048 |
| 31 | GLU | 8.173 | 119.756 | 176.902 | 56.584 | 30.220 | 4.015 |
| 32 | LYS | 8.146 | 122.065 | 177.17 | 56.353 | 32.893 | 4.152 |
| 33 | THR | 8 | 115.268 | 174.87 | 62.136 | 69.781 | 4.096 |
| 34 | LYS | 8.217 | 123.528 | 176.736 | 56.523 | 32.795 | 4.064 |
| 35 | GLU | 8.232 | 121.541 | 177.156 | 56.585 | 30.198 | 4.038 |
| 36 | GLY | 8.255 | 109.754 | 174.165 | 45.307 | n/a | 3.743 |
| 37 | VAL | 7.73 | 119.375 | 176.092 | 62.351 | 32.638 | 3.851 |
| 38 | LEU | 8.104 | 125.525 | 176.813 | 54.835 | 42.433 | 4.128 |
| 39 | TYR | 8.1 | 122.238 | 175.724 | 57.799 | 38.731 | 4.361 |
| 40 | VAL | 7.908 | 123.185 | 176.296 | 62.211 | 32.703 | 3.845 |

| 41 | GLY | 7.874 | 111.987 | 174.083 | 45.145 | n/a | 3.72 |
|----|-----|-------|---------|---------|--------|--------|-------|
| 42 | SER | 8.082 | 115.435 | 174.929 | 58.357 | 63.754 | 4.23 |
| 43 | LYS | 8.306 | 123.238 | 176.99 | 56.358 | 32.924 | 4.211 |
| 44 | THR | 8.012 | 115.218 | 174.686 | 61.920 | 69.774 | 4.095 |
| 45 | ARG | 8.264 | 123.233 | 176.322 | 56.155 | 30.643 | 4.601 |
| 46 | GLU | 8.304 | 121.977 | 177.12 | 56.648 | 30.212 | 4.045 |
| 47 | GLY | 8.286 | 109.929 | 174.023 | 45.218 | n/a | 3.739 |
| 48 | VAL | 7.762 | 119.76 | 176.425 | 62.311 | 32.678 | 3.91 |
| 49 | VAL | 8.204 | 125.405 | 176.189 | 62.336 | 32.666 | 3.878 |
| 50 | GLN | 8.419 | 125.197 | 176.441 | 55.763 | 29.445 | 4.114 |
| 51 | GLY | 8.319 | 110.627 | 174.002 | 45.239 | n/a | 3.762 |
| 52 | VAL | 7.881 | 119.413 | 176.183 | 62.161 | 32.768 | 3.913 |
| 53 | ALA | 8.314 | 127.937 | 177.907 | 52.407 | 19.126 | 4.136 |
| 54 | SER | 8.178 | 115.776 | 174.814 | 58.045 | 63.748 | 4.24 |
| 55 | VAL | 8.065 | 121.926 | 176.336 | 62.617 | 32.617 | 3.891 |
| 56 | ALA | 8.189 | 127.123 | 178.207 | 52.769 | 19.016 | 4.07 |
| 57 | GLU | 8.159 | 120.511 | 177.079 | 56.518 | 30.338 | 4.08 |
| 58 | LYS | 8.229 | 122.397 | 177.375 | 56.592 | 32.783 | 4.142 |
| 59 | THR | 8.027 | 115.447 | 175.036 | 62.465 | 69.709 | 4.052 |
| 60 | LYS | 8.178 | 123.328 | 177.259 | 56.917 | 32.716 | 4.075 |
| 61 | GLU | 8.246 | 121.703 | 177.143 | 57.299 | 30.022 | 4.007 |
| 62 | GLN | 8.193 | 121.085 | 176.336 | 56.116 | 29.377 | 4.04 |
| 63 | ALA | 8.158 | 124.539 | 178.171 | 52.770 | 19.028 | 4.084 |
| 64 | SER | 8.061 | 114.472 | 174.682 | 58.565 | 63.654 | 4.159 |
| 65 | HIS | 8.16 | 120.46 | 175.064 | 55.983 | 29.595 | n/a |
| 66 | LEU | 8.036 | 122.969 | 178.042 | 55.272 | 42.104 | 4.076 |
| 67 | GLY | 8.257 | 109.554 | 174.754 | 45.253 | n/a | 3.746 |
| 68 | GLY | 8.086 | 108.542 | 173.934 | 44.990 | n/a | 3.75 |
| 69 | ALA | 8.014 | 123.665 | 177.755 | 52.345 | 19.312 | 4.105 |
| 70 | VAL | 7.921 | 119.236 | 176.053 | 62.196 | 32.753 | 3.833 |
| 71 | PHE | 8.254 | 124.397 | 175.831 | 57.555 | 39.674 | 4.483 |
| 72 | SER | 8.166 | 118.497 | 174.813 | 57.948 | 63.764 | 4.202 |
| 73 | GLY | 7.675 | 110.485 | 173.927 | 45.267 | n/a | 3.705 |
| 74 | ALA | 8.049 | 123.536 | 178.453 | 52.654 | 19.130 | 4.114 |
| 75 | GLY | 8.267 | 107.657 | 174.003 | 45.226 | n/a | 3.711 |
| 76 | ASN | 8.077 | 118.481 | 175.4 | 53.028 | 38.906 | 4.503 |
| 77 | ILE | 7.949 | 121.408 | 176.281 | 61.278 | 38.604 | 3.917 |
| 78 | ALA | 8.207 | 127.943 | 177.685 | 52.461 | 18.932 | 4.061 |
| 79 | ALA | 8.026 | 123.185 | 177.895 | 52.356 | 19.026 | 4.048 |
| 80 | ALA | 8.133 | 123.194 | 178.291 | 52.510 | 19.006 | 4.149 |
| 81 | THR | 7.912 | 112.354 | 175.343 | 61.936 | 69.809 | 4.111 |
| 82 | GLY | 8.177 | 110.603 | 173.986 | 45.262 | n/a | 3.743 |
| 83 | LEU | 7.889 | 121.445 | 177.406 | 55.084 | 42.397 | 4.15 |
| 84 | VAL | 7.981 | 122.06 | 175.973 | 62.181 | 32.871 | 3.859 |
| 85 | LYS | 8.312 | 126.623 | 176.28 | 56.062 | 32.951 | 4.095 |
| 86 | ARG | 8.332 | 124.159 | 176.192 | 56.103 | 30.809 | 4.374 |
| 87 | GLU | 8.407 | 122.854 | 175.985 | 56.327 | 30.302 | 4.015 |
| 88 | GLU | 8.198 | 122.112 | 175.799 | 56.225 | 30.463 | 3.969 |
| 89 | PHE | 8.152 | 121.156 | 173.891 | 55.344 | 39.125 | 4.698 |
| 90 | PRO | n/a | n/a | 177.315 | 63.223 | 32.158 | n/a |
| 91 | THR | 8.124 | 113.926 | 174.41 | 61.792 | 69.776 | 4.127 |
| 92 | ASP | 8.185 | 122.239 | 175.931 | 54.234 | 40.978 | 4.405 |

| 93 | LEU | 7.942 | 122.322 | 177.189 | 54.749 | 42.383 | 4.126 |
|---|---|---|---|---|---|---|---|
| 94 | LYS | 8.323 | 124.338 | 174.639 | 54.217 | 32.399 | 4.381 |
| 95 | PRO | n/a | n/a | 177.325 | 63.354 | 32.048 | n/a |
| 96 | GLU | 8.536 | 120.402 | 176.792 | 56.656 | 29.967 | 4.009 |
| 97 | GLU | 8.21 | 122.198 | 176.448 | 56.253 | 30.394 | 4.118 |
| 98 | VAL | 7.988 | 121.921 | 175.993 | 62.158 | 32.731 | 3.859 |
| 99 | ALA | 8.287 | 128.34 | 177.787 | 52.374 | 19.034 | 4.074 |
| 100 | GLN | 8.264 | 120.435 | 176.175 | 55.614 | 29.581 | 4.082 |
| 101 | GLU | 8.345 | 122.772 | 176.226 | 56.212 | 30.304 | 4.04 |
| 102 | ALA | 8.259 | 125.68 | 177.386 | 52.120 | 19.186 | 4.085 |
| 103 | ALA | 8.171 | 124.083 | 177.746 | 52.060 | 19.427 | 4.094 |
| 104 | GLU | 8.23 | 120.664 | 176.348 | 56.061 | 30.446 | 4.058 |
| 105 | GLU | 8.326 | 124.026 | 174.574 | 54.241 | 30.156 | 4.056 |
| 106 | PRO | n/a | n/a | 176.626 | 62.859 | 32.123 | n/a |
| 107 | LEU | 8.22 | 123.068 | 177.259 | 54.836 | 42.134 | 4.1 |
| 108 | ILE | 8.101 | 123.681 | 176.057 | 60.430 | 38.586 | 3.972 |
| 109 | GLU | 8.326 | 127.334 | 174.323 | 54.160 | 29.798 | 4.362 |
| 110 | PRO | n/a | n/a | 176.721 | 62.829 | 32.157 | n/a |
| 111 | LEU | 8.194 | 122.592 | 177.44 | 54.895 | 42.201 | 4.115 |
| 112 | MET | 8.274 | 122.388 | 175.974 | 54.644 | 33.014 | 4.304 |
| 113 | GLU | 8.306 | 124.054 | 174.553 | 54.186 | 29.642 | 4.366 |
| 114 | PRO | n/a | n/a | 177.064 | 63.080 | 32.130 | n/a |
| 115 | GLU | 8.432 | 121.597 | 177.174 | 56.548 | 30.386 | 4.063 |
| 116 | GLY | 8.276 | 110.098 | 173.978 | 45.046 | n/a | 3.747 |
| 117 | GLU | 8.16 | 120.416 | 176.442 | 56.307 | 30.470 | 4.045 |
| 118 | SER | 8.22 | 116.986 | 174.02 | 57.797 | 63.809 | 4.231 |
| 119 | TYR | 8.169 | 122.877 | 175.476 | 57.764 | 39.072 | 4.376 |
| 120 | GLU | 7.97 | 123.059 | 175.5 | 55.615 | 31.006 | 4.074 |
| 121 | ASP | 8.272 | 123.458 | 173.804 | 52.739 | 40.379 | 4.109 |
| 122 | PRO | n/a | n/a | n/a | n/a | n/a | n/a |
| 123 | PRO | n/a | n/a | 177.013 | 62.746 | 32.073 | n/a |
| 124 | GLN | 8.383 | 121.122 | 176.156 | 55.476 | 29.622 | 4.077 |
| 125 | GLU | 8.371 | 122.943 | 176.259 | 56.125 | 30.444 | 4.041 |
| 126 | GLU | 8.328 | 122.39 | 176.057 | 56.389 | 30.439 | 4.036 |
| 127 | TYR | 8.218 | 122.46 | 175.417 | 57.928 | 38.788 | n/a |
| 128 | GLN | 7.98 | 123.694 | 174.887 | 54.820 | 29.978 | 4.051 |
| 129 | GLU | 8.19 | 122.905 | 175.932 | 56.182 | 30.346 | 3.943 |
| 130 | TYR | 8.113 | 121.902 | 175.181 | 57.527 | 39.155 | 4.36 |
| 131 | GLU | 8.14 | 125.47 | 173.782 | 53.465 | 30.210 | 4.331 |
| 132 | PRO | n/a | n/a | 176.98 | 62.879 | 32.203 | n/a |
| 133 | GLU | 8.355 | 121.508 | 175.535 | 56.467 | 30.287 | 4.003 |
| 134 | ALA | 7.839 | 107.823 | 173.99 | 53.788 | 20.076 | 3.892 |

*Miscellaneous*

**Acknowledgments**

## Publications

*Original articles:*

- **Bertoncini, C.W.**, Y.-S., Jung, C.O. Fernandez, W. Hoyer, C. Griesinger, T.M. Jovin and M. Zweckstetter (2005) "Release of long-range structure triggers aggregation of natively unfolded α-synuclein". *Proc. Natl Acad. Sci.* **102**: 1430-1435.

- Rasia, R.M., **C.W. Bertoncini**, D.Marsh, W.Hoyer, D.Cherny, M, Zweckstetter, C. Griesinger, T.M. Jovin and C.O. Fernandez (2005) "Structural characterization of copper (II) binding to α-synuclein: New insights into the bioinorganic chemistry of Parkinson's disease". *Proc. Natl Acad. Sci.* **102**: 4294-4299.

- **Bertoncini, C.W.**, C.O. Fernandez, C. Griesinger, T.M. Jovin and M. Zweckstetter (2005) "Familial mutants of α-synuclein with increased neurotoxicity have a destabilized conformation". *J. Biol. Chem.* **280**: 30649-30652.

- Bernado, P., **C.W. Bertoncini**, C. Griesinger, M. Zweckstetter, and M. Blackledge (2005) "Defining long-range order and local disorder in native α-synuclein using residual dipolar couplings". *J. Am. Chem. Soc.* **127**: 17968-17969.

- Binolfi, A., R.M. Rasia, **C.W. Bertoncini**, M. Ceolin, M. Zweckstetter, C. Griesinger, T.M. Jovin and C.O. Fernandez (2006) "Interaction of α-synuclein with divalent metal ions reveals key differences: A link between structure, binding specificity and fibrillation enhancement". *J. Am. Chem. Soc.* 128: 9893-9901.

- Roberti, M.J., **C.W. Bertoncini**, R. Klement, E.A. Jares-Erijman and T.M. Jovin (2006) "Shedding light on Parkinson´s disease: Tetracysteine-tagged α-synuclein, a probe for amyloid-protein formation in living cells". *Submitted*.

*Scientific meetings and Symposia:*

- **Bertoncini, C.W.**, C.O. Fernandez, W. Hoyer, C. Griesinger, T.M. Jovin, <u>M. Zweckstetter.</u> "Becoming Mr. Hyde: Residual structure and slow dynamics in α-synuclein". 17th EENC/32nd Ampere, September 6th-11th, 2004, Lille, France.

- <u>Fernandez, C.O.</u>, R.M. Rasia, **C.W. Bertoncini**, W. Hoyer, M. Zweckstetter, D. Marsh, C. Griesinger, T.M. Jovin. "Cu(II) binding to α-synuclein: A natively unfolded protein?". 1$^{st}$ Latin American Protein Society Meeting, November 8$^{th}$-12$^{th}$, 2004, Angra dos Reis, Brazil.

- **Bertoncini, C.W**., C.O. Fernandez, W. Hoyer, <u>C. Griesinger</u>, T.M. Jovin, M. Zweckstetter. "Residual structure and slow dynamics in α-synuclein". XXI International Conference on  Magnetic Resonance in Biological Systems (XXI ICMRBS), January 16$^{th}$-21$^{st}$, 2005, Hyderabad, India.

- **Bertoncini, C.W.**, M. Cho, C.O. Fernandez, H. Heise, M. Reese, F. Rodriguez-Castaneda, V. Sanchez, M. Baldus, T. Carlomagno, T.M. Jovin, M. Zweckstetter and <u>C. Griesinger</u>. "Studies of protein dynamics and a new method to study drug/target interactions". XXI International Conference on Magnetic Resonance in Biological Systems (XXI ICMRBS), January 16$^{th}$-21$^{st}$, 2005, Hyderabad, India.

- <u>**Bertoncini, C.W.**</u>, C.O. Fernandez, C. Griesinger, T.M. Jovin, M. Zweckstetter. "Structural investigation of A30P and A53T α-synuclein diseased-related mutants by NMR residual  dipolar couplings and paramagnetic relaxation enhancement". Keystone Symposia Meeting, Frontiers of NMR in Molecular Biology IX, January 29$^{th}$-February 4$^{th}$, 2005, Banff, Alberta,  Canada.

- C.O. Fernandez, R.M. Rasia, <u>**C.W. Bertoncini**</u>, W. Hoyer, M. Zweckstetter, E.A. Jares-Erijman, V. Subramaniam, D. Marsh, C. Griesinger, T.M. Jovin. "Ligand binding to α-synuclein reveals important long-range contacts: Biological implications". Keystone Symposia Meeting, Frontiers of NMR in Molecular Biology IX, January 29$^{th}$-February 4$^{th}$, 2005, Banff, Alberta, Canada.

- **Bertoncini, C.W.**, Y-S. Jung, C.O. Fernandez, W.Hoyer, C. Griesinger, T.M. Jovin, <u>M. Zweckstetter</u>. Becoming Mr. Hyde: Residual structure and slow dynamics in α-synuclein. Keystone Symposia Meeting, Frontiers of NMR in Molecular Biology IX, January 29$^{th}$-February 4$^{th}$, 2005, Banff, Alberta, Canada.

- **Bertoncini, C.W.**, D. Cherny, C.O. Fernandez, E. Garfinkel, C. Griesinger, W. Hoyer, E.A. Jares-Erijman, <u>T.M. Jovin</u>, D. Marsh, R.M. Rasia, M.J. Roberti, V. Subramaniam and M. Zweckstetter. "3D structure, ligand binding, autoinhibition,

aggregation, and cellular distribution of wild-type, mutant, and labeled α-synuclein". 49th Biophysical Society Annual Meeting. February 12$^{th}$-16$^{th}$, 2005. Long Beach, California, USA.

- Rasia, R.M., **C. W. Bertoncini**, D. Marsh, W. Hoyer, D. Cherny, M, Zweckstetter, C. Griesinger, T. M. Jovin and C. O. Fernandez. "Structural characterization of copper (II) binding to α-synuclein: New insights into the bioinorganic chemistry of Parkinson's disease". 16th International Congress on Parkinson's Disease and Related Disorders. June 5$^{th}$-9$^{th}$, 2005, Berlin, Germany.

- **Bertoncini, C.W.**, Y-S. Jung, C.O. Fernandez, W.Hoyer, C. Griesinger, T.M. Jovin, M. Zweckstetter. "Residual structure and slow dynamics in α-synuclein: biological implications for Parkinson's disease". EMBO-FEBS Spetsai Summer School on Protein Misfolding, Protein Modification and Age-Related Diseases. September 5$^{th}$-15$^{th}$, 2005, Island of Spetses, Greece.

- Kim, H-Y., **C.W. Bertoncini**, M-K. Cho, P. Kapinar, C.O. Fernandez, C. Griesinger, T.M. Jovin and M. Zweckstetter. "α-synuclein: Beyond a single 3D structure". EMBO-FEBS workshop on amyloid formation. March 25$^{th}$-28$^{th}$, 2006, Florence, Italy.

- Rasia, R.M., A. Binolfi, **C.W. Bertoncini**, M. Zweckstetter, C. Griesinger, T.M. Jovin and C.O. Fernandez. "Metallobiology of Parkinson's disease: Structural basis and hierarchy of α-synuclein-metal interactions". EMBO-FEBS workshop on amyloid formation. March 25$^{th}$-28$^{th}$, 2006, Florence, Italy.

- **Bertoncini, C.W.**, R.M. Rasia, A. Binolfi, M. Zweckstetter, C. Griesinger, T.M. Jovin and C.O. Fernandez. "NMR characterization of the α-synuclein/β-synuclein interaction, a molecular complex implicated in Parkinson's disease". EMBO-FEBS workshop on amyloid formation. March 25$^{th}$-28$^{th}$, 2006, Florence, Italy.

- Roberti, M.J., **C.W. Bertoncini**, E.A. Jares-Erijman and T.M. Jovin. "Shedding light on Parkinson´s disease: In vitro and in vivo properties of a recombinant α-synuclein fused to a FlAsH-binding domain". EMBO-FEBS workshop on amyloid formation. March 25$^{th}$-28$^{th}$, 2006, Florence, Italy.

**Lebenslauf**

| | |
|---|---|
| Name: | Carlos Walter Bertoncini |
| Geburtsdatum: | 10. April 1977 |
| Geburtsort: | Santa Fe, Argentinien |
| Nationalität: | argentinisch |
| Adresse: | Hainbuchenring 1 |
| | 37077 Göttingen |

Bildungsweg

| | |
|---|---|
| 1983 - 1989 | Grundschule „ Escuela N° 6 Mariano Moreno", Santa Fe, Argentinien. |
| 1990 - 1996 | Gymnasium „ Escuela Industrial Superior – Universidad Nacional del Litoral", Santa Fe, Argentinien, mit einem technischem Abschluss für Chemie verliess. |
| 1997 - 2001 | Studium der Biotechnologie an der „Universidad Nacional del Litoral", Santa Fe, Argentinien, mit einem Diplomabschluss in Biotechnologie. |
| 2002 | Wissenschaftlicher am Zelltek, SRL, Santa Fe, Argentinien. |
| 2002 | Wissenschaftlicher am Max-Planck-Institut für Biophysikalische Chemie, Göttingen. |
| seit 2003 | Dissertation im Max-Planck-Institut für Biophysikalische Chemie, Göttingen, mit dem Thema „ Structure, Dynamics and aggregation mechanism of the Parkinson´s-disease associated protein α-synuclein" bei Prof. Christian Griesinger and Prof. Thomas Jovin. |